

AD-A076 248

DELAWARE UNIV NEWARK COLL OF MARINE STUDIES

F/G 8/10

WAVELIKE BAROCLINIC DISTURBANCES ON SHALLOW UPPER OCEAN DENSITY--ETC(U)

MAR 79 R A FORMATO

N00014-78-C-0071

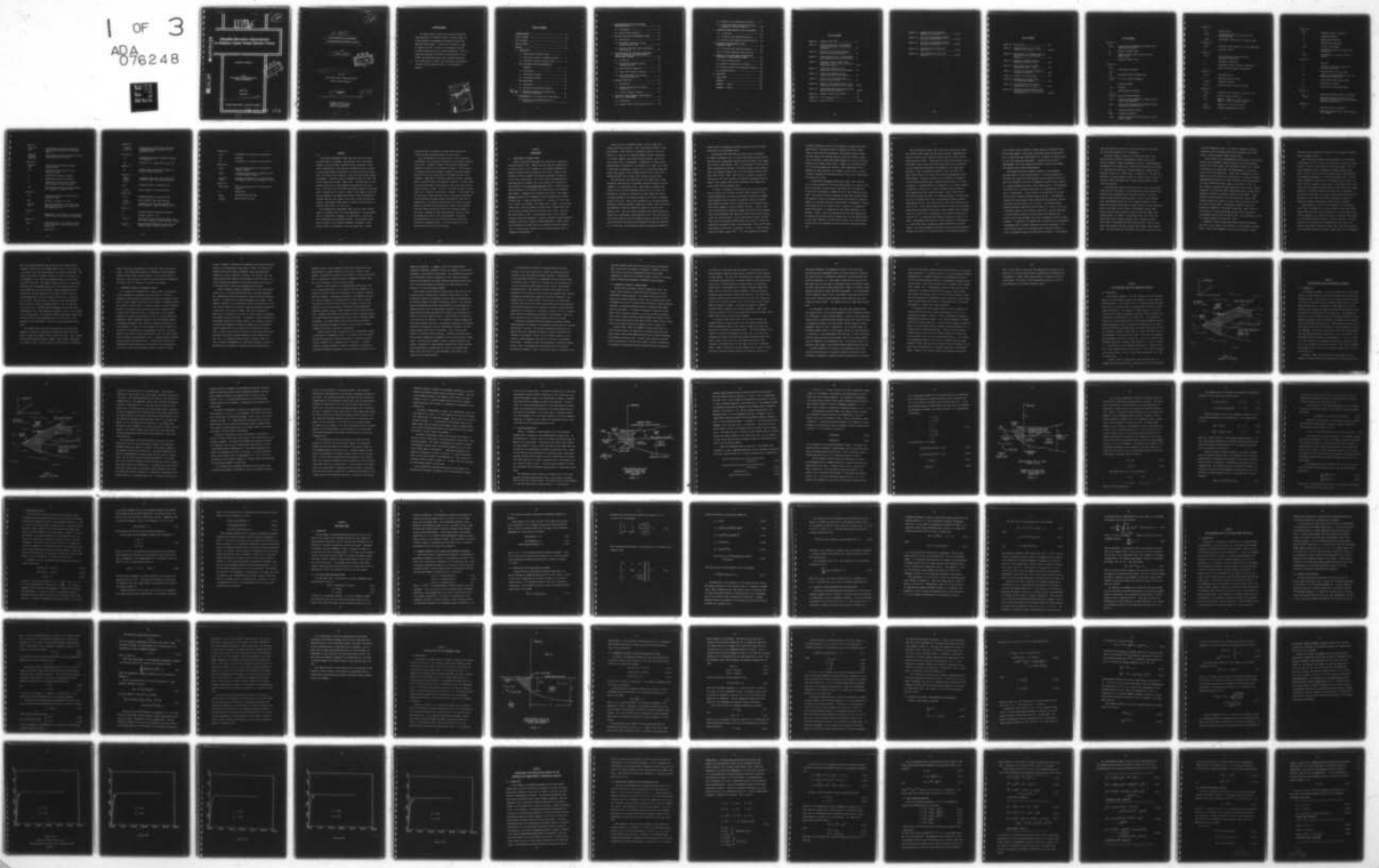
UNCLASSIFIED

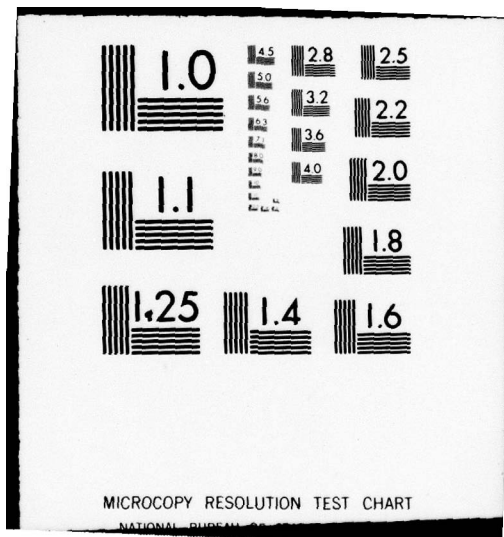
CMS-C-1-79

NL

1 OF 3

ADA
076248





MICROCOPY RESOLUTION TEST CHART
NATIONAL BUREAU OF STANDARDS-1963-A

LEVEL II

12

AD A 076248

Wavelike Baroclinic Disturbances on Shallow Upper Ocean Density Fronts

RICHARD A. FORMATO

For the
Ocean Science and Technology Division
Office of Naval Research

✓
CMS-C-1-79

March 1979

APPROVED FOR PUBLIC RELEASE; DISTRIBUTION UNLIMITED

✓
College of Marine Studies • University of Delaware

DDC
NOV 7 1979
E

79 11 06 073

79 06 12 008

DDC FILE COPY.

12

14 CMS-C-1-79

6 WAVELIKE BAROCLINIC DISTURBANCES
ON SHALLOW UPPER OCEAN DENSITY FRONTS

by

10 Richard A. Formato

DDC
R
NOV 7 1979
E

15 N00014-78-C-0071 *new*

for the

Ocean Science and Technology Division

Office of Naval Research

11 Mar ~~1979~~

12 224

APPROVED FOR PUBLIC RELEASE; DISTRIBUTION UNLIMITED

College of Marine Studies
University of Delaware
Newark, Delaware 19711

407 178

mx

ACKNOWLEDGEMENTS

The author wishes to express his sincere gratitude and deep appreciation to Professor Richard W. Garvine, whose continuing guidance, encouragement and personal interest have made this work possible. I also wish to thank Mssrs. James E. Hazelton and John J. Petillo of Northeastern University for their assistance with the computer programming. This research was supported by the Office of Naval Research, Ocean Science and Technology Division under Contract N00014-75-C-0714, Modification No. P0004 at the University of Connecticut and under Contract N00014-78-C-0071 at the University of Delaware.

new

Accession For	
NTIS GMA&I	<input checked="" type="checkbox"/>
DDC TAB	<input type="checkbox"/>
Unannounced	<input type="checkbox"/>
Justification	<input type="checkbox"/>
By _____	
Distribution/	
Availability Codes	
Dist	Avail and/or special

TABLE OF CONTENTS

ACKNOWLEDGEMENTS	iii
LIST OF FIGURES	vii
LIST OF TABLES	ix
LIST OF SYMBOLS	x
<hr/>	
ABSTRACT	xvi
1. INTRODUCTION	1
1.1 Observations of Oceanic Fronts	1
1.2 Theoretical Studies of Atmospheric Fronts	11
1.3 Theoretical Studies of Oceanic Fronts	16
2. THE EQUILIBRIUM STATE AND PERTURBATION	
EXPANSION	21
2.1 Introduction	21
2.2 The Equilibrium State	25
2.3 Perturbation Analysis	35
3. THE PLANAR FRONT	38
3.1 Introduction	38
3.2 The Planar Front Equilibrium State	38
3.3 Harmonic Solutions to the Planar Front Perturbation Equations	39
3.4 Derivation of the Planar Front DPA Equation ...	40
3.5 Solution of the DPA Equation for the Planar Front	43

4.	NON-DIMENSIONALIZATION OF THE PLANAR FRONT ODE FOR $Z(x)$	47
4.1	Introduction	47
4.2	Inviscid Scale Variables	48
5.	THE BASIC STATE FOR THE EXPONENTIAL FRONT	53
5.1	Introduction	53
5.2	Differential Equations for the Exponential Basic State	55
5.3	Solution of the Basic State Interfacial Depth Equation	58
6.	LINEARIZATION OF THE TIME-VARYING EQUATIONS FOR THE EXPONENTIAL AND PLANAR FRONTS IN DIMENSIONLESS VARIABLES	68
6.1	Introduction	68
6.2	Perturbation Variables and Non-Dimensionalization	69
6.3	Small-Parameter Expansions	72
6.4	Zeroth Order Harmonic Solutions	75
6.5	Zeroth Order ODE's for the Depth Perturbation Amplitude	77
7.	BOUNDARY CONDITIONS	80
7.1	Introduction	80
7.2	Boundary Conditions on the Depth Perturbation	83
7.3	Velocity Boundary Conditions	84
8.	ANALYSIS OF THE EXPONENTIAL FRONT EQUATION FOR $Z(\eta)$ TO LOWEST ORDER	88
8.1	Introduction	88
8.2	Singular Points of the Equation for $Z(\eta)$...	88

8.3	Behavior of the Solution Near Infinity	91
8.4	Typical Mode Shapes for the Zeroth Order Exponential Front DPA Equation	106
9.	DISPERSION CHARACTERISTICS OF THE PLANAR FRONT ..	111
9.1	Introduction	111
9.2	The Zeroth Order Dispersion Relation	114
9.3	The First Order Dispersion Characteristics .	115
10.	DISPERSION CHARACTERISTICS OF THE EXPONENTIAL FRONT	123
10.1	The Zeroth Order Dispersion Relation	123
10.2	First Order Dispersion Characteristics	124
11.	ANALYSIS OF THE FIRST ORDER DISPERSION CHAR- ACTERISTICS OF THE EXPONENTIAL FRONT	137
11.1	The Low Frequency Limit	137
11.3	Regions of Instability in $k\lambda$ -Space	140
11.3	Further Analysis of the Dispersion Relation.	146
11.4	Numerical Results	150
12.	CONCLUSION	192
	BIBLIOGRAPHY	199
	APPENDIX 1	202
	APPENDIX 2 - PART I	205
	APPENDIX 2 - PART II	206

LIST OF FIGURES

Figure 2.1	Geometry of the Front	22
Figure 2.2	Cross-Sectional View of the Idealized Frontal Zone Geometry in Earth-Fixed Coordinates	26
Figure 2.3	Geometry of the Equilibrium Frontal Zone in Translating Coordinates	30
Figure 5.1	Cross-Sectional View of the Equilibrium State Exponential Frontal Zone Geometry .	54
Figure 5.2	Comparison of Exact (Curve A) and Approximate (Curve B) Basic State Inter- facial Depth Profiles	63-67
Figure 7.1	Frontal Zone Geometry for the Exponential Front With Wave Disturbance .	81
Figure 7.2	Frontal Zone Geometry for the Planar Front With Wave Disturbance	82
Figure 8.1	Location of the Singular Points τ_1 , τ_2 and τ_3 in The $k\lambda$ - ω Plane	92
Figure 8.2	Regions of Divergent Solutions to the Zeroth Order DPA Equation in $k\lambda$ - ω Space .	96-102
Figure 8.3	Typical Mode Shapes for the Zeroth Order Depth Perturbation Amplitude	108-110
Figure 9.1	Duxbury's Frontal Zone Geometry	112
Figure 10.1	Plot of $C_{ph(gr)}^{+V_\infty}$ vs δ_0	125
Figure 11.1	Plots of M vs $k\lambda$	141-145

Figure 11.2	Imaginary Part of the Complex Frequency for $\delta_0=0.1-0.5$	166-170
Figure 11.3	Real Part of the Complex Frequency for $V_\infty=0.2$ and $\delta_0=0.1-0.5$	172-176
Figure 11.4	Real Part of the Complex Frequency for $\delta_0=0.4$ and $V_\infty=0.1-0.5$	177-181
Figure 11.5	Phase Velocity for $V_\infty=0.2$ and $\delta_0=0.1-0.5$	182-186
Figure 11.6	Group Velocity for $\delta_0=0.4$ and $V_\infty=0.1-0.5$	187-191

LIST OF TABLES

Table 8.1	Zeros of $A(\eta)$	89
Table 8.2	Computed Values of ω for Various Values of $k\lambda$, δ_0 and V_∞	103-105
Table 11.1	Comparison of Low Frequency Limit and Exact Solution to the Dispersion Relation	151
Table 11.2	Maximum and Minimum Normalized Wavenumber for Bands 1 and 2	158
Table 11.3	Characteristics of the Fastest Growing Mode, Band 1, $V_\infty=0.2$	159
Table 11.4	Values of the Coriolis Parameter as a Function of Latitude	160
Table 11.5	Period at Various Latitudes	161
Table 11.6	Wavelength for Various Values of $k\lambda$ and Rossby Radius	162
Table 11.7	Characteristics of the Fastest Growing Mode, Band 1, $V_\infty=0.6$	163
Table 11.8	Phase and Group Velocities and Dis- turbance Periods for Various Values of δ_0 and V_∞	164-165

LIST OF SYMBOLS

Section 2.1

U_f, V_f	x and y velocity components of frontal zone in earth-fixed coordinates
ρ_∞	density of ambient fluid
$\Delta\rho$	density contrast between frontal zone and ambient fluid
λ	baroclinic Rossby radius

Section 2.2

h_1, h'_1	free surface elevations
h_2, h'_2	
D, D'	interfacial depth in frontal zone
u', v', w' u, v, w	x, y and z velocity components
f	Coriolis parameter
p', p	pressure
g	gravitational acceleration
x', y', z' t', x, y, z	space and time coordinates
U_a, V_a	x and y velocity components of ambient fluid in earth-fixed coordinates
U_∞, V_∞	x and y velocity components of ambient fluid in translating coordinate system
∇_h	horizontal gradient operator
D/Dt	convective derivative
w_s, w_i	vertical velocity at sea surface and at discontinuity surface

Section 2.3

g' reduced gravity
 $\bar{u}, \bar{v}, \bar{D}$ time-invariant basic state velocities and interfacial depth
 $\hat{u}, \hat{v}, \hat{D}$ perturbation velocities and interfacial depth

Section 3.2

$D_f(0)$ interfacial depth beneath the origin (dimensional)
 β arbitrary constant

Section 3.3

X, Y, Z velocity field and interfacial depth
perturbation amplitudes
 k wavenumber (dimensional)
 Ω disturbance circular frequency (dimensional)
 ω Doppler shifted frequency (dimensional)

Section 3.4

a_1, a_2 interfacial slopes
 p derivative operator ($=d/dx$)
 $L_i, \Delta(p)$ derivative operators
 v_n, γ_n complex constants in the DPA equation

Section 3.5

r, α, w_1 constants in the asymptotic solution for $Z(x)$
 $W(x)$ series in inverse powers of x
 α_d, z Duxbury's quantities α and z (used only in equations (3.17), (3.18) and (3.21))
 A_n, B_n constants in the solution for $Z(x)$
 $U(\alpha_d, 1; z)$ confluent hypergeometric function

Section 4.2

\tilde{x}, \tilde{y}	normalized spatial coordinates
σ	normalized frequency
ϵ, ϵ'	dimensionless parameters
c	internal wave phase speed
F_x, F_y	internal Froude numbers
τ	dimensionless transport parameter (only in Chapter 4)
$\tilde{\nu}_n, \tilde{\gamma}_n$	non-dimensional constants in the DPA equation

Section 5.2

Λ	vorticity
u_b	(constant) cross-stream velocity far from the surface front
δ	non-dimensional interfacial depth
D_b	asymptotic interfacial depth far from the surface front (dimensional)
F_b	cross-stream internal Froude number
ξ	normalized x coordinate
F_y	long-stream internal Froude number

Section 5.3

δ_0	normalized interfacial depth at the origin
$\delta^{(0)}, \delta^{(2)}$	zeroth and second order functions in the basic state interfacial depth small parameter expansion (dimensionless)

Section 6.2

ξ, ζ	normalized x and y coordinates
*	superscript asterisk used to mark dimensionless variables

Section 6.3

$\bar{\delta}(0), \bar{\delta}(1)$
 $\bar{\delta}(2)$

small parameter expansion functions for the scaled equilibrium state interfacial depth

$\hat{u}(0), \hat{u}(1)$
 $\hat{v}(0), \hat{v}(1)$
 $\hat{\delta}(0), \hat{\delta}(1)$

small parameter expansion functions for the scaled perturbation variables

Section 6.4

$X(\xi), Y(\xi)$
 $Z(\xi)$

zeroth order perturbation amplitudes (dimensionless)

$\tau(\xi)$

zeroth order normalized basic state interfacial depth

Ω

dimensional disturbance frequency

ω

dimensionless disturbance frequency

σ

dimensionless Doppler shifted disturbance frequency - Planar Front only

$g(\xi)$

position dependent Doppler shifted disturbance frequency - Exponential Front

Section 6.5

$\eta(\tau)$

transformed independent variable for the exponential front

$f(\eta)$

function of η defined in (6.22)

$A(\eta), B(\eta)$
 $C(\eta)$

variable coefficients in the lowest order depth perturbation amplitude equation for the exponential front

Section 7.1

h

displacement of the frontal zone equilibrium boundary under wave disturbance (dimensional)

Section 7.2

$\bar{\delta}_{eq}$

equilibrium value of the interfacial depth at the inner/outer region boundary in the frontal zone

h_o

amplitude of h

Section 8.2

$\tau_i (i=0,4)$
 $n_i^1 (i=0,4)$ singular points of the zeroth order depth perturbation amplitude equation for the exponential front

Section 8.3

μ, s transformed independent variables, equations (8.1) and (8.2)

a, d functions of μ , equations (8.4) and (8.5)

Section 9.1

D_o constant depth (dimensional) in Region 2 of Duxbury's frontal zone model

Section 9.3

$X^{(1)}(\xi)$
 $Y^{(1)}(\xi)$
 $Z^{(1)}(\xi)$ ξ dependent first order velocity field and interfacial depth perturbation amplitudes

A to E parameters defined in equation (9.10)

a_{ij}, b_{ij} matrix elements (row-column notation)

Section 10.2

A to F parameters defined in equation (10.19)

a_{ij}, b_{ij} matrix elements (row-column notation)

$C_i (i=1,5)$ constants in the first order exponential front dispersion relation, equation (10.25)

Section 11.1

$\hat{\omega}$ strained-coordinate disturbance frequency

G constant, equation (11.4)

$\omega_i (i=1,3)$ three roots of the low frequency limit of the first order exponential front dispersion relation

C_{ph_i}, C_{g_i} phase and group velocities for the three low frequency limit dispersion relation roots

Section 11.2

p, q, r coefficients in the general cubic equation
 a, b constants
 M discriminant for the general cubic equation

Section 11.3

ω_R, ω_i real and imaginary parts of the scaled disturbance frequency
 $\tilde{\omega}_R, \tilde{\omega}_i$ coordinate-stretched real and imaginary parts of the disturbance frequency
 $e_i (i=0,6)$ constants and parameters in the equation for the imaginary part of the disturbance frequency
 $\Delta, f(\Delta)$

Section 11.4

$\text{Re}(\omega), \text{Im}(\omega)$ real and imaginary parts of the disturbance frequency
 t_d doubling time
 T_{days} disturbance period in days
 $C_{\text{ph}}, C_{\text{gr}}$ phase and group velocity

ABSTRACT

A theoretical development of small amplitude wave disturbances on oceanic fronts is presented. The prototype front is the inshore boundary of the Gulf Stream, although the model encompasses a wider range of applicability. This work is an extension of recent research by Garvine which showed the importance of dissipation near the surface front, and earlier work by Duxbury on large scale time varying inviscid flow regimes. A two-layer model is considered in which the lower layer is much deeper than the upper, lighter layer. The upper layer, including the frontal zone, is then dynamically uncoupled from the lower layer. The frontal zone that forms the horizontal boundary of the upper layer is divided into two regions, a smaller, inner region in which the flow is dissipative and depends upon interfacial mass entrainment and turbulent friction, and a larger, outer region in which the motion is inviscid. The boundary between these two regions is placed where the internal Froude number is of order one.

Both geostrophic and ageostrophic basic state (non time varying) flows are considered under the f-plane approximation. The geostrophic case is a modification of Duxbury's two-layer model to include the inner dissipative zone described by Garvine. The ageostrophic basic state is similar to one originally suggested by Stommel as a more realistic model of the geometry of the Gulf Stream front. Nonzero

cross-stream flow is allowed in each basic state which is consistent with mass entrainment within the inner region.

Small perturbations to the basic state are then assumed with time-harmonic and space-harmonic dependence in the direction parallel to the front. A system of coupled, linear ordinary differential equations is derived in the perturbation variables. Their solution is developed using a small parameter expansion, the small parameter being the ratio of the cross-stream to the downstream basic state velocities. Application of appropriate physical boundary conditions leads to zeroth and first order dispersion relations. To lowest order, for both the geostrophic and ageostrophic basic state flows, the dispersion relation is linear. All waves are therefore stable to lowest order, and a continuum of wave modes is allowed. To first order, that is, when finite cross-stream flow occurs, the dispersion characteristics are nonlinear and admit complex wave frequencies that lead to instabilities. The stability characteristics are found to be independent of the shear velocity between the frontal zone and ambient fluid and depend only upon the frontal zone interfacial depth at the origin. Comparison is made between Duxbury's analytical model and observational data for Gulf Stream meanders. Disturbance periods generally in the range 3-20 days are predicted which decrease with increasing latitude. The results compare well with recent satellite data for the Gulf Stream.

CHAPTER 1

INTRODUCTION

1.1 OBSERVATIONS OF OCEANIC FRONTS

Oceanic fronts have undoubtedly been observed for centuries by those who sailed the sea. Perhaps they have even been understood on an intuitive level, as, for example, by the Japanese fishermen who regularly exploited their biologically rich waters. However, their scientific study as prominent and important geophysical features is of a far more recent origin. One of the earliest published accounts describing what we recognize today as an oceanic front appeared in William Beebe's book The Arcturus Adventure (1926), in which he developed the metaphor of an invisible wall separating two very different water masses. Steaming in the mid-Pacific just north of the equator, Arcturus encountered the filamentary surface manifestation of Beebe's invisible wall, a region he described as "...a world, not of two, but to all intents and purposes, of a single plane - length." He continued: "From first to last we followed its course along a hundred miles, and yet ten yards on either side of the central line of foam, the water was almost barren of life. The thread-like artery of the currents' juncture seethed with organisms - literally billions of living creatures, clinging to its erratic angles as though magnetized." Beebe's qualitative description included many of the important features characteristic of oceanic fronts, features which have been observed often in subsequent investigations.

Fronts occur at the boundary between two water masses with different physical properties. Thus, they generally exhibit a long, thin geometry. Their presence is frequently revealed at the sea-surface by a foam line (as observed by Beebe), debris accumulation, or an abrupt change in some visible surface property, such as sea state, water color or transparency. Although none of these surface manifestations is necessary for the existence of a front, one or more of them often accompanies an oceanic front, as observed by Beebe and others (Amos, et al., 1972; Cromwell and Reid, 1956; Knauss, 1957; Garvine and Monk, 1974; Stommel, 1976; Zaneveld, et al., 1969).

The near-surface zone associated with an oceanic front is also frequently characterized by considerably enhanced biological activity compared to the surrounding waters. Beebe (1926) considered this discovery one of the most remarkable features of the "current rip" described in his book, and attributed the large number and variety of living organisms to the shelter provided by the debris accumulated along the foam line. There is not necessarily any correlation between biological activity and debris accumulation, however, since fronts have been observed in which the former was present but not the latter (Knauss, 1957). The front studied by Knauss in the eastern equatorial Pacific was, nevertheless, easily observed by eye. The colder water on one side was darker in color with shorter-crested waves than the water on the warm side, where most of the biological activity was concentrated. In this case, the biological activity was apparently promoted by

higher levels of suspended and dissolved nutrients near the surface front than in the surrounding waters.

Observational data also show that fronts tend to be regions of surface convergence, that is, surface water moves toward the front from both sides, subsequently sinking (Garvine and Monk, 1974; Ingram, 1976; Voorhis, 1969; Wooster, 1969). No observation of surface divergence has apparently been made. In addition, fronts are not fixed in space, but frequently wander about the ocean (Garvine and Monk, 1974; Katz, 1969; Wooster, 1969). They occur on a variety of length and time scales, from tens of meters to thousands of kilometers and from hours to years (Beebe, 1926; Garvine and Monk, 1974; Ingram, 1976; Knauss, 1957; Pak and Zaneveld, 1974).

In view of the number of characteristics that may be associated with an oceanic front, Cromwell and Reid (1956) provided the first precise definition of the term in an attempt to introduce a standardized nomenclature and to isolate the essential physical processes. They defined an oceanic front as a band along the sea surface across which abrupt changes in the water density occurred. In their study, they correlated abrupt temperature changes with abrupt density changes, since their measurements were made where appreciable salinity contrast across the front was absent. More recent studies, however, have been made of fronts with nearly uniform density as a result of offsetting temperature and salinity effects (Maul and Hansen, 1972), and of fronts whose density contrast was a consequence, instead, of salinity differences alone (Amos, et al., 1972). It is thus apparent that Cromwell

and Reid's definition should now be broadened to include these other possibilities. The essential notion conveyed by the term "oceanic front" is that the front constitutes a well-defined boundary between two water masses with different physical properties (density, temperature or salinity), across which sharp changes occur with little mixing between the two regions (Katz, 1969). Changes in the physical properties of the water masses are, moreover, often accompanied by sharp gradients in other properties, for example, current velocity, concentration of suspended and dissolved materials, water color, transparency, and surface wave action.

In describing the Arcturus observations, Beebe (1926) referred to the surface expression of the water mass boundary as a "current rip", since he observed a strong velocity shear parallel to the foam line, as have other investigators (Cromwell and Reid, 1956; Zaneveld, et al., 1969). But Cromwell and Reid recognized the similarity between oceanic and atmospheric fronts as boundaries between fluid masses of different density, and therefore adopted the meteorologist's terminology. However, their definition was too limited, since, in addition to allowing only density differences, it considered only the surface expression of the boundary. Instead, the surface separating the two water masses generally slopes down and away from the surface front into the ambient water. In this paper, therefore, the term "front" refers to the entire discontinuity surface that separates two water masses with different properties.

Three observational papers that provide some quantitative insight into typical frontal length and time scales, density, temperature and salinity contrasts, and circulation patterns are Katz (1969), Voorhis (1969) and Knauss (1957). These papers are particularly relevant, since they examine typical large scale upper ocean fronts, and the theoretical work presented here addresses the dynamics of such large scale structures. Katz' investigation involved a front near 30° N, 70° W whose linear extent was at least 200 km oriented approximately northwest-southeast. The entire frontal zone was observed to translate in a west-southwest direction with a maximum average velocity of 15 cm/s. In addition, a definite meander (or "wiggling") of the frontal boundary was observed, giving rise to a roughly sinusoidal surface shape of small amplitude and about 180 km wavelength. Water to the north of the frontal boundary was found to be characteristically 1° C colder than water on the southern side, with a corresponding salinity contrast of approximately $0.1^{\circ}/\text{oo}$. The variation of σ_t across the front was on the order of 0.25. Over a surface range of 20 km, the depth of the boundary between the warm southern water and the colder northern water increased from zero to about 150 m, corresponding to an interfacial slope on the order of 10^{-2} , and thereafter more gradually increased to about 175 m depth. Measurements were made with a depth resolution of approximately 2 m, and on that scale no mixing was observed between the two water masses. The frontal boundary was therefore very sharp and well-defined. Evidence was found for a circulation pattern that included convergence

of the surface waters followed by sinking along the interface between the two water masses. The frontal zone Rossby number was estimated to be 0.1, indicating nearly geostrophic flow. Estimates of surface velocity were then based upon geostrophy. A surface velocity shear of approximately 80 cm/s was computed and found to agree quite favorably with limited direct velocity measurements.

The Sargasso Sea front studied by Voorhis in 1969 exhibited features similar to those described above. The surface expression of the front was tracked over 1000 km extent and was marked by the 21.5°C and 23.5°C isotherms, with the 2°C temperature contrast being confined to a region sometimes less than 1 km in lateral extent. The corresponding salinity and σ_t contrasts were found to be approximately 0.1‰ and 0.4, respectively. A high velocity jet was observed on the warm water side with central currents as high as 80 cm/s. The oppositely directed cold water current, which provided the characteristic frontal zone shear, was much lower at 10 to 30 cm/s. The warm-cold water boundary gradually sloped down from the surface to a depth of 50 m over a horizontal range of 10 km (slope of order 10^{-3}), with the less dense warm water wedge floating on the more dense colder ambient water. A drogue study provided evidence for surface convergence along the frontal interface. In addition, the surface front was marked by the accumulation of Sargassum weed, a further indication of surface convergence. Aircraft infrared studies were performed during a five month period in order to determine frontal zone persistence and motion. A well-defined

front was observed to preserve its identity throughout this period, but with marked changes in its configuration.

The front studied by Knauss in the Pacific was close to the equator ($2^{\circ}46'N$, $120^{\circ}39'W$) corresponding to small values of the Coriolis parameter, unlike the Sargasso Sea fronts. Bathythermograph measurements in the frontal zone, whose surface expression was confined to a band some 100 yards wide, revealed temperature, salinity and σ_t contrasts of about $3^{\circ}C$, $0.08^{\circ}/\text{oo}$ and 1.0, respectively. The front was observed to translate normal to itself at a speed of about 50 cm/s. In addition, surface convergence and a strong velocity shear of nearly 2 m/s were observed.

A very important feature of oceanic fronts, and the one addressed theoretically in this paper, is their tendency to develop wavelike disturbances which propagate along the frontal interface. On fronts marked by some visible surface expression, such as a foam or debris line, these wavelike distortions of the boundary between two water masses are frequently manifested as roughly sinusoidal lateral displacements of the surface foam or debris line (Zaneveld, et al., 1969). Frontal waves have been observed on several large scale upper ocean frontal systems, for example, the Kuroshio Current (Uda, 1964), the California Current (Bernstein, et al., 1977), Sargasso Sea fronts (Katz, 1969), the Norwegian Current (Mysak and Schott, 1977), and the Gulf Stream (Hansen, 1970; Maul, et al., 1978; Stommel, 1976; Webster, 1961). The Gulf Stream Front separates cold Atlantic slope water from

the warmer Sargasso Sea water. The waves, or meanders as they are frequently called, sometimes grow to such an amplitude that vortex rings, or eddies, actually detach from the front.

In his study of Gulf Stream meanders off Onslow Bay, North Carolina, Webster (1961) performed a spectral analysis that revealed dominant periods of 6.9 and 3.9 days, with amplitudes of about 10 km. Periods on the order of 1-2 weeks seem to be characteristic of wave disturbances on the Gulf Stream Front. Hansen (1970) examined wave disturbances on the Gulf Stream east of Cape Hatteras. He found an eastward propagating wave pattern out to about 60°W with typical wavelengths in the range 200-400 km and phase speeds on the order of 5 cm/s. He also observed a generally increasing amplitude with the wave's eastward progression, with initially small disturbances growing to some 200 km amplitude, indicating a possible instability in the system. Recent satellite infrared studies of the Gulf Stream (Maul, et al., 1978) revealed dominant wave periods of 30 and 6 days off Onslow Bay and 45 and 5 days off New England. Wavelengths of 500-900 km have been observed for meanders of the Kuroshio system (Uda, 1964); 300-500 km in the California Current (Bernstein, et al., 1977); 50-125 km in the Norwegian Current (Mysak and Schott, 1977); and approximately 100 km in a typical Sargasso Sea front (Katz, 1969).

Atmospheric frontal systems also support wavelike disturbances which are, in many respects, quite similar to those observed on oceanic fronts. Oceanic and atmospheric fronts are not isomorphic, however.

The latter may be conveniently divided into two categories, lower and upper tropospheric fronts.

Lower tropospheric fronts, the first category, are those where a thin wedge of cold air at the earth's surface is overlain by a warm air mass. These are least similar to upper ocean fronts. For the lower tropospheric front, the important external boundary is the earth's surface. There the no-slip condition must be satisfied with the consequent development of a frictional boundary layer. The horizontal convergence of this layer at the surface front, in turn, produces a vertical component of flow there. In the oceanic case, on the other hand, the relevant external boundary is the ocean's free surface, along which a specified pressure distribution must be maintained. In the absence of wind shear, frictional surface boundary layers will not be present, so that some other physical mechanism is required to explain the observed sinking along oceanic frontal interfaces.

Upper tropospheric fronts in the atmosphere, the jet stream or polar front, for example, are far more similar to upper ocean fronts. Newton (1978) has made a detailed comparison of the Gulf Stream front and the atmospheric jet stream front under the assumption that similarity of structure implies similarity of physical processes. The Gulf Stream and jet stream fronts are geometrically very similar, each having a high velocity filament of fluid ("jet") that floats buoyantly on a relatively deep layer of denser, ambient fluid (the "troposphere").

The fully developed frontal zone in each case has a depth which is typically 10-20% of the total ambient depth, that is, on the order of 1.2 km and 12 km for the Gulf Stream and jet stream, respectively. The frontal zone width is likewise in the ratio 1/10 for the oceanic vs. the atmospheric front, while the interfacial slopes are of the same order (10^{-2}) for each. The velocity fields, however, are considerably different, with the maximum velocity in the jet stream being some 30 times larger than in the Gulf Stream. Typical wavelengths for disturbances on the Gulf Stream are on the order of 200 km, while the corresponding value for the jet stream is on the order of 4000 km, a ratio of 1/20. The same ratio is preserved for the small amplitude phase velocities, which, according to Newton (1978), are typically 0.4 m/s and 8 m/s. The amplitude-to-wavelength ratio in both cases is approximately 1/10. Small amplitude disturbances, which are the subject of this investigation, thus apparently exhibit considerably larger phase velocities than the large amplitude waves into which some of them eventually evolve (only about 5 cm/s for the Gulf Stream from Hansen, 1970).

The limited observations that have been made of oceanic fronts emphasize the variety of phenomena associated with them and the wide range of spatial and temporal scales on which they exist. Their complex structure and dynamical behavior, however, remain largely unexplained by available theory. The work presented in this paper is a theoretical

model of baroclinic instabilities on large-scale upper ocean density fronts. Such instabilities produce the meanders and eddy detachment observed on many oceanic frontal systems. In view of the nature of this work, a brief review of earlier theoretical models for atmospheric and oceanic fronts is presented in the next two sections.

1.2 THEORETICAL STUDIES OF ATMOSPHERIC FRONTS

In a theoretical consideration of oceanic fronts, the similarity to their atmospheric counterparts leads naturally to a review of attempts at understanding the dynamical processes in atmospheric fronts. One of the most complete discussions of the theory of atmospheric fronts was provided by Stoker (1953). He made no attempt to solve the frontal problem, but pursued the more limited objective of rigorously formulating the full nonlinear problem. Starting with the fluid dynamic equations for momentum and continuity, as well as certain simplifying assumptions, Stoker developed a sequence of four hydrodynamic models of decreasing complexity, each, however, being more restrictive than its predecessor. In each of these problems, the flow was taken to be inviscid and incompressible (no thermodynamic processes), the earth's sphericity was ignored (f -plane approximation), and the initial steady state was taken to be geostrophic, that is, a balance between horizontal pressure gradient and Coriolis force. The front was defined as the discontinuity surface separating a thin wedge of cold air adjacent to the earth's surface from an overlying region of warm air of lower

density. Problem I consisted of the momentum and continuity equations subject to the restrictions listed above, in which the velocity and pressure fields were treated as unknowns, along with appropriate boundary and initial conditions as follows: the pressure field and normal velocity were required to be continuous across the front, the no-slip condition was imposed at the earth's surface, and the shape of the discontinuity surface was presumed known initially.

Stoker's Problem II added the assumption of vertical hydrostatic balance, that is, vertical accelerations were considered negligible, as a consequence of which the horizontal velocity field was vertically uniform. In Problem III, two further assumptions were added: fluid elements initially on the discontinuity surface remained there for all time, and the motion of the warm air region was completely unaffected by the motion of the cold air region. This latter assumption is equivalent to requiring that the cold air (lower) layer is vanishingly thin compared to the upper layer. In Problem IV, Stoker introduced the displacement distance of the front normal to its stationary position as an additional dependent variable and assumed that the horizontal velocity perpendicular to the initial front vanished far from the front. However, even Problem IV could not be solved analytically and presented difficulties that made numerical solution impractical at that time. In a companion paper to Stoker's, Whitham (1953) provided a heuristic development of an essentially graphical solution to Problem IV using the method of characteristics which exhibited the

nonlinear nature of wave propagation along frontal surfaces and also demonstrated the tendency towards occlusion and, ultimately, cyclogenesis. Unfortunately, Problem IV was burdened by so many restrictions that it constituted a rather poor model of atmospheric frontal zones, and, as a consequence, it was of limited utility.

Stoker's frontal models led to mathematical problems that could not be solved analytically. At the time his work was completed, even numerical solutions could not be implemented, since adequate computers were not available. Recognizing the futility of attempting a solution for even the simplest of his frontal models, Stoker went no further. The problem of nonlinear frontal dynamics lay dormant for more than ten years, when, with the advent of sufficiently large, high-speed computers, Kasahara, et al., (1965) provided the first numerical solution. Kasahara built directly upon Stoker's previous modelling efforts, and solved Problem III described above using a finite difference numerical method. His results showed clearly that initially sinusoidal frontal disturbances propagate from west to east and have a tendency towards occlusion and, eventually, cyclogenesis.

Another numerical study of essentially the same nonlinear problem was performed by Grammelvedt (1970). His results also clearly demonstrated the tendency for frontal disturbances to develop the characteristic asymmetry that ultimately leads to occlusion. To obtain numerical solutions, however, he found it necessary to introduce an artificial dissipative mechanism in order to maintain stability in the

numerical integration. It appears, in fact, that some physical dissipative mechanism, turbulent friction, for example, is an essential ingredient in any realistic frontal model. The instabilities encountered in performing a numerical integration of the nonlinear dynamical equations are apparently not simply numerical instabilities associated with a particular integration algorithm, but rather important consequences of the inviscid dynamics assumed.

Even though no known method of exact solution exists for the complicated system of equations that describes frontal motion, certain theoretical results are nonetheless available using the approximations of classical stability and small perturbation analysis. The numerical models that demonstrated frontal wave instability provided impetus for renewed analysis, since even approximate solutions to the dynamical equations can provide considerably more insight into the physical processes at work than numerical results. Since wavelike disturbances of the frontal zone are observed, it is reasonable to assume a priori that there exist wavelike solutions to the dynamical equations; in particular, solutions which contain an explicit time-harmonic dependence and which permit complex-valued circular frequencies. This is the approach adopted in classical stability analysis. Solutions exhibiting purely real circular frequencies are bounded for all time and therefore termed stable. Solutions whose frequency contains a nonzero imaginary part, however, correspond to a time-dependent amplitude that either decays or grows exponentially, depending upon the sign of the imaginary part. Waves of the first type are termed evanescent, while those of the second type are termed unstable.

The simplification afforded by assuming wavelike solutions, however, is not alone sufficient to render the dynamical equations tractable, since they remain inherently nonlinear. Linearization of the fundamental equations is accomplished by using classical small perturbation theory, in which it is assumed that wave disturbances to the system constitute small departures from a known, time invariant equilibrium state. Each dependent variable in the problem is thus decomposed into the sum of an equilibrium state component and a harmonic perturbation component whose amplitude is small by comparison. This scheme results in a linear system of equations for the perturbation variables which may then be solved using standard analytical techniques. The principal objective of this synthesis of stability and perturbation analysis is the derivation of a dispersion relation, that is, a function which relates the disturbance wavelength to the frequency. This relation then can be used to identify unstable modes in the system.

Using such a combined stability/perturbation approach, Orlanski (1968) examined the propagation of atmospheric frontal waves and achieved some measure of success. The system he modelled was essentially the same as that used by Kasahara and Stoker, although he considered the coupling of the dynamics in each of the two frontal regions to first order in a small parameter, which was not a feature of the Kasahara/Stoker model. Orlanski's efforts were subsequently extended by Kasahara and Rao (1972), who employed the same frontal model and stability/perturbation treatment in order to extend the analysis to regions of the

problem's parameter space that had not been previously considered. Their results were very similar to Orlanski's. However, like his, theirs did not include any dissipative effects, even though Grammelvedt's numerical work provided indirect evidence of the importance of dissipative mechanisms in modelling frontal dynamics.

1.3 THEORETICAL STUDIES OF OCEANIC FRONTS

Garvine (1974) published a model of quasisteady, small scale oceanic frontal dynamics in which frictional dissipation and mass entrainment figured prominently. His model showed clearly that a steady state frontal structure can exist only if friction and/or mass entrainment are present to balance the net horizontal pressure gradient. Otherwise, the sloping interface between two different water masses cannot be maintained. In contrast, the models of large scale atmospheric fronts described in Section 1.2 are all inviscid and invoke a basic balance between horizontal pressure gradient and Coriolis force. Only in large scale oceanic fronts where Coriolis effects will be significant can dissipative effects be expected to play a lesser role.

Garvine (1979a, 1979b) has expanded his small scale model, in which Coriolis effects were neglected, to include quasisteady large scale oceanic fronts whose dynamics involve friction, mass entrainment, wind stress and Coriolis force. In view of the inherently turbulent nature of geophysical flows and the attendant analytical difficulties in treating the turbulence structure in detail, Garvine parameterized

the effects of friction and mass entrainment by introducing friction and entrainment coefficients whose values reflected the bulk influence of these effects. He also wrote the momentum and continuity equations in vertically integrated form. His model showed that the steady state frontal zone is characterized by two length scales, the baroclinic Rossby radius of deformation and a turbulent transport length scale. Their ratio he called the "rotation parameter", which was the major parameter characterizing the frontal zone structure. For nearly non-rotating systems in which Coriolis effects are small, the frontal zone scale is the turbulent transport scale, and the frontal zone is dissipative throughout its domain. This limit corresponds to Garvine's 1974 model which considered only nonrotating systems. Small scale frontal structures, such as a river plume front (Garvine and Monk, 1974), exhibit small values of the rotation parameter.

In contrast, large scale fronts, such as the Gulf Stream, are strongly affected by earth rotation, but only weakly by dissipation. Their corresponding values of the rotation parameter are large, and the scale of the front is the Rossby radius. The weak dissipative processes of friction and entrainment are active only in an inner zone bordering the surface front where the gradient Richardson number falls below a value of order one due to the large vertical shear there. Typically, the lateral extent of this region is 10-20% of the Rossby radius. Hence, in this zone, inviscid dynamics are not valid. Beyond this zone, the flow is nearly inviscid; but even here the motion is

indirectly affected by the dissipative effects of the inner zone. Any vertical mass entrainment across the frontal interface occurring in the inner zone must be balanced by horizontal, cross-stream mass flux above the interface; i.e., flow toward or away from the surface front. This mass flux, in turn, must be continuous across the boundary between the inner region and the outer inviscid one. Hence, the inviscid region responds indirectly to inner zone mass entrainment. If the entrainment there is downward, mass is lost to the ambient water below, and the inviscid outer zone must supply balancing cross-stream mass flux (flow toward the surface front). The opposite occurs for upward mass entrainment.

In this paper, we will consider only upper ocean density fronts with large values of the rotation parameter, so that dissipative effects are subordinated to earth rotation effects. Typical of the large-scale oceanic fronts to which this model applies are the Gulf Stream Front and the Sargasso Sea fronts, for which Garvine (1979b) estimates rotation parameter values of 9 and 4, respectively. For the Gulf Stream, the baroclinic Rossby radius is on the order of 100 km, so that dissipation is confined to a zone approximately 10-20 km wide. It will be seen below that there does exist a third length scale in the frontal problem which is imbedded in the dissipative zone. On this scale, which is an advective scale length, the cross-flow Rossby number becomes order one.

The work presented in this paper is an analytical study of the stability characteristics of large-scale upper ocean density fronts. The model is developed by assuming wavelike disturbances to the system,

which are then treated as small amplitude perturbations to a stationary equilibrium flow. As outlined in Section 1.2, the perturbation variable decomposition is a standard technique in the atmospheric literature, and also in prior modelling efforts on time-dependent, inviscid oceanic fronts (Duxbury, 1963; Mysak and Schott, 1977; Orlandi, 1969; Stommel, 1953; Stommel, 1976). Time-dependent numerical models have also been developed of both small scale fronts (Kao, et al., 1977) and large scale fronts (Kao, et al., 1978), but not with the objective of studying wave disturbances on established frontal structures. Both of these papers instead address the problem of frontogenesis with the ultimate development of a steady state frontal structure.

The present model first extends Duxbury's (1963) treatment of an inviscid density front with a planar discontinuity surface. It is significantly different, however, in that it subsequently examines an exponential discontinuity surface. This form was suggested by Stommel (1976) for the Gulf Stream front. The model also includes the important effect of a cross-stream velocity component (flow perpendicular to the surface front) in the equilibrium flow. Duxbury's system included a constant velocity shear across the boundary between the frontal zone and the ambient ocean, but had no cross-stream velocity. It was found to be dynamically stable for all values of frequency and wave number. Orlandi's (1969) work showed that systems in which the dynamics of the lower layer are neglected in a two-layer frontal model are inherently stable. However, he too did not admit any equilibrium cross-stream

flow. In this paper, we see that, even neglecting the dynamics of the lower layer, a frontal system subject to harmonic wave disturbances may be unstable if a nonzero cross-stream velocity is present in the equilibrium state. The source of this cross-stream velocity, in turn, is mass entrainment in the inner dissipative region.

CHAPTER 2

THE EQUILIBRIUM STATE AND PERTURBATION EXPANSION

2.1 INTRODUCTION

As discussed in Chapter 1, the term "oceanic front" in this paper refers to the discontinuity surface that separates two water masses of different density. The "frontal zone" is a wedge shaped body of fluid that floats on an ambient ocean of slightly greater density, as illustrated in Figure 2.1. Its thickness is small compared to the total depth, and, as a result, the ambient horizontal pressure gradient field is unaltered by the presence of the frontal zone. The dynamical behavior of the frontal zone and that of the underlying ambient fluid are therefore uncoupled, which is equivalent to assuming that the ambient fluid is effectively infinitely deep. Recall that this restriction was also implicit in Stoker's (1953) model of a lower tropospheric front in the atmosphere. The frontal zone is free to move about and propagates into the ambient fluid with a velocity $\vec{Q}_f = (U_f, V_f, 0)$ relative to an earthfixed Cartesian coordinate system labeled x' , y' and z' in Figure 2.1. The location of the coordinate system origin is arbitrary, and the z' axis coincides with the local vertical. The y' axis is parallel to the surface front, with the x' axis being perpendicular to it into the frontal zone.

In nature, oceanic frontal zones, the Gulf Stream front, for example, are long and thin with a characteristic velocity shear across

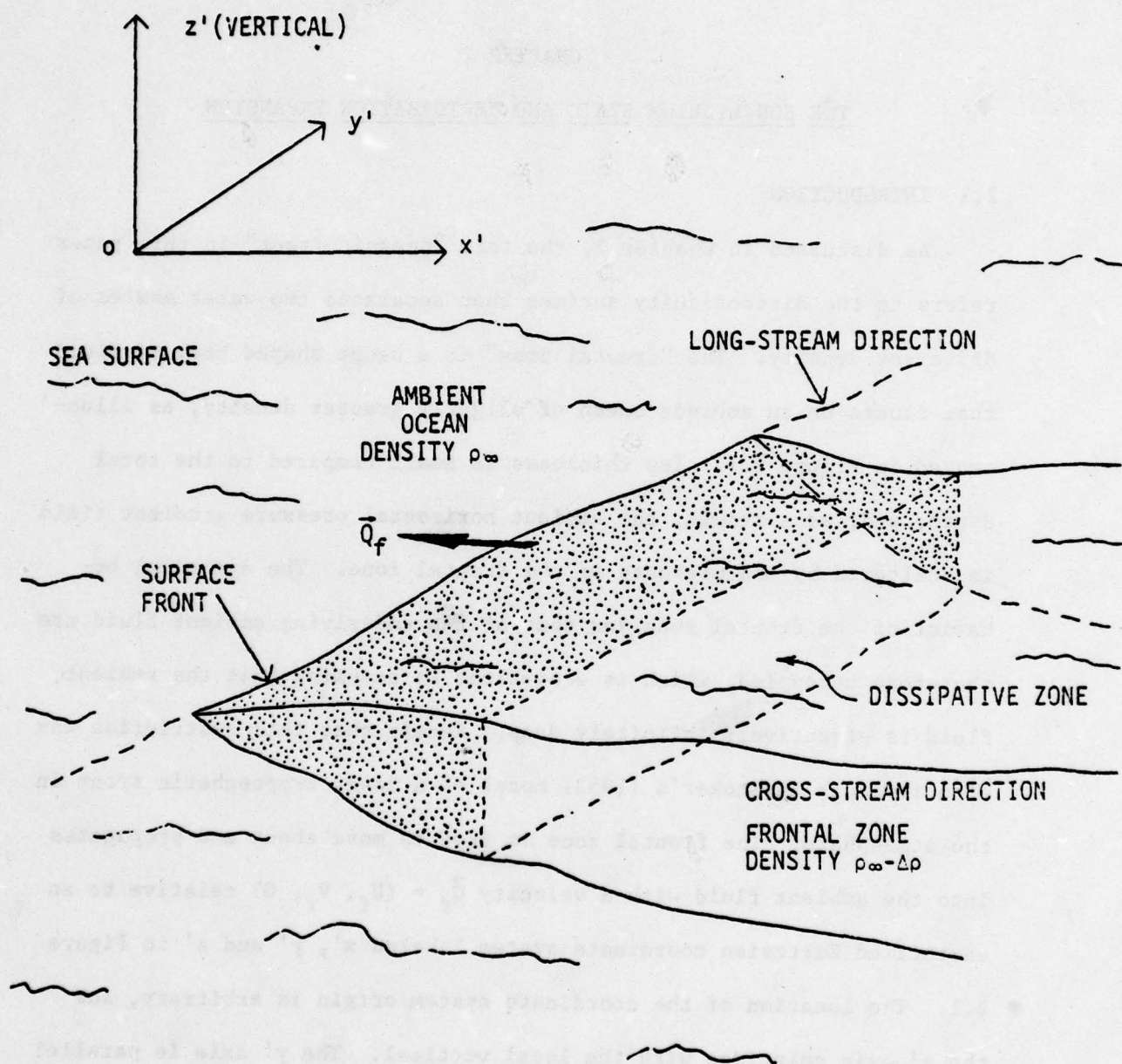


FIGURE 2.1
 GEOMETRY OF THE FRONT

CHAPTER 2

THE EQUILIBRIUM STATE AND PERTURBATION EXPANSION

2.1 INTRODUCTION

As discussed in Chapter 1, the term "oceanic front" in this paper refers to the discontinuity surface that separates two water masses of different density. The "frontal zone" is a wedge shaped body of fluid that floats on an ambient ocean of slightly greater density, as illustrated in Figure 2.1. Its thickness is small compared to the total depth, and, as a result, the ambient horizontal pressure gradient field is unaltered by the presence of the frontal zone. The dynamical behavior of the frontal zone and that of the underlying ambient fluid are therefore uncoupled, which is equivalent to assuming that the ambient fluid is effectively infinitely deep. Recall that this restriction was also implicit in Stoker's (1953) model of a lower tropospheric front in the atmosphere. The frontal zone is free to move about and propagates into the ambient fluid with a velocity $\vec{Q}_f = (U_f, V_f, 0)$ relative to an earthfixed Cartesian coordinate system labeled x' , y' and z' in Figure 2.1. The location of the coordinate system origin is arbitrary, and the z' axis coincides with the local vertical. The y' axis is parallel to the surface front, with the x' axis being perpendicular to it into the frontal zone.

In nature, oceanic frontal zones, the Gulf Stream front, for example, are long and thin with a characteristic velocity shear across

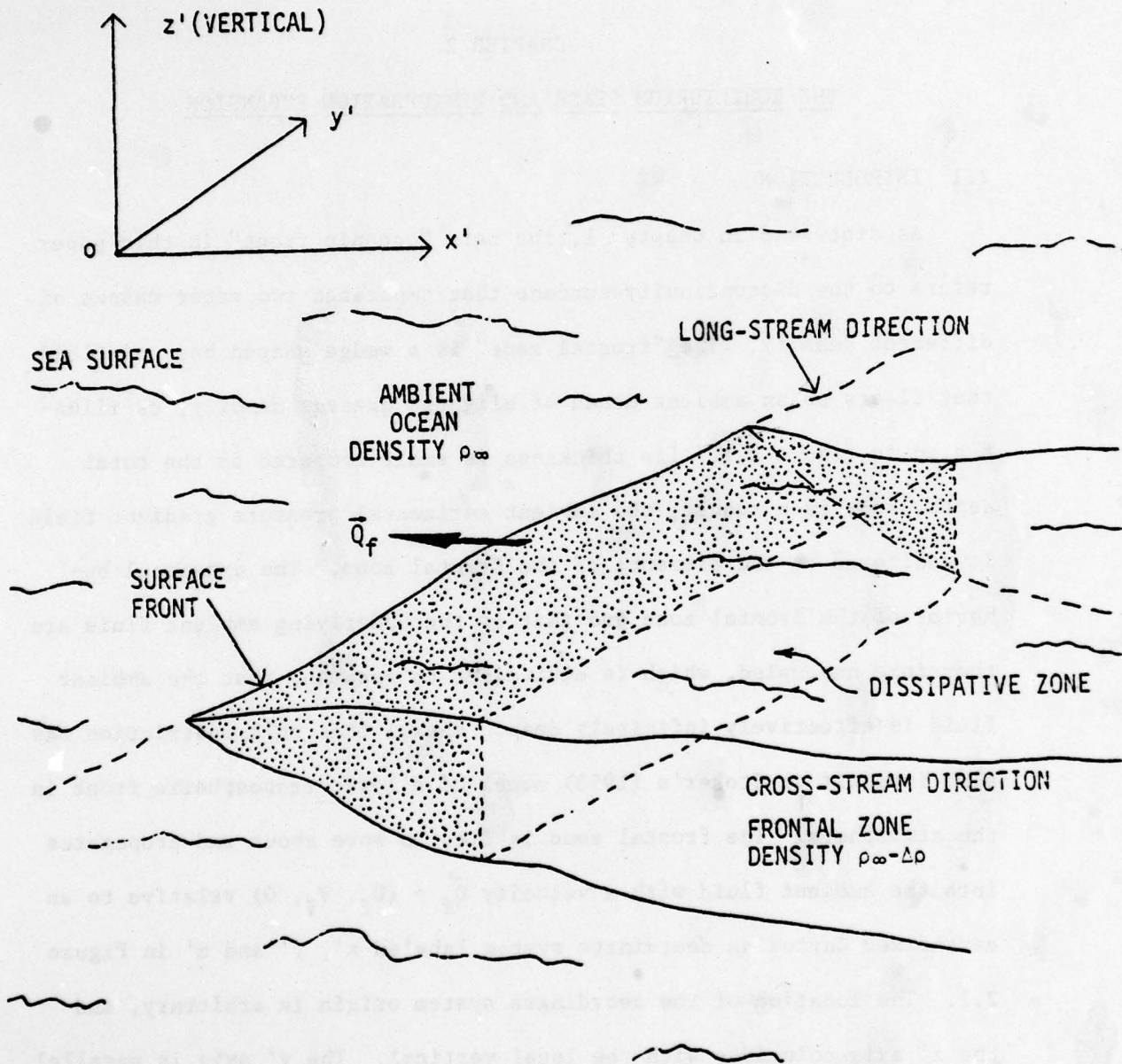


FIGURE 2.1
GEOMETRY OF THE FRONT

the front in the direction of its maximum extent. These features motivate the "long-stream" and "cross-stream" terminology introduced in the figure. The long-stream direction coincides with the direction of maximum extent of the filamentary frontal zone, while the cross-stream direction is perpendicular to it and taken positive toward the less dense fluid. The frontal zone's long-stream length scale is typically an order of magnitude or more larger than its cross-stream length scale. The velocity field in the frontal zone exhibits similar behavior, with the long-stream component being much larger than the cross-stream component, but not necessarily in the same ratio as the length scales. The spatial rate of change of the velocity and pressure fields, however, behaves in the opposite manner, with derivatives in the long-stream direction being generally much smaller than derivatives in the cross-stream direction.

The discontinuity surface which defines an oceanic front thus divides the fluid into two quite distinct regions, the (uncoupled) dynamics of which are taken to be inviscid in this model, except for the innermost portion of the upper layer. The model assumes that the fluid is incompressible, and ignores surface wind stress as a driving force. We will later introduce wavelike disturbances of the frontal zone, such as would be initiated by some driving agent (such as surface wind stress) which is no longer active. In typical upper ocean frontal zones, the lateral extent is sufficiently small compared to the planetary scale that Coriolis acceleration is adequately approximated on the f -plane, which is the assumption made here. In addition, the vertical

dynamical balance is assumed to be everywhere hydrostatic, in view of which the horizontal velocity field is vertically uniform. The horizontal dynamical balance in the ambient fluid is taken to be geostrophic, that is, a balance between Coriolis force and horizontal pressure gradient, and, moreover, is unaltered by the presence of the frontal zone.

The model is hydrodynamic in nature, not thermodynamic, since the fluid densities, ρ_∞ and $\rho_\infty - \Delta\rho$ in the ambient fluid and in the frontal zone, respectively, are specified a priori. Both ρ_∞ and $\Delta\rho$ are positive constants with $\frac{\Delta\rho}{\rho_\infty} \ll 1$. Specification of the density field in this manner leaves only the velocity and pressure fields as unknown quantities, thereby eliminating the need for an energy equation that couples the density field and frontal zone dynamics.

The model is restricted to upper ocean density fronts which, in Garvine's (1979a, 1979b) model, are characterized by large values of the rotation parameter. The frontal zone dynamics are therefore rotationally dominated, and the zone's cross-stream length scale is the baroclinic Rossby radius of deformation λ . Even though dissipative processes are unimportant over most of the scale λ , a narrow dissipative region, whose lateral extent is approximately $0.1\lambda - 0.2\lambda$, exists near the surface front as shown in Figure 2.1. Garvine (1979a) has developed the quasi-steady dynamics for this case.

In the present work, wavelike disturbances of the frontal zone, including those leading to instability, will be investigated in detail

the front in the direction of its maximum extent. These features motivate the "long-stream" and "cross-stream" terminology introduced in the figure. The long-stream direction coincides with the direction of maximum extent of the filamentary frontal zone, while the cross-stream direction is perpendicular to it and taken positive toward the less dense fluid. The frontal zone's long-stream length scale is typically an order of magnitude or more larger than its cross-stream length scale. The velocity field in the frontal zone exhibits similar behavior, with the long-stream component being much larger than the cross-stream component, but not necessarily in the same ratio as the length scales. The spatial rate of change of the velocity and pressure fields, however, behaves in the opposite manner, with derivatives in the long-stream direction being generally much smaller than derivatives in the cross-stream direction.

The discontinuity surface which defines an oceanic front thus divides the fluid into two quite distinct regions, the (uncoupled) dynamics of which are taken to be inviscid in this model, except for the innermost portion of the upper layer. The model assumes that the fluid is incompressible, and ignores surface wind stress as a driving force. We will later introduce wavelike disturbances of the frontal zone, such as would be initiated by some driving agent (such as surface wind stress) which is no longer active. In typical upper ocean frontal zones, the lateral extent is sufficiently small compared to the planetary scale that Coriolis acceleration is adequately approximated on the f -plane, which is the assumption made here. In addition, the vertical

dynamical balance is assumed to be everywhere hydrostatic, in view of which the horizontal velocity field is vertically uniform. The horizontal dynamical balance in the ambient fluid is taken to be geostrophic, that is, a balance between Coriolis force and horizontal pressure gradient, and, moreover, is unaltered by the presence of the frontal zone.

The model is hydrodynamic in nature, not thermodynamic, since the fluid densities, ρ_∞ and $\rho_\infty - \Delta\rho$ in the ambient fluid and in the frontal zone, respectively, are specified a priori. Both ρ_∞ and $\Delta\rho$ are positive constants with $\frac{\Delta\rho}{\rho_\infty} \ll 1$. Specification of the density field in this manner leaves only the velocity and pressure fields as unknown quantities, thereby eliminating the need for an energy equation that couples the density field and frontal zone dynamics.

The model is restricted to upper ocean density fronts which, in Garvine's (1979a, 1979b) model, are characterized by large values of the rotation parameter. The frontal zone dynamics are therefore rotationally dominated, and the zone's cross-stream length scale is the baroclinic Rossby radius of deformation λ . Even though dissipative processes are unimportant over most of the scale λ , a narrow dissipative region, whose lateral extent is approximately 0.1λ - 0.2λ , exists near the surface front as shown in Figure 2.1. Garvine (1979a) has developed the quasi-steady dynamics for this case.

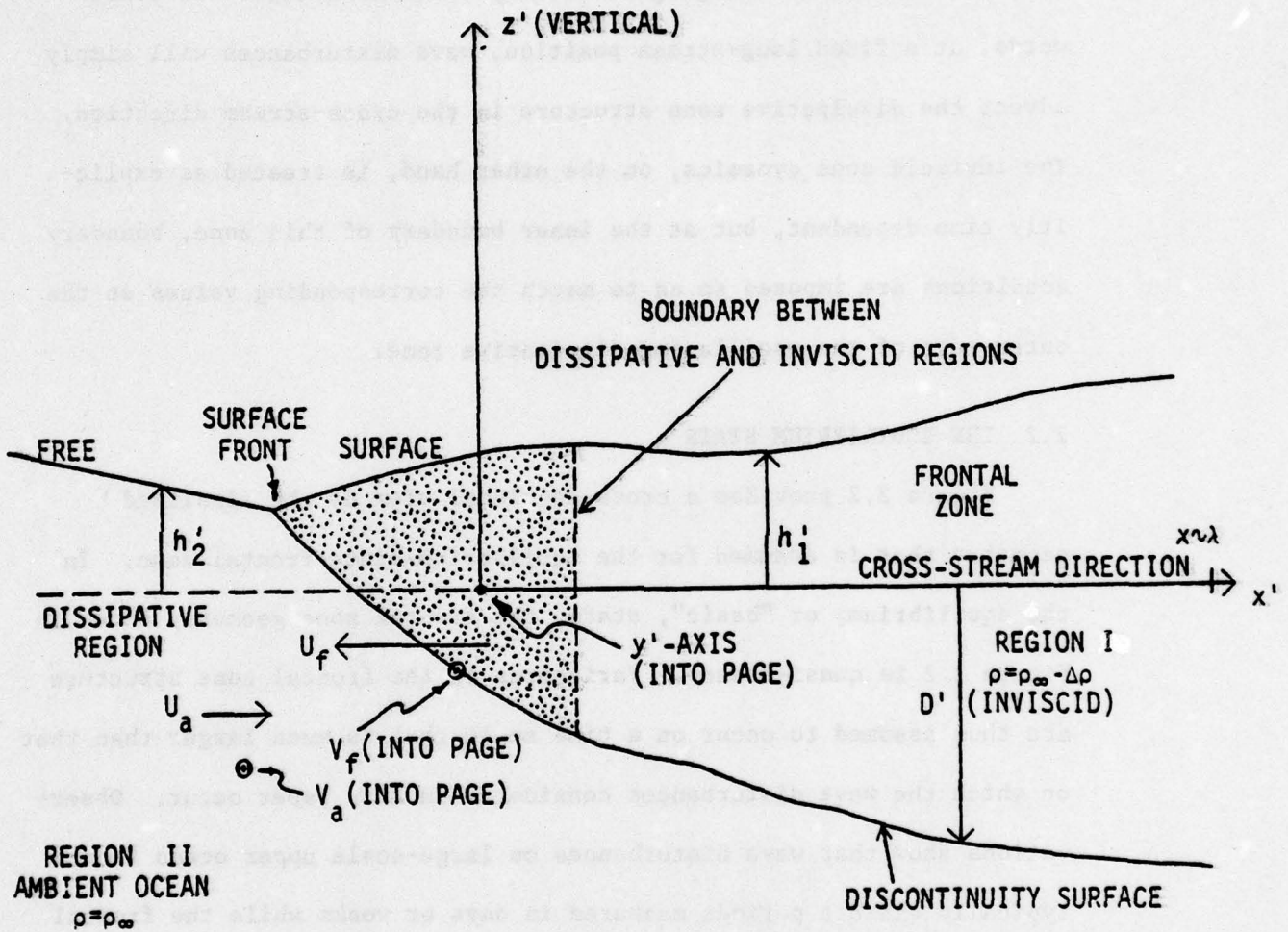
In the present work, wavelike disturbances of the frontal zone, including those leading to instability, will be investigated in detail

for the outer inviscid scale. The model will assume that, as the wave disturbances develop horizontal distortions of the surface front and adjacent dissipative region, the response there is simply to displace this region without changing its steady state structure. In other words, at a fixed long-stream position, wave disturbances will simply advect the dissipative zone structure in the cross-stream direction. The inviscid zone dynamics, on the other hand, is treated as explicitly time dependent, but at the inner boundary of this zone, boundary conditions are imposed so as to match the corresponding values at the outer edge of the oscillating dissipative zone.

2.2 THE EQUILIBRIUM STATE

Figure 2.2 provides a cross-sectional view of the idealized geometry that is assumed for the equilibrium-state frontal zone. In the equilibrium, or "basic", state, the frontal zone geometry shown in Figure 2.2 is quasi-steady. Variations in the frontal zone structure are thus assumed to occur on a time scale that is much larger than that on which the wave disturbances considered in this paper occur. Observations show that wave disturbances on large-scale upper ocean fronts typically exhibit periods measured in days or weeks while the frontal zone itself persists in a stable configuration for a much longer interval, typically months or years. The quasi-steady assumption is therefore consistent with the observed characteristics of large-scale frontal zones.

The dissipative region, whose cross-stream extent is some small fraction of the baroclinic Rossby radius, λ , lies between the surface front and the outer inviscid region. The ambient ocean is labeled Region II, while the frontal zone is labeled Region I. An earth-fixed



CROSS-SECTIONAL VIEW OF THE IDEALIZED FRONTAL-ZONE GEOMETRY IN EARTH-FIXED COORDINATES

FIGURE 2.2

(primed) right-handed Cartesian coordinate system is established in which the spatial axes are labeled x' , y' and z' , with t' designating the time. The z' axis is taken to be along the local vertical, and the y' axis is oriented parallel to the surface front. The boundary between the dissipative and inviscid domains in the frontal zone is therefore parallel to the plane $x' = 0$. The sea surface elevation above the reference plane $z' = 0$ is designated h_1' and h_2' in Regions I and II, respectively, while the depth of the discontinuity surface in Region I, that is, the "interfacial depth", is denoted D' . The fluid densities in Regions I and II are $\rho_\infty - \Delta\rho$ and ρ_∞ , respectively. Note that the dissipative region is part of the frontal zone and contains fluid of density $\rho_\infty - \Delta\rho$. Note also that the x' velocity at the boundary between the dissipative and inviscid domains in the frontal zone will not, in general, be zero, which reflects mass entrainment through the discontinuity surface in the dissipative region.

Under the assumptions made in Section 2.1, the general time-varying x' , y' and z' momentum equations, and the continuity equation for the outer, inviscid region in the primed coordinates are, respectively:

$$\begin{aligned} \partial u' / \partial t' + u' (\partial u' / \partial x') + v' (\partial u' / \partial y') + w' (\partial u' / \partial z') - f v' \\ = -(\partial p' / \partial x') / \rho \end{aligned} \quad (2.1a)$$

$$\begin{aligned} \partial v' / \partial t' + u' (\partial v' / \partial x') + v' (\partial v' / \partial y') + w' (\partial v' / \partial z') + f u' \\ = -(\partial p' / \partial y') / \rho \end{aligned} \quad (2.1b)$$

$$0 = \rho g + (\partial p' / \partial z') \quad (2.1c)$$

$$\partial u' / \partial x' + \partial v' / \partial y' + \partial w' / \partial z' = 0 \quad (2.1d)$$

In (2.1), u' , v' and w' are the x' , y' and z' velocities, respectively, p' the pressure, ρ the density, g the gravitational acceleration, and f the Coriolis parameter. All variables are dimensional.

(2.1) constitutes a system of four coupled nonlinear partial differential equations (PDE's) for the four dependent variables u' , v' , w' and p' , each of which is a function of position and time (x' , y' , z' , t').

The horizontal velocity field in the ambient ocean is assumed to be invariant in space and time, and is denoted $\vec{Q}_a = (U_a, V_a, 0)$, where U_a and V_a are the ambient x' and y' velocity components as shown in Figure 2.2. Horizontal pressure gradients in the ambient fluid are induced by the sloping free surface in Region II, whose elevation above the plane $z' = 0$ is related to U_a and V_a by

$$fV_a = g\partial h_2'/\partial x' \quad (2.2a)$$

$$-fU_a = g\partial h_2'/\partial y' \quad (2.2b)$$

as a consequence of the assumed geostrophic balance. The ambient sea surface height is therefore a time-invariant plane in the primed coordinate system whose uniform slope in the x' and y' directions drives a uniform geostrophic flow in the orthogonal coordinate direction.

The thin wedge of lighter fluid that constitutes the frontal zone propagates into the ambient fluid with a constant velocity in the primed system, U_f in the x' direction and V_f in the y' direction as shown in Figure 2.2. The free surface elevation in Region I, the frontal zone, is therefore time-dependent in earth-fixed coordinates, $h_1' = h_1'(x', y', t')$, as is the interfacial depth $D' = D'(x', y', t')$. The explicit time dependence in h_1' and D' is analytically cumbersome, and

it is conveniently removed from the equilibrium state by transforming into a new Cartesian coordinate system whose origin translates relative to the earth at the frontal zone velocity $\vec{Q}_f = (U_f, V_f, 0)$. In the new coordinate system, the same symbols are retained for the dependent and independent variables, but without the prime. The transformation is defined by

$$\begin{aligned}
 x &= x' - U_f t \\
 y &= y' - V_f t \\
 z &= z' \\
 t &= t' \\
 u &= u' - U_f \\
 v &= v' - V_f \\
 w &= w'
 \end{aligned}
 \tag{2.3}$$

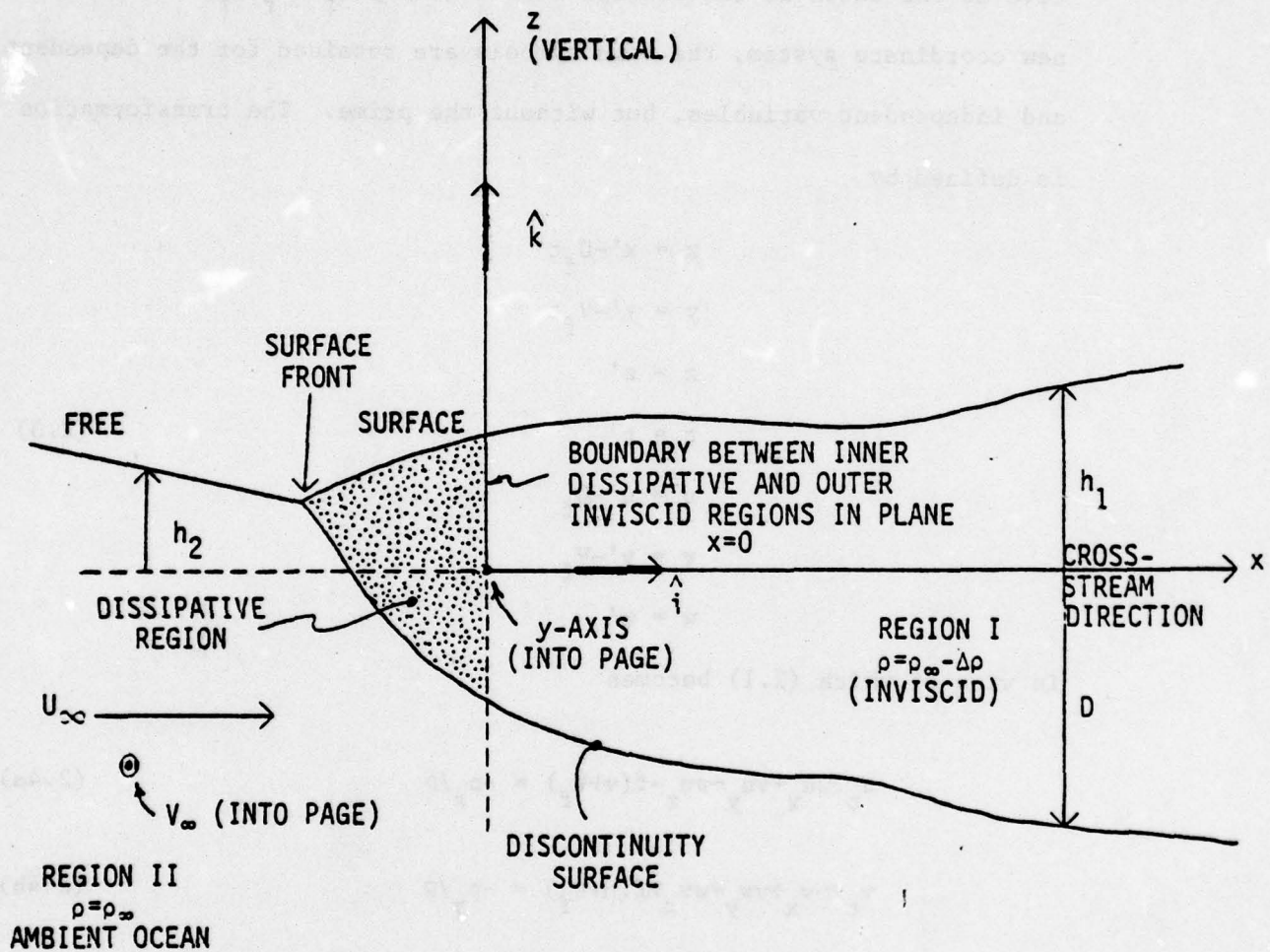
in view of which (2.1) becomes

$$u \frac{\partial u}{\partial t} + u \frac{\partial u}{\partial x} + v \frac{\partial u}{\partial y} + w \frac{\partial u}{\partial z} - f(v + V_f) = -p_x / \rho
 \tag{2.4a}$$

$$v \frac{\partial v}{\partial t} + u \frac{\partial v}{\partial x} + v \frac{\partial v}{\partial y} + w \frac{\partial v}{\partial z} + f(u + U_f) = -p_y / \rho
 \tag{2.4b}$$

$$0 = g + p_z / \rho
 \tag{2.4c}$$

$$u \frac{\partial v}{\partial x} + v \frac{\partial w}{\partial y} + w \frac{\partial z}{\partial z} = 0
 \tag{2.4d}$$



CROSS-SECTIONAL VIEW IN A PLANE
PARALLEL TO $y=0$

GEOMETRY OF THE EQUILIBRIUM
FRONTAL ZONE IN TRANSLATING
COORDINATES

FIGURE 2.3

(2.4) has been simplified notationally by marking partial derivatives with a subscript following accepted convention. This notation is used hereafter whenever possible, with the significance of subscripted variables that are not derivatives being clear from context. Figure 2.3 provides a cross-sectional view of the frontal zone geometry in the translating coordinate system. As before, the sea surface elevations in Regions I and II are denoted h_1 and h_2 , respectively, while D denotes the interfacial depth. The free surface height h_2 is now explicitly time-dependent, as was h_1' previously; but h_1 and D in the equilibrium state are not. It will be seen in what follows, however, that only the uniform, constant velocity in the ambient ocean enters the equilibrium state equations for the frontal zone velocity field and interfacial depth, so that the time dependence in $h_2(x,y,t)$ is of no consequence. The ambient fluid velocity in the translating coordinate system is labeled u_∞ along the x -axis and v_∞ along the y -axis, where u_∞ and v_∞ are constants related to the earth-fixed ambient and frontal zone velocities by

$$u_\infty = U_a - U_f \quad (2.5a)$$

$$v_\infty = V_a - V_f \quad (2.5b)$$

The density field for $x \geq 0$ is specified as

$$\rho = \rho_\infty, \quad z < -D \quad (2.6)$$

$$\rho = \rho_\infty - \Delta\rho, \quad -D \leq z \leq h_1,$$

where $\Delta\rho > 0$, $D > 0$ and $(\Delta\rho/\rho_\infty) \ll 1$.

The pressure field is calculated by integrating the hydrostatic equation, (2.4c), using (2.6), with the result

$$p = g(\rho_\infty - \Delta\rho)(h_1 - z) \quad , \quad -D \leq z \leq h_1 \quad (2.7a)$$

$$p = g(\rho_\infty - \Delta\rho)h_1 - g(\rho_\infty z + \Delta\rho D) \quad , \quad z \leq -D \quad (2.7b)$$

Neglecting terms of order $(\Delta\rho/\rho_\infty)$ compared to unity, the horizontal pressure gradients in the half space $x \geq 0$ are computed from (2.7) as

$$\nabla_h p/\rho = g \nabla_h h_1 \quad -D \leq z \leq h_1 \quad (2.8a)$$

$$\nabla_h p/\rho = g \nabla_h (h_1 - \Delta\rho D/\rho_\infty) \quad z \leq -D \quad , \quad (2.8b)$$

where $\nabla_h = (\partial/\partial x)\hat{i} + (\partial/\partial y)\hat{j}$ is the horizontal gradient operator. Note that the horizontal gradients of the pressure field are discontinuous across the frontal interface marked by $z = -D$, whereas the pressure field is continuous, as it must be.

Below the frontal interface in Region I, the fluid is assumed to be in isostatic balance, that is, the ambient horizontal pressure gradient field is unchanged by the presence of the frontal zone above. This restriction is equivalent to assuming that the ambient fluid is infinitely deep, and, therefore, that its (geostrophic) dynamics are unaltered as the frontal zone propagates into the ambient fluid. The velocity and pressure gradient fields in the ambient fluid are then related by

$$\nabla_h p/\rho = f\{(\mathbf{v}_\infty + \mathbf{V}_f)\hat{i} - (\mathbf{u}_\infty + \mathbf{U}_f)\hat{j}\} \quad . \quad (2.9)$$

(2.9) follows from (2.4a) and (2.4b) and is analogous to (2.2) in earth-fixed coordinates in which the pressure gradients have been written in terms of the free surface slope.

In view of (2.8), the horizontal gradients of the sea surface elevation and interfacial depth, and the velocity field are related as follows:

$$\nabla_h (h_1 - \Delta\rho D / \rho_\infty) = (f/g) \{ (v_\infty + V_f) \hat{i} - (u_\infty + U_f) \hat{j} \} \quad (2.10)$$

Integrating (2.10) subject to the boundary conditions $h_1(0,0)=0$ and $D(0,0)=D_f(0)$, where $D_f(0)$ is some known constant, yields the following relationship between h_1 and D :

$$h_1(x,y) = (\Delta\rho/\rho_\infty) \{ D(x,y) - D_f(0) \} + (f/g) \{ (v_\infty + V_f)x - (u_\infty + U_f)y \} \quad (2.11)$$

In the inviscid zone, mass entrainment is not permitted through the discontinuity surface. However, entrainment through the discontinuity surface is allowed in the dissipative zone shown in Figure 2.3, which produces a nonzero cross-stream volume flux in the plane $x=0$. This, in turn, leads to a velocity boundary condition at $x=0$, since we demand that the cross-stream velocity component be continuous across the boundary between the inner dissipative region and the outer inviscid region.

The requirement that fluid elements initially on the inviscid zone discontinuity surface remain there for all time may be stated rigorously as

$$\lim_{z \rightarrow h_1} \frac{D}{Dt} (h_1 - z) = 0 \quad (2.12a)$$

$$\lim_{z \rightarrow D} \frac{D}{Dt} (D + z) = 0 \quad (2.12b)$$

where $D/Dt = \partial/\partial t + u(\partial/\partial x) + v(\partial/\partial y) + w(\partial/\partial z)$ is the convective derivative.

Denoting the frontal zone vertical

2.3 PERTURBATION ANALYSIS

In this section, the general nonlinear time dependent frontal zone momentum and continuity equations will be linearized by assuming a perturbation expansion for each of the dependent variables u , v , and D . Such a linearization scheme is applicable only if the perturbation amplitude is small compared to the time invariant equilibrium state value of a given variable, and this restriction is implicit in all of what follows. For large deviations from the equilibrium state, the frontal zone dynamics are essentially nonlinear and must be treated accordingly. The purpose of this paper, however, is to address the question of stability of the frontal zone flow, and instabilities that grow to large amplitude in time must be small initially. Large amplitude frontal disturbances are therefore not within the purview of this analysis, but the conditions under which they develop are.

In analogy to (2.16), the general time varying momentum and continuity equations are

$$u_t + uu_x + vu_y - fv = -g'D_x - fv_\infty \quad (2.17a)$$

$$v_t + uv_x + vv_y + fu = -g'D_y + fu_\infty \quad (2.17b)$$

$$u_x + v_y + w_z = 0, \quad (2.17c)$$

in which u , v and D are functions of (x, y, t) and $w = w(x, y, z, t)$. g' is the "reduced gravity" defined as $g' \equiv g \left(\frac{\Delta\rho}{\rho_\infty} \right)$. (2.17) makes no assumption about the frontal zone geometry. As before, all variables are dimensional. In (2.17a) and (2.17b), the horizontal pressure gradients have been written in terms of the interfacial slopes, $\partial D/\partial x$ and $\partial D/\partial y$. In order to eliminate the vertical velocity, w , in (2.17c),

a vertically integrated form of the continuity equation is introduced by following the same procedure employed in the previous section, but with h_1 and D now functions of time as well as space. Neglecting terms of order h_1/D compared to unity, the counterpart of (2.15) is then

$$(uD)_x + (vD)_y + D_t = 0, \quad (2.18)$$

which replaces (2.17c) and is used exclusively hereafter.

We now assume that the dependent variables may be expanded as

$$\begin{aligned} u &= \bar{u} + \hat{u} \\ v &= \bar{v} + \hat{v} \\ D &= \bar{D} + \hat{D} \end{aligned} \quad (2.19)$$

where \bar{u} , \bar{v} and \bar{D} are the equilibrium state velocities and interfacial depth, respectively, and where the perturbation (caret) variables are small by comparison. This decomposition and the subsequent linearization of (2.17) are therefore valid only if

$$|\hat{u}/\bar{u}| \ll 1, \quad |\hat{v}/\bar{v}| \ll 1, \quad |\hat{D}/\bar{D}| \ll 1. \quad (2.20)$$

The basic state variables in (2.19) are solutions to the basic state equations given in (2.16). The planar front solution to this system is developed in the next chapter, while the exponential front solution is derived in Chapter 5.

Substituting (2.19) into (2.17a), (2.17b) and (2.18), expanding, and neglecting second order terms (products of perturbation variables)

leads to the following system of linear partial differential equations (PDE's) in the new unknowns \hat{u} , \hat{v} and \hat{D} :

$$\hat{u}_t + \bar{u}\hat{u}_x + \bar{v}\hat{u}_y + \bar{u}\hat{u} - f\hat{v} + g'\hat{D}_x = 0 \quad (2.21a)$$

$$\hat{v}_t + \bar{u}\hat{v}_x + \bar{v}\hat{v}_y + \bar{v}\hat{v} + f\hat{u} + g'\hat{D}_y = 0 \quad (2.21b)$$

$$(\bar{u}\hat{D})_x + (\bar{v}\hat{D})_y + (\bar{D}\hat{u})_x + (\bar{D}\hat{v})_y + \hat{D}_t = 0 . \quad (2.21c)$$

The linearized system in (2.21), written in dimensional variables, is general and therefore applies to both the planar and exponential fronts. In the planar front case, which is developed in detail in the next two chapters, (2.21) simplifies considerably, since the equilibrium velocity is spatially invariant and its spatial derivatives consequently vanish. In Chapter 5, which introduces the exponential front, an ageostrophic equilibrium state is considered. Terms in (2.21) involving spatial derivatives of the basic state flow must then be retained, leading to a more complicated system of perturbation equations. Note that the time independent equilibrium state variables appear in (2.21) as non-constant coefficients, but not as forcing terms. The perturbation system is thus homogeneous. Perturbations to the basic state flow are assumed to have developed from an external forcing, surface wind stress, for example, which is no longer active. Moreover, in view of the homogeneity of (2.21), the perturbations are not forced by the equilibrium state variables.

CHAPTER 3

THE PLANAR FRONT

3.1 INTRODUCTION

In this chapter, the equilibrium state solution to (2.16) is presented for the planar front, wavelike solutions are then assumed for the perturbation equations in (2.21), and the general equation for the amplitude of the depth perturbation is derived and solved. Dimensional variables are used throughout in order to compare the results developed here with those of Duxbury (1963). It is shown that the general ordinary differential equation (ODE) for the depth perturbation amplitude (DPA) reduces to Duxbury's second order equation for the case of zero cross-stream flow. In its general form, however, which allows nonzero cross-stream flow, the DPA equation is a seventh order ODE, the implications of which are discussed in this and the next chapter.

3.2 THE PLANAR FRONT EQUILIBRIUM STATE

For the planar front, the solutions to the time independent basic state equations (2.16) are

$$\bar{D}(x,y) = D_f(0) + (f\beta/g')(-v_\infty x + u_\infty y) \quad (3.1)$$

$$\bar{u} = (1-\beta)u_\infty \quad (3.2)$$

$$\bar{v} = (1-\beta)v_\infty \quad (3.3)$$

in which β is an arbitrary constant. (3.1)-(3.3) completely specify the equilibrium state velocity field and interfacial depth for the planar front, which then appear in the perturbation system (2.21) as

variable coefficients. The discontinuity surface that separates the frontal zone from the ambient ocean is, in view of (3.1), a plane; hence, the term planar front. The free-surface elevation, which is related to the interfacial depth by (2.11), is therefore also a plane. The horizontal velocity field is spatially invariant, and includes a nonzero cross-stream velocity. The resulting nonzero cross-stream volume flux at $x = 0$ is driven by mass entrainment through the discontinuity surface in the dissipative region. The bulk effect on the outer (inviscid) region of dissipation near the surface front is therefore parameterized here by the single free constant β .

3.3 HARMONIC SOLUTIONS TO THE PLANAR FRONT PERTURBATION EQUATIONS

Even with the level of simplification achieved by introducing the perturbation expansion in Section 2.3, the analytical solution of the system (2.21) constitutes a formidable, if not impossible, task. Since we anticipate wavelike disturbances of the frontal zone flow field and interfacial depth, a further simplification is introduced by assuming time and space-harmonic solutions to (2.21) of the form

$$\hat{u}(x, y, t) = X(x) \exp\{i(ky - \Omega t)\} \quad (3.4a)$$

$$\hat{v}(x, y, t) = Y(x) \exp\{i(ky - \Omega t)\} \quad (3.4b)$$

$$\hat{D}(x, y, t) = Z(x) \exp\{i(ky - \Omega t)\} \quad (3.5)$$

where $i = (-1)^{1/2}$, Ω is the disturbance circular frequency, and k the wavenumber. $X(x)$, $Y(x)$ and $Z(x)$ are the (complex-valued) x -dependent amplitudes of the perturbations to the x and y velocities and interfacial depth, respectively. In addition to specifying the y and t dependence explicitly, solutions harmonic in these variables provide the additional advantage of not requiring boundary conditions in y or

c. The x-direction boundary conditions are formulated rigorously in Chapter 7.

Substitution of (3.4) and (3.5) into (2.21) along with the basic state equations (3.1)-(3.3) reduces the system of perturbation PDE's for \hat{u} , \hat{v} and \hat{D} to a system of ODE's for the planar front perturbation amplitudes $X(x)$, $Y(x)$ and $Z(x)$ as follows:

$$i\omega X - fY + \bar{u}X' + g'Z' = 0 \quad (3.6a)$$

$$i\omega Y + fX + \bar{u}Y + ik_g Z = 0 \quad (3.6b)$$

$$i\omega Z + \bar{u}Z' + (\bar{D}_y + ik\bar{D})Y + \bar{D}_x X + \bar{D}X' = 0, \quad (3.6c)$$

where $\omega = k\bar{v} - \Omega$ is the Doppler-shifted disturbance frequency. Since (3.6) contains only derivatives with respect to x , it has been simplified notationally by marking derivatives with a prime; for example, $Z' = dZ/dx$.

3.4 DERIVATION OF THE PLANAR FRONT DPA EQUATION

A single ODE for the DPA (depth perturbation amplitude), $Z(x)$, may be developed by eliminating $X(x)$ and $Y(x)$ in (3.6), which, in turn, is most easily accomplished by writing the system (3.6) in operator matrix notation. The interfacial slopes in the x and y directions, respectively, will be denoted a_1 and a_2 , so that the equilibrium interfacial depth (3.1) becomes

$$\bar{D}(x,y) = D_f(0) + a_1 x + a_2 y. \quad (3.7)$$

Replacing the total derivative operator by the symbol p ; i.e.,

$p = d/dx$, (3.6) thus becomes

$$\begin{bmatrix} L_1 & -f & g'p \\ f & L_1 & ikg' \\ a_1 + \bar{D}p & a_2 + ik\bar{D} & L_1 \end{bmatrix} \begin{bmatrix} X \\ Y \\ Z \end{bmatrix} = 0, \quad (3.8)$$

After considerable manipulation, this matrix may now be reduced to the triangular form:

$$\begin{bmatrix} L_1 & -f & g'p \\ 0 & f^2 + L_1^2 & L_4 \\ 0 & 0 & (f^2 + L_1^2)L_5 + \Delta(p)L_4 \end{bmatrix} \begin{bmatrix} X \\ Y \\ Z \end{bmatrix} = 0, \quad (3.9)$$

where the operators L_1 and $\Delta(p)$ are defined by

$$L_1 = i\omega + \bar{u}p \quad (3.10a)$$

$$L_2 = a_1 f \bar{u} p + f L_1 (a_1 + \bar{D}p) + L_1^2 (a_2 + ik\bar{D}) \quad (3.10b)$$

$$L_3 = a_1 g' \bar{u} p^2 + g' L_1 (a_1 + \bar{D}p) p - L_1^3 \quad (3.10c)$$

$$L_4 = -fg'p + ikg'L_1 \quad (3.10d)$$

$$L_5 = L_2 L_4 + (f^2 + L_1^2) L_3 \quad (3.10e)$$

$$\Delta(p) / (2a_1 \bar{u}) = k\omega^3 - \omega^2 (f + 3iku) p + \omega \bar{u} (2if - 3k\bar{u}) p^2 + \bar{u}^2 (f + ik\bar{u}) p^3 \quad (3.10f)$$

The final form of the ODE satisfied by $Z(x)$ is therefore

$$\{(f^2 + L_1^2) L_5 + \Delta(p) L_4\} Z(x) = 0. \quad (3.11)$$

An examination of the operators in (3.11) shows that the order of the highest derivative of $Z(x)$ is seven; that is, Z satisfies a seventh order, linear, homogeneous ODE. The explicit form of the equation for the depth perturbation amplitude is obtained from (3.11) by expanding each of the operators using the appropriate definitions. Although straight forward, the expansion for the general case is tedious, and is therefore not reproduced here.

The special case of zero equilibrium cross-stream flow ($\bar{u} = 0$), however, is readily derived and is of considerable interest, since it corresponds to Duxbury's (1963) model of the planar front. In (3.11) we set $\bar{u} = u_\infty = \bar{D}_y = a_2 = 0$, and upon simplification arrive at the following equation for $Z(x)$:

$$\{(\omega^2 - f^2)/g' + fa_1 k / \omega - k^2 \bar{D}\} Z(x) + a_1 (dZ/dx) + \bar{D} (d^2 Z/dx^2) = 0. \quad (3.12)$$

Rewriting (3.12) in Duxbury's notation, which is discussed in Appendix 2, recovers precisely his equation (49), thereby verifying (3.11) in this limiting case.

For the general case ($\bar{u} \neq 0$), the explicit form of the equation satisfied by $Z(x)$ is

$$\sum_{n=0}^7 (v_n x + \gamma_n) (d^n Z/dx^n) = 0, \quad (3.13)$$

where the v_n and γ_n are complex constants given in Appendix 1, eq. (A.1.). Note that the γ_n may contain a parametric dependence on y .

3.5 SOLUTION OF THE DPA EQUATION FOR THE PLANAR FRONT

The ODE for the depth perturbation amplitude $Z(x)$, (3.13), has an irregular singular point at infinity. Its nature there is ascertained by transforming to the new independent variable $s = 1/x$ and considering the behavior of the solution $Z(s)$ for $s \rightarrow 0$. The details are not included here. However, one finds that the point at infinity is an

irregular singularity, so that no power series expansion exists for the solution $Z(x)$ as $x \rightarrow \infty$. Thus, the method of Frobenius (Hildebrand, 1962, Ch. 4) is not useful in developing the solution for large x . An asymptotic normal form solution does exist, however, as x grows arbitrarily large (Ince, 1956, Ch. XVII), its form being

$$Z(x) \sim x^r e^{\alpha x} W(x) \quad \text{for } x \rightarrow \infty \quad (3.14)$$

where

$$W(x) = 1 + (w_1/x) + (w_2/x^2) + \dots \quad (3.15)$$

α , r , and the w_n are all constants to be determined. Both the exponential factor in (3.14) and the series $W(x)$ in (3.15) are non-dimensional. It is therefore understood that the constant 1 with dimensions of length raised to the $(1-r)$ power multiplies the right-hand side of (3.14), rendering $Z(x)$ dimensionally correct. The constants α , r and w_n are determined by substituting (3.14) with (3.15) into (3.13), expanding in powers of x , and equating coefficients of like powers.

The significance of (3.14) is that it sets the cross-stream decay scale through the parameter α . This scale length turns out upon expansion to be just $1/k$. Determining it explicitly is also crucial to the normalization scheme introduced in Chapter 6. In addition, the parameter α serves to connect the asymptotic form of the solution for $x \rightarrow \infty$ to an integral representation of the solution for finite x .

For the case of no cross-stream flow, (3.14) becomes

$$Z(z) \sim z^{-\alpha_d} \cdot e^{-z/2} \cdot \{1 - (\alpha_d^2/z) + \dots\}, \quad (3.16)$$

where

$$\alpha_d = \frac{1}{2} \{1 + (f^2 - \omega^2) / a_1 g' k - f/\omega\} \quad (3.17)$$

and
$$z = (2k/a_1) \{D_f(0) + a_1 x\} \quad (3.18)$$

are the same as Duxbury's (1963) quantities α and z . (3.16), which is written in Duxbury's notation, recovers his expression for the asymptotic behavior of the DPA which appears in Appendix A of his paper. Note that z above should not be confused with the vertical coordinate, nor α_d with α in (3.14). This notation is employed only in (3.17), (3.18) and (3.21) in order to compare these equations with Duxbury's expressions. From (3.16) and (3.18), we see clearly that the natural scale in the cross-stream direction is the decay scale for the DPA, $1/k$.

Since only the point at infinity is an irregular singularity of the DPA ODE, (3.13), a valid power series expansion of $Z(x)$ exists in any finite and bounded interval in x . The series may be developed by employing the method of Frobenius, a technique which is straightforward in principle and well suited to numerical computation. This procedure is not particularly illuminating from an analytical viewpoint, however, since it does not provide the relationship between the series expansion for finite x and the asymptotic form of $Z(x)$ as $x \rightarrow \infty$ in (3.14). This limitation is overcome by Laplace transforming (3.13) and using the

the property that its coefficients are at most linear in x , whereupon the solution for $Z(x)$ may be written

$$Z(x) = \sum_{n=1}^7 B_n \int_{-\infty + i\text{Im}(\alpha_n)}^{\alpha_n} \prod_{j=1}^7 (t - \alpha_j)^{A_j - 1} \cdot \exp\{t(x + \gamma_7 / v_7)\} dt \quad (3.19)$$

The α_n in (3.19), all assumed distinct, are the roots of the polynomial equation

$$\sum_{n=0}^7 v_n \alpha^n = 0, \quad (3.20)$$

and the integration is carried out along a line parallel to the real axis in the complex t -space. The A_j and B_n in (3.19) are constants. For the case of zero cross-stream flow, (3.19) reduces to an integral representation of the confluent hypergeometric function U (Abramowitz and Stegun, 1970, Ch. 13). $Z(x)$ then becomes

$$Z(x) = B e^{-z/2} \cdot U(\alpha_d, 1; z), \quad (3.21)$$

which is precisely Duxbury's equation (66) in which the solution that is singular at infinity has been removed. The α 's in (3.19) are exactly the same α 's appearing in the asymptotic form (3.14), thereby establishing the connection between the solution for finite x and its behavior at infinity.

In principle, the problem of the planar front with cross-stream flow has been solved, since the determination of the DPA $Z(x)$ has been reduced to quadratures, and the associated perturbations to the flow field may then be computed from (3.6). Note that once $Z(x)$, and consequently its first derivative, are known explicitly, (3.6) reduces to an algebraic system for the three unknown functions $X(x)$, $X'(x)$ and $Y(x)$.

CHAPTER 4

NON-DIMENSIONALIZATION OF THE PLANAR FRONT ODE FOR $Z(x)$

4.1 INTRODUCTION

In Chapter 3, a single ODE was developed for the depth perturbation amplitude in the planar front case. The analysis was presented entirely in dimensional variables, as was Duxbury's (1963) treatment of the special case of zero cross-stream flow. It led to an asymptotic normal form solution for large x , an integral representation of the solution for finite x , and the connection between the two via the parameters α_n . In principle, then, the formal solution of the planar front problem with allowance for cross-stream flow has been obtained, at least in the sense that it has been reduced to quadratures. In Duxbury's model, the cross-stream flow was taken to be zero at the outset, and the resulting ODE for the depth perturbation amplitude was second order. In this model, Duxbury's second order ODE and all of his subsequent results are recovered if the cross-stream velocity component vanishes; however, the ODE for the depth perturbation amplitude is inherently order seven, not two, as long as any cross-stream flow exists, however small. This observation is somewhat disquieting, and is reminiscent of the singular perturbation problems that frequently occur in fluid dynamics in which the order of a system changes abruptly as some parameter of the problem becomes zero. This peculiarity

demands closer examination, and motivates the non-dimensionalization of the DPA equation that is presented in this chapter.

It was pointed out earlier that the frontal zone is characterized by the baroclinic Rossby radius length scale, λ , on which the dynamics are inviscid except in a narrow dissipative region near the surface front. A second natural length scale also exists for the problem, however, the ratio of the basic state cross-stream velocity to the Coriolis parameter. This is an advective scale and is much smaller than the Rossby radius scale. It is the scale on which the cross-stream Rossby number becomes order one; i.e., \bar{u}/f . In a typical example with $\bar{u} = 10$ cm/s and $f = 10^{-4}$ /s, this scale would be only 1 km. Thus, it would generally lie well within the inner dissipative zone so that it would not require separate treatment in this paper. In what follows, the ODE for the planar front depth perturbation amplitude will be non-dimensionalized by introducing coordinates scaled to the outer (inviscid) and advective cross-stream scale lengths.

4.2 INVISCID SCALE VARIABLES

For time varying wave disturbances on the planar front, the natural long-stream length scale is clearly the disturbance wavelength, or, equivalently, the reciprocal wavenumber $1/k$. From the asymptotic form of the solution to the DPA in Section 3.5, in which an explicit e^{-kx} dependence appears, it is clear that the decay scale for the DPA in the cross-stream direction is also $1/k$, and, consequently, that the x - and y - scales for wavelike disturbances of the planar front are the

same. A careful scaling analysis (cf. Section 5.2 for details), moreover, reveals that the only nontrivial perturbation of interest corresponds to $k \sim 1/\lambda$, where λ is the baroclinic Rossby radius defined below. Dimensionless x and y coordinates, marked by a tilde ($\tilde{}$), are therefore introduced as follows:

$$\tilde{x} = x/\lambda \quad (4.1a)$$

$$\tilde{y} = ky \quad (4.1b)$$

The natural time scale is the inertial period $1/f$, and the appropriate dimensionless circular frequency is thus

$$\sigma = \omega/f \quad (4.1c)$$

The advective scale is characterized by the x - and y - direction lengths \bar{u}/f and \bar{v}/f , respectively, where \bar{u} and \bar{v} are the equilibrium state velocities introduced in Chapter 2. The ratios of the advective to inviscid length scales for the x and y directions form two non-dimensional parameters of the problem, which are denoted

$$\epsilon = \bar{u}/f \quad (4.1d)$$

and

$$\epsilon' = k\bar{v}/f \quad (4.1e)$$

In general, we anticipate $\epsilon \ll 1$ while $\epsilon' \sim 1$, since $|\bar{u}/\bar{v}| \ll 1$ for large scale fronts with large values of the rotation parameter.

Two internal Froude numbers exist which measure the ratio of the fluid velocity to the internal wave phase speed. The latter is defined

$$c^2 = g'D_f(0) \quad (4.1f)$$

The two Froude numbers are then,

$$F_x = \bar{u}/c \quad (4.1g)$$

for the x -direction, and

$$F_y = \bar{v}/c \quad (4.1h)$$

for the y -direction. We anticipate $F_x \ll 1$ while $F_y \sim 1$ for the same reasons as above for ϵ and ϵ' .

The baroclinic Rossby radius is defined as

$$\lambda = c/f. \quad (4.11)$$

The free parameter β appearing in the basic state velocity field developed in Chapter 3 for the planar front is absorbed into a new dimensionless transport parameter defined by

$$\tau = 1 - \beta^{-1}, \quad (4.1j)$$

which is order one.

With these definitions, the non-dimensional differential equation for the planar front DPA in inviscid scale variables becomes

$$\sum_{n=0}^7 (\tilde{\nu}_n \tilde{x} + \tilde{\gamma}_n) (d^n Z(\tilde{x}) / d\tilde{x}^n) = 0, \quad (4.2)$$

where the dimensionless complex constants $\tilde{\nu}_n$ and $\tilde{\gamma}_n$ are defined in Appendix 2B.

We now assume that $Z(\tilde{x})$ in (4.2) may be developed in a small parameter expansion as follows

$$Z(\tilde{x}) = Z^{(0)} + F_x Z^{(1)} + F_x^2 Z^{(2)} + \dots, \quad (4.3)$$

in view of which, at order F_x^0 , (4.2) becomes

$$\begin{aligned} \{ \tilde{x} + \tau \{ 1 - \sigma^2 - (k\lambda)^2 \} / k\lambda F_y - 1 / \sigma \} Z^{(0)}(\tilde{x}) - dZ^{(0)} / d\tilde{x} \\ + \{ k\lambda \tau / F_y - \tilde{x} \} (d^2 Z^{(0)} / d\tilde{x}^2) = 0. \end{aligned} \quad (4.4)$$

The case of zero cross-stream flow corresponds to $F_x = 0$ in (4.2) and (4.3), which again recovers Duxbury's (1963) second order ODE for $Z(x)$, as it must. The details are not reproduced here. Even for nonzero F_x , however, we see that at order F_x^0 the equation for $Z(\tilde{x})$ is still second order, not seventh order as in the general, dimensional

formulation. On the outer (inviscid) scale, therefore, which is the only region of applicability of this model, the lowest order ODE for the depth perturbation amplitude is still second order. An extension to first order in F_x leads to a similar result: the equation for $Z(\tilde{x})$ is still second order, but with the addition of lowest order forcing terms. The first order dynamics in the small parameter F_x are thus no longer homogeneous, but instead are driven by the zeroth order solutions. On the outer scale, the third and higher derivative terms in Z can enter the dynamics at most at order F_x^2 in the small parameter expansion, if at all. Thus, the inviscid scale dynamics of the planar front are fundamentally second order, even with nonzero cross-stream flow, a conclusion which is consistent with Duxbury's second order model. This conclusion, however, has been reached only by having introduced appropriate scalings for the problem, not by developing the general dimensional form presented in Chapter 3 or in Duxbury's (1963) work.

The effect of nonzero cross-stream flow on the outer scale is simply to modify the constants in the coefficients of the ODE for $Z(\tilde{x})$ by introducing terms which vanish with zero cross-stream flow; the functional dependence of the coefficients on \tilde{x} remains unchanged even for nonzero cross-stream flow. The formalism developed in Chapter 3 for the solution of the depth perturbation amplitude ODE is therefore directly applicable to the DPA equation at lowest order in the parameter F_x , but the results thus obtained are only a minor extension of Duxbury's original problem.

It is interesting to note that normalizing the cross-stream coordinate to the advective length scale, \bar{u}/f , and redoing the above analysis leads to a fifth order ODE for $Z(\hat{x})$ at order F_x^0 . The details are not reproduced here, but this observation is important, since it shows that the higher order derivative terms in the DPA equation are significant at order F_x^0 only in the very narrow advective zone. However, since this region is imbedded in the dissipative zone, the kind of inviscid dynamics which would develop on this scale are never realized.

The insight provided by this analysis will be incorporated in what follows in order to develop a more realistic frontal model that includes nonzero cross-stream flow and more accurately reflects observed frontal zone geometry.

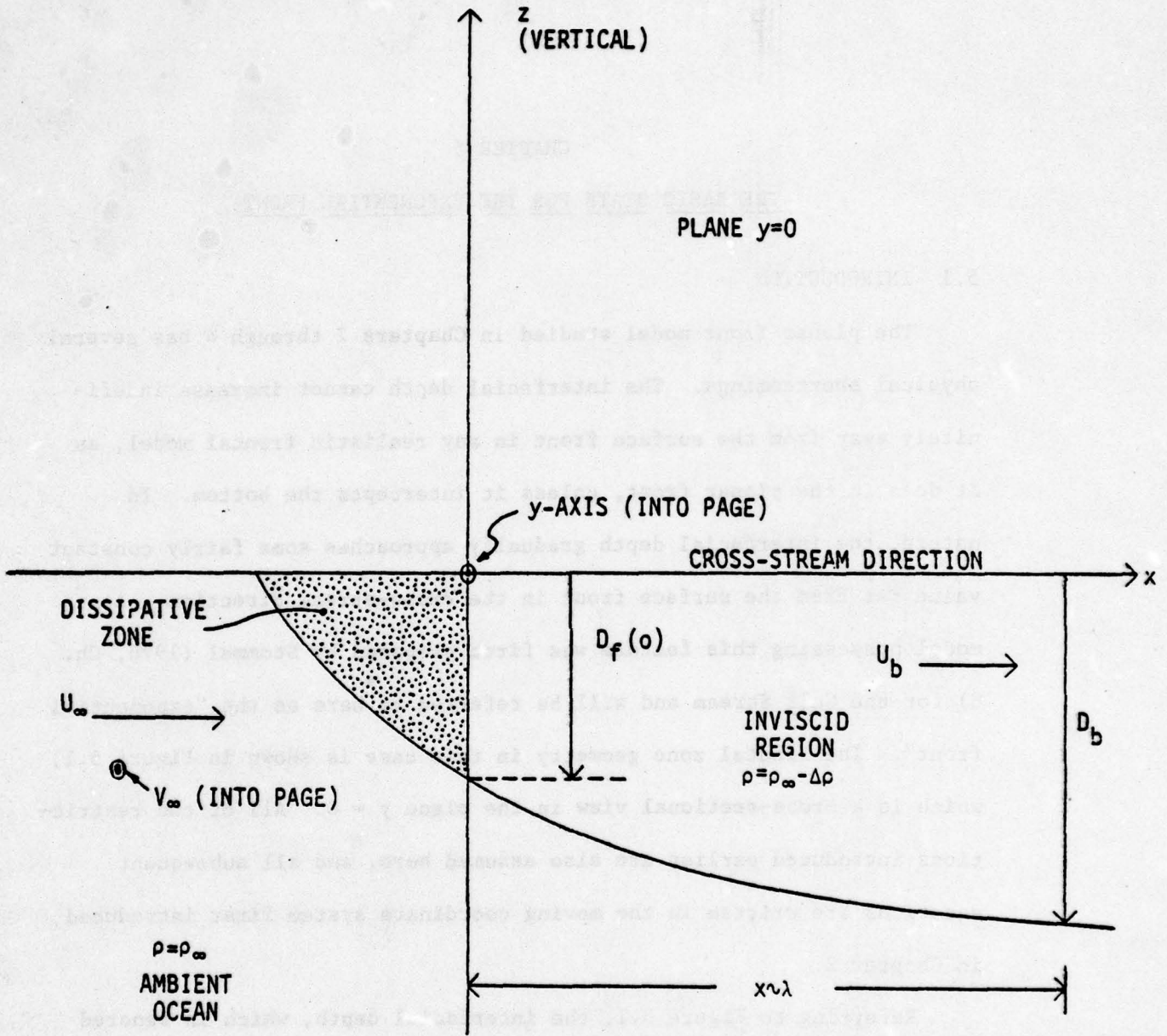
CHAPTER 5

THE BASIC STATE FOR THE EXPONENTIAL FRONT

5.1 INTRODUCTION

The planar front model studied in Chapters 2 through 4 has several physical shortcomings. The interfacial depth cannot increase indefinitely away from the surface front in any realistic frontal model, as it does in the planar front, unless it intercepts the bottom. In nature, the interfacial depth gradually approaches some fairly constant value far from the surface front in the cross-stream direction. A model possessing this feature was first proposed by Stommel (1976, Ch. 8) for the Gulf Stream and will be referred to here as the "exponential front". The frontal zone geometry in this case is shown in Figure 5.1, which is a cross-sectional view in the plane $y = 0$. All of the restrictions introduced earlier are also assumed here, and all subsequent equations are written in the moving coordinate system first introduced in Chapter 2.

Referring to Figure 5.1, the interfacial depth, which is denoted $D_f(0)$ at the origin, as before, gradually increases in the cross-stream (x) direction and asymptotically approaches the value D_b far from the dissipative zone. All dissipation through mass entrainment, mixing, and turbulent friction is again confined to the narrow dissipative region. The interfacial depth increases from $D_f(0)$ to D_b in the inviscid (outer) region on its natural length scale, λ , the baroclinic



CROSS-SECTIONAL VIEW OF THE
EQUILIBRIUM STATE EXPONENTIAL
FRONTAL ZONE GEOMETRY

FIGURE 5.1

Rossby radius. With the spatial coordinates scaled by λ we anticipate that spatial derivatives are order one in the x-direction and very small in the y-direction.

5.2 DIFFERENTIAL EQUATIONS FOR THE EXPONENTIAL BASIC STATE

The general time dependent momentum and continuity equations for the inviscid (outer) region appear in (2.17) and (2.18) and are reproduced here for convenient reference:

$$u \frac{\partial u}{\partial t} + v \frac{\partial u}{\partial x} - f v = -g' D_x - f v_\infty \quad (5.1a)$$

$$v \frac{\partial v}{\partial t} + u \frac{\partial v}{\partial x} + f u = -g' D_y + f u_\infty \quad (5.1b)$$

$$D_t + (u D_x + v D_y) = 0 \quad (5.1c)$$

in which all variables are dimensional. (5.1) makes no assumption about the frontal zone geometry.

Differentiating the x-momentum equation with respect to y and the y-momentum equation with respect to x, subtracting and using (5.1c) leads to the result

$$\frac{D}{Dt} \left(\frac{f + \Lambda}{D} \right) = 0 \quad (5.2)$$

where $\Lambda = v_x - u_y$ and where D/Dt is the convective derivative. The quantity $(f + \Lambda)/D$ is recognized as the potential vorticity, and (5.2) is a statement of conservation of potential vorticity following a fluid element. This result follows from the assumption of inviscid dynamics which permit no mechanism for altering the angular momentum of a fluid column.

The equilibrium state equations for the exponential front are formulated by setting $\frac{\partial}{\partial t} = 0$ and $u_y = v_x = (vD)_y = 0$ in (5.1), reflecting the fact that, in the basic state, y-variations are assumed very

small compared to x-variations. Although the long stream rate of change of the y-direction volume flux, vD , is negligible compared to the cross-stream rate of change of the x-direction volume flux, uD , the derivative D_y in the y-momentum equation is retained. This is necessary since D_y must be present for large x to provide the y-pressure gradient which is compatible with the cross-stream flow u_b there. The simplified basic state continuity and momentum equations thus become

$$(uD)_x = 0 \quad (5.3a)$$

$$uu_x - fv = -g'D_x - fv_\infty \quad (5.3b)$$

$$uv_x + fu = -g'D_y + fu_\infty, \quad (5.3c)$$

while the potential vorticity equation is now

$$(\partial/\partial x)\{(f+v_x)/D\} = 0. \quad (5.3d)$$

Each of the dependent variables, u , v , and D in (5.3) is a function of x and y , but the y -dependence is weak. In addition, since (5.3d) was derived by combining (5.3b) and (5.3c), only two of these three equations are independent. The two independent equations are here taken to be the x-momentum and potential vorticity equations.

(5.3a) and (5.3d) may be integrated immediately to obtain

$$uD = u_b D_b \quad (5.4)$$

and

$$f+v_x = f\delta, \quad (5.5)$$

where u_b is the (constant) x-direction velocity in the frontal zone far from the dissipative region, and δ is the non-dimensional interfacial depth defined by

$$\delta = D/D_b. \quad (5.6)$$

Differentiating the x-momentum equation (5.3b) with respect to x and substituting for v_x and u from (5.4) and (5.5) produces the following equation for the normalized basic state interfacial depth:

$$(1-F_b^2/\delta^3)\delta_{\xi\xi} + (3F_b^2/\delta^4)\delta_{\xi}^2 + 1 - \delta = 0, \quad (5.7)$$

where

$$c = (g'D_b)^{1/2} \quad (5.8a)$$

$$F_b = u_b/c \quad (5.8b)$$

$$\lambda = c/f \quad (5.8c)$$

$$\xi = x/\lambda \quad (5.8d)$$

In (5.8), c is the frontal zone internal wave phase speed (note that it is defined somewhat differently here than in Chapter 4), F_b is the x-direction Froude number and measures the strength of the frontal zone cross-stream flow, λ is the baroclinic Rossby radius of deformation, and ξ is the normalized x-coordinate. Under the linearization scheme that is introduced in Chapter 6, F_b constitutes the fundamental parameter for the frontal zone.

In general, we seek solutions for which the disturbance frequency is small compared to the inertial frequency; i.e., we are interested in low subinertial frequency behavior. Similarly, we are interested in fronts for which the inviscid region scale length is of order λ . A careful scaling analysis applied to the general equations in (5.1) then reveals that the only conditions of interest are that $k\lambda \sim F_y^2 \sim 1$, where F_y is the y-direction internal Froude number (ratio of the basic state long stream velocity to the internal wave phase speed). The reciprocal wavenumber, $1/k$, is therefore of the order of the Rossby radius, λ , and either of these length scales may be used to normalize

the inviscid scale spatial coordinates. (5.8d) is thus consistent with the earlier observation for the planar front that the inviscid scale length is order $1/k$. For large scale upper ocean fronts, observations tend to show $|F_b| \ll 1$, while for smaller scale fronts $|F_b|$ may be order 1 (Garvine, 1979b). In addition, consistent observation of the high velocity long-stream shear characteristics of large scale fronts is reflected in the condition $|F_y| \sim 1$. For analytical convenience, however, any explicit F_y dependence will be avoided in the sequel by choosing $F_y = 1$ identically. This is tantamount to scaling the long-stream velocity by c .

(5.7) provides now a second order, nonlinear, inhomogeneous ODE for the non-dimensional interfacial depth, δ . Recall that δ is only weakly y -dependent, and that its y -dependence may be computed from the y -momentum equation once the remaining three equations in the system (5.3) have been solved. The solution to (5.7) will be developed in the next section.

5.3 SOLUTION OF THE BASIC STATE INTERFACIAL DEPTH EQUATION

Subject to the boundary conditions

$$\lim_{\xi \rightarrow \infty} \delta(\xi) = 1 \quad (5.9a)$$

$$\delta(0) = \delta_0 = D_f(0)/D_b, \quad (5.9b)$$

the exact solution for $\delta(\xi)$ in (5.7) is given implicitly by

$$\begin{aligned} \xi = & (\Psi/\delta_0) - (\Phi/\delta) + \ln\{(\delta_0 + \Psi)/(\delta + \Phi)\} \\ & + F_b \{\sin^{-1}(F_b/\delta) - \sin^{-1}(F_b/\delta_0)\} \\ & - (1-F_b^2)^{3/2} \ln \left\{ \frac{(\delta-1)\{\delta_0 - F_b^2 + (1-F_b^2)^{1/2}\Psi\}}{(\delta_0-1)\{\delta - F_b^2 + (1-F_b^2)^{1/2}\Phi\}} \right\} \end{aligned} \quad (5.10a)$$

where

$$\Psi = (\delta_0^2 - F_b^2)^{1/2} \quad (5.10b)$$

$$\Phi = (\delta^2 - F_b^2)^{1/2} \quad (5.10c)$$

Principal values are to be understood for the arcsine terms, and we require $F_b^2 \ll \delta_0 < 1$. Note also that δ_0 is order one.

Although the exact solution is very useful for numerical computation, it is very cumbersome for analytical purposes, since the dependent variable is represented implicitly. An approximate, but explicit representation may be developed, however, by introducing a small parameter expansion for $\delta(\xi)$ in terms of the Froude number F_b .

We assume that $\delta(\xi)$ may be written

$$\delta(\xi) = \delta^{(0)}(\xi) + F_b^2 \delta^{(2)}(\xi) + F_b^4 \delta^{(4)}(\xi) + \dots, \quad (5.11)$$

in which only even powers of F_b appear, since (5.7) contains only F_b^2 . Each of the functions $\delta^{(n)}(\xi)$ is order one, and the error introduced by truncating the series at $\delta^{(n)}(\xi)$ is order F_b^n . Substituting (5.11) into (5.7) yields the following equations for $\delta^{(0)}$ and $\delta^{(2)}$:

$$\delta_{\xi\xi}^{(0)} - \delta^{(0)} + 1 = 0 \quad (5.12)$$

$$\delta_{\xi\xi}^{(2)} - \delta^{(2)} = -\frac{1}{2} \left(\frac{d^2}{d\xi^2} \right) \left\{ 1 / \{ \delta^{(0)} \}^2 \right\} \quad (5.13)$$

The approximate solution will not be carried beyond second order in F_b . (5.12) and (5.13) are both second order, linear and inhomogeneous. The inhomogeneity in (5.12) is a result of the inhomogeneity in the original equation for $\delta(\xi)$, while the inhomogeneity in (5.13) is characteristic of the small parameter expansion formulation, in which each successive solution beyond zeroth order is dependent on the lower order solutions.

The boundary conditions (5.9) will be satisfied exactly to zeroth order in F_b , that is,

$$\delta^{(0)}(0) = \delta_0 \quad (5.14a)$$

$$\lim_{\xi \rightarrow \infty} \delta^{(0)}(\xi) = 1 \quad (5.14b)$$

In view of (5.9) and (5.14), all higher order terms in F_b in the expansion for $\delta(\xi)$ must satisfy zero boundary conditions, that is,

$$\delta^{(n)}(0) = 0 \quad \left. \vphantom{\delta^{(n)}(0)} \right\} n \geq 2 \quad (5.15a)$$

$$\lim_{\xi \rightarrow \infty} \delta^{(n)}(\xi) = 0 \quad (5.15b)$$

The lowest order solution to (5.12) subject to the boundary conditions (5.14) is

$$\delta^{(0)}(\xi) = 1 - (1 - \delta_0) e^{-\xi}, \quad (5.16)$$

which is, of course, also the solution to the original equation for $\delta(\xi)$ with $F_b = 0$. This is the form of the solution found by Stommel in his *Gulf Stream model* and it motivates the "exponential front" nomenclature. The second order solution to (5.13) subject to the boundary conditions (5.15) is

$$\begin{aligned} \delta^{(2)}(\xi) / \{\delta^{(0)} - 1\} = \ln \sqrt{\frac{\delta_0 (1 - \delta^{(0)})}{(1 - \delta_0) \delta^{(0)}}} \\ + \frac{(\delta^{(0)} - \delta_0)(\delta^{(0)} + \delta_0 + 2)}{4\{\delta^{(0)}\}^2} \end{aligned} \quad (5.17)$$

The set of equations (5.11), (5.16) and (5.17) provides an explicit, although approximate, representation for the time invariant basic state interfacial depth to second order in the small parameter F_b . The difference between the exact and approximate solutions is expected to

be order F_b^2 . Having developed an explicit form for $\delta(\xi)$, the basic state x and y velocities in the frontal zone may now be computed from (5.4) and (5.3b) if desired.

Figures 5.2a through 5.2e compare the exact equilibrium interfacial depth computed from (5.10) (curve A) with the approximate representation computed to order F_b^2 using (5.11) with (5.16) and (5.17) (curve B). The value of δ_0 is fixed at 0.4, and F_b ranges over 0.1 to 0.3 in steps of 0.05. For $F_b = 0.1$ and 0.15, the approximate solution is greater than the exact solution, while at $F_b = 0.25$ and 0.3, this is reversed. For $F_b = 0.2$, the two curves are essentially indistinguishable. The absolute error in the approximate solution therefore passes through a minimum near $F_b \approx 0.2$. Agreement between the two solutions at order F_b^2 is excellent over the range of F_b that is considered, and the error is generally even less than F_b^2 . Although several other cases were computed, the results are not included here, since Figure 5.2 serves well to illustrate the behavior of the approximate and exact solutions.

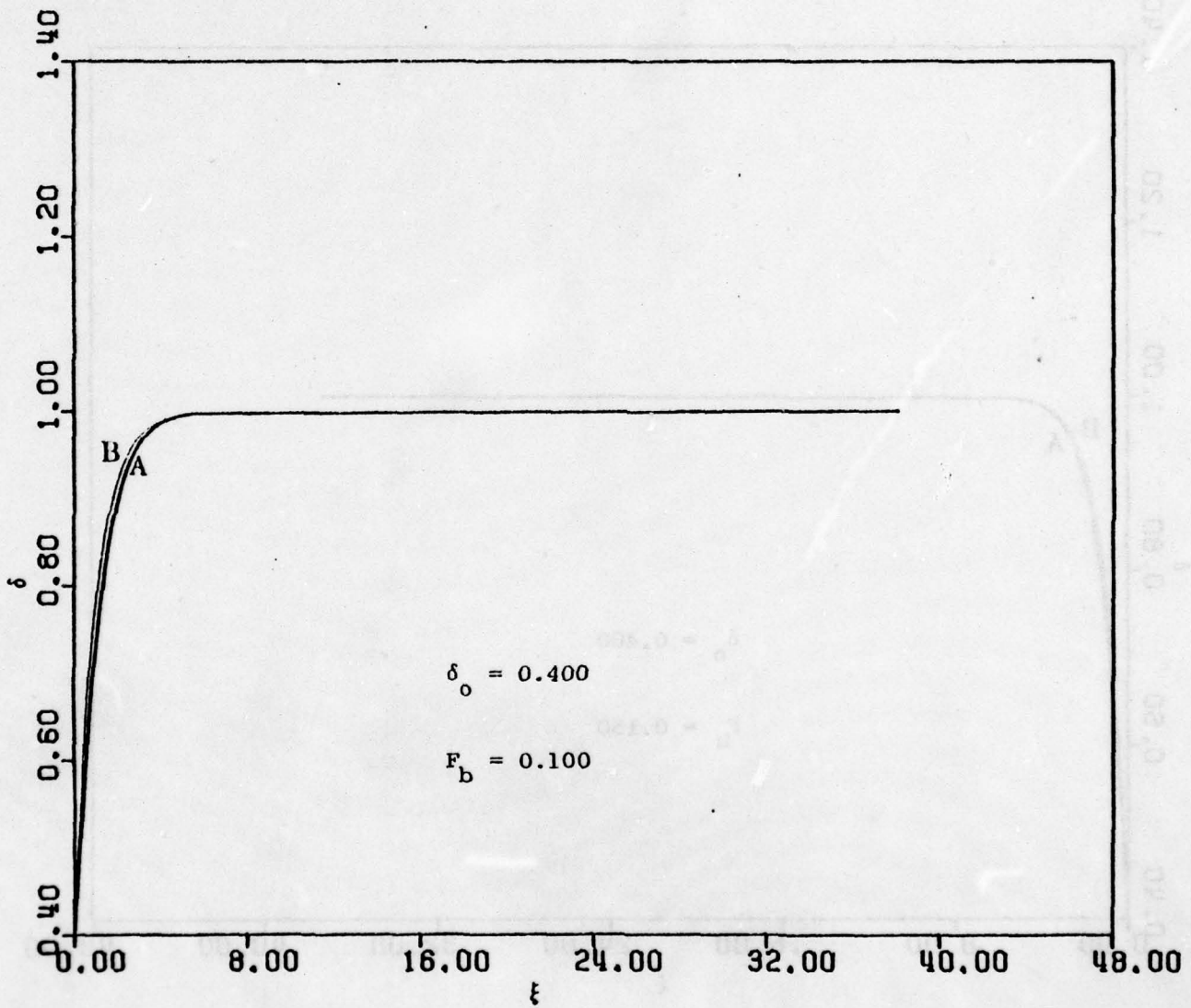


Figure 5.2(a)

Comparison of Exact (Curve A) and
Approximate (Curve B) Basic State Interfacial Depth
Profiles

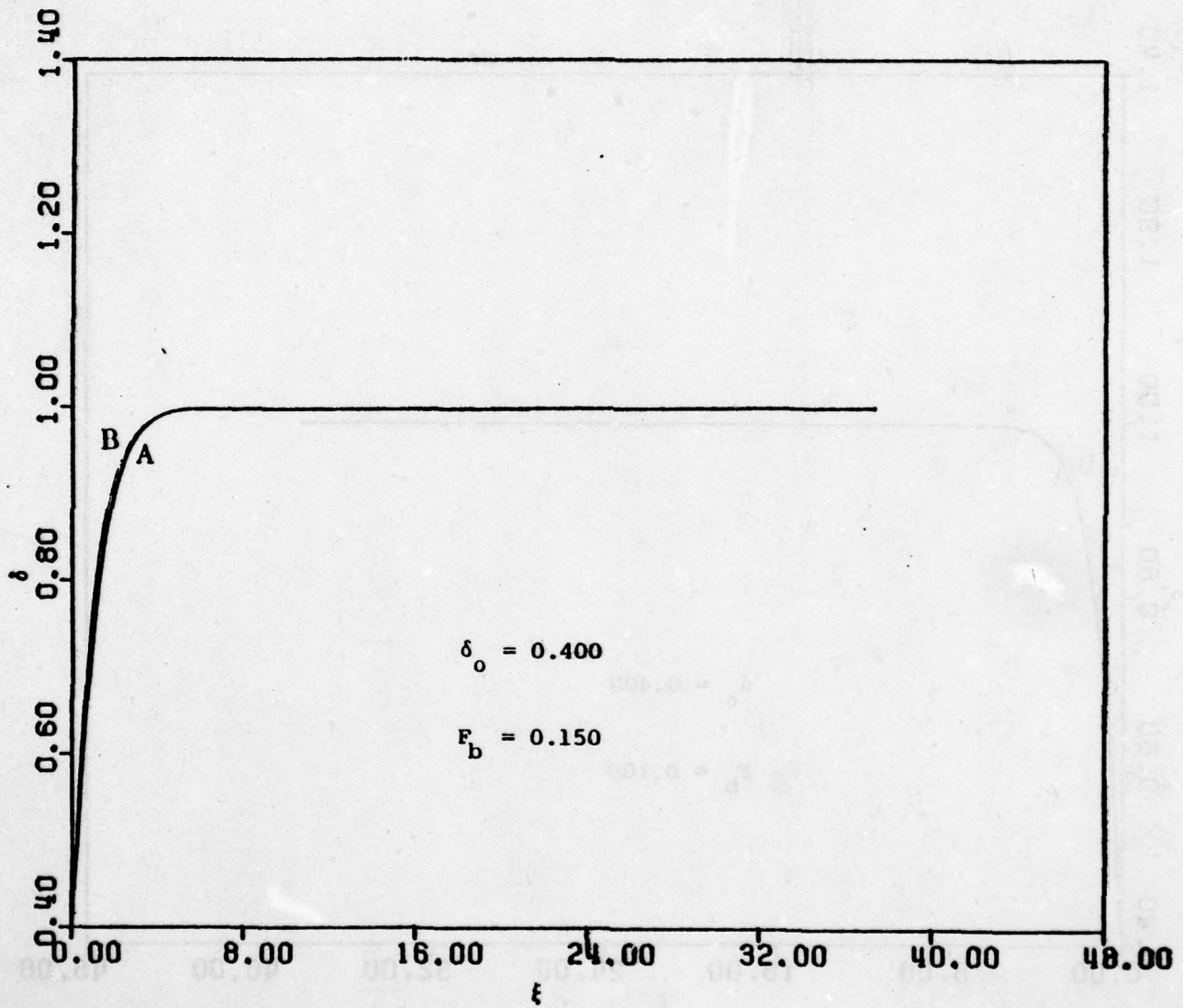


Figure 5.2(b)

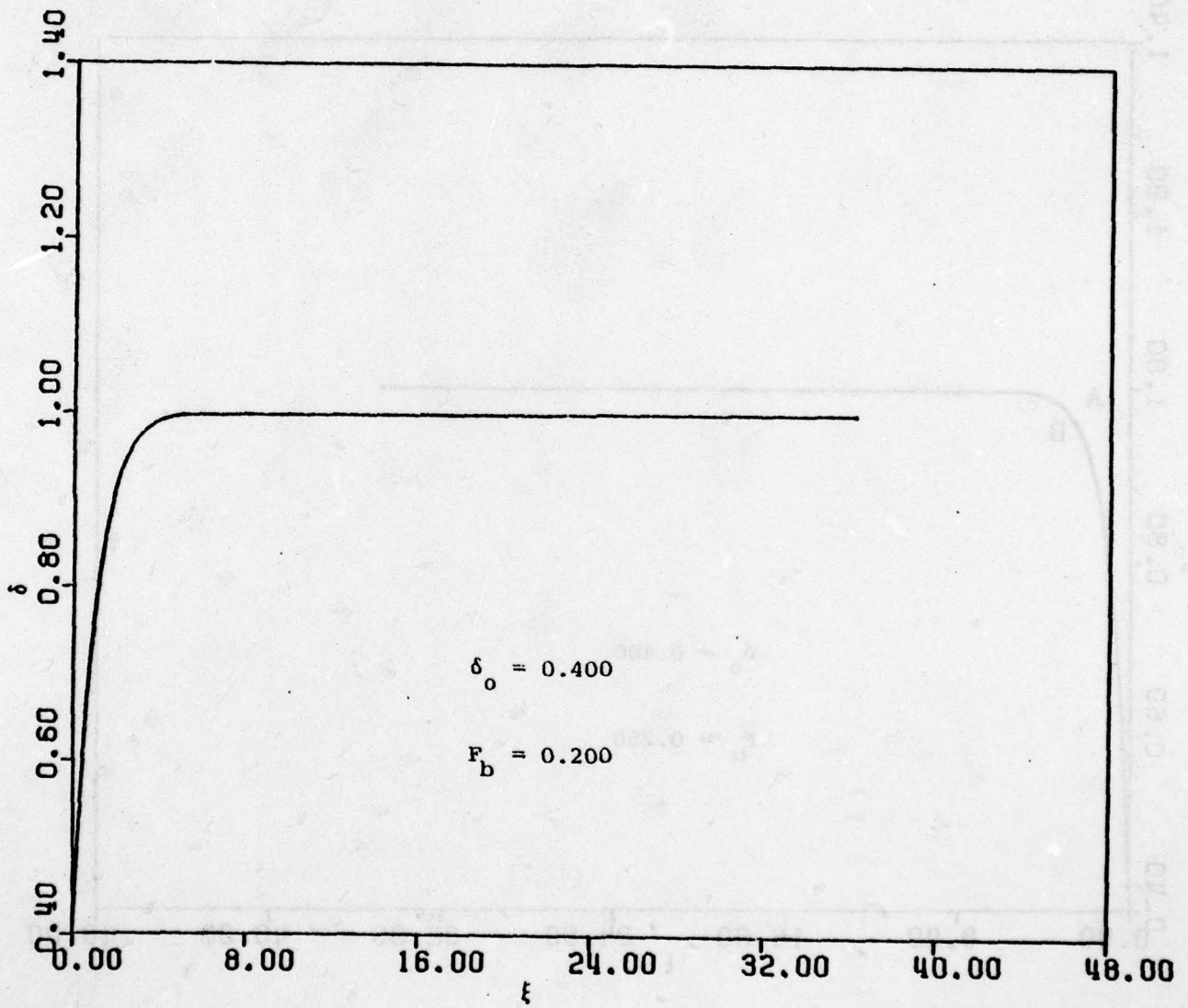


Figure 5.2(c)

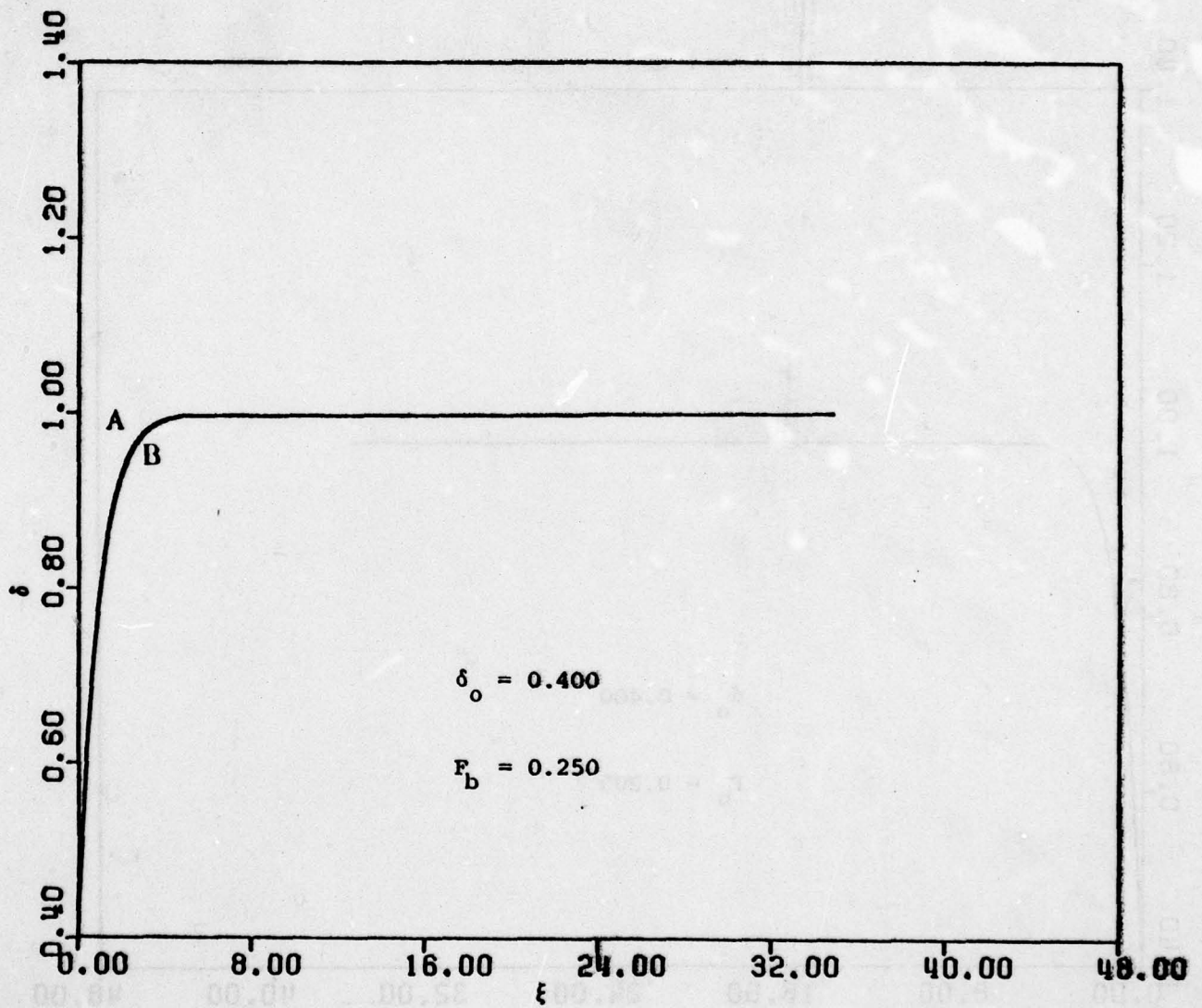


Figure 5.2(d)

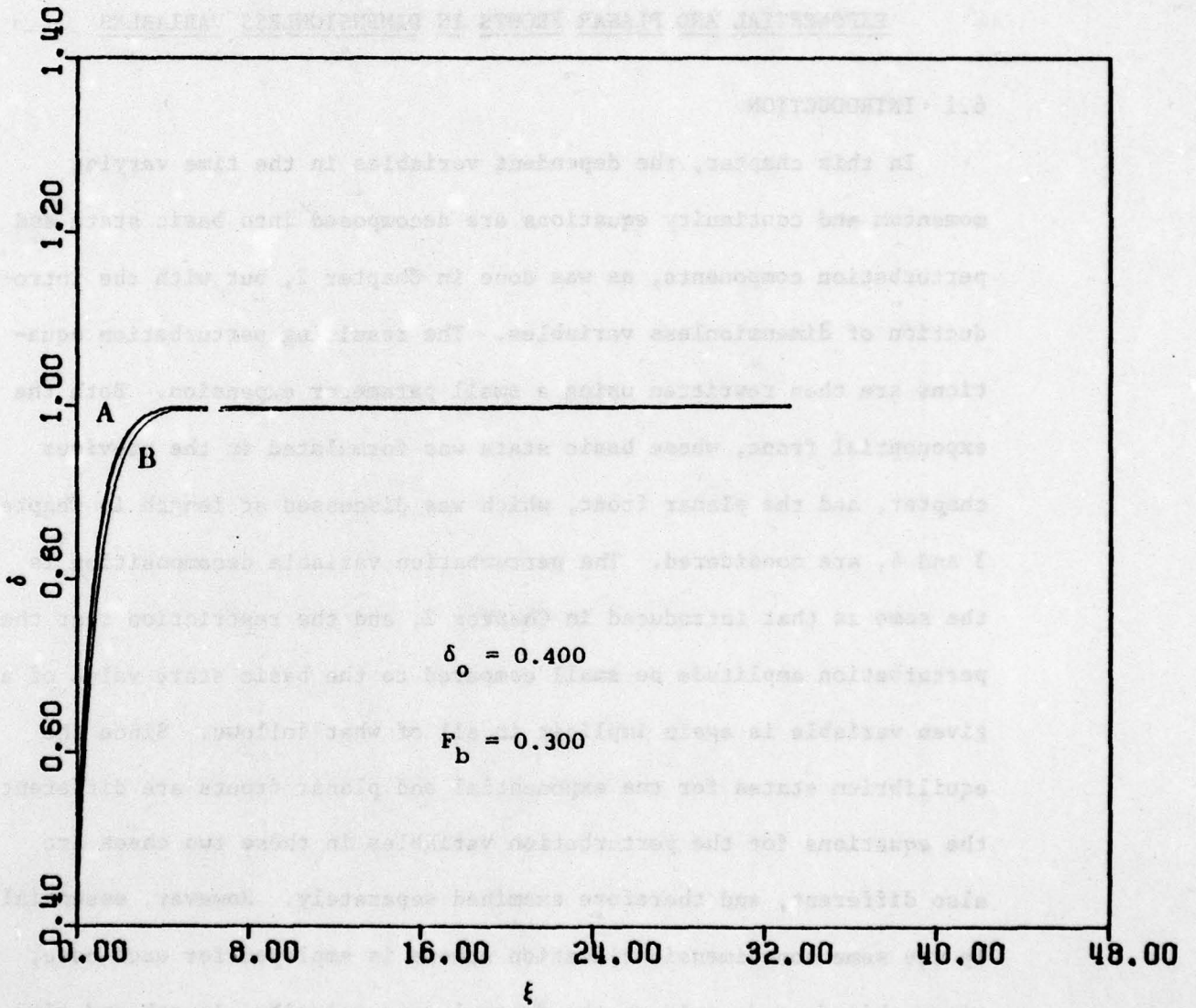


Figure 5.2(e)

CHAPTER 6

LINEARIZATION OF THE TIME-VARYING EQUATIONS FOR THE EXPONENTIAL AND PLANAR FRONTS IN DIMENSIONLESS VARIABLES

6.1 INTRODUCTION

In this chapter, the dependent variables in the time varying momentum and continuity equations are decomposed into basic state and perturbation components, as was done in Chapter 2, but with the introduction of dimensionless variables. The resulting perturbation equations are then rewritten using a small parameter expansion. Both the exponential front, whose basic state was formulated in the previous chapter, and the planar front, which was discussed at length in Chapters 3 and 4, are considered. The perturbation variable decomposition is the same as that introduced in Chapter 2, and the restriction that the perturbation amplitude be small compared to the basic state value of a given variable is again implicit in all of what follows. Since the equilibrium states for the exponential and planar fronts are different, the equations for the perturbation variables in these two cases are also different, and therefore examined separately. However, essentially the same non-dimensionalization scheme is employed for each case, since this depends only on the frontal zone velocity, length and time scales, which, in turn, are only weakly dependent upon the model geometry. The perturbation variable decomposition requires an explicit

form for the basic state variables \bar{u} , \bar{v} and \bar{D} , which then appear as coefficients in the perturbation equations. This is accomplished by introducing the same small parameter expansion in terms of F_b that was used in the previous chapter for both the exponential and planar front cases. This provides the additional advantage of facilitating comparison between the two.

6.2 PERTURBATION VARIABLES AND NON-DIMENSIONALIZATION

The time varying momentum and continuity equations are (2.17a), (2.17b), and (2.18) for both the exponential and planar fronts, in which u , v and D are each functions of (x, y, t) . These equations are general, and apply to the basic state as well as the time varying flow. As before, each of the dependent variables is decomposed into a basic state component and a perturbation component which is small by comparison, that is, the decomposition (2.19) is again assumed. For the exponential front, the resulting perturbation equations are different from those for the planar front, since the spatial variation of the equilibrium velocity field introduces derivatives of the basic state flow.

The variables for the planar and exponential front models are scaled as follows: x is scaled by λ , y by $1/k$, the interfacial depth by $D_f(0)$ or D_b , u by the characteristic x velocity u_b , v by c , and t by the inertial time scale $1/f$. As before, k is the (dimensional) y -direction wavenumber for harmonic frontal disturbances, and λ is the (dimensional) baroclinic Rossby radius. The product $k\lambda$ is, therefore,

dimensionless. The long-stream equilibrium state velocity scale reflects the characteristic frontal zone jet predicted by other authors (Charney, 1955; Garvine, 1979a; Morgan, 1956). Since perturbations to the system are homogeneous, as we have seen in section 2.3, the normalization for the perturbation velocities is arbitrary, and therefore set equal to c for convenience. The dimensionless x and y coordinates are ξ and ζ , respectively, while δ is the dimensionless interfacial depth. F_b is the x -direction internal Froude number introduced in Chapter 5, while its y -direction counterpart, F_y in the previous chapter, is set identically equal to 1. Other non-dimensional variables are marked by an asterisk. Thus, we define

$$\begin{aligned} x &= \lambda \xi, & y &= \zeta/k, & \bar{u} &= u_b \bar{u}^* \\ \bar{v} &= c \bar{v}^*, & \hat{u} &= c \hat{u}^*, & \hat{v} &= c \hat{v}^* \\ u_\infty &= u_b u_\infty^*, & v_\infty &= c v_\infty^*, & F_b &= u_b/c \\ t &= t^*/f, & \lambda &= c/f \quad (\text{Rossby radius}) \end{aligned}$$

(6.1)

$$\left. \begin{aligned} \bar{D} &= D_b \bar{\delta} \\ \hat{D} &= D_b \hat{\delta} \\ c^2 &= g' D_b \end{aligned} \right\} \text{Exponential Front}$$

$$\left. \begin{aligned} \bar{D} &= D_f(0) \bar{\delta} \\ \hat{D} &= D_f(0) \hat{\delta} \\ c^2 &= g' D_f(0) \end{aligned} \right\} \text{Planar Front}$$

In view of (6.1), the fundamental system of perturbation equations for both the planar and exponential fronts in non-dimensional variables is:

$$\hat{u}_t + F_b \bar{u} \hat{u}_\xi + k\lambda \bar{v} \hat{u}_\zeta + F_b \bar{u}_\xi \hat{u} - \hat{v} + \hat{\delta}_\xi = 0 \quad (6.2a)$$

$$\hat{v}_t + F_b \bar{u} \hat{v}_\xi + k\lambda \bar{v} \hat{v}_\zeta + \bar{v}_\xi \hat{u} + \hat{u} + k\lambda \hat{\delta}_\zeta = 0 \quad (6.2b)$$

$$\hat{\delta}_t + F_b (\bar{u} \hat{\delta})_\xi + k\lambda \bar{v} \hat{\delta}_\zeta + (\bar{\delta} \hat{u})_\xi + k\lambda (\bar{\delta} \hat{v})_\zeta = 0 \quad (6.2c)$$

The planar front equilibrium (overbar) velocities are then

$$\bar{u} = (1-\beta)u_\infty \quad (6.3a)$$

$$\bar{v} = (1-\beta)v_\infty \quad (6.3b)$$

where β is the dimensionless transport parameter introduced in (3.1). Note that the asterisks have now been dropped for notational convenience, and it is understood that all quantities, except k and λ , which always appear as a product, are non-dimensional. The planar front basic state interfacial depth is

$$\bar{\delta}(\xi, \zeta) = \bar{\delta}^{(0)} + F_b \bar{\delta}^{(1)}, \quad (6.4a)$$

where

$$\bar{\delta}^{(0)} = 1 - \beta v_\infty \xi \quad (6.4b)$$

$$\bar{\delta}^{(1)} = (\beta F_b u_\infty / k\lambda) \zeta \quad (6.4c)$$

Note that the cross-stream flow enters the scaled basic state only at order F_b^1 .

For the exponential front, the scaled basic state (overbar) variables, which were developed explicitly in the previous chapter, are given by

$$\bar{u} = 1/\bar{\delta} \quad (6.5a)$$

$$\bar{v} = \bar{\delta}_\xi - F_b^2 \bar{\delta}_\xi / \bar{\delta}^3 + v_\infty \quad (6.5b)$$

and

$$\bar{\delta}(\xi) = \bar{\delta}^{(0)} + F_b^2 \bar{\delta}^{(2)}, \quad (6.5c)$$

where $\bar{\delta}^{(0)}$ and $\bar{\delta}^{(2)}$ appear in (5.16) and (5.17), respectively. The basic state flow is derived from (5.3b) and (5.4) using (5.11).

6.3 SMALL-PARAMETER EXPANSIONS

Each of the dependent variables in (6.2) is now expanded in terms of the small parameter F_b as follows:

$$\hat{u} = \hat{u}^{(0)} + F_b \hat{u}^{(1)} + F_b^2 \hat{u}^{(2)} + \dots \quad (6.6a)$$

$$\hat{v} = \hat{v}^{(0)} + F_b \hat{v}^{(1)} + F_b^2 \hat{v}^{(2)} + \dots \quad (6.6b)$$

$$\hat{\delta} = \hat{\delta}^{(0)} + F_b \hat{\delta}^{(1)} + F_b^2 \hat{\delta}^{(2)} + \dots \quad (6.6c)$$

$$\bar{\delta} = \bar{\delta}^{(0)} + F_b^2 \bar{\delta}^{(2)} + \dots \quad (6.6d)$$

$$\bar{\delta} = \bar{\delta}^{(0)} + F_b \bar{\delta}^{(1)} \quad (6.6e)$$

where (6.6d) and (6.6e) apply to the exponential and planar fronts, respectively.

In (6.6), each of the functions $\hat{u}^{(0)}$, $\hat{u}^{(2)}$, etc., is presumably order one, as is the product $k\lambda$. The exponential front expansion in (6.6d) is the same as (5.11) in which the overbar had not yet been used, and only even powers of F_b appear for the reason discussed in section 5.3. For the planar front, the basic state expansion for the interfacial

depth terminates at order F_b^1 , even though the expression is exact; and none is introduced for the velocity field, since it is constant.

Substituting (6.6) into (6.2) leads to the following zeroth and first order non-dimensional perturbation equations for the planar front:

$$\hat{u}_t^{(0)} + k\lambda\bar{v}\hat{u}_\zeta^{(0)} - \hat{v}^{(0)} + \hat{\delta}_\xi^{(0)} = 0 \quad (6.7a)$$

$$\hat{v}_t^{(0)} + k\lambda\bar{v}\hat{v}_\zeta^{(0)} + \hat{u}^{(0)} + k\lambda\hat{\delta}_\zeta^{(0)} = 0 \quad (6.7b)$$

$$\begin{aligned} \hat{\delta}_t^{(0)} + k\lambda\bar{v}\hat{\delta}_\zeta^{(0)} - \beta v_\infty \hat{u}^{(0)} + (1-\beta v_\infty \xi)\hat{u}_\xi^{(0)} \\ + k\lambda(1-\beta v_\infty \xi)\hat{v}_\zeta^{(0)} = 0 \end{aligned} \quad (6.7c)$$

(PLANAR FRONT, ORDER F_b^0)

$$\hat{u}_t^{(1)} + k\lambda\bar{v}\hat{u}_\zeta^{(1)} - \hat{v}^{(1)} + \hat{\delta}_\xi^{(1)} = -\bar{u}\hat{u}_\xi^{(0)} \quad (6.8a)$$

$$\hat{v}_t^{(1)} + k\lambda\bar{v}\hat{v}_\zeta^{(1)} + \hat{u}^{(1)} + k\lambda\hat{\delta}_\zeta^{(1)} = -\bar{u}\hat{v}_\xi^{(0)} \quad (6.8b)$$

$$\begin{aligned} \hat{\delta}_t^{(1)} + k\lambda\bar{v}\hat{\delta}_\zeta^{(1)} + \bar{\delta}_\xi^{(0)}\hat{u}^{(1)} + \bar{\delta}^{(0)}\hat{u}_\xi^{(1)} + k\lambda\bar{\delta}^{(0)}\hat{v}_\zeta^{(1)} \\ = -\bar{u}\hat{\delta}_\xi^{(0)} - \bar{\delta}^{(1)}\hat{u}_\xi^{(0)} - k\lambda\bar{\delta}^{(1)}\hat{v}_\zeta^{(0)} - k\lambda\bar{\delta}^{(1)}\hat{v}_\zeta^{(0)} \end{aligned} \quad (6.8c)$$

(PLANAR FRONT, ORDER F_b^1)

To order F_b^0 for the planar front, the basic state enters as nonconstant coefficients in the resulting perturbation equations. The lowest order system, however, is homogeneous, whereas the first order system is not, as a result of forcing by the lowest order terms. The lowest order solutions also appear as nonconstant coefficients in the first order system.

The corresponding systems of zeroth and first order equations for the exponential front, which are derived by using (6.6) in (6.2) and then eliminating the basic state velocities with (6.5), are as follows:

$$\hat{u}_t^{(0)} + k\lambda(\bar{\delta}_\xi^{(0)} + v_\infty)\hat{u}_\zeta^{(0)} - \hat{v}^{(0)} + \hat{\delta}_\xi^{(0)} = 0 \quad (6.9a)$$

$$\hat{v}_t^{(0)} + k\lambda(\bar{\delta}_\xi^{(0)} + v_\infty)\hat{v}_\zeta^{(0)} + (1 + \bar{\delta}_{\xi\xi}^{(0)})\hat{u}^{(0)} + k\lambda\hat{\delta}_\zeta^{(0)} = 0 \quad (6.9b)$$

$$\begin{aligned} \hat{\delta}_t^{(0)} + \bar{\delta}^{(0)}\hat{u}_\xi^{(0)} + k\lambda\bar{\delta}^{(0)}\hat{v}_\zeta^{(0)} + k\lambda(\bar{\delta}_\xi^{(0)} + v_\infty)\hat{\delta}_\zeta^{(0)} \\ + \bar{\delta}_\xi^{(0)}\hat{u}^{(0)} = 0 \end{aligned} \quad (6.9c)$$

(EXPONENTIAL FRONT, ORDER F_b^0)

$$\begin{aligned} \hat{u}_t^{(1)} + k\lambda(1 + v_\infty - \bar{\delta}^{(0)})\hat{u}_\zeta^{(1)} - \hat{v}^{(1)} + \hat{\delta}_\xi^{(1)} \\ = (1 - \bar{\delta}^{(0)})\hat{u}^{(0)} / \{\bar{\delta}^{(0)}\}^2 - \hat{u}_\xi^{(0)} / \bar{\delta}^{(0)} \end{aligned} \quad (6.10a)$$

$$\begin{aligned} \hat{v}_t^{(1)} + k\lambda(1 + v_\infty - \bar{\delta}^{(0)})\hat{v}_\zeta^{(1)} + \bar{\delta}^{(0)}\hat{u}^{(1)} + k\lambda\hat{\delta}_\zeta^{(1)} \\ = -\hat{v}_\xi^{(0)} / \bar{\delta}^{(0)} \end{aligned} \quad (6.10b)$$

$$\begin{aligned} \hat{\delta}_t^{(1)} + \bar{\delta}^{(0)}\hat{u}_\xi^{(1)} + k\lambda\bar{\delta}^{(0)}\hat{v}_\zeta^{(1)} + k\lambda(1 + v_\infty - \bar{\delta}^{(0)})\hat{\delta}_\zeta^{(1)} \\ + (1 - \bar{\delta}^{(0)})\hat{u}^{(1)} \\ = (1 - \bar{\delta}^{(0)})\hat{\delta}^{(0)} / \{\bar{\delta}^{(0)}\}^2 - \hat{\delta}_\xi^{(0)} / \bar{\delta}^{(0)} \end{aligned} \quad (6.10c)$$

(EXPONENTIAL FRONT, ORDER F_b^1)

As with the planar front, the lowest order system is homogeneous, while the first order system is not. Note that the coefficients in (6.10) have been simplified somewhat by using the basic state relations

$$\bar{\delta}_{\xi}^{(0)} = 1 - \bar{\delta}^{(0)} \quad (6.11a)$$

and
$$\bar{\delta}_{\xi\xi}^{(0)} = \bar{\delta}^{(0)} - 1 \quad (6.11b)$$

6.4 ZEROth ORDER HARMONIC SOLUTIONS

In order to simplify the notation, the caret will now be dropped from the perturbation variables. In addition, the lowest order exponential basic state interfacial depth, $\bar{\delta}^{(0)}$, will be denoted by τ ; i.e.

$$\tau(\xi) = \bar{\delta}^{(0)}(\xi) \quad , \quad (6.12)$$

where $\bar{\delta}^{(0)}$ is defined in (5.16). We now assume time and space harmonic solutions, as in Section 3.3, but only for the lowest order systems (6.7) and (6.9). Harmonic solutions to the first order systems (6.8) and (6.10) will be considered later and boundary conditions will be addressed in the next chapter.

Thus, we let

$$\hat{u}^{(0)} = X(\xi) \exp\{i(\zeta + \omega t)\} \quad (6.13a)$$

$$\hat{\varphi}^{(0)} = Y(\xi) \exp\{i(\zeta + \omega t)\} \quad (6.13b)$$

$$\hat{\delta}^{(0)} = Z(\xi) \exp\{i(\zeta + \omega t)\} \quad , \quad (6.13c)$$

where X , Y and Z are the (complex-valued) non-dimensional perturbation amplitudes for the x - and y -velocities, and the interfacial depth, respectively. Note that the time dependence assumed in Chapter 3 differs in sign from the one assumed here. ω is the dimensionless circular frequency of the disturbance, which is related to the dimensional frequency, Ω , by

$$\omega = \Omega/f \quad . \quad (6.14)$$

Using (6.13) in (6.7) and (6.9) reduces the system of PDE's in each case to the following systems of ODE's for the ξ -dependent perturbation amplitudes:

$$i\sigma X - Y + Z_{\xi} = 0 \quad (6.15a)$$

$$i\sigma Y + X + ik\lambda Z = 0 \quad (6.15b)$$

$$i\sigma Z + ik\lambda(1-\beta v_{\infty}\xi)Y - \beta v_{\infty}X + (1-\beta v_{\infty}\xi)X_{\xi} = 0 \quad (6.15c)$$

(PLANAR FRONT, ORDER F_b^0)

$$ig(\xi)X - Y + Z_{\xi} = 0 \quad (6.16a)$$

$$ig(\xi)Y + \tau X + ik\lambda Z = 0 \quad (6.16b)$$

$$ig(\xi)Z + ik\lambda\tau Y + (1-\tau)X + \tau X_{\xi} = 0 \quad (6.16b)$$

(EXPONENTIAL FRONT, ORDER F_b^0)

AD-A076 248

DELAWARE UNIV NEWARK COLL OF MARINE STUDIES

F/G 8/10

WAVELIKE BAROCLINIC DISTURBANCES ON SHALLOW UPPER OCEAN DENSITY--ETC(U)

MAR 79 R A FORMATO

N00014-78-C-0071

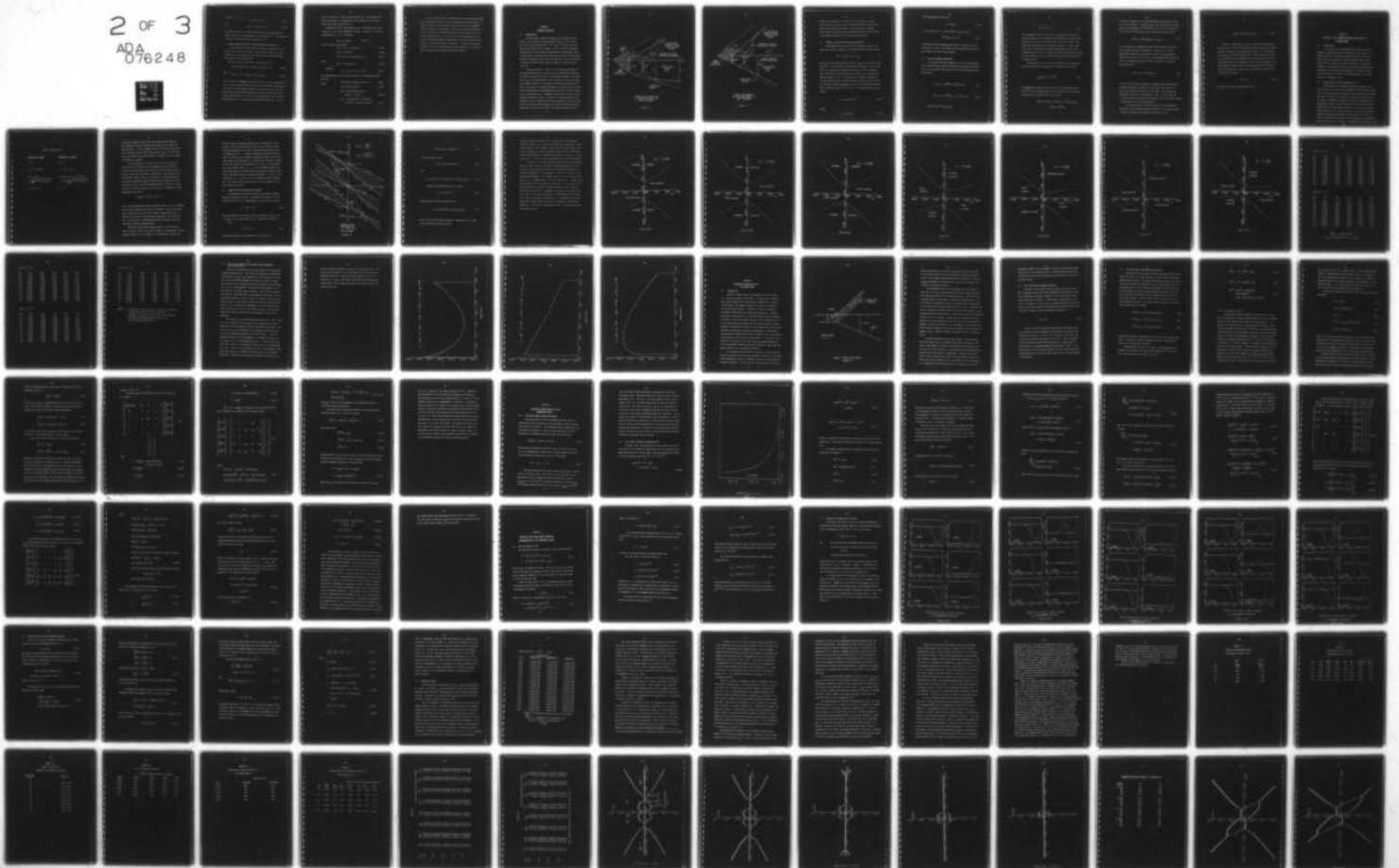
UNCLASSIFIED

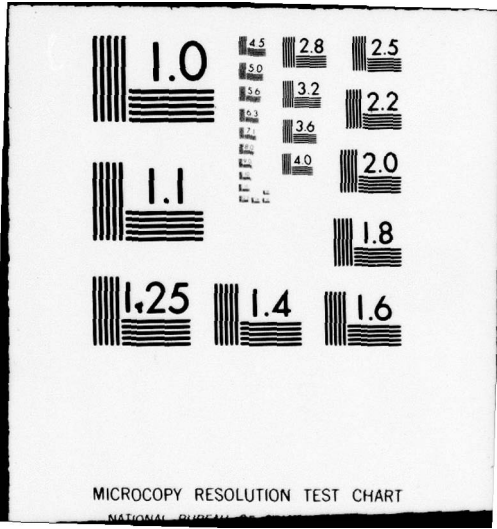
CMS-C-1-79

NL

2 OF 3

ADA
076248





MICROCOPY RESOLUTION TEST CHART

NATIONAL BUREAU OF STANDARDS

in which

$$\sigma = \omega + k\lambda(1-\beta)v_{\infty} \quad (6.17)$$

and

$$g(\xi) = \omega + k\lambda\{1+v_{\infty}^{-1}\tau(\xi)\} \quad (6.18)$$

For the planar front, σ is the non-dimensional Doppler shifted frequency, and $g(\xi)$ is the exponential front analogue of σ . The subscript ξ denotes a total derivative with respect to ξ .

6.5 ZEROth ORDER ODE'S FOR THE DEPTH PERTURBATION AMPLITUDE

A single equation for the depth perturbation amplitude, $Z(\xi)$, is derived from (6.15) for the planar front and from (6.16) for the exponential front by eliminating the velocity perturbation amplitudes, $X(\xi)$ and $Y(\xi)$, from these systems.

The planar front result, which follows directly, is

$$(\beta v_{\infty} \xi - 1)(d^2 Z/d\xi^2) + \beta v_{\infty} (dZ/d\xi) + A(\xi)Z(\xi) = 0, \quad (6.19)$$

where

$$A(\xi) = 1 - \sigma^2 + k\lambda\beta v_{\infty}/\sigma + (k\lambda)^2(1-\beta v_{\infty}\xi). \quad (6.20)$$

(6.19) is linear, homogeneous, second order in $Z(\xi)$, and independent of u_{∞} . The cross-stream flow does not enter the perturbation dynamics nor, as we will see, the boundary conditions to lowest order in F_b for the planar front, and therefore contributes nothing to the system's stability characteristics. If (6.19) is redimensionalized, the equations developed earlier for the depth perturbation amplitude, viz., (3.12)

and (4.2) with $F_x = 0$, are recovered identically. The analysis presented in Chapter 3 is therefore directly applicable to the lowest order planar front equation for Z.

Uncoupling (6.16) is more involved, but is facilitated by transforming to τ as the new independent variable. Viewing X, Y and Z now as functions of τ , not ξ , we obtain

$$d/d\xi = (1-\tau)(d/d\tau) \quad , \quad \text{and so on,}$$

and the system (6.16) becomes

$$i\eta\tau X - \tau Y + \tau(1-\tau)(dZ/d\tau) = 0 \quad (6.21a)$$

$$i\eta Y + \tau X + ik\lambda Z = 0 \quad (6.21b)$$

$$i\eta Z + ik\lambda\tau Y + (1-\tau)\{d(\tau X)/d\tau\} = 0 \quad , \quad (6.21c)$$

where

$$\eta(\tau) = \omega + k\lambda(1+v_\infty - \tau) \quad . \quad (6.21d)$$

Defining

$$f(\eta) = \omega/k\lambda + 1 + v_\infty - \eta/k\lambda \quad , \quad (6.22)$$

and eliminating X and Y from (6.21) leads to the following equation

for Z(n):

$$A(d^2Z/d\eta^2) + B(dZ/d\eta) + CZ(\eta) = 0, \quad (6.23)$$

where

$$A(\eta) = \eta^2 f(f-\eta^2)(f-1)^2 \quad (6.24a)$$

$$B(\eta) = \eta^2(1-f)\{\eta^2(1-2f)/k\lambda + 2\eta f(1-f) + f^2/k\lambda\} \quad (6.24b)$$

$$C(\eta) = (1-f)\{f(f-\eta^2) - \eta^2(\eta/k\lambda + 2f)\} + f(\eta^2 - f) + (\eta^2 - f)^2 \{f - (\eta/k\lambda)^2\} \quad . \quad (6.24c)$$

As for the planar front, the depth perturbation amplitude equation for the exponential front is linear, homogeneous and second order. We again note that the cross-stream flow does not enter the exponential front's dynamics to lowest order. Since we are primarily interested in the influence of the cross-stream flow on the frontal zone's stability characteristics, it is now clear that an examination of the zeroth-order dynamics alone is inadequate. The cross-stream flow has, at most, a first order effect on stability. In subsequent chapters, therefore, the first order dynamics will be developed, and attention will be focused on the attendant dispersion relation.

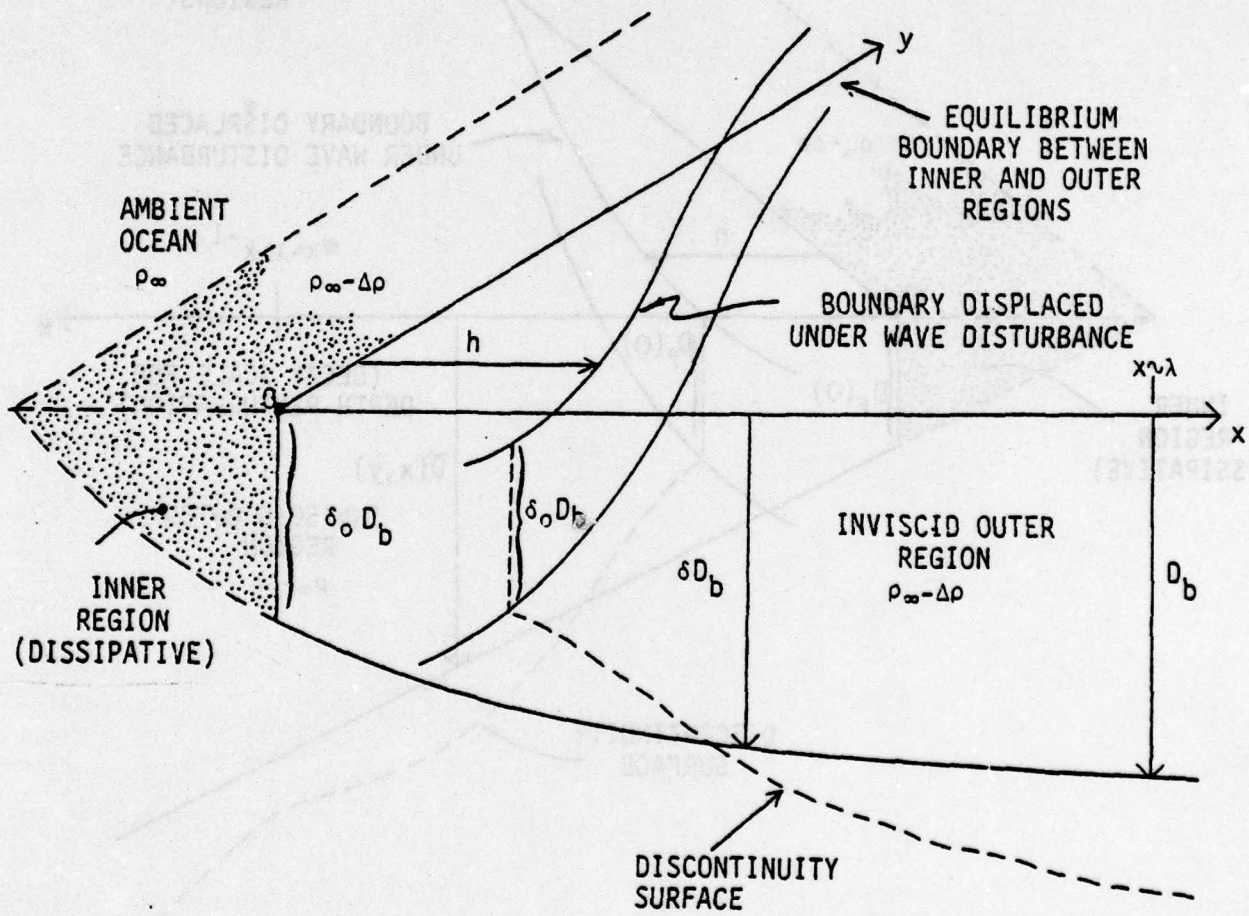
CHAPTER 7

BOUNDARY CONDITIONS

7.1 INTRODUCTION

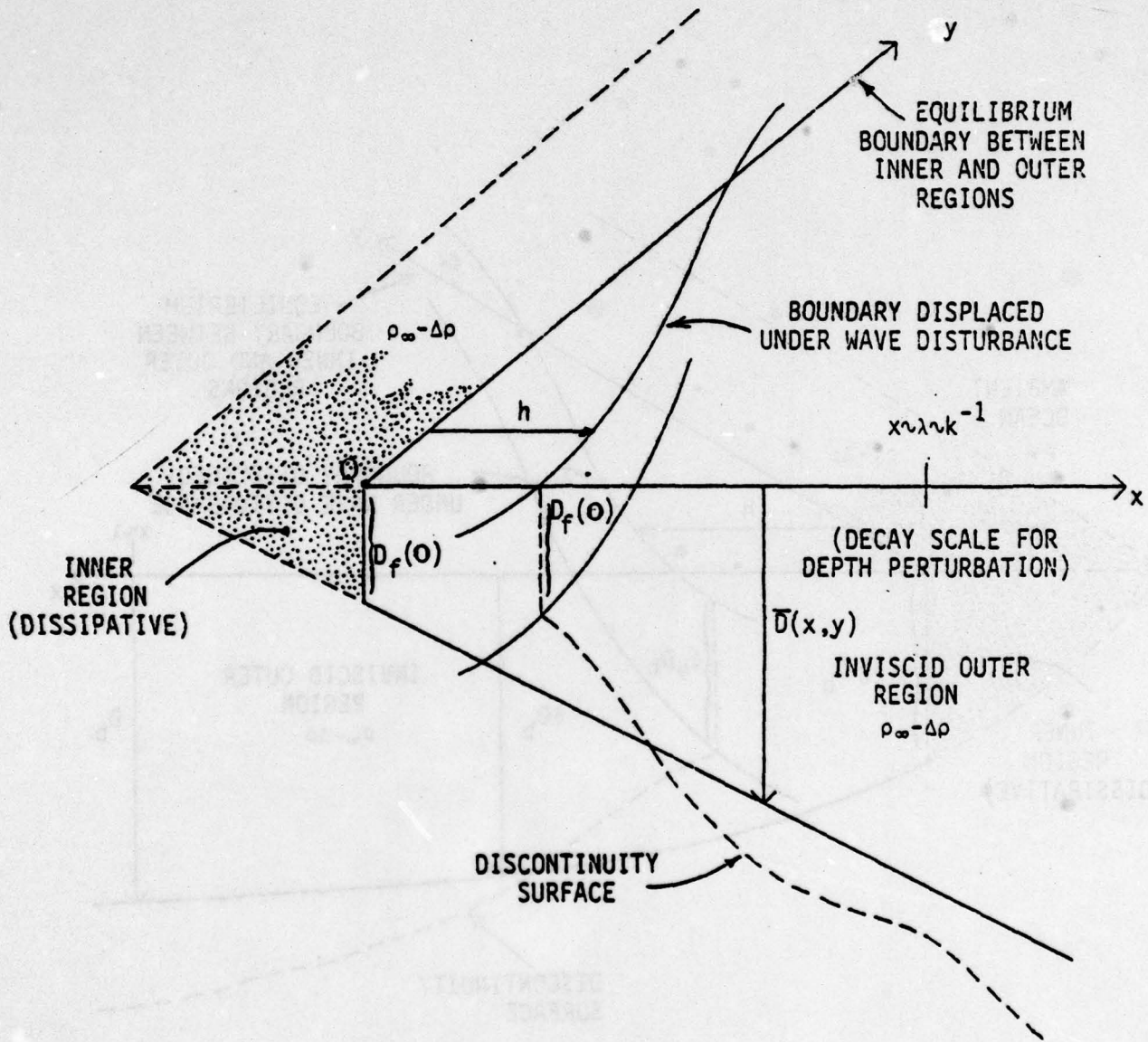
In this chapter, boundary conditions are formulated for the lowest order perturbation amplitudes $X(\xi)$, $Y(\xi)$ and $Z(\xi)$, and for the first order perturbations $\hat{u}^{(1)}$, $\hat{v}^{(1)}$ and $\hat{\delta}^{(1)}$ for both the exponential and planar fronts. Figures 7.1 and 7.2 show the simplified exponential and planar frontal zone geometries, respectively, under the influence of a wavelike disturbance that distorts the equilibrium boundary separating the inner and outer regions. With no disturbance, the surface boundary between these two regions is contained in the plane $x=0$.

As shown in Figures 7.1 and 7.2, the surface displacement of the equilibrium boundary is denoted $h(y,t)$ in dimensional variables. For small perturbations, $|h|/\lambda \ll 1$. The interfacial depth in the plane $x=0$ is $\delta_0 D_b$ for the exponential front, and $D_f(0)$ for the planar front. The boundary condition on the lowest order depth perturbation amplitude Z is derived by invoking the kinematic restriction that the interfacial depth beneath the displaced inner-outer region boundary remain at its equilibrium value, a reasonable restriction as long as the perturbation amplitude is small. In addition to being plausible, this condition may be formulated rigorously by taking only the lowest order term in the Taylor series expansion for the time-varying interfacial depth about its basic state value. The boundary condition on the



FRONTAL ZONE GEOMETRY FOR THE EXPONENTIAL FRONT WITH WAVE DISTURBANCE

FIGURE 7.1



FRONTAL ZONE GEOMETRY
FOR THE PLANAR FRONT WITH
WAVE DISTURBANCE

FIGURE 7.2

x-velocity perturbation is derived from the kinematic condition that the normal velocity across the boundary between the inner and outer regions must be continuous. We also require no velocity shear across the boundary in the long-stream direction, which leads to a boundary condition on the y-velocity perturbation.

7.2 BOUNDARY CONDITION ON THE DEPTH PERTURBATION

The kinematic restriction that the interfacial depth at the inner-outer boundary remains at its equilibrium value may be written

$$\bar{\delta}(h) + \hat{\delta}\{h(\zeta, t), \zeta, t\} = \bar{\delta}_{eq} \quad , \quad (7.1)$$

where $\bar{\delta}_{eq} = \delta_0$ for the exponential front and $\bar{\delta}_{eq} = 1$ for the planar front. Note that (7.1) is written in dimensionless variables, that is, with $h^* = h/\lambda$ and subsequently dropping the asterisk. $\bar{\delta}(h)$ is the basic state interfacial depth evaluated at $\xi = h$, that is, at the displaced surface boundary. (7.1) is translated into boundary conditions on the depth perturbations to lowest and first orders in F_b by substituting the small parameter expansions in (6.6) and invoking the approximations $Z(h) \approx Z(0)$ and $e^{-h} \approx (1-h)$ for $h \ll 1$. To lowest order in F_b , we obtain

$$h = h_0 \exp\{i(\zeta + \omega t)\} \quad , \quad (7.2a)$$

where

$$h_0 = Z(0)/(\delta_0 - 1) \quad (7.2b)$$

for the exponential front, and

$$h_0 = Z(0)/\beta v_\infty \quad (7.2c)$$

for the planar front. At first order in F_b , we obtain

$$\hat{\delta}^{(1)}\{h(\zeta, t), \zeta, t\} = 0 \quad (7.3)$$

for both the planar and exponential fronts. Condition (7.3) requires that the first order depth perturbation amplitude vanish in both cases at the inner-outer boundary.

7.3 VELOCITY BOUNDARY CONDITIONS

If the small parameter expansions in (6.6) are substituted into the perturbation variable decomposition introduced in Section 6.2, the lowest order flow field for $\xi \geq h$ in the exponential front case becomes

$$u(\xi, \zeta, t) = 1/\bar{\delta}^{(0)}(\xi) + \hat{u}^{(0)}(\xi, \zeta, t) \quad (7.4a)$$

$$v(\xi, \zeta, t) = 1 - \bar{\delta}^{(0)}(\xi) + v_\infty + \hat{v}^{(0)}(\xi, \zeta, t) \quad (7.4b)$$

To first order in F_b , we have

$$\hat{u}^{(1)} = \hat{v}^{(1)} = 0 \quad (7.5)$$

as a consequence of only even powers of F_b appearing in the small parameter expansion of the exponential basic state interfacial depth. Condition (7.5) is found to apply also for the planar front, since there the equilibrium flow is spatially invariant. At first order in F_b , then, the velocity perturbation amplitudes in the x- and y-directions must be zero for both the planar and exponential fronts. At zeroth order, of course, the velocity perturbations are not zero, as discussed next.

The restriction that the normal velocity at the boundary between the inner and outer regions be continuous may be written

$$\lim_{x \rightarrow h} \frac{D}{Dt} (x-h) = \bar{u}^{(0)}(0) \quad (7.6)$$

in dimensional variables, where D/Dt is the convective derivative and $\bar{u}^{(0)}(0)$ is the equilibrium x-velocity evaluated at the boundary. Expanding (7.6) to lowest order in F_b yields

$$\begin{aligned} \bar{u}^{(0)}(h) + \hat{u}^{(0)}(h) - \{\bar{v}^{(0)}(h) + \hat{v}^{(0)}(h)\}(\partial h / \partial y) \\ - (\partial h / \partial t) = \bar{u}^{(0)}(0) \end{aligned} ,$$

in which all velocities on the left-hand-side are evaluated at $x=h$, i.e., at the boundary. The basic state terms involving \bar{u} are eliminated by the approximation $\bar{u}^{(0)}(h) \approx \bar{u}^{(0)}(0)$ for $|h|/\lambda \ll 1$, and the second order term $\hat{v}^{(0)}(h) \partial h / \partial y$ may be neglected altogether, giving

$$\hat{u}^{(0)}(h) - \bar{v}^{(0)}(h) (\partial h / \partial y) - (\partial h / \partial t) = 0 \quad (7.7)$$

(7.7) constitutes the fundamental zeroth order boundary condition on the x-velocity perturbation amplitude. Rewriting (7.7) in non-dimensional variables in accordance with (6.1), substituting the explicit form for $h(\zeta, t)$ in (7.2a,b), approximating $X(h)$ by $X(0)$ for $|h| \ll 1$, and neglecting terms of order h compared to 1 yields the following result:

$$X(0) = ih_0 \{ \omega + k\lambda(v_\infty + \delta_0 - 1) \} \quad (7.8)$$

(7.8), written in scaled variables, provides the connection between the depth perturbation amplitude at the origin, $Z(0)$, and the x-velocity perturbation amplitude at the origin, $X(0)$, through the displacement amplitude h_0 appearing in (7.2b). We note that, for a fixed disturbance frequency and wavelength, $X(0)$ and $Z(0)$ are directly proportional, but in phase quadrature.

For the planar front, we follow exactly the same procedure and arrive at the following boundary condition on the (dimensionless) x-velocity perturbation amplitude to lowest order in F_b :

$$X(0) = ih_0 \{ \omega + k\lambda(1-\beta)v_\infty \} \quad (7.9)$$

Again to lowest order in F_b , we require for the long-stream velocity that no velocity shear exist across the inner-outer region boundary, although a long-stream velocity shear can exist between the frontal zone and the ambient ocean. This restriction is physically realistic for small amplitude wave disturbances, and may be justified rigorously by performing a Taylor series expansion of the time-varying y -velocity about its equilibrium value and retaining only the leading term. Therefore, as a boundary condition on $Y(\xi)$ at order F_b^0 , we require

$$Y(0) = 0 \quad (7.10)$$

for both the planar and exponential fronts.

CHAPTER 8

ANALYSIS OF THE EXPONENTIAL FRONT EQUATION FOR $Z(\eta)$ TO LOWEST ORDER

8.1 INTRODUCTION

In this chapter, the exponential front depth perturbation amplitude equation (6.23) will be analyzed in some detail. Its singular points in τ -space and η -space are located, the asymptotic form of the solution far from the surface front is presented, and the condition for stable solutions at infinity is developed. The equation for $Z(\eta)$ is then integrated numerically, and several of the resulting mode shapes are discussed. Recall that the analysis of the planar front DPA equation, (6.19), was performed in Chapters 3 and 4.

8.2 SINGULAR POINTS OF THE EQUATION FOR $Z(\eta)$

Singularities in the depth perturbation amplitude, $Z(\eta)$, occur at most at the zeros of the polynomial $A(\eta)$ in (6.24a). Since $A(\eta)$ is presented in factored form, its zeros are readily determined and appear in Table 8.1. Recall that the domain of definition of the original independent variable ξ is $0 \leq \xi < \infty$. Transforming to the independent variable τ maps the interval $0 \leq \xi < \infty$ into the interval $\delta_0 \leq \tau \leq 1$, while the transformation from τ to η in (6.23) maps the domain of definition for τ into an interval in η -space with variable endpoints whose locations depend on the values of ω , $\kappa\lambda$ and V_∞ . Since, in general, the locations of the singular points also depend upon the values of ω , $\kappa\lambda$ and V_∞ , a determination of whether or not

TABLE 8.1 ZEROS OF A(η)LOCATION IN η -SPACELOCATION IN τ -SPACE

$$\eta_0 = 0$$

$$\tau_0 = 0$$

$$\eta_1 = \omega + k\lambda(v_\infty + 1)$$

$$\tau_1 = \omega/k\lambda + v_\infty + 1$$

$$\eta_{3,2} = -1/2k\lambda$$

$$\tau_{2,3} = \omega/k\lambda + v_\infty + 1 + 1/2(k\lambda)^2$$

$$\pm \frac{1}{2} \sqrt{1/(k\lambda)^2 + 4(\omega/k\lambda + v_\infty + 1)}$$

$$\pm (1/2k\lambda) \sqrt{1/(k\lambda)^2 + 4(\omega/k\lambda + v_\infty + 1)}$$

$$\eta_4 = \omega + k\lambda v_\infty$$

$$\tau_4 = 1$$

a particular singular point lies in the domain of definition of the independent variable is most easily made when the domain has fixed endpoints. For this reason, Table 8.1 includes the locations of the singular points in both η -space and τ -space. We will hereafter deal almost exclusively with the τ variable, since its domain of definition is fixed.

If the parameters ω , $\kappa\lambda$ and V_∞ are such that the $\tau_i \neq \tau_j$ in Table 8.1 for $i \neq j$, that is, if the singular points are distinct, then the ratios $B(\eta)/A(\eta)$ and $C(\eta)/A(\eta)$ in (6.24) possess poles of, at most, first and second order, respectively. Each singular point is therefore regular if the τ_i are distinct. Irregular singularities, and the attendant analytical difficulties, result from the coalescence of two or more of the singular points in Table 8.1, which can occur for certain values of ω , $\kappa\lambda$ and V_∞ . For example, if these quantities are such that

$$1/(\kappa\lambda)^2 = -4(\omega/\kappa\lambda + v_\infty + 1) ,$$

the two otherwise distinct regular singular points τ_2 and τ_3 coalesce into a single singular point which is irregular. Since the development of analytical solutions near irregular singular points is, in general, very difficult, we will require hereafter that all five of the τ_i are distinct, thereby insuring regular singular points for the depth perturbation amplitude ODE.

Physically significant singular behavior in the solution Z must, of course, occur in the interval $0 \leq \xi \leq \infty$, or, equivalently, $\delta_0 \leq \tau \leq 1$. Singular behavior in Z for values of the independent variable out-

side this range is physically meaningless and consequently of no concern. The fixed singular point $\tau_0=0$ is thus irrelevant, while the fixed singular point $\tau_4=1$ is of considerable importance, since it corresponds to $\xi=\infty$. It thereby determines the nature of the solution at infinity in the original x -coordinate system. The ODE for Z thus admits the possibility of a solution that "blows up" at infinity for some values of the parameters ω , $\kappa\lambda$ and V_∞ . At the remaining three singular points, τ_1 , τ_2 , and τ_3 , divergent solutions for Z are also possible, but these points may be placed outside the physically significant interval by suitably choosing ω , $\kappa\lambda$ and V_∞ . The locations of τ_1 , τ_2 and τ_3 in the $\kappa\lambda$ - ω plane are shown in Figure 8.1. The nature of the solution near $\tau_4=1$ will be examined in detail in the next section.

8.3 BEHAVIOR OF THE SOLUTION NEAR INFINITY

Since physically acceptable solutions must exhibit regular behavior at infinity, we wish to investigate the nature of the solution to (6.23) as $\xi \rightarrow \infty$, or, equivalently, $\mu \rightarrow 1$ and $\eta \rightarrow \kappa\lambda(\mu-1)$, where

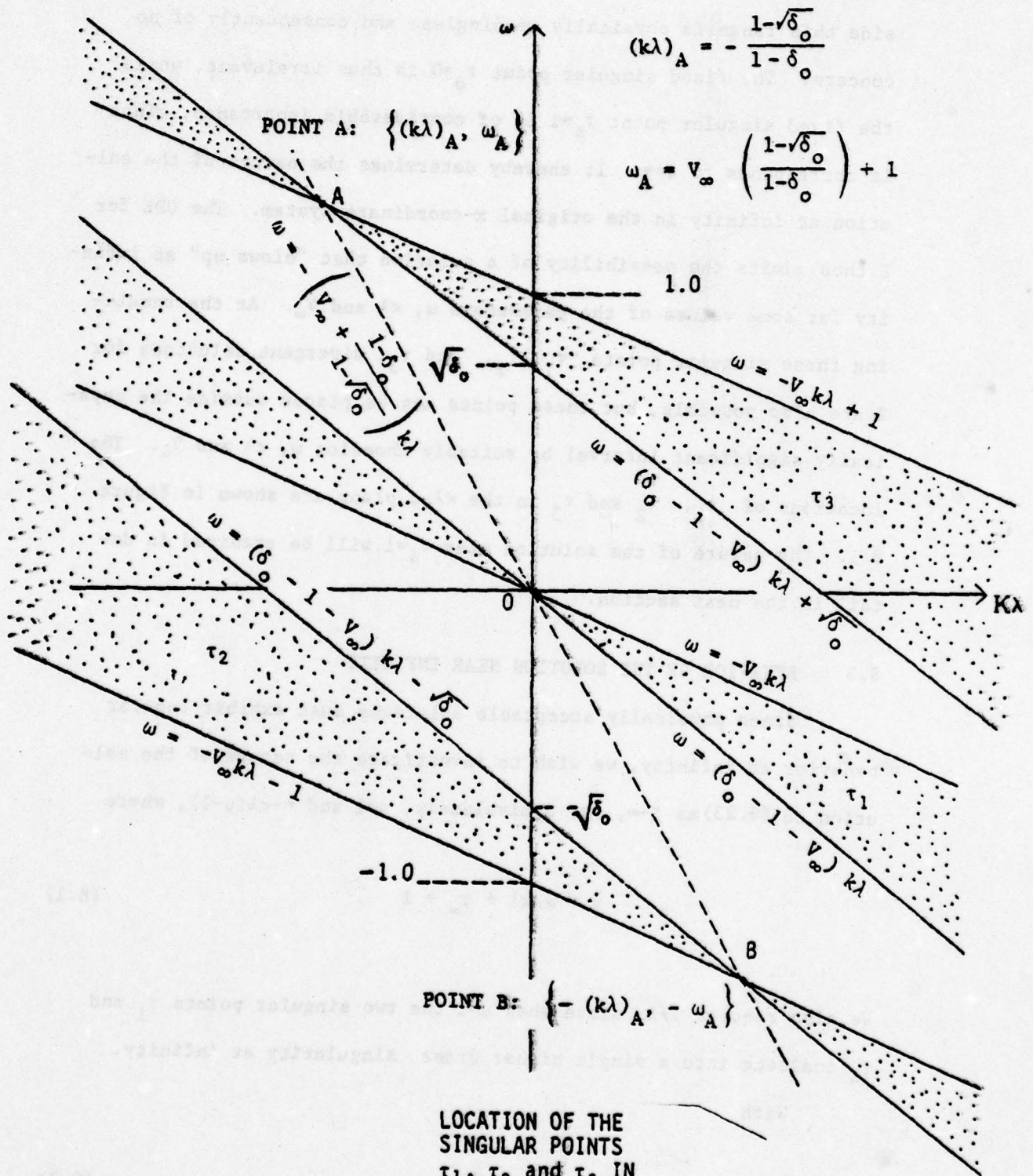
$$\mu = \omega/\kappa\lambda + v_\infty + 1 \quad . \quad (8.1)$$

We also require $\mu \neq 1$, since when $\mu=1$ the two singular points τ_1 and τ_4 coalesce into a single higher order singularity at infinity.

With

$$s = 1 + \eta/\kappa\lambda - \mu \quad , \quad (8.2)$$

the problem reduces to an examination of the solution to



LOCATION OF THE SINGULAR POINTS τ_1, τ_2 and τ_3 IN THE $k\lambda-\omega$ PLANE

FIGURE 8.1

$$s^2 Z_{ss} + s Z_s + (d/a)Z(s) = 0 \quad (8.3)$$

as $s \rightarrow 0$ from above, where

$$a = (1-\mu)^2 \{1 - (k\lambda)^2 (1-\mu)^2\} \quad (8.4)$$

and

$$d = (k\lambda)^2 (1-\mu)^2 + \{(k\lambda)^2 (1-\mu)^2 - 1\}^2 \{1 - (1-\mu)^2\} - 1. \quad (8.5)$$

Under the transformation $s = e^t$, we obtain

$$Z_{tt} + (d/a)Z(t) = 0, \quad (8.6)$$

whose solution is written immediately as

$$Z = A \exp\{(-d/a)^{1/2} t\} + B \exp\{-(-d/a)^{1/2} t\}, \quad (8.7)$$

where A and B are arbitrary constants. Rewriting (8.7) in terms of the original ξ -coordinate yields

ating the domain of allowable $(\kappa\lambda, \omega)$ values from that in which divergent solutions exist. Since the disturbance wavelength on a large scale oceanic front is generally larger than the Rossby radius, that is, $\kappa\lambda < 1$ typically, (8.10) and Figure 8.2 show that the disturbance periods will generally be longer than the inertial period, or, equivalently, $\omega < 1$. In other words, we anticipate sub-inertial frequencies.

In Table 8.2, the exact dispersion relation for the exponential front at lowest order in F_b , which is developed analytically in Section 10.1, has been used to tabulate the disturbance frequency for various combinations of the parameters δ_0 and V_∞ as a function of the normalized wavenumber $\kappa\lambda$. V_∞ ranges from 0.1 to 0.5 in steps of 0.1, as does δ_0 . $\kappa\lambda$ ranges from 0.1 to 1.9 in steps of 0.1. Entries carrying a superscript "a" correspond to values of ω , $\kappa\lambda$ and V_∞ which violate the stability criterion at infinity given in (8.9). Entries carrying a superscript "b" correspond to parameter values that place one or more of the singular points of the DPA equation in the interval $\delta_0 \leq \tau \leq 1$, as discussed in Section 8.2. An examination of the tabulated results again clearly shows that the system is sub-inertially dominated. In no case is an allowable value of the disturbance frequency greater than 1.

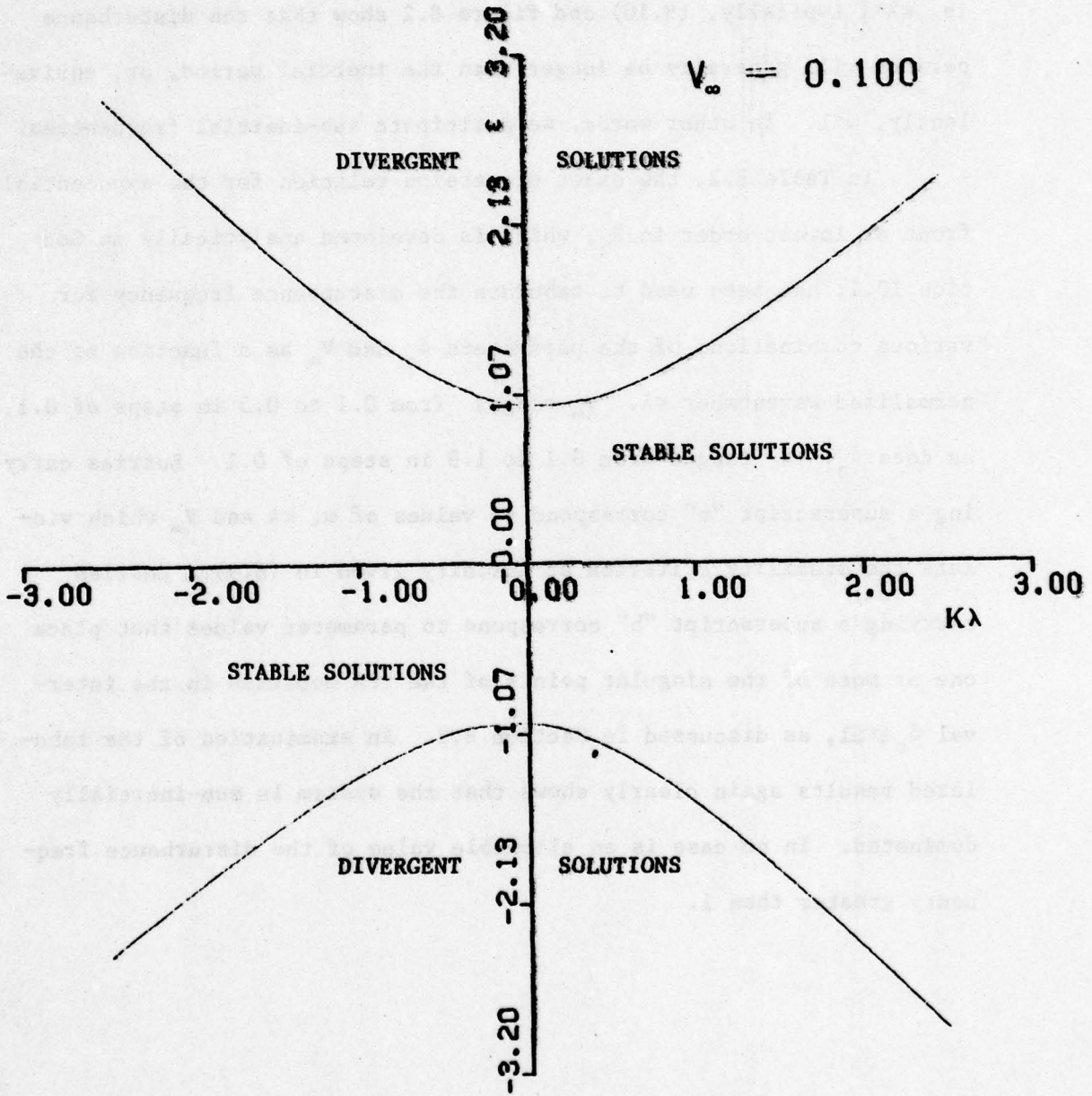


Figure 8.2(a)

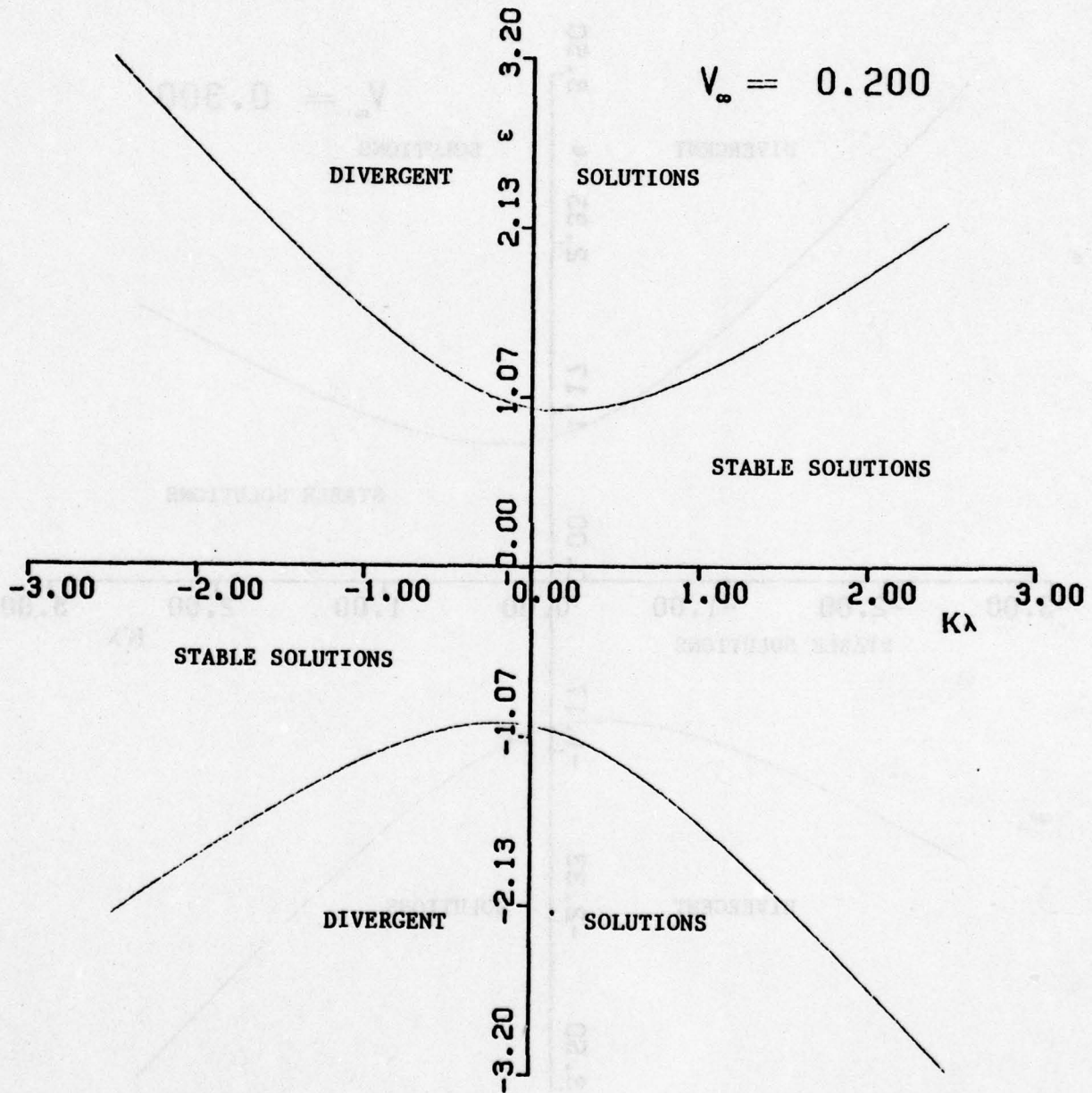


Figure 8.2(b)

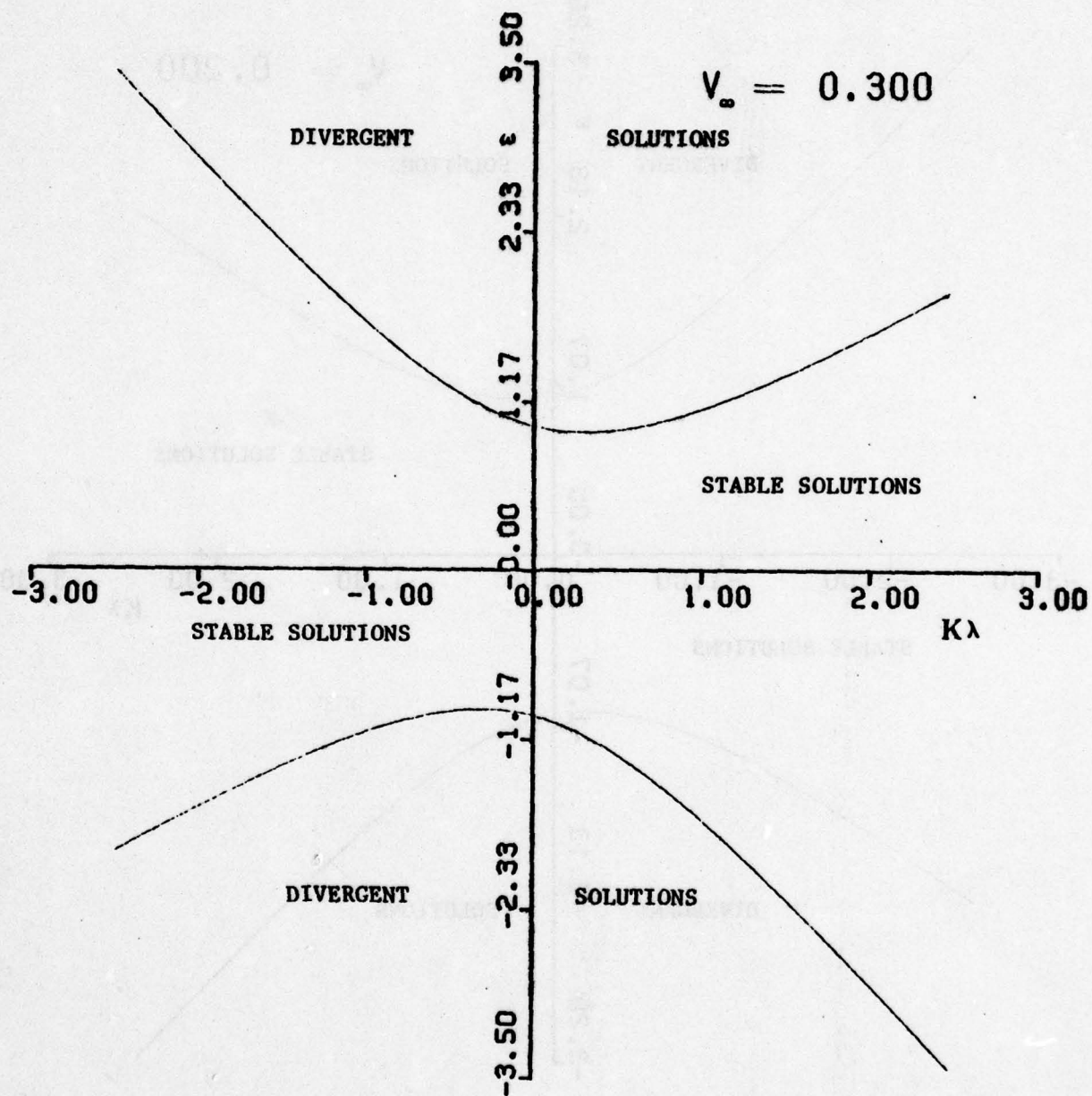


Figure 8.2(c)

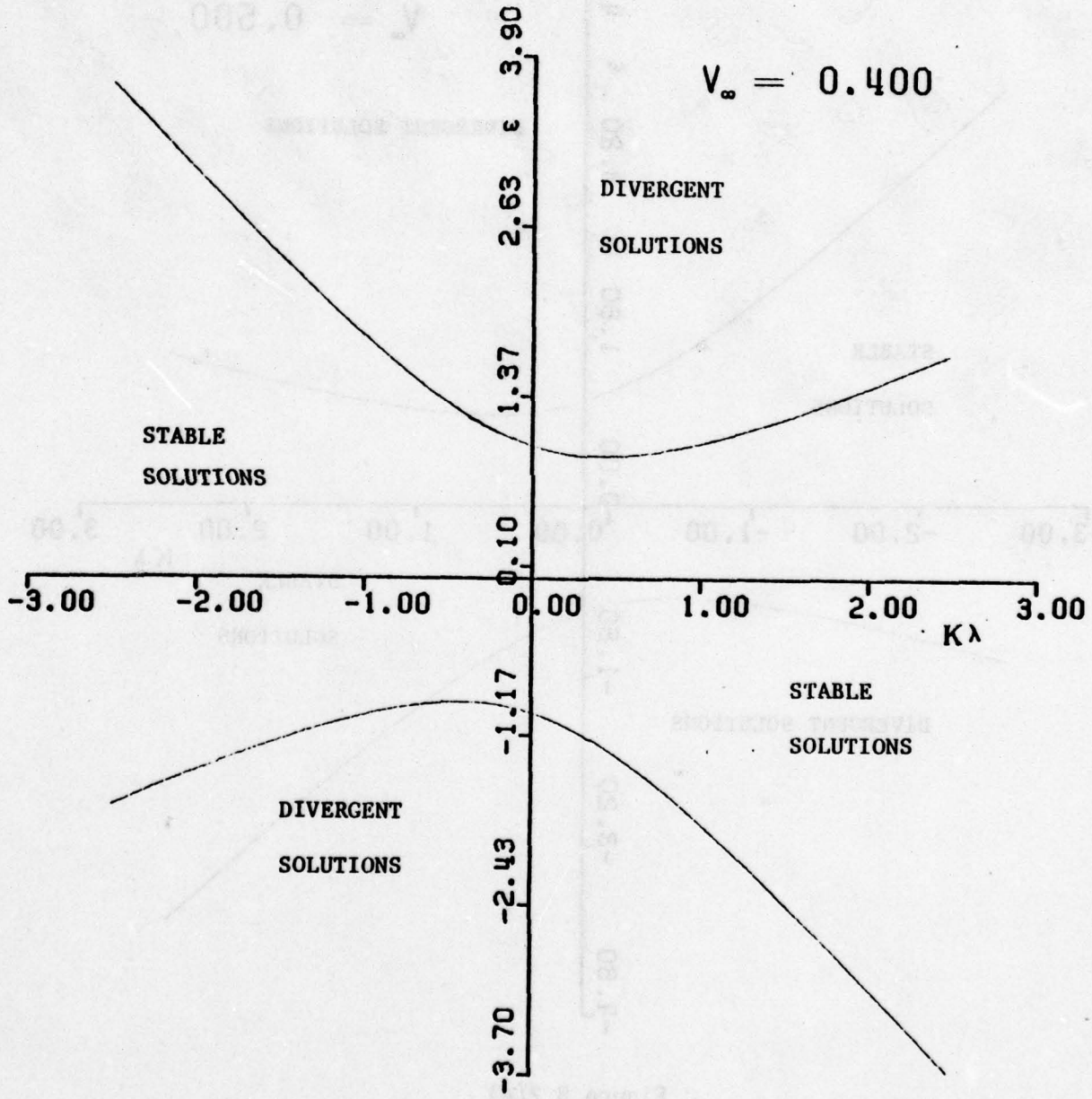


Figure 8.2(d)

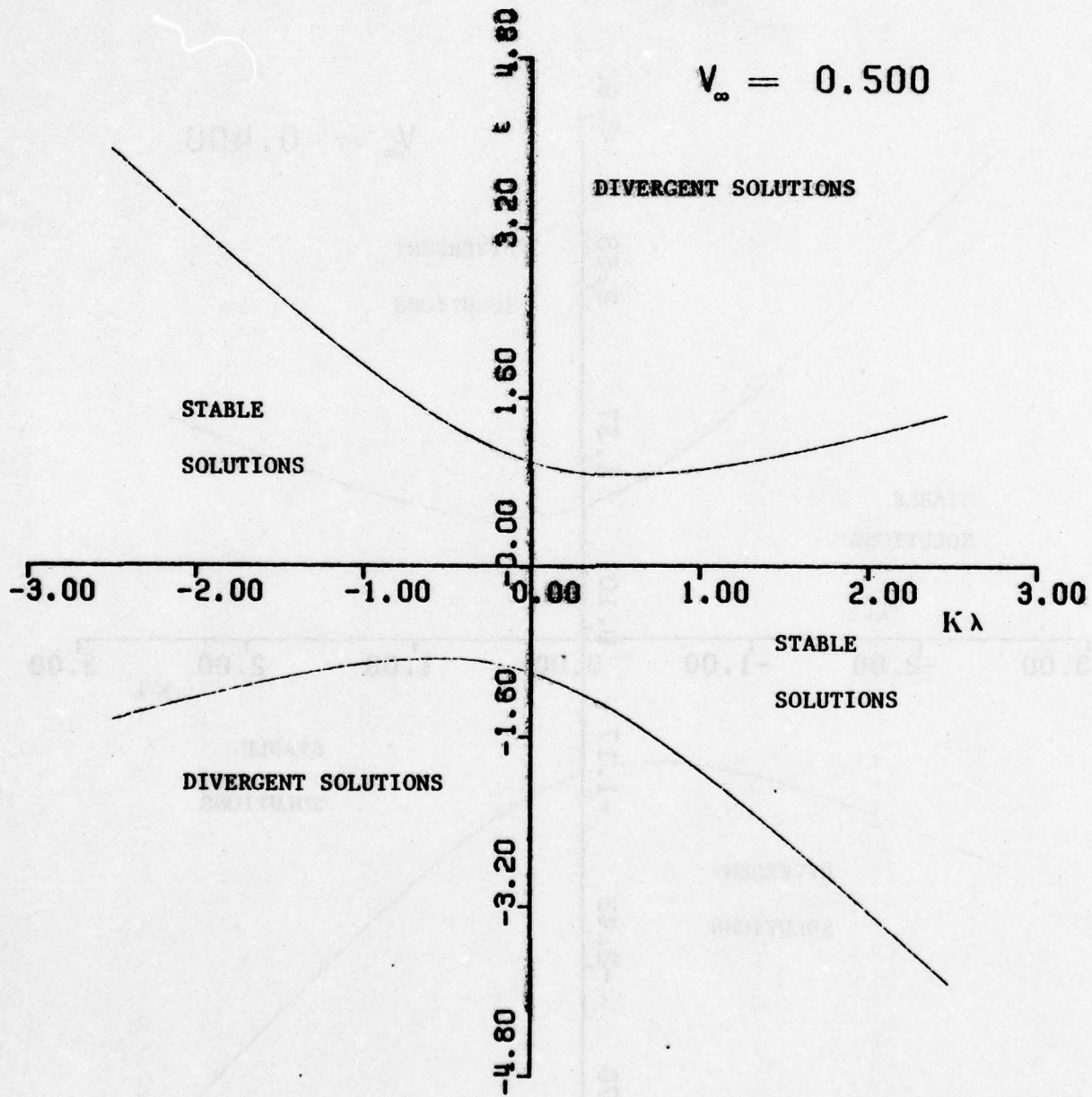


Figure 8.2(e)

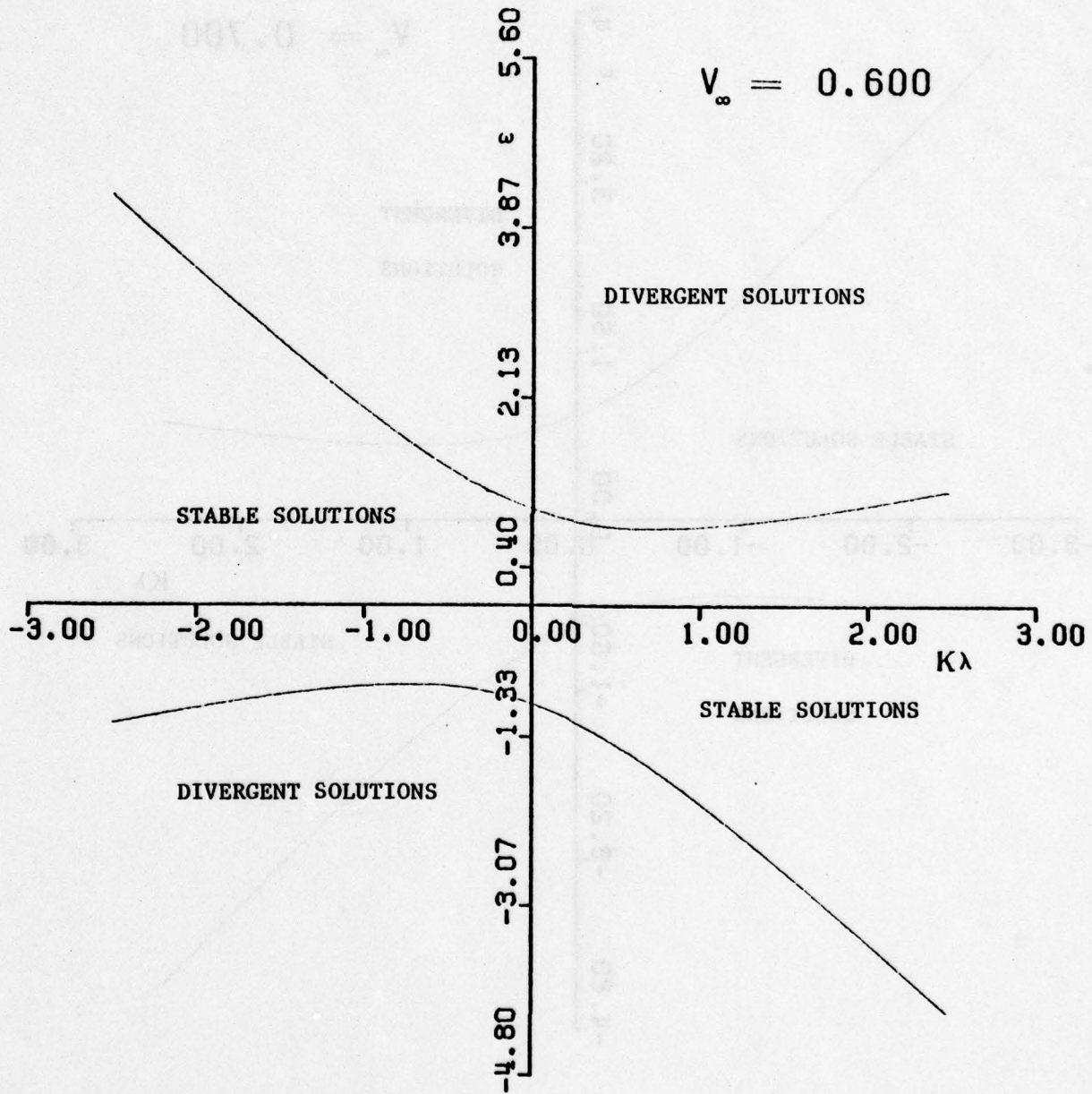


Figure 8.2(f)

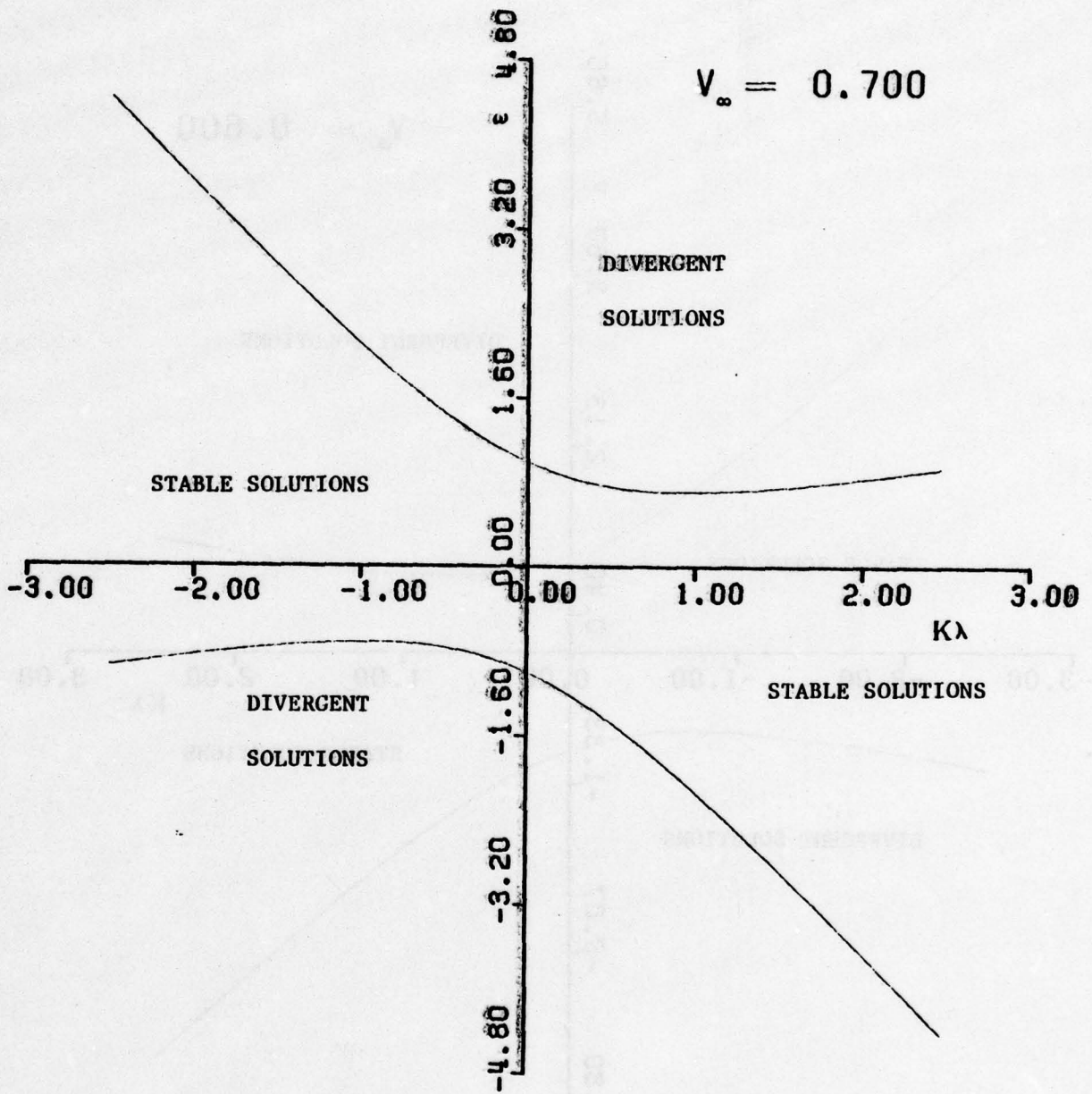


Figure 8.2(g)

Case 1: $V_\infty = 0.1$

$\kappa\lambda$	0.1	0.2	0.3	0.4	0.5
0.1	0.98 ^b	0.47 ^b	0.29	0.20	0.14
0.3	2.94 ^a	1.41 ^a	0.88 ^b	0.60 ^b	0.42
0.5	4.90 ^a	2.35 ^a	1.47 ^a	1.00	0.70 ^b
0.7	6.86 ^a	3.29 ^a	2.05 ^a	1.40 ^a	0.98
0.9	8.82 ^a	4.23 ^a	2.64 ^a	1.80 ^a	1.26 ^a
1.1	10.78 ^a	5.17 ^a	3.23 ^a	2.20 ^a	1.54 ^a
1.3	12.74 ^a	6.11 ^a	3.81 ^a	2.60 ^a	1.82 ^a
1.5	14.70 ^a	7.05 ^a	4.40 ^a	3.00 ^a	2.10 ^a
1.7	16.66 ^a	7.99 ^a	4.99 ^a	3.40 ^a	2.38 ^a
1.9	18.62 ^a	8.93 ^a	5.57 ^a	3.80 ^a	2.66 ^a

Case 2: $V_\infty = 0.2$

$\kappa\lambda$	0.1	0.2	0.3	0.4	0.5
0.1	0.97 ^b	0.46 ^b	0.28	0.19	0.13
0.3	2.91 ^a	1.38 ^a	0.85 ^b	0.57 ^b	0.39
0.5	4.85 ^a	2.30 ^a	1.42 ^a	0.95	0.65 ^b
0.7	6.79 ^a	3.22 ^a	1.98 ^a	1.33 ^a	0.91
0.9	8.73 ^a	4.14 ^a	2.55 ^a	1.71 ^a	1.17 ^a
1.1	10.67 ^a	5.06 ^a	3.12 ^a	2.09 ^a	1.43 ^a
1.3	12.61 ^a	5.98 ^a	3.68 ^a	2.47 ^a	1.69 ^a
1.5	14.55 ^a	6.90 ^a	4.25 ^a	2.85 ^a	1.95 ^a
1.7	16.49 ^a	7.82 ^a	4.85 ^a	3.23 ^a	2.21 ^a
1.9	18.43 ^a	8.74 ^a	5.38 ^a	3.61 ^a	2.27 ^a

TABLE 8.2 Computed Values

of ω for Various Values of $\kappa\lambda$, δ_0 and V_∞

Case 3: $V_{\infty} = 0.3$

$\kappa\lambda$	<u>0.1</u>	<u>0.2</u>	<u>0.3</u>	<u>0.4</u>	<u>0.5</u>
0.1	0.96 ^b	0.45 ^b	0.27	0.18	0.12
0.3	2.88 ^a	1.35 ^a	0.82 ^b	0.54 ^b	0.36
0.5	4.80 ^a	2.25 ^a	1.37 ^a	0.90	0.60 ^b
0.7	6.72 ^a	3.15 ^a	1.91 ^a	1.26 ^a	0.84
0.9	8.64 ^a	4.05 ^a	2.46 ^a	1.62 ^a	1.08 ^a
1.1	10.56 ^a	4.95 ^a	3.01 ^a	1.98 ^a	1.32 ^a
1.3	12.48 ^a	5.85 ^a	3.55 ^a	2.34 ^a	1.56 ^a
1.5	14.40 ^a	6.75 ^a	4.10 ^a	2.70 ^a	1.80 ^a
1.7	16.32 ^a	7.65 ^a	4.65 ^a	3.06 ^a	2.04 ^a
1.9	18.24 ^a	8.55 ^a	5.19 ^a	3.42 ^a	2.28 ^a

Case 4: $V_{\infty} = 0.4$

$\kappa\lambda$	<u>0.1</u>	<u>0.2</u>	<u>0.3</u>	<u>0.4</u>	<u>0.5</u>
0.1	0.95 ^b	0.44 ^b	0.26	0.17	0.11
0.3	2.85 ^a	1.32 ^a	0.79 ^b	0.51 ^b	0.33
0.5	4.75 ^a	2.20 ^a	1.32 ^a	0.85	0.55 ^b
0.7	6.65 ^a	3.08 ^a	1.84 ^a	1.19 ^a	0.77
0.9	8.55 ^a	3.96 ^a	2.37 ^a	1.53 ^a	0.99 ^a
1.1	10.45 ^a	4.84 ^a	2.90 ^a	1.87 ^a	1.21 ^a
1.3	12.35 ^a	5.72 ^a	3.42 ^a	2.21 ^a	1.43 ^a
1.5	14.25 ^a	6.60 ^a	3.95 ^a	2.55 ^a	1.65 ^a
1.7	16.15 ^a	7.48 ^a	4.48 ^a	2.89 ^a	1.87 ^a
1.9	18.05 ^a	8.36 ^a	5.00 ^a	3.23 ^a	2.09 ^a

Case 5: $V_\infty = 0.5$

$\kappa\lambda$	<u>0.1</u>	<u>0.2</u>	<u>0.3</u>	<u>0.4</u>	<u>0.5</u>
0.1	0.94 ^b	0.43 ^b	0.25	0.16	0.10
0.3	2.82 ^a	1.29 ^a	0.76 ^b	0.48 ^b	0.30
0.5	4.70 ^a	2.15 ^a	1.27 ^a	0.80	0.50 ^b
0.7	6.58 ^a	3.01 ^a	1.77 ^a	1.12 ^a	0.70
0.9	8.46 ^a	3.87 ^a	2.28 ^a	1.44 ^a	0.90 ^a
1.1	10.34 ^a	4.73 ^a	2.79 ^a	1.76 ^a	1.10 ^a
1.3	12.22 ^a	5.59 ^a	3.29 ^a	2.08 ^a	1.30 ^a
1.5	14.10 ^a	6.45 ^a	3.80 ^a	2.40 ^a	1.50 ^a
1.7	15.98 ^a	7.31 ^a	4.31 ^a	2.72 ^a	1.70 ^a
1.9	17.86 ^a	8.17 ^a	4.81 ^a	3.04 ^a	1.90 ^a

NOTES: a - the values of $\kappa\lambda$, δ_0 and V_∞ are such that the stability criterion at infinity, (8.9), is violated

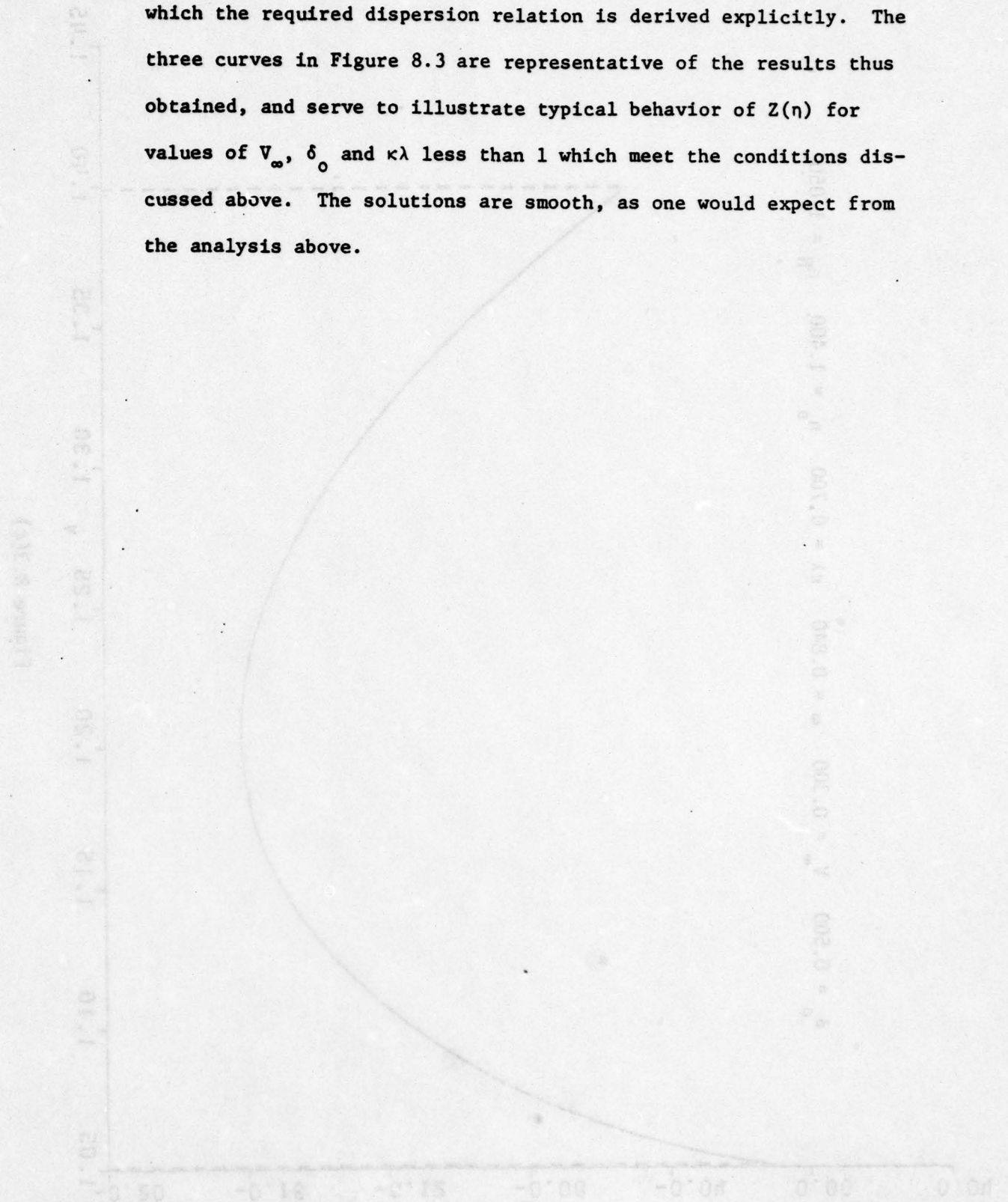
b - parameter values are such that one or more singular points are contained in the interval $\delta_0 < \tau_i < 1$:
see discussion in Section 8.2.

8.4 TYPICAL MODE SHAPES FOR THE ZEROth ORDER EXPONENTIAL FRONT DPA EQUATION

Figure 8.3 illustrates typical mode shapes for the depth perturbation amplitude $Z(\eta)$. The curves were generated by numerically integrating the lowest order exponential front DPA equation, (6.23), using a finite difference method that reduces the ODE to an algebraic system which is then solved by matrix methods (Conte and deBoor, 1972, Ch. 5). The algorithm's accuracy was checked against a second order ODE with known analytic solution. The curves in Figure 8.3 were generated using 380 steps in the numerical integration, and the accuracy is expected to be well within 1%. Values of the input parameters V_∞ and $\kappa\lambda$ were chosen so that the stability criterion at infinity in (8.9) was met and, additionally, so that none of the singular points τ_i ($i=1,3$) fell in the interval $\delta_0 \leq \tau_i \leq 1$. These restrictions insure regular behavior of $Z(\eta)$ throughout its interval of definition.

The value of Z at $\xi=0$ was arbitrarily set equal to -0.05 , -0.07 and -0.06 in Figures 8.3(a) through 8.3(c), respectively, which is consistent with the assumption of small amplitude perturbations. The points η_0 and η_N in these figures are the images of $\xi=0$ and $\xi=\infty$ under the transformations defined in (6.12) and (6.21d). At $\xi=\infty$ the boundary condition is $Z=0$ as demanded by the asymptotic behavior of the solution for $Z(\eta)$ developed in Section 8.3. Since the DPA equation (6.23) involves ω as a parameter, specification of an appropriate $(\kappa\lambda, \omega)$ pair, that is, one satisfying the lowest order exponential front dispersion relation, is required in order to perform the numerical integration. This was done by using the results of Section 10.1, in

which the required dispersion relation is derived explicitly. The three curves in Figure 8.3 are representative of the results thus obtained, and serve to illustrate typical behavior of $Z(\eta)$ for values of V_∞ , δ_0 and $\kappa\lambda$ less than 1 which meet the conditions discussed above. The solutions are smooth, as one would expect from the analysis above.



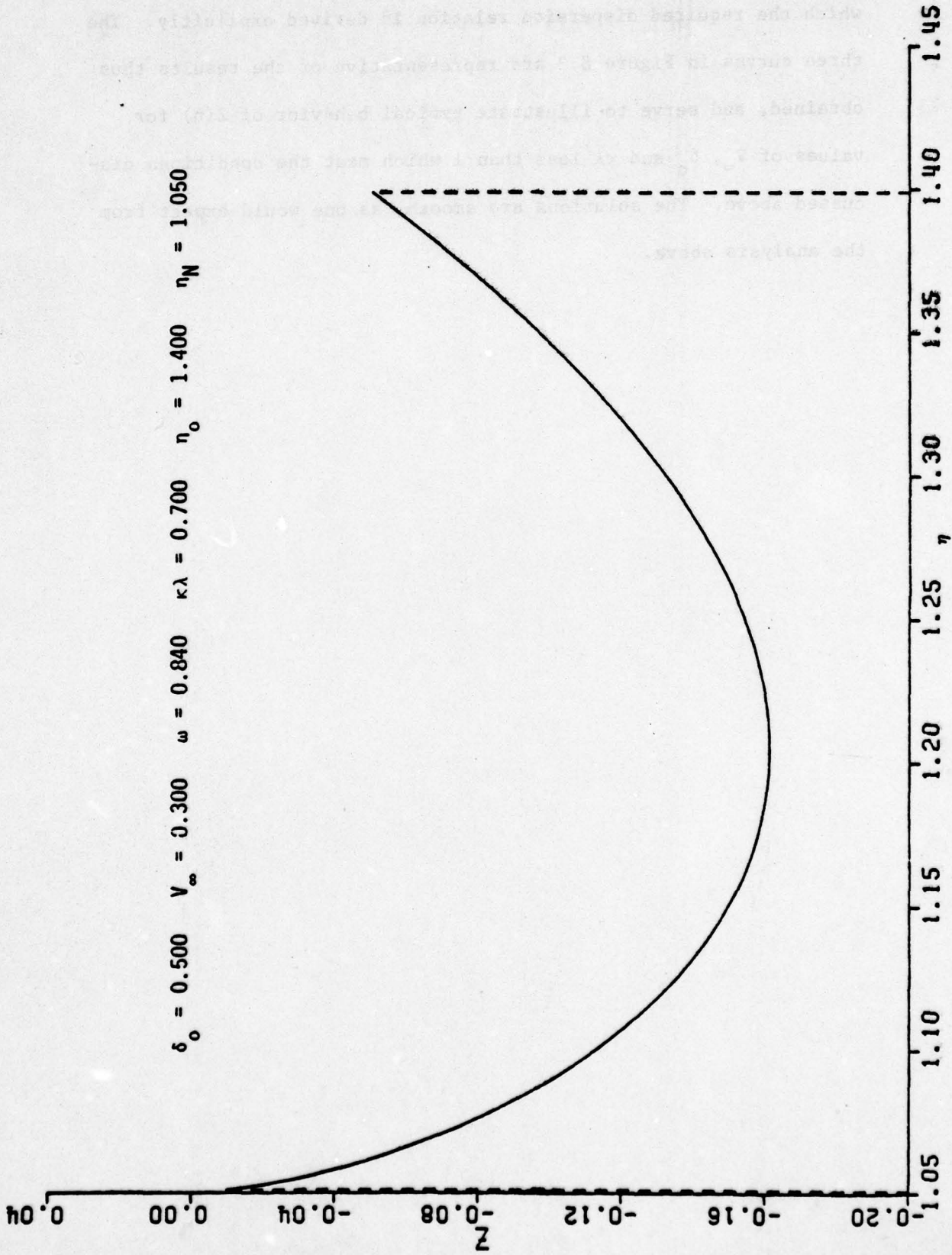


Figure 8.3(c)

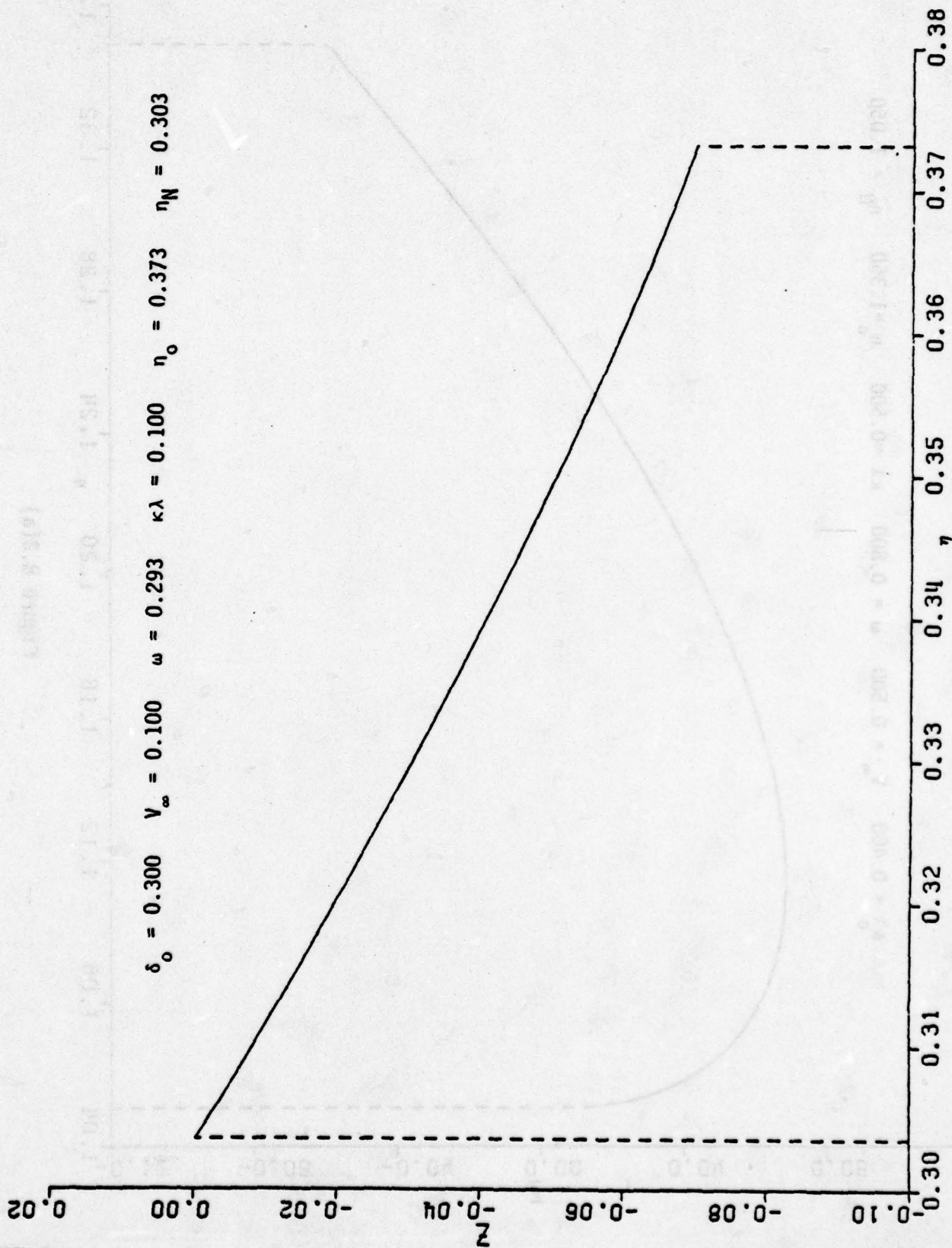


Figure 8.3(b)

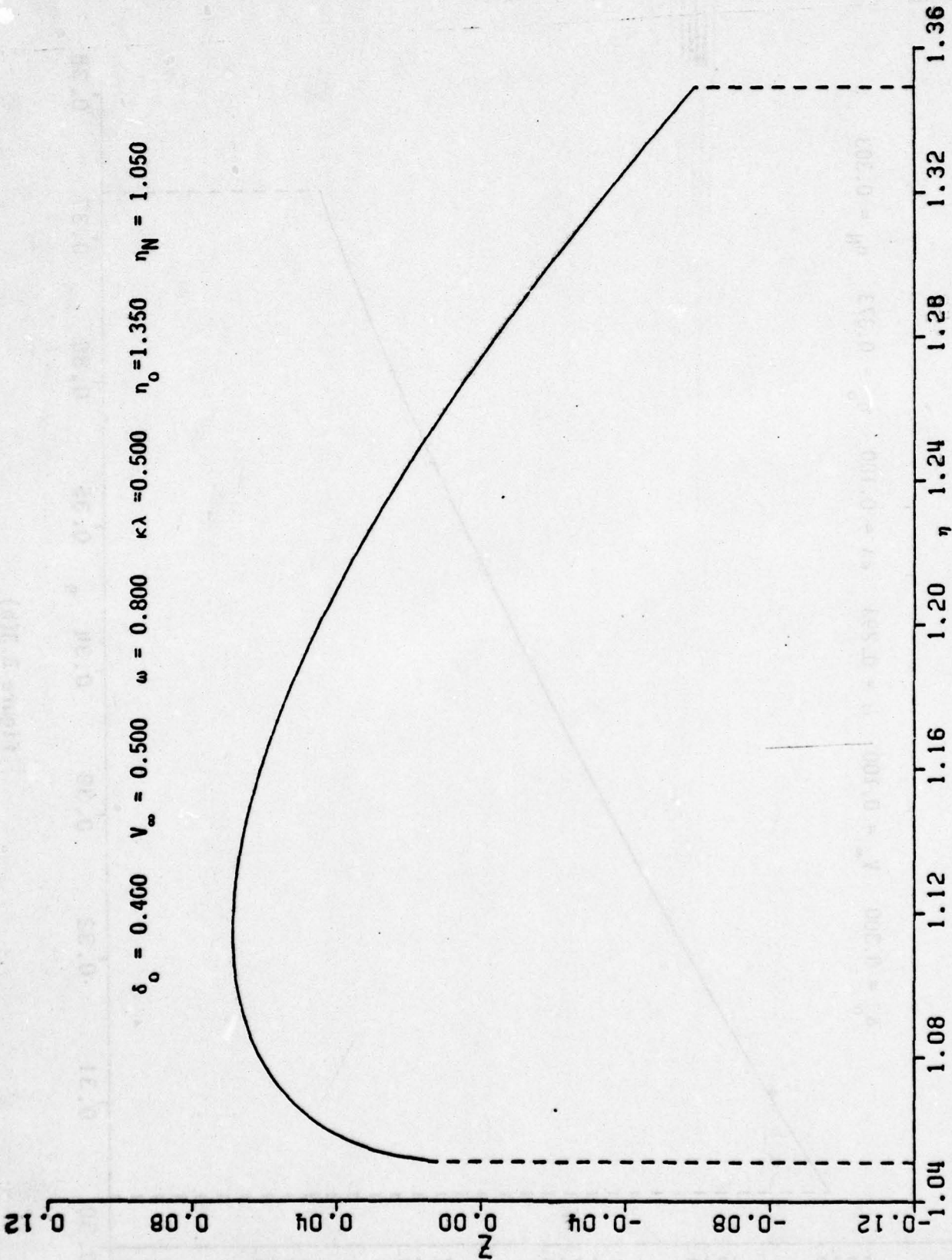


Figure 8.3(a)

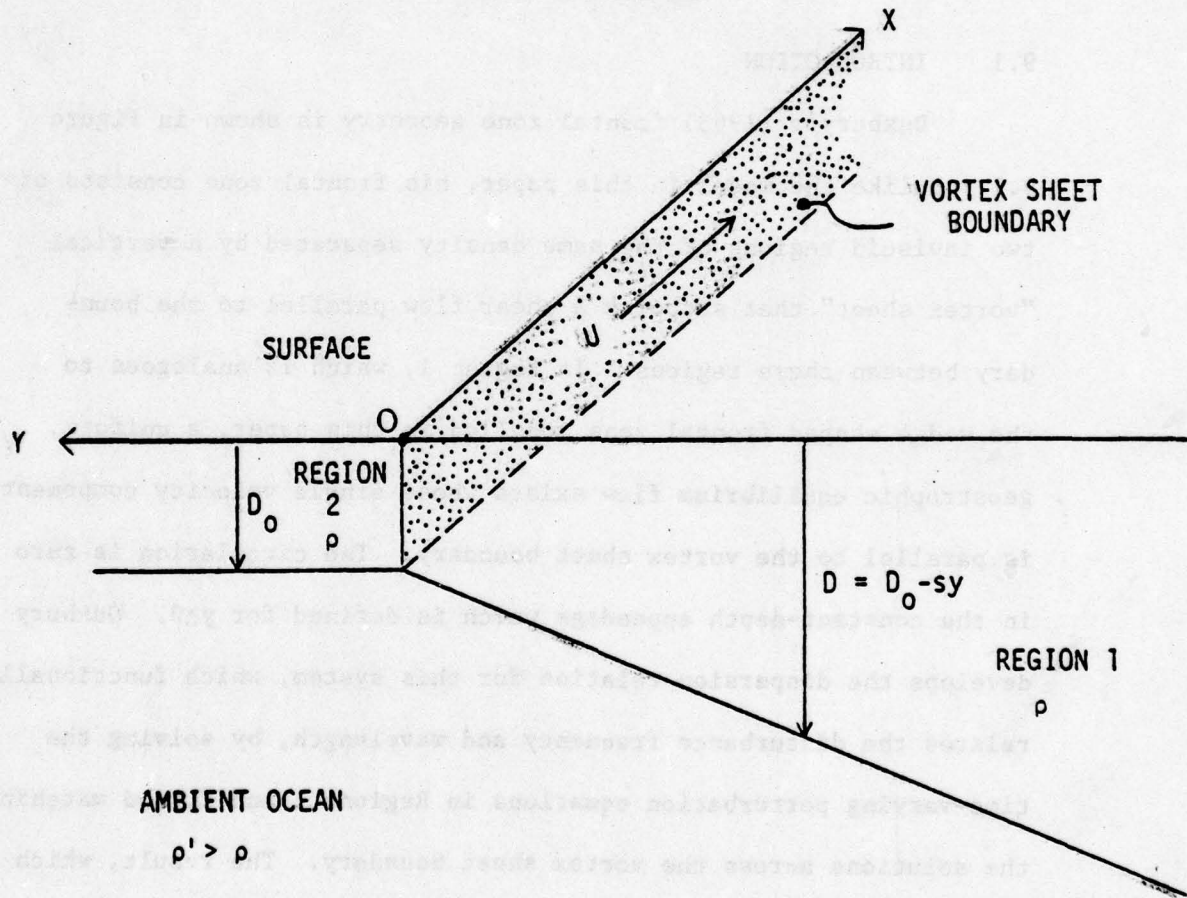
CHAPTER 9

DISPERSION CHARACTERISTICS OF THE PLANAR FRONT

9.1 INTRODUCTION

Duxbury's (1963) frontal zone geometry is shown in Figure 9.1. Unlike the model in this paper, his frontal zone consists of two inviscid regions of the same density separated by a vertical "vortex sheet" that supports a shear flow parallel to the boundary between these regions. In Region 1, which is analogous to the wedge shaped frontal zone modelled in this paper, a uniform, geostrophic equilibrium flow exists whose single velocity component is parallel to the vortex sheet boundary. The circulation is zero in the constant-depth appendage which is defined for $y \geq 0$. Duxbury develops the dispersion relation for this system, which functionally relates the disturbance frequency and wavelength, by solving the time-varying perturbation equations in Regions 1 and 2, and matching the solutions across the vortex sheet boundary. The result, which appears as his equation (75), thus requires a priori knowledge of the time-dependent perturbation equation solutions, since these then appear explicitly in the dispersion relation.

The dispersion characteristics of Duxbury's system rest upon boundary conditions that are quite different from those in this model, which consequently leads to a different formalism in developing the dispersion relation. It will be seen in what follows that the dis-



DUXBURY'S FRONTAL ZONE GEOMETRY

Figure 9.1

persion characteristics of both the exponential and planar fronts are available directly from the perturbation equations upon application of the boundary conditions developed in Chapter 7. Since no a priori knowledge of the perturbation solutions is required, considerable simplification results.

The fundamental nature of the difference between Duxbury's model and this one is readily appreciated by more closely examining his dispersion relation in the limiting case $D_0 \rightarrow 0$. Since D_0 is the (constant) depth in his Region 2, letting $D_0 \rightarrow 0$ removes Region 2 from the problem and presumably recovers the planar frontal zone geometry in this model with the inner region width set to zero. We expect that this is a physically realistic limit which should correspond to well-behaved dispersion characteristics. Taking the limit $D_0 \rightarrow 0$ in Duxbury's equations (75)-(77), however, reveals that his dispersion relation exhibits no regular behavior in this limit and, in fact, becomes undefined. This peculiar behavior is a consequence of the boundary conditions that are imposed, which require a coupling of the dynamics in Regions 1 and 2. Removal of Region 2 therefore leads to a singular result.

The model developed in this paper, however, does not suffer this shortcoming, since the boundary conditions are different. The frontal zone geometry, moreover, is formulated more realistically at the outset, and the artifice of a vortex sheet barrier separating two regions of the same density is unnecessary. Garvine's work (1974, 1979a, 1979b) has shown clearly that the steep interface between the frontal zone and the ambient ocean is maintained by local dissipation, viz., turbulent friction, mixing and mass entrainment in the inner

dissipative region, which eliminates the need for an artificial vertical barrier, as in Duxbury's model. In the following two sections, the zeroth and first order dispersion characteristics are derived for the planar front.

9.2 THE ZEROth ORDER DISPERSION RELATION

Derivation of the planar front dispersion relation at order F_b^0 is remarkably simple and follows immediately by applying the boundary conditions formulated in Chapter 7 to the lowest order perturbation equations in Chapter 6. Specifically, we substitute (7.10) and (7.9) along with (7.2c) into the y-momentum equation (6.15b) evaluated at $\xi=0$, which imposes the following characteristic condition on the scaled frequency ω and the normalized wavenumber $\kappa\lambda$:

$$\omega/\kappa\lambda = -V_\infty \quad (9.1)$$

Thus, at order F_b^0 , wavelike disturbances on the planar front in the moving coordinate system are non-dispersive with equal phase and group velocities. For real $\kappa\lambda$, the frequency is also real, and therefore no unstable modes exist in the system. Since the planar front is inherently stable and non-dispersive to lowest order, it cannot support a disturbance whose amplitude grows in time. In the next section, we will therefore consider the first order dispersion characteristics for the planar front and are led to a rather surprising conclusion.

9.3 THE FIRST ORDER DISPERSION CHARACTERISTICS

Recall that the perturbation variable decomposition was introduced in Chapter 6, and that the zeroth and first order perturbation equations were derived. The lowest order systems appear in (6.7) and (6.9) for the planar and exponential fronts, respectively, while the corresponding first order systems are contained in (6.8) and (6.10). We then assumed the time- and space-harmonic solutions in (6.13) for the zeroth order perturbations, but proceeded no further with the first order systems. In this section, we will introduce time- and space-harmonic solutions for the first order velocity and interfacial depth perturbations as follows:

$$\hat{u}^{(1)}(\xi, \zeta, t) = X^{(1)}(\xi) \exp\{i(\zeta + \omega t)\} \quad (9.2a)$$

$$\hat{v}^{(1)}(\xi, \zeta, t) = Y^{(1)}(\xi) \exp\{i(\zeta + \omega t)\} \quad (9.2b)$$

$$\hat{\delta}^{(1)}(\xi, \zeta, t) = Z^{(1)}(\xi) \exp\{i(\zeta + \omega t)\} \quad (9.2c)$$

The circular frequency ω appearing in (9.2) is the same as the zeroth order ω in Chapter 6, since the inhomogeneous first order system is driven by the lowest order solutions.

Substituting (9.2) into (6.8) leads to the following system of ODE's for the first order perturbation amplitudes $X^{(1)}$, $Y^{(1)}$ and $Z^{(1)}$, each of which is a function of ξ alone:

$$i\sigma X^{(1)} - Y^{(1)} + Z_{\xi}^{(1)} = -\bar{u}X_{\xi} \quad (9.3a)$$

$$i\sigma Y^{(1)} + X^{(1)} + ik\lambda Z^{(1)} = -\bar{u}Y_{\xi} \quad (9.3b)$$

$$\begin{aligned} i\sigma Z^{(1)} + Z_{\xi} X^{(1)} + (1-\beta v_{\infty} \xi) X_{\xi}^{(1)} \\ + ik\lambda(1-\beta v_{\infty} \xi) Y^{(1)} \\ = -\bar{u}Z_{\xi} - (\beta u_{\infty}/k\lambda) \zeta X_{\xi} - \beta u_{\infty}(1+i\zeta)Y \end{aligned} \quad (9.3c)$$

where σ is defined in (6.17).

Following the notation introduced in Chapter 6, X , Y and Z with no superscript are lowest order quantities, while the corresponding first order quantities are marked by a superscript (1). As before, the overbar denotes an equilibrium state variable. We note that the equilibrium state and the solutions to order F_b^0 appear both as driving terms and as non-constant coefficients in the first order system. The first order dispersion relation may now be derived by applying the boundary conditions on $X^{(1)}$, $Y^{(1)}$ and $Z^{(1)}$ directly to the system (9.3). Doing so, however, is somewhat involved algebraically for the following reason. If each of the functions in (9.3) is evaluated at $\xi=0$, the point at which the boundary conditions are applied, we see that (9.3) reduces to a system of three algebraic equations for five unknowns, viz., $X^{(1)}$, $Y^{(1)}$, $Z^{(1)}$, $X_{\xi}^{(1)}$ and $Z_{\xi}^{(1)}$, each evaluated at $\xi=0$. The lowest order solutions and their deriva-

tives evaluated at $\xi=0$ are presumed known. In order to successfully develop a characteristic relation between ω and $\kappa\lambda$, therefore, we must first manipulate the system in (9.3) to generate a number of equations equal to the number of unknowns. This procedure is unfortunately tedious. It is nevertheless outlined here, since it will be used again for the exponential front at order F_b^1 .

We begin by restating the known zeroth and first order boundary conditions:

$$Z(0) = \beta V_\infty h_0 \quad (7.2c)$$

$$X(0) = ih_0 \{ \omega + \kappa\lambda(1-\beta)V_\infty \} \quad (7.9)$$

$$Y(0) = 0 \quad (7.10)$$

$$Z^{(1)} = 0 \quad (\text{with } Z^{(1)}(h) = Z^{(1)}(0)) \quad (7.3)$$

$$X^{(1)}(0) = Y^{(1)}(0) = 0 \quad , \quad (7.5)$$

where h_0 is the wave disturbance amplitude. Since the lowest order perturbations are homogeneous, vanishing with h_0 , and the first order solutions are driven by the lowest order solutions, h_0 should factor out of the dispersion relation. We note that the perturbation equations at order F_b^0 appear in (6.15) and are not reproduced here.

Evaluating (6.15a) and (6.15c) at $\xi=0$ using (7.2c), (7.9) and (7.10) provides explicit representations for $X_\xi(0)$ and $Z_\xi(0)$. (9.3b) evaluated at $\xi=0$ subject to (7.3) and (7.5) gives $Y_\xi(0)=0$. Thus, each of the lowest order perturbation amplitudes and its first der-

ivative is known explicitly at the origin. Taking $d/d\xi$ of (6.15a) determines $Z_{\xi\xi}(0)$ as

$$Z_{\xi\xi}(0) = -i\sigma X_{\xi}(0) \quad , \quad (9.4)$$

where $X_{\xi}(0)$ is known. Differentiating (6.15c) once with respect to ξ and (6.15b) twice provides the following expressions for $X_{\xi\xi}(0)$ and $Y_{\xi\xi}(0)$ in terms of previously computed quantities:

$$X_{\xi\xi}(0) = -(2V_{\infty}/k\lambda)X_{\xi}(0) - i\sigma Z_{\xi}(0) \quad (9.5)$$

$$Y_{\xi\xi}(0) = (i/\sigma)\{X_{\xi\xi}(0) + ik\lambda Z_{\xi\xi}(0)\} \quad (9.6)$$

All relevant lowest order quantities are now known, and we proceed to close the first order system in a similar manner.

From (9.3a) and (9.3c) with $\xi=0$, we obtain, respectively,

$$Z_{\xi}^{(1)}(0) = -\bar{u}X_{\xi}(0) \quad (9.7)$$

$$X_{\xi}^{(1)}(0) = -\bar{u}Z_{\xi}^{(0)} + \{u_{\infty}\zeta/(k\lambda)^2\}X_{\xi}(0) \quad , \quad (9.8)$$

wherein the previously derived results have been used. Note that \bar{u} , which is constant, is defined in (6.3a). Finally, differentiating in order (9.3b), (9.3a) and (9.3c) once with respect to ξ and setting $\xi=0$ closes the algebraic system by providing five equations for the five unknowns $X_{\xi}^{(1)}(0)$, $Y_{\xi}^{(1)}(0)$, $Z_{\xi}^{(1)}(0)$, $X_{\xi\xi}^{(1)}(0)$ and $Z_{\xi\xi}^{(1)}(0)$. Note that, as a consequence of the successive differentiations, these are not the same five unknowns obtained by simply setting $\xi=0$ in the

original system (9.3).

The final result is conveniently written in matrix form as follows:

$$\begin{bmatrix} Z_{\xi}(0) + v_{\infty}/k\lambda & ik\lambda & i\sigma & 1 & 0 \\ i\sigma & -1 & 0 & 0 & 1 \\ 1 & i\sigma & ik\lambda & 0 & 0 \\ 1 & 0 & 0 & 0 & 0 \\ 0 & 0 & 1 & 0 & 0 \end{bmatrix} \begin{bmatrix} X_{\xi}^{(1)}(0) \\ Y_{\xi}^{(1)}(0) \\ Z_{\xi}^{(1)}(0) \\ X_{\xi\xi}^{(1)}(0) \\ Z_{\xi\xi}^{(1)}(0) \end{bmatrix} \quad (9.9)$$

$$= \begin{bmatrix} A \\ B \\ C \\ D \\ E \end{bmatrix}$$

where

$$A = -\bar{u}Z_{\xi\xi}(0) + \{u_{\infty}\zeta/(k\lambda)^2\}X_{\xi\xi}(0) + (u_{\infty}/k\lambda)(1+i\zeta)Y_{\xi\xi}(0) \quad (9.10a)$$

$$B = -\bar{u}X_{\xi\xi}(0) \quad (9.10b)$$

$$C = -\bar{u}Y_{\xi\xi}(0) \quad (9.10c)$$

$$D = -\bar{u}Z_{\xi}(0) + \{u_{\infty}\zeta/(k\lambda)^2\}X_{\xi}(0) \quad (9.10d)$$

$$E = -\bar{u}X_{\xi}(0) \quad (9.10e)$$

With a bit of algebra, the inverse of the coefficient matrix may be derived and the system in (9.9) solved to give

$$\begin{bmatrix} X_{\xi}^{(1)}(0) \\ Y_{\xi}^{(1)}(0) \\ Z_{\xi}^{(1)}(0) \\ X_{\xi\xi}^{(1)}(0) \\ Z_{\xi\xi}^{(1)}(0) \end{bmatrix} = \begin{bmatrix} 0 & 0 & 0 & b_{14} & 0 \\ 0 & 0 & b_{23} & b_{24} & b_{25} \\ 0 & 0 & 0 & 0 & 1 \\ b_{41} & 0 & b_{43} & b_{44} & b_{45} \\ 0 & b_{52} & b_{53} & b_{54} & b_{55} \end{bmatrix} \begin{bmatrix} A \\ B \\ C \\ D \\ E \end{bmatrix} \quad (9.11)$$

where

$$\begin{aligned} b_{14} &= 1/a_{14}, & b_{23} &= 1/a_{13}, & b_{24} &= -1/a_{13}a_{14} \\ b_{25} &= -a_{12}/a_{13}a_{14}^2, & b_{41} &= 1/a_{14}, & b_{43} &= -a_{12}/a_{13}a_{14} \\ b_{44} &= (a_{12}/a_{13} - a_{11})/a_{14}^2, & b_{45} &= (a_{12}^2/a_{13}a_{14}^3) - a_{13}/a_{14} \end{aligned} \quad (9.12)$$

$$b_{52} = a_{14}, \quad b_{53} = a_{14}/a_{13}, \quad b_{54} = -(a_{13} + 1/a_{13}) \quad (9.12 - \text{cont.})$$

$$b_{55} = -a_{12}/a_{13}a_{14}$$

The a_{ij} in (9.12) are the elements of the coefficient matrix in (9.9) with obvious equivalences.

The first order dispersion relation is now derived directly from (9.9) and (9.11). From (9.9), we have

$$X_{\xi}^{(1)}(0) + i\sigma Y_{\xi}^{(1)}(0) + ik\lambda Z_{\xi}^{(1)}(0) = C \quad (9.13)$$

And, from (9.11),

$$X_{\xi}^{(1)}(0) = b_{14}D \quad (9.14a)$$

$$Y_{\xi}^{(1)}(0) = b_{23}C + b_{24}D + b_{25}E \quad (9.14b)$$

$$Z_{\xi}^{(1)}(0) = E \quad (9.14c)$$

Substituting (9.14) into (9.13) results in the characteristic relation between ω and $\kappa\lambda$ demanded by internal consistency within the original system of dynamical equations, the result being

$$\begin{aligned} &(-1 + a_{13}b_{23})C + (b_{14} + a_{13}b_{24})D \\ &+ (a_{13}b_{25} + a_{12}/a_{14}^2)E = 0 \quad , \quad (9.15) \end{aligned}$$

where the a_{ij} are elements of the coefficient matrix in (9.9) and

the b_{ij} are elements of its inverse defined in (9.12). Expanding the coefficients in (9.15) using (9.12) leads to the rather surprising result that each of the coefficients of C, D and E in (9.15) vanishes identically and independently. Therefore, no dispersion relation exists to first order for the planar front, and the original system of perturbation equations is internally self-consistent without the constraint of any characteristic relation between ω and $\kappa\lambda$. In view of the lowest order dispersion relation, which is physically uninteresting, the first order result developed here shows a grave deficiency in the planar front model. The planar front model, even with appropriate boundary conditions and scaling, is incapable of reproducing the dynamical behavior of waves on oceanic fronts. In the next chapter, however, the procedures outlined above are applied to the exponential front with far more satisfying results.

CHAPTER 10

DISPERSION CHARACTERISTICS OF THE EXPONENTIAL FRONT

10.1 THE ZEROth ORDER DISPERSION RELATION

The zeroth and first order dispersion relations for the exponential front are derived in the same manner as were the planar front results in Chapter 9. The exponential front equations for the perturbation amplitudes X, Y and Z at order F_b^0 appear in (6.16). Evaluating the y-momentum equation (6.16b) at $\xi=0$ then gives

$$ig(0)Y(0) + \delta_0 X(0) + ik\lambda Z(0) = 0 \quad (10.1)$$

Substituting the boundary conditions (7.10), (7.8) and (7.2b) into (10.1) and eliminating a common factor of $iZ(0)$ imposes the following characteristic condition on ω and $\kappa\lambda$ at order F_b^0 :

$$\omega/k\lambda = (1/\delta_0) - \delta_0 - V_\infty \quad (10.2)$$

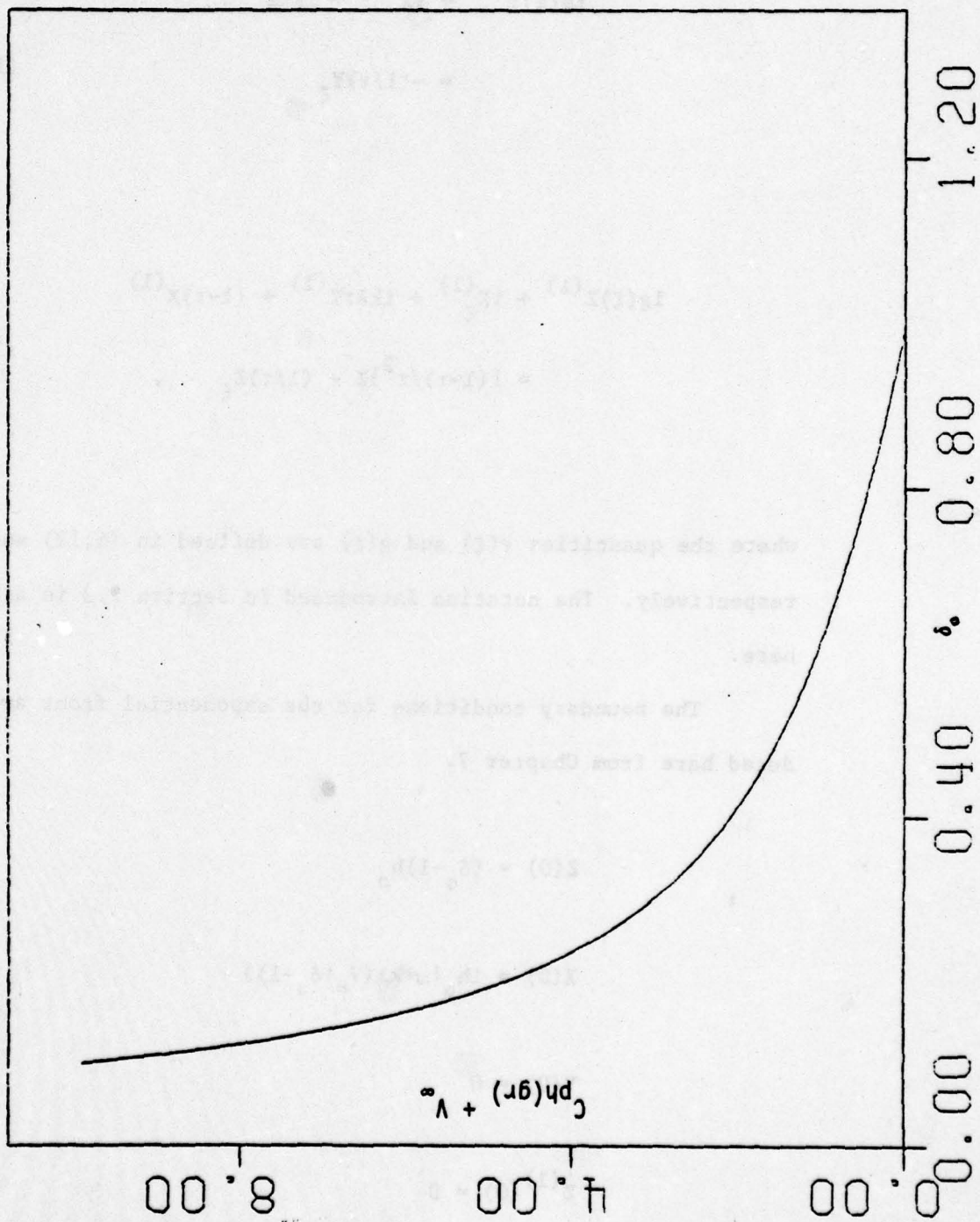
The phase and group velocities are equal and constant, as they were for the planar front. And, since ω is real for real $\kappa\lambda$, the exponential front is dynamically stable at order F_b^0 . A plot of $C_{ph(gr)} + V_\infty$ as a function of δ_0 appears in Figure 10.1, where $C_{ph(gr)}$ is the phase (group) velocity. For $V_\infty > (1/\delta_0 - \delta_0)$, $C_{ph(gr)} < 0$; other-

wise, the phase and group velocities are positive in the moving coordinate system. Realistic values of V_∞ are not likely to exceed approximately 0.5. For $V_\infty=0.5$, the phase (group) velocity will be negative only if δ_0 is greater than about 0.8, which is unrealistically large. The range of V_∞ and δ_0 likely to be encountered in an oceanic frontal zone is therefore such that the phase and group velocities in the moving coordinate system will be positive. Stable lowest order waves on the exponential front are expected to propagate in the positive y -direction in a right-handed coordinate system with the x -axis oriented perpendicular to the long-stream direction and into the frontal zone. This result is consistent with observed meander patterns on the Gulf Stream, in which disturbances propagate northward and eastward along the Stream.

10.2 FIRST ORDER DISPERSION CHARACTERISTICS

As before, time- and space-harmonic first order solutions of the form (9.2) are assumed and substituted into the perturbation variable equations (6.10), which leads to the following system of ODE's for the perturbation amplitudes $X^{(1)}$, $Y^{(1)}$ and $Z^{(1)}$:

$$\begin{aligned} ig(\xi)X^{(1)} - Y^{(1)} + Z_\xi^{(1)} \\ = \{(1-\tau)/\tau^2\}X - (1/\tau)X_\xi \end{aligned} \tag{10.3a}$$



PLOT OF $C_{ph}(gr) + V_{\infty}$ vs δ_0

$$\begin{aligned}
 ig(\xi)Y^{(1)} + \tau X^{(1)} + ik\lambda Z^{(1)} \\
 = -(1/\tau)Y_{\xi}
 \end{aligned}
 \tag{10.3b}$$

$$\begin{aligned}
 ig(\xi)Z^{(1)} + \tau X_{\xi}^{(1)} + ik\lambda\tau Y^{(1)} + (1-\tau)X^{(1)} \\
 = \{(1-\tau)/\tau^2\}Z - (1/\tau)Z_{\xi}
 \end{aligned}
 \tag{10.3c}$$

where the quantities $\tau(\xi)$ and $g(\xi)$ are defined in (6.12) and (6.18), respectively. The notation introduced in Section 9.3 is also employed here.

The boundary conditions for the exponential front are reproduced here from Chapter 7:

$$Z(0) = (\delta_0 - 1)h_0 \tag{7.2b}$$

$$X(0) = ih_0 \{\omega + k\lambda(V_{\infty} + \delta_0 - 1)\} \tag{7.8}$$

$$Y(0) = 0 \tag{7.10}$$

$$Z^{(1)}(0) = 0 \tag{7.3}$$

$$X^{(1)}(0) = Y^{(1)}(0) = 0 \quad (7.5)$$

Once again, we expect the disturbance amplitude, h_0 , to factor out of the dispersion relation, since the perturbations at order F_b^0 are homogeneous. Following the procedure outlined in Section 9.3, the system (10.3) is closed by manipulating it to produce a number of equations equal to the number of unknowns.

The first step is to compute the relevant lowest order quantities, which are the first, second and third derivatives of the perturbation amplitudes X , Y and Z evaluated at $\xi=0$. This is done iteratively using the zeroth order system of ODE's in (6.16). Thus, from (6.16a) using (7.10) and setting $\xi=0$,

$$Z_\xi(0) = -ig(0)X(0) \quad (10.4)$$

Evaluating (6.16c) at $\xi=0$ with (7.10) gives

$$X_\xi(0) = -(1/\delta_0)\{ig(0)Z(0) + (1-\delta_0)X(0)\} \quad (10.5a)$$

while (10.3b) with (7.3) and (7.5) at $\xi=0$ yields

$$Y_\xi(0) = 0 \quad (10.5b)$$

Differentiating in order (6.16a) and (6.16c) once with respect to ξ , using $\tau_{\xi} = \tau_{\xi\xi\xi} = -\tau_{\xi\xi} = 1 - \tau$, and setting $\xi=0$ gives

$$Z_{\xi\xi}(0) = -1\{g_{\xi}(0)X(0) + g(0)X_{\xi}(0)\} \quad (10.6)$$

$$\begin{aligned} X_{\xi\xi}(0) &= -(1/\delta_0)\{g_{\xi}(0)Z(0) + g(0)Z_{\xi}(0)\} \\ &+ \{(\delta_0 - 1)/\delta_0\}\{X(0) - 2X_{\xi}(0)\} \end{aligned} \quad (10.7)$$

Taking $d^2/d\xi^2$ of (6.16b) with $\xi=0$ determines $Y_{\xi\xi}(0)$ as

$$\begin{aligned} Y_{\xi\xi}(0) &= \{1/g(0)\}\{(\delta_0 - 1)\{X(0) - 2X_{\xi}(0)\} \\ &+ \delta_0 X_{\xi\xi}(0) + ik\lambda Z_{\xi\xi}(0)\} \end{aligned} \quad (10.8)$$

Computing the third derivative of Z from (6.16a) and setting $\xi=0$ gives

$$\left. \frac{d^3 Z}{d\xi^3} \right|_{\xi=0} = -1\{g_{\xi\xi}(0)X(0) + 2g_{\xi}(0)X_{\xi}(0) + g(0)X_{\xi\xi}(0)\} + Y_{\xi\xi}(0) \quad (10.9)$$

Taking $d^2/d\xi^2$ of (6.16c) with $\xi=0$ and the previous results yields

$$\begin{aligned}
\left. \frac{d^3 X}{d\xi^3} \right|_{\xi=0} &= -(1/\delta_0) \{ g_{\xi\xi}(0) Z(0) + 2g_{\xi}(0) Z_{\xi}(0) \\
&+ g(0) Z_{\xi\xi}(0) + k\lambda \delta_0 Y_{\xi\xi}(0) \} \\
&+ \{ (\delta_0 - 1)/\delta_0 \} \{ X(0) - 3X_{\xi}(0) + 3X_{\xi\xi}(0) \}
\end{aligned} \tag{10.10}$$

And, from (6.16b), computing the third derivative with respect to ξ leads to

$$\begin{aligned}
\left. \frac{d^3 Y}{d\xi^3} \right|_{\xi=0} &= (1/g(0)) \{ 3ig_{\xi}(0) Y_{\xi\xi}(0) \\
&+ (1-\delta_0) \{ X(0) - 3X_{\xi}(0) + 3X_{\xi\xi}(0) \} \\
&+ \delta_0 X_{\xi\xi\xi}(0) + ik\lambda Z_{\xi\xi\xi}(0) \}
\end{aligned} \tag{10.11}$$

All relevant lowest order quantities at $\xi=0$ thus appear in (7.2b), (7.8), (7.10) and (10.4)-(10.11).

The system is now closed at order F_b^1 by working with (10.3). Substituting the above results into (10.3a,c) and setting $\xi=0$ yields

$$Z_{\xi}^{(1)}(0) = (1/\delta_0) \left[\{ (1-\delta_0)/\delta_0 \} X(0) - X_{\xi}(0) \right] \tag{10.12}$$

$$X_{\xi}^{(1)}(0) = (1/\delta_0^2) \left[\{ (1-\delta_0)/\delta_0 \} Z(0) - Z_{\xi}(0) \right] \tag{10.13}$$

The quantities that remain to be computed are the first derivative of $Y^{(1)}$, and the second derivatives of $X^{(1)}$, $Y^{(1)}$ and $Z^{(1)}$, each evaluated at the origin. This is accomplished by sequentially differentiating (10.3b), (10.3a) and (10.3c) once with respect to ξ and then (10.3b) twice. Putting $\xi=0$ and employing the previous results leads to the following equations which determine, respectively, $Y_{\xi}^{(1)}(0)$, $Z_{\xi\xi}^{(1)}(0)$, $X_{\xi\xi}^{(1)}(0)$ and $Y_{\xi\xi}^{(1)}(0)$:

$$\begin{aligned} ig(0)Y_{\xi}^{(1)}(0) + \delta_0 X_{\xi}^{(1)}(0) + ik\lambda Z_{\xi}^{(1)}(0) \\ = \{(1-\delta_0)/\delta_0^2\}Y_{\xi}(0) - (1/\delta_0)Y_{\xi\xi}(0) \end{aligned} \quad (10.14)$$

$$\begin{aligned} ig(0)X_{\xi}^{(1)}(0) - Y_{\xi}^{(1)}(0) + Z_{\xi\xi}^{(1)}(0) \\ = \frac{d}{d\xi} \left\{ \{(1-\tau)/\tau^2\}X - (1/\tau)X_{\xi} \right\}_{\xi=0} \end{aligned} \quad (10.15)$$

$$\begin{aligned} ig(0)Z_{\xi}^{(1)}(0) + 2(1-\delta_0)X_{\xi}^{(1)}(0) + \delta_0 X_{\xi\xi}^{(1)}(0) + ik\lambda\delta_0 Y_{\xi}^{(1)}(0) \\ = \frac{d}{d\xi} \left\{ \{(1-\tau)/\tau^2\}Z - (1/\tau)Z_{\xi} \right\}_{\xi=0} \end{aligned} \quad (10.16)$$

$$\begin{aligned} 2ig_{\xi}(0)Y_{\xi}^{(1)}(0) + ig(0)Y_{\xi\xi}^{(1)}(0) + 2(1-\delta_0)X_{\xi}^{(1)}(0) \\ + \delta_0 X_{\xi\xi}^{(1)}(0) + ik\lambda Z_{\xi\xi}^{(1)}(0) \\ = \frac{d}{d\xi} \left\{ \{(1-\tau)/\tau^2\}Y_{\xi} - (1/\tau)Y_{\xi\xi} \right\}_{\xi=0} \end{aligned} \quad (10.17)$$

We have now generated a closed algebraic system of six equations for the six unknowns $X_{\xi}^{(1)}(0)$, $Y_{\xi}^{(1)}(0)$, $Z_{\xi}^{(1)}(0)$, $X_{\xi\xi}^{(1)}(0)$, $Y_{\xi\xi}^{(1)}(0)$ and $Z_{\xi\xi}^{(1)}(0)$. It is conveniently written in matrix form as follows:

$$\begin{bmatrix}
 2(1-\delta_0) & 2ig_{\xi}(0) & 0 & \delta_0 & ig(0) & ik\lambda \\
 2(1-\delta_0) & ik\lambda\delta_0 & ig(0) & \delta_0 & 0 & 0 \\
 ig(0) & -1 & 0 & 0 & 0 & 1 \\
 \delta_0 & ig(0) & ik\lambda & 0 & 0 & 0 \\
 0 & 0 & 1 & 0 & 0 & 0 \\
 \delta_0 & 0 & 0 & 0 & 0 & 0
 \end{bmatrix}
 \begin{bmatrix}
 X_{\xi}^{(1)}(0) \\
 Y_{\xi}^{(1)}(0) \\
 Z_{\xi}^{(1)}(0) \\
 X_{\xi\xi}^{(1)}(0) \\
 Y_{\xi\xi}^{(1)}(0) \\
 Z_{\xi\xi}^{(1)}(0)
 \end{bmatrix}
 =
 \begin{bmatrix}
 A \\
 B \\
 C \\
 D \\
 E \\
 F
 \end{bmatrix}
 \quad (10.18)$$

where the six constants A through F on the right-hand-side of (10.18) are all known in terms of the zeroth order perturbation amplitudes evaluated at $\xi=0$ as follows:

$$A = \frac{d}{d\xi} \left(\left\{ \frac{(1-\tau)}{\tau^2} Y_{\xi} - \frac{1}{\tau} Y_{\xi\xi} \right\} \right)_{\xi=0} \quad (10.19a)$$

$$B = \frac{d}{d\xi} \left(\left\{ \frac{(1-\tau)}{\tau^2} Z - \frac{1}{\tau} Z_{\xi} \right\} \right)_{\xi=0} \quad (10.19b)$$

$$C = \frac{d}{d\xi} \left(\left\{ \frac{(1-\tau)}{\tau^2} X - \frac{1}{\tau} X_{\xi} \right\} \right)_{\xi=0} \quad (10.19c)$$

$$D = \{(1-\delta_0)/\delta_0^2\}Y_\xi(0) - (1/\delta_0)Y_{\xi\xi}(0) \quad (10.19d)$$

$$E = \{(1-\delta_0)/\delta_0^2\}X(0) - (1/\delta_0)X_\xi(0) \quad (10.19e)$$

$$F = \{(1-\delta_0)/\delta_0^2\}Z(0) - (1/\delta_0)Z_\xi(0) \quad (10.19f)$$

Writing the elements of the coefficient matrix in (10.18) as a_{ij} , where standard row-column notation is employed, and the elements of its inverse matrix as b_{ij} , we have

$$\begin{bmatrix} X_\xi^{(1)}(0) \\ Y_\xi^{(1)}(0) \\ Z_\xi^{(1)}(0) \\ X_{\xi\xi}^{(1)}(0) \\ Y_{\xi\xi}^{(1)}(0) \\ Z_{\xi\xi}^{(1)}(0) \end{bmatrix} = \begin{bmatrix} 0 & 0 & 0 & 0 & 0 & b_{16} \\ 0 & 0 & 0 & b_{24} & b_{25} & b_{26} \\ 0 & 0 & 0 & 0 & b_{35} & 0 \\ 0 & b_{42} & 0 & b_{44} & b_{45} & b_{46} \\ b_{51} & b_{52} & b_{53} & b_{54} & b_{55} & b_{56} \\ 0 & 0 & b_{63} & b_{64} & b_{65} & b_{66} \end{bmatrix} \begin{bmatrix} A \\ B \\ C \\ D \\ E \\ F \end{bmatrix} \quad (10.20a)$$

where

$$b_{51} = 1/a_{15}, \quad b_{42} = 1/a_{24}, \quad b_{52} = -a_{14}/a_{24}a_{15}$$

$$b_{53} = -a_{16}/a_{15}a_{36}, \quad b_{63} = 1/a_{36}, \quad b_{24} = b_{51}$$

$$b_{44} = -a_{22}/a_{24}a_{15}, \quad b_{64} = b_{63}b_{51}$$

$$b_{54} = (-a_{16}/a_{36} + a_{22}a_{14}/a_{24} - a_{12})/a_{15}^2$$

$$b_{25} = b_{53}, \quad b_{35} = b_{63}$$

$$b_{45} = (a_{22}a_{16}/a_{15} - a_{15})/(a_{36}a_{24})$$

$$b_{55} = a_{16}(a_{16}/a_{36} - a_{22}a_{14}/a_{24} + a_{12} + a_{15}^2a_{14}/a_{16}a_{24})/(a_{36}a_{15}^2)$$

$$b_{65} = b_{63}b_{53}, \quad b_{16} = b_{42}, \quad b_{26} = b_{52}$$

$$b_{46} = (a_{22}a_{14}/a_{15} - a_{21})/a_{24}^2 \quad (10.20b)$$

$$b_{56} = -(a_{11}/a_{15} - a_{14}a_{21}/a_{15}a_{24} - a_{16}/a_{36} + (a_{14}/a_{15}^2)(-a_{16}/a_{36} + a_{22}a_{14}/a_{24} - a_{12}))/a_{24}$$

$$b_{66} = -(a_{15} + a_{14}/a_{15})/(a_{24}a_{36})$$

The dispersion relation is developed directly from (10.18) and (10.20a). Returning to (10.18), we have

$$a_{24}X_{\xi}^{(1)}(0) = F \quad (10.21a)$$

$$a_{36}Z_{\xi}^{(1)}(0) = E \quad (10.21b)$$

$$a_{14}x_{\xi}^{(1)}(0) + a_{15}y_{\xi}^{(1)}(0) + a_{16}z_{\xi}^{(1)}(0) = D \quad (10.21c)$$

And, from (10.20a), we have

$$y_{\xi}^{(1)}(0) = b_{24}D + b_{25}E + b_{26}F \quad (10.22)$$

Substituting (10.22) into (10.21c) and then (10.21a,b) into the resulting expression yields the following simple form for the dispersion relation at order F_b^1 :

$$D = 0 \quad (10.23)$$

where D is defined in (10.19d), which, in turn, involves only zeroth order quantities that are known functions of ω , $\kappa\lambda$ and V_{∞} . The final explicit form for the dispersion relation is thus obtained by substituting the required expressions into (10.23) from the set of equations (7.2b) through (10.8), which leads to

$$\begin{aligned} & (\omega/k\lambda)^3 + C_1(\omega/k\lambda)^2 + C_2(\omega/k\lambda) \\ & + \{(\delta_0 - 1)/k\lambda\}^2 + \{(\delta_0 - 1)/\delta_0\}C_3^2 \\ & + C_4C_5 = 0 \end{aligned} \quad (10.24)$$

where the constants C_1 through C_5 are

$$C_1 = 2V_{\infty} + C_3 \quad (10.25a)$$

$$C_2 = (1-\delta_0)(1-2V_\infty) - (1-\delta_0)^2(1+2/\delta_0) + V_\infty(4C_3 - V_\infty) \quad (10.25b)$$

$$C_3 = 1 + V_\infty - \delta_0 \quad (10.25c)$$

$$C_4 = 1 - \delta_0 + C_3^2 + \{(1-\delta_0)/\delta_0\}C_3 \quad (10.25d)$$

$$C_5 = 2V_\infty - C_3 \quad (10.25e)$$

Given values for δ_0 and V_∞ , condition (10.24), which is imposed by the requirement of self-consistency within the set of perturbation equations at order F_b^1 , provides the functional relationship between the disturbance frequency ω and the normalized wavenumber $\kappa\lambda$, which is always a real quantity. Since (10.24) is cubic in ω with real coefficients, fixing $\kappa\lambda$ leads to three roots for ω . Thus, they are either (i) all real or (ii) one is real and the other two a complex conjugate pair. Disturbances whose wavelength is such that the solutions to (10.24) are all real are, of course, stable, the amplitude neither increasing nor decreasing with time. Those for which $\text{Im}(\omega) < 0$ (> 0) are unstable (evanescent), where $\text{Im}(\omega)$ is the imaginary part of the complex frequency. Since complex roots of (10.24) must occur in conjugate pairs, each unstable mode, i.e., one whose amplitude increases exponentially with time, is necessarily accompanied by an evanescent mode, i.e., one whose amplitude decays exponentially with time. The real parts of ω for these two modes are equal. Thus, implicit in the exponential front's perturbation dynamics at order F_b^1

are unstable modes whose amplitudes can grow in time. In addition, the first order perturbation dynamics are inherently dispersive, whereas the lowest order dynamics are non-dispersive.

CHAPTER 11

ANALYSIS OF THE FIRST ORDER DISPERSION CHARACTERISTICS OF THE EXPONENTIAL FRONT

11.1 THE LOW FREQUENCY LIMIT

The dispersion relation at order F_b^1 , (10.24), may be written

$$\begin{aligned} \omega^3 + C_1 k \lambda \omega^2 + C_2 (k \lambda)^2 \omega + k \lambda (1 - \delta_0)^2 \\ + (k \lambda)^3 \left\{ ((\delta_0 - 1) / \delta_0) C_3^2 + C_4 C_5 \right\} = 0 \quad , \end{aligned} \quad (11.1)$$

where the C_i are defined in (10.25). The point (0,0) in $(k\lambda, \omega)$ space lies on the curve $\omega(k\lambda)$ defined by (11.1), and we wish to investigate now the asymptotic behavior of (11.1) in the limit $\omega \rightarrow 0$ and $k\lambda \rightarrow 0$, that is, the low frequency limit.

Since all quantities in (11.1) are presumably order one under the scaling introduced earlier, the asymptotic form of $\omega(k\lambda)$ as $k\lambda \rightarrow 0$ is determined by assuming

$$\omega = \hat{\omega} (k\lambda)^n \quad , \quad (11.2)$$

where $\hat{\omega}$ is order one. Substituting (11.2) into (11.1) gives

$$\begin{aligned} \hat{\omega}^3 + C_1 \hat{\omega}^2 (k\lambda)^{1-n} + C_2 \hat{\omega} (k\lambda)^{2(1-n)} \\ + (1 - \delta_0)^2 (k\lambda)^{1-3n} + (k\lambda)^{3(1-n)} G = 0 \quad , \end{aligned} \quad (11.3)$$

where the constant G is

$$G = \{(\delta_0 - 1)/\delta_0\} C_3^2 + C_4 C_5 \quad (11.4)$$

If all quantities are to remain finite for $k\lambda \rightarrow 0$, (11.3) implies that $1-3n=0$, or $n=1/3$. This condition leads to the following asymptotic form

$$\omega^3 \sim -(1-\delta_0)^2 k\lambda \quad (11.5)$$

in which the original variables have been reintroduced.

The three roots of (11.5) for $k\lambda > 0$ are

$$\omega_1 = -\{(1-\delta_0)^2 k\lambda\}^{1/3} \quad (11.6a)$$

$$\omega_2 = \frac{1}{2}(1+i\sqrt{3})\{(1-\delta_0)^2 k\lambda\}^{1/3} \quad (11.6b)$$

$$\omega_3 = \frac{1}{2}(1-i\sqrt{3})\{(1-\delta_0)^2 k\lambda\}^{1/3} \quad (11.6c)$$

where $0 < k\lambda \ll 1$. ω_1 corresponds to a stable mode, whereas ω_2 and ω_3 correspond to evanescent and unstable modes, respectively. We note that the low frequency limit of the first order dispersion relation is independent of V_∞ and depends parametrically only on δ_0 .

The phase velocities associated with these three frequencies, which are computed from $\text{Re}(\omega_n)/k\lambda$, are:

$$C_{ph_1} = -(1-\delta_0)^{2/3} (k\lambda)^{-2/3} \quad (11.7a)$$

$$C_{ph_2} = C_{ph_3} = \frac{1}{2}(1-\delta_0)^{2/3} (k\lambda)^{-2/3} \quad (11.7b)$$

The stable wave thus travels in the $-y$ direction with twice the phase velocity of the evanescent and unstable waves, both of which propagate in the $+y$ direction.

The group velocities for the three modes are computed from $d\text{Re}(\omega_n)/d(k\lambda)$ as

$$C_{g_1} = -(1/3)(1-\delta_0)^{2/3} (k\lambda)^{-2/3} \quad (11.8a)$$

$$C_{g_2} = (1/6)(1-\delta_0)^{2/3} (k\lambda)^{-2/3} \quad (11.8b)$$

The group velocity of a particular mode is thus $1/3$ of its phase velocity, and both the group and phase velocities are proportional to $(k\lambda)^{-2/3}$ for all disturbances. As $k\lambda \rightarrow 0$, C_g and C_{ph} become infinite.

11.2 REGIONS OF INSTABILITY IN $k\lambda$ -SPACE

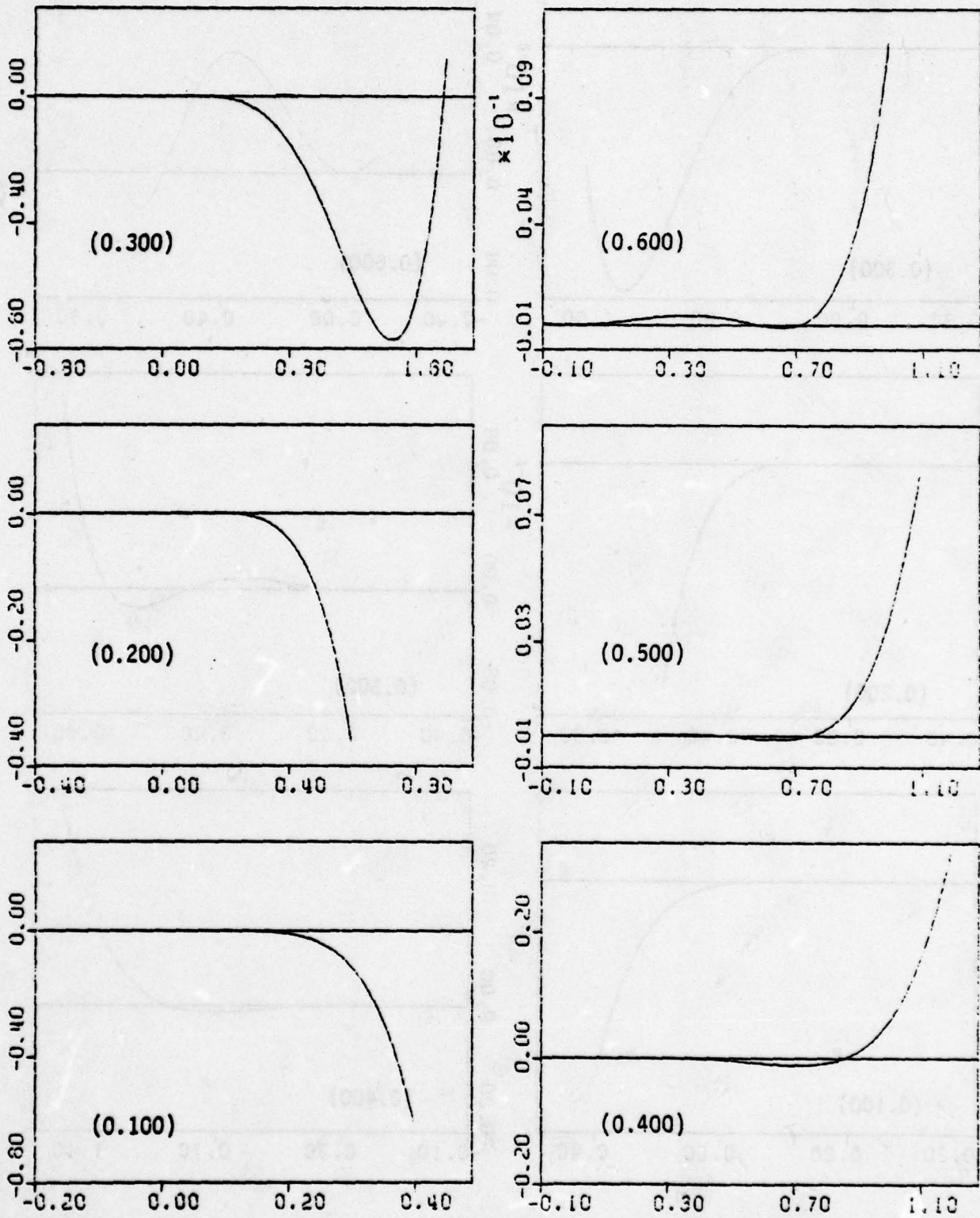
The nature of the roots of (11.1) are easily determined by employing the following general result for cubic equations (CRC Handbook of Mathematical Tables, 1962, p. 387). The equation

$$y^3 + py^2 + qy + r = 0$$

- has
- (A) one real and two conjugate complex roots for $M > 0$
 - (B) three real roots, of which at least two are equal, for $M = 0$
 - (C) three real and unequal roots for $M < 0$,

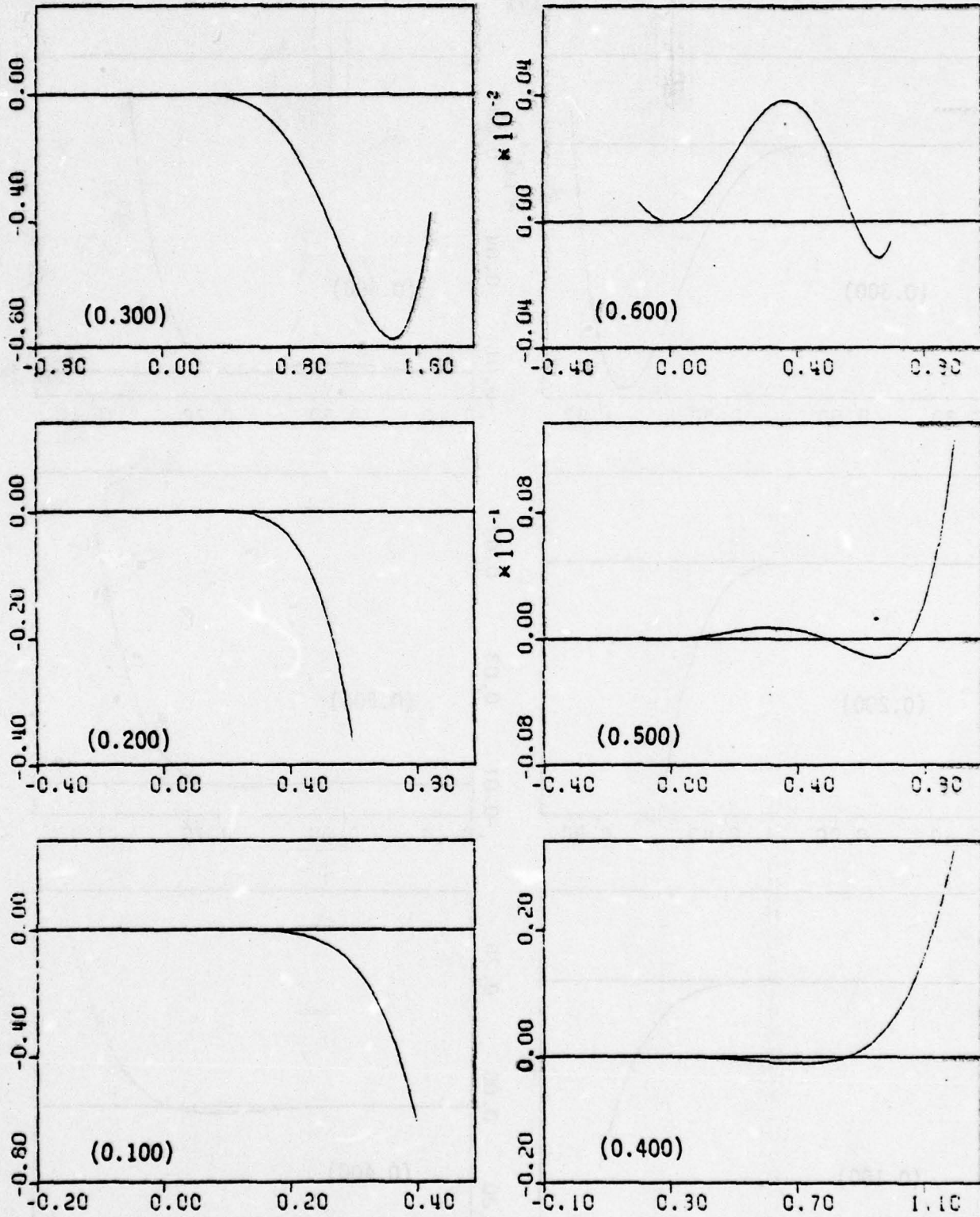
where $M = b^2/4 + a^3/27$, and where a and b are defined in terms of the coefficients p , q and r as follows: $a = q - p^2/3$, $b = 2p^3/27 - pq/3 + r$. The obvious equivalences between the quantities p , q and r above and the coefficients in (11.1) are not reproduced here.

For several values of the parameters δ_0 and V_∞ , the discriminant M is plotted for (11.1) as a function of $k\lambda$ in Figures 11.1a through 11.1e. Ranges of $k\lambda$ for which the discriminant is zero or negative correspond to three stable modes on the exponential front, while values of $k\lambda$ giving a positive discriminant result in one stable, one evanescent and one unstable mode as discussed earlier. Since $M(k\lambda)$ is an even function of $k\lambda$, only the domain $k\lambda \geq 0$ is plotted in Figure 11.1.



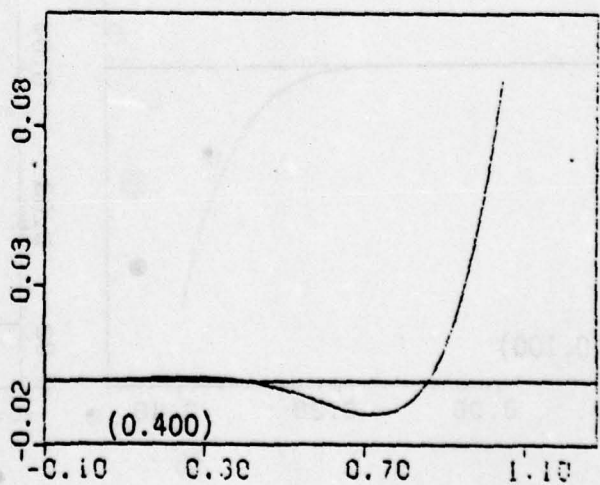
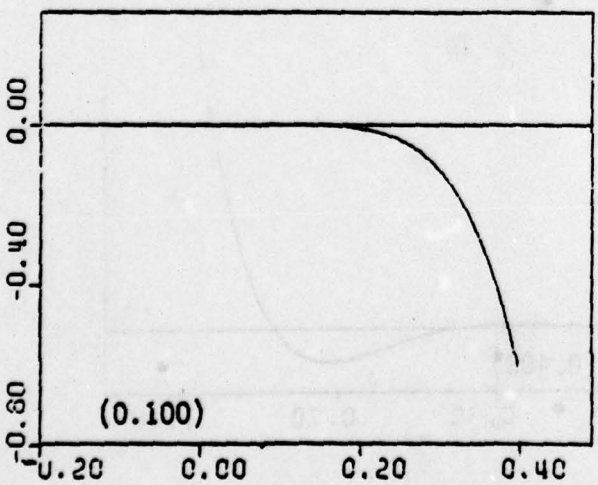
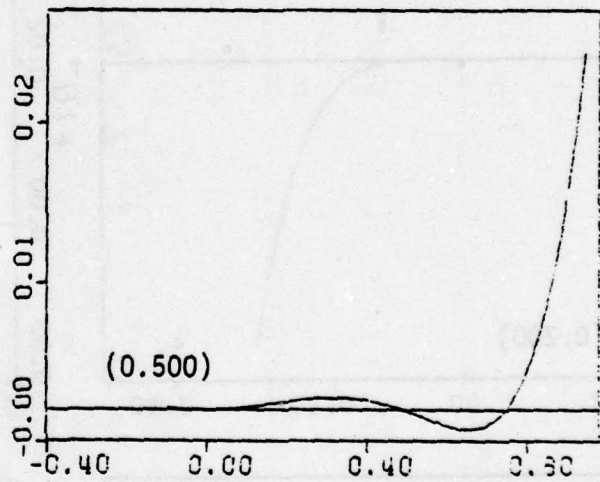
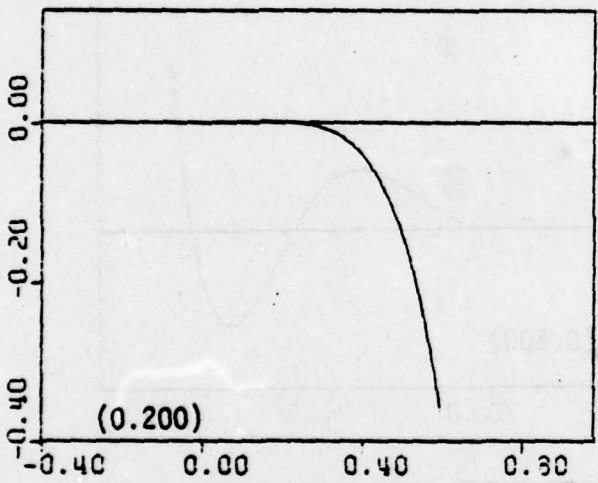
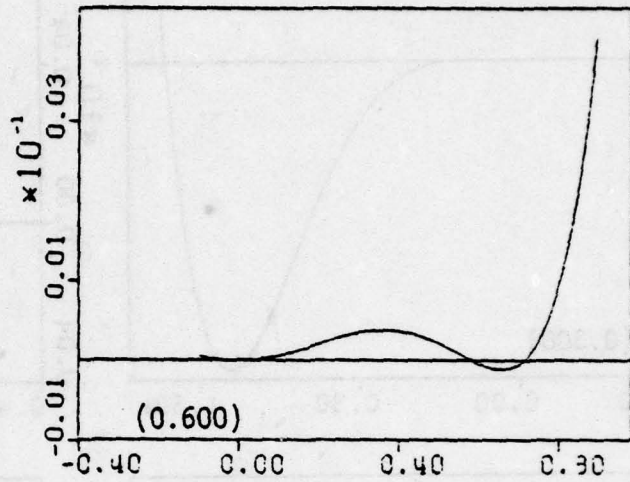
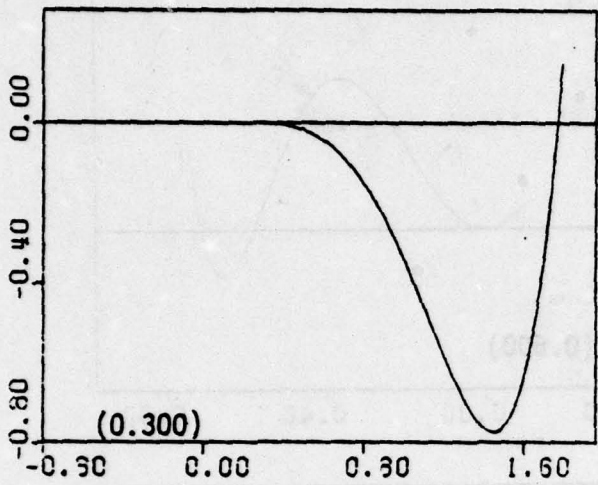
Plots of M vs $\kappa\lambda$ for $V_\infty = 0.100$. Value of δ_0 in Parentheses on Each Plot.

Figure 11.1(a)

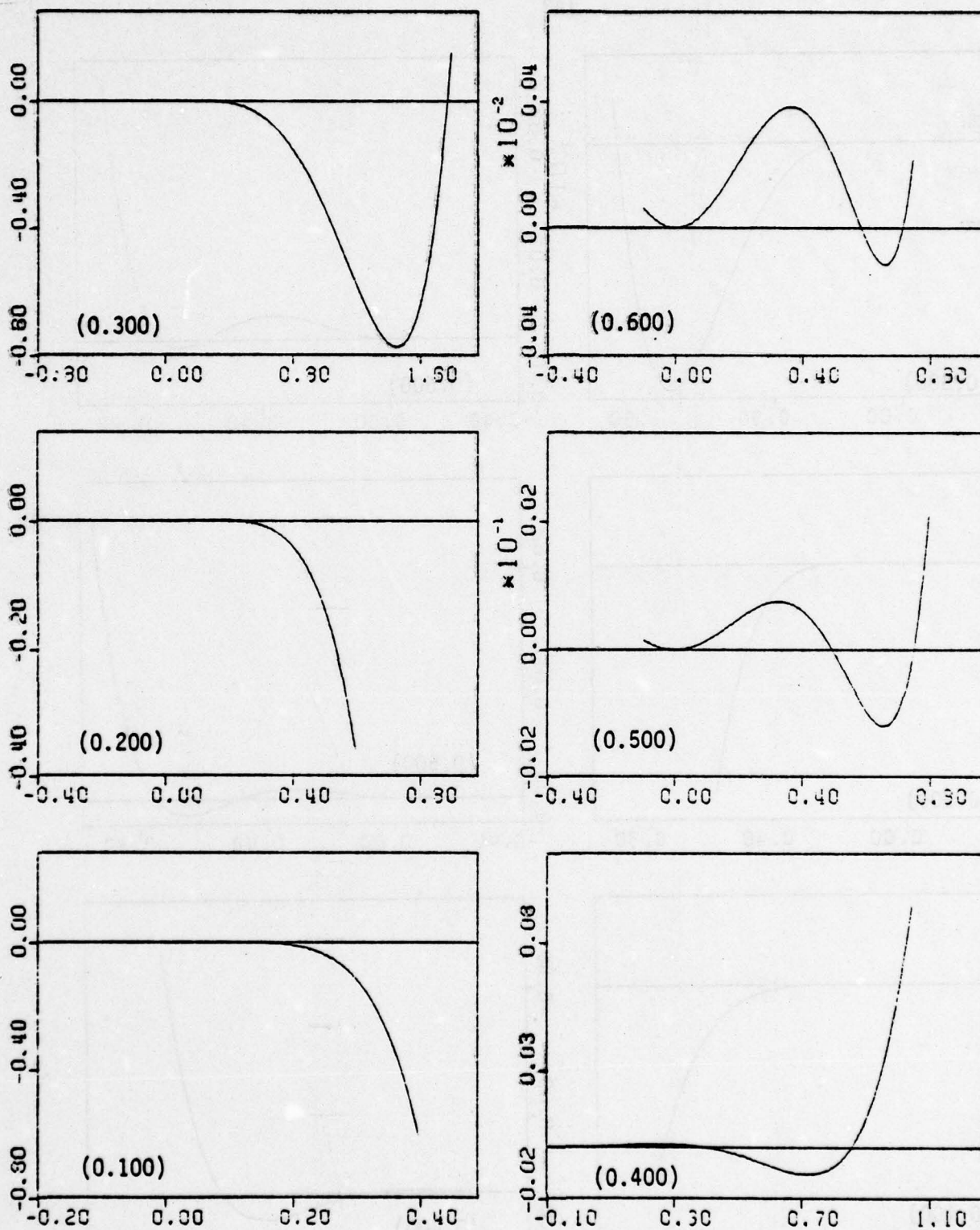


Plots of M vs $\kappa\lambda$ for $V_\infty = 0.200$. Value of δ_0 in Parentheses on Each Plot.

Figure 11.1(b)

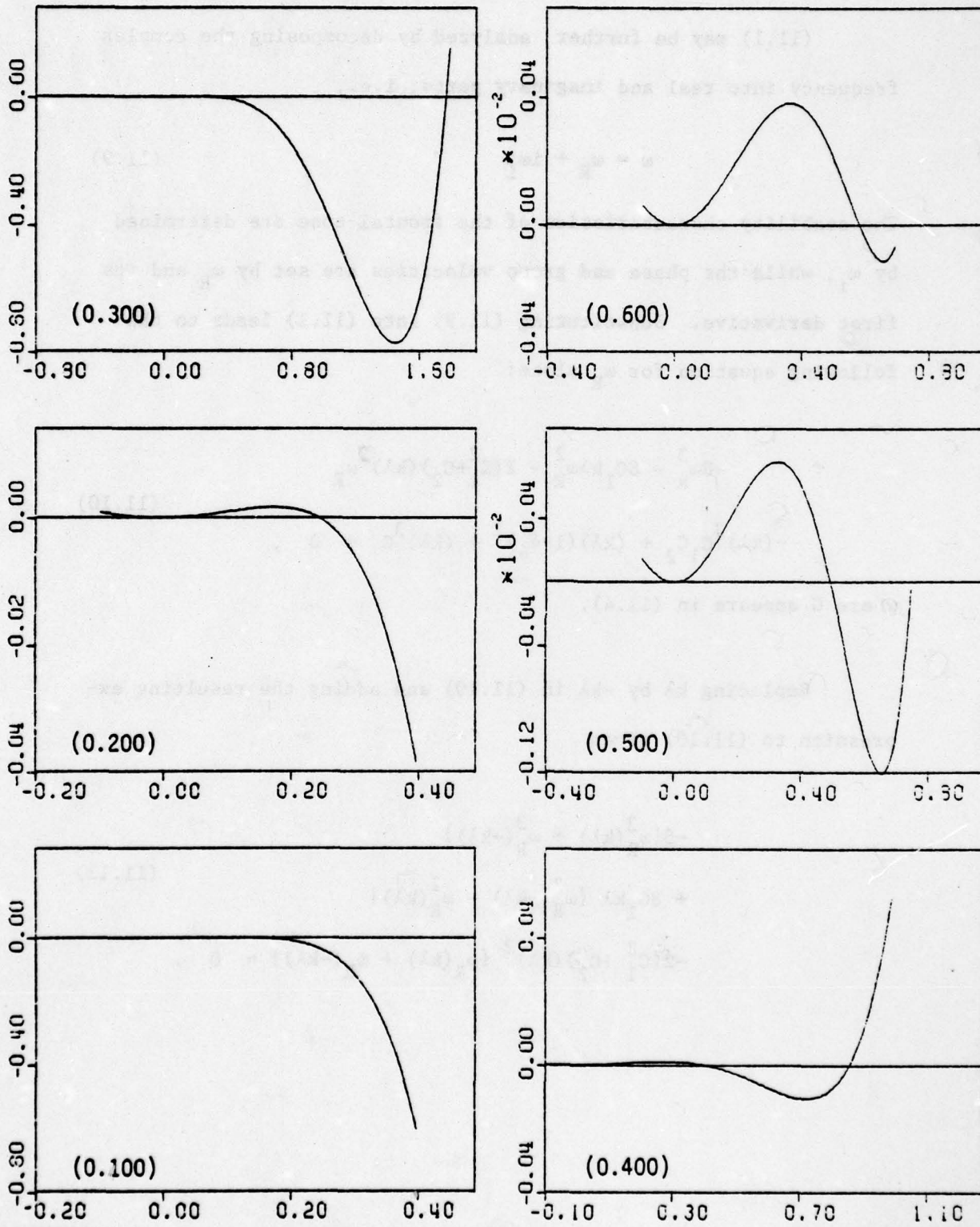


Plots of M vs $\kappa\lambda$ for $V_\infty = 0.300$. Values of ϵ_c in Parentheses on Each Plot.
Figure 11.1(c)



Plots of M vs $\kappa\lambda$ for $V_\infty = 0.400$. Values of δ_0 in Parentheses on Each Plot.

Figure 11.1(d)



Plots of M vs $\kappa\lambda$ for $V_\infty = 0.500$. Values of δ_0 in Parentheses on Each Plot.

Figure 11.1(e)

11.3 FURTHER ANALYSIS OF THE DISPERSION RELATION

(11.1) may be further analyzed by decomposing the complex frequency into real and imaginary parts, i.e.,

$$\omega = \omega_R + i\omega_I \quad (11.9)$$

The stability characteristics of the frontal zone are determined by ω_I , while the phase and group velocities are set by ω_R and its first derivative. Substituting (11.9) into (11.1) leads to the following equation for ω_R alone:

$$\begin{aligned} -8\omega_R^3 - 8C_1 k \lambda \omega_R^2 - 2(C_1^2 + C_2)(k\lambda)^2 \omega_R \\ - (k\lambda)^3 C_1 C_2 + (k\lambda)(1 - \delta_0)^2 + (k\lambda)^3 G = 0, \end{aligned} \quad (11.10)$$

where G appears in (11.4).

Replacing $k\lambda$ by $-k\lambda$ in (11.10) and adding the resulting expression to (11.10) gives

$$\begin{aligned} -8\{\omega_R^3(k\lambda) + \omega_R^3(-k\lambda)\} \\ + 8C_1 k \lambda \{\omega_R^2(-k\lambda) - \omega_R^2(k\lambda)\} \\ - 2(C_1^2 + C_2)(k\lambda)^2 \{\omega_R(k\lambda) + \omega_R(-k\lambda)\} = 0. \end{aligned} \quad (11.11)$$

This last expression is satisfied only if the coefficient of each power of $k\lambda$ vanishes independently, i.e.,

$$\begin{aligned}\omega_R^3(k\lambda) + \omega_R^3(-k\lambda) &= 0 \\ \omega_R^2(-k\lambda) - \omega_R^2(k\lambda) &= 0 \\ \omega_R(k\lambda) + \omega_R(-k\lambda) &= 0\end{aligned}\tag{11.12}$$

These three conditions, in turn, require

$$\omega_R(-k\lambda) = -\omega_R(k\lambda) \quad , \tag{11.13}$$

from which we see that the real part of the complex frequency is an odd function of $k\lambda$.

Proceeding in a similar manner, we can quickly generate the following result that expresses $\omega_i(k\lambda)$ in terms of $\omega_R(k\lambda)$:

$$\begin{aligned}\omega_i^2(k\lambda) - \omega_i^2(-k\lambda) &= 3\{\omega_R^2(k\lambda) - \omega_R^2(-k\lambda)\} \\ &+ 2C_1 k\lambda\{\omega_R(k\lambda) + \omega_R(-k\lambda)\}\end{aligned}\tag{11.14}$$

But, in view of (11.13), the right-hand-side of (11.14) vanishes identically, leaving

$$\omega_i(-k\lambda) = +\omega_i(k\lambda) \quad . \tag{11.15}$$

This result at first appears unusual, since it seems to imply that $\omega_1(k\lambda)$ simultaneously exhibits both even and odd symmetry. This apparent inconsistency is resolved, however, by realizing that complex roots of (11.1) must occur as a conjugate pair, which is the fact reflected in (11.15).

The real and imaginary parts of (11.1) are

$$\tilde{\omega}_R^3 - 3\tilde{\omega}_R\tilde{\omega}_I^2 + C_1(\tilde{\omega}_R^2 - \tilde{\omega}_I^2) \quad (11.16)$$

$$+ C_2\tilde{\omega}_R + \{(1-\delta_0)/k\lambda\}^2 + G = 0$$

and

$$3\tilde{\omega}_R^2 - \tilde{\omega}_I^2 + 2C_1\tilde{\omega}_R + C_2 = 0 \quad , \quad (11.17)$$

respectively, where

$$\tilde{\omega} = \omega/k\lambda = \tilde{\omega}_R + i\tilde{\omega}_I \quad . \quad (11.18)$$

Eliminating $\tilde{\omega}_R$ between (11.16) and (11.17) generates a single equation for $\tilde{\omega}_I(k\lambda)$, which is analogous to (11.10) for the real part of ω . The derivation, however, is considerably more involved algebraically than the one leading to (11.10), and the details are not reproduced here. The final form is

$$e_6 \omega_1^6 + e_4 \omega_1^4 + e_2 \omega_1^2 + e_0 = 0 \quad (11.19)$$

where

$$e_6 = 192/81 \quad (11.20a)$$

$$e_4 = (32/27)\Delta\{2\Delta(2 + 3/\delta_0) - 3\} \quad (11.20b)$$

$$e_2 = (1/27)\{36f^2(\Delta) - 24f(\Delta)\Delta^2 + 4\Delta^4\} \quad (11.20c)$$

$$\begin{aligned} e_0 = & 4\Delta^4(2\Delta/27 - 1) - (4/27)f^3(\Delta) \\ & + (4/27)f(\Delta)\Delta^2\{18\Delta - \Delta^2 - 2f(\Delta)\} \\ & + 4\Delta\{\Delta - \Delta^2/27 - (1/3)\cdot f(\Delta)\}(\Delta/k\lambda)^2 \\ & - (\Delta/k\lambda)^4 \end{aligned} \quad (11.20d)$$

$$f(\Delta) = \Delta\{1 - \Delta(1+2/\delta_0)\} \quad (11.20e)$$

$$\Delta = 1 - \delta_0 \quad (11.20f)$$

This is a remarkable result, in that the coefficients e_0 through e_6 do not depend on the shear velocity V_∞ . Thus, $\tilde{\omega}_1$ is independent of V_∞ , or, equivalently, the frontal zone's stability characteristics are independent of V_∞ . The real part of ω , on the other hand, does, in general, depend on V_∞ , so that the phase and group velocities of first order frontal disturbances do exhibit a parametric dependence on V_∞ . As we have seen in Section 11.1, only in the low frequency limit is the real part of ω independent of V_∞ . We also note that only e_0 contains any $\kappa\lambda$ dependence; each of the other coefficients is a function of δ_0 alone. Thus, δ_0 appears to be the dominant parameter in determining the frontal zone's stability.

11.4 NUMERICAL RESULTS

(10.24) has been solved numerically for a range of the parameters δ_0 and V_∞ . For fixed $\kappa\lambda$, the three roots of (10.24) were computed iteratively using the IMSL⁽¹⁾ algorithm ZRPOLY, which provided exceptional accuracy. Substitution of the calculated roots back into (10.24) gave equality to within typically one part in 10^{13} .

Table 11.1 compares the frequencies calculated from the exact dispersion relation, (10.24), with those calculated from its low frequency asymptotic form in (11.6) for the case $\delta_0=0.35$ and $V_\infty=0.20$. Since the complex frequencies (roots) must occur as a conjugate pair, only one complex root is tabulated in Table 11.1, along with the purely real root. Results obtained with the low frequency limit are in parentheses. It is apparent from the table that the low frequency limit is a good approximation only for large disturbance wavelengths, or, conversely, small $\kappa\lambda$. Agreement to within 20% or so is obtained out to $\kappa\lambda=0.10$. As $\kappa\lambda$ increases, the low frequency limit becomes a progressively poorer approximation.

Parameter Values: $\delta_0 = 0.35$, $V_\infty = 0.20$

$\kappa\lambda$	Complex Root		Real Root
	Real Part	Imag Part	
0.00	0.000(0.000)*	0.000(0.000)	0.000(0.000)
0.01	0.077(0.081)	0.140(0.140)	-0.166(-0.162)
0.02	0.094(0.102)	0.175(0.176)	-0.213(-0.204)
0.03	0.105(0.117)	0.199(0.202)	-0.248(-0.233)
0.04	0.114(0.128)	0.218(0.222)	-0.278(-0.257)
0.05	0.120(0.138)	0.232(0.239)	-0.303(-0.276)
0.06	0.126(0.147)	0.245(0.254)	-0.327(-0.294)
0.07	0.131(0.155)	0.255(0.268)	-0.349(-0.309)
0.08	0.135(0.162)	0.264(0.280)	-0.369(-0.323)
0.09	0.138(0.168)	0.271(0.291)	-0.389(-0.336)
0.10	0.141(0.174)	0.278(0.302)	-0.408(-0.348)
0.15	0.153(0.199)	0.295(0.345)	-0.493(-0.399)
0.20	0.160(0.219)	0.291(0.380)	-0.571(-0.439)
0.25	0.165(0.236)	0.269(0.409)	-0.643(-0.473)
0.30	0.168(0.251)	0.220(0.435)	-0.712(-0.502)
0.35	0.170(0.264)	0.119(0.458)	-0.777(-0.529)
0.40	-0.006(0.276)	0.000(0.479)	-0.841(-0.553)
0.45	-0.126(0.288)	0.000(0.498)	-0.903(-0.575)
0.50	-0.226(0.298)	0.000(0.516)	-0.962(-0.596)

*Results in parentheses computed from the low frequency limit

Table 11.1 Comparison of Low Frequency Limit
and Exact Solution to the Dispersion
Relation

The exact frequencies show a band of instability for $0 < \kappa\lambda < 0.40$ as a result of the nonzero imaginary part of the complex root. For $\kappa\lambda \geq 0.40$, all three modes are stable, since the imaginary part of the complex frequency is zero. The real part of the complex frequency increases from zero at $\kappa\lambda = 0$ to a maximum positive value near $\kappa\lambda = 0.35$, and then quickly decreases to negative values for $\kappa\lambda \geq 0.40$. The behavior of the real and imaginary parts of the complex frequency is thus clearly not monotonic in $\kappa\lambda$. The low frequency limit, however, is monotonic in $\kappa\lambda$, which, in part, accounts for its poor performance as an approximation when $\kappa\lambda$ is large.

Figures 11.2 through 11.4 show plots of the exact dispersion relation (real and imaginary parts of ω vs $\kappa\lambda$) at order F_b^1 for the exponential front computed from (10.24). They illustrate the qualitative behavior of the dispersion characteristics as the parameters δ_0 and V_∞ are varied. Figures 11.5 and 11.6 provide typical phase and group velocity plots, computed from $C_{ph} = \text{Re}(\omega)/\kappa\lambda$ and $C_{gr} = d\text{Re}(\omega)/d(\kappa\lambda)$, respectively, for various values of δ_0 and V_∞ .

Figures 11.2a through 11.2e plot the imaginary part of each of the three complex roots (frequencies) as a function of $\kappa\lambda$ for $\delta_0 = 0.5$ to 0.1 in increments of 0.1, respectively. Since ω_1 is independent of V_∞ , the results in this set of curves apply for any value of V_∞ . The real part of the complex frequency does depend on V_∞ , however, and its value therefore appears in the plot annotation. Each of the three roots of the dispersion relation is marked by a different symbol on the plots in Figures 11.2 through 11.6 (circle, diamond and triangle).

In Figure 11.2, the $\kappa\lambda$ axis is always overplotted because the cubic dispersion relation must always contain at least one purely real root with a corresponding zero imaginary part. Since the complex-valued dispersion relation roots must occur always as a conjugate pair, unstable and evanescent modes, corresponding to $\text{Im}(\omega) < 0$ and $\text{Im}(\omega) > 0$, respectively, must also occur as a pair. Thus, every unstable mode is accompanied by an evanescent mode, and this fact is reflected in the mirror image symmetry about the $\kappa\lambda$ -axis in Figure 11.2. In addition, $\text{Im}(\omega)$ is also symmetrical about the ω -axis, as discussed in Section 11.3. It is therefore sufficient to consider only $\kappa\lambda \geq 0$ in discussing stability.

Figure 11.2 reveals two symmetric bands of instability, that is, two regions on nonzero $\text{Im}(\omega)$. The one referred to as Band 1 is centered about the $\kappa\lambda$ origin, while the other, Band 2, is bounded away from $\kappa\lambda=0$. Band 1 is characterized by the maximum normalized wavenumber for modes in this band, which is labeled $\kappa\lambda_{\text{max}}$ in Figure 11.2a, and by the $(\kappa\lambda, \omega)$ pair that gives the fastest growing unstable mode in this band. This point on the dispersion curve is marked by the largest value of $|\text{Im}(\omega)|$, as shown in Figure 11.2a. Examination of Figure 11.2 shows that $|\text{Im}(\omega)|$ is monotonically increasing with increasing $\kappa\lambda$ for modes in Band 2, so that modes in Band 2 exhibit progressively larger imaginary parts of the disturbance frequency with increasing wavenumber. Therefore, no fastest growing mode exists in Band 2. The only parameter characterizing Band 2 is the minimum wavenumber for modes contained in it, labeled $\kappa\lambda_{\text{min}}$ in Figure 11.2a.

Each unstable mode possesses a time dependent amplitude which doubles in the interval $t_d = \ln(2/F_b) / |\text{Im}(\omega)|$. The point (0,0) is always contained in the dispersion curve. Thus, for any finite values of the

parameters δ_0 and F_b , as the wavelength becomes arbitrarily large, so does the doubling time. The doubling time also becomes infinite for unstable modes with nonzero frequencies as $F_b \rightarrow 0$. At order F_b^1 for the exponential front, therefore, unstable modes evolve continuously from stable ones with increasing cross-stream flow. For zero cross-stream velocity, all modes are stable, but the doubling time for a given unstable mode decreases from infinity with increasing cross-stream flow. The existence of nonzero cross-stream velocity is therefore of paramount importance in determining the stability characteristics of the exponential front.

The limiting normalized wavenumbers for Bands 1 and 2, $\kappa\lambda_{\max}$ and $\kappa\lambda_{\min}$ as discussed above, are tabulated as functions of δ_0 in Table 11.2. The maximum wavenumber for modes in Band 1 increases with increasing δ_0 , as does the minimum wavenumber for Band 2 modes. $\kappa\lambda_{\max}$ is nearly equal to δ_0 , and this observation serves as a useful rule of thumb for setting the limits of Band 1 modes in the range $0.1 \leq \delta_0 \leq 0.5$. Recall that the results in Table 11.2 are independent of V_∞ .

The characteristics of the fastest growing mode in Band 1 are tabulated as functions of δ_0 in Table 11.3 for $V_\infty = 0.2$. Knowing V_∞ is important in this case, since $\text{Re}(\omega)$, C_{ph} and C_{gr} depend upon it. $\kappa\lambda$, $\text{Im}(\omega)$ and t_d , however, do not depend on V_∞ , so that the tabulated results for these quantities apply generally for δ_0 in the range considered. Observational data tend to show that F_b , or, equivalently, the cross-stream flow, is quite small in large scale upper ocean density fronts. It is unlikely, therefore, that values of F_b much larger than 0.2 would be associated with the frontal structures considered in this paper. Doubling times in Table 11.3 are therefore computed for $F_b = 0.05$ and $F_b = 0.20$, which are taken as reasonable representative limits for this parameter.

Table 11.3 shows that the wavenumber of the fastest growing mode is nearly equal to $\delta_0/2$, which is a useful rule of thumb for estimating its value. As δ_0 increases by a factor of 5, $\kappa\lambda$ increases by a factor of about 4. The real and imaginary parts of the disturbance frequency, however, are far less sensitive to changes in δ_0 . The real part of ω increases very slightly as δ_0 increases from 0.1 to 0.2, and thereafter decreases by a factor of less than 1/3 as δ_0 continues to 0.5. The imaginary part of ω is even less sensitive to varying δ_0 , and remains between -0.263 and -0.297 as δ_0 ranges over 0.1-0.5. The phase and group velocities both decrease with increasing δ_0 and show considerable variation. The shortest doubling time, normalized by the inertial period, occurs for $\delta_0=0.3$. It is not particularly sensitive to changes in F_b as a result of the logarithmic dependence on F_b . As F_b increases by a factor of 4, the doubling time decreases by somewhat less than 50%. Note that all entries in Table 11.3 are dimensionless.

In order to compare these results with observational data, Tables 11.4 through 11.6 provide the most important characteristics of the fastest growing mode as dimensional quantities for the data in Table 11.3. The disturbance period in days is computed from $T_{\text{days}} = 2\pi/\text{Re}(\omega) \cdot f \cdot 8.64 \times 10^4$, where f is the Coriolis parameter. For convenient reference, the Coriolis parameter is tabulated in Table 11.4. The wavelength is computed from $2\pi\lambda/(\kappa\lambda)$. Table 11.5 shows the disturbance period in days at various latitudes as a function of $\text{Re}(\omega)$, whose values are given in Table 11.3 for the fastest growing mode. We see that the disturbance period decreases with increasing latitude, and increases with decreasing $\text{Re}(\omega)$. For latitudes between 20° and 50° , the fastest growing mode with $V_\infty=0.2$ exhibits periods between 3.63 days and 12.50

days for $0.1 < \delta_0 < 0.5$. For $\delta_0 = 0.3$, corresponding to $\text{Re}(\omega) = 0.166$, the periods at 20° , 30° and 40° latitude are 8.81, 6.02 and 4.69 days, respectively. These values are in fair agreement with the dominant periods observed using satellite imagery of the Gulf Stream by Maul, *et. al* (1978). Their spectral analysis of Gulf Stream Meanders revealed dominant periods of 10, 5.8 and 4.8 days, respectively, at latitudes of approximately 27°N , 33°N and 38°N . The variation of meander period with latitude seems to be strongly influenced by Coriolis effects. Using the fastest growing mode wavenumbers in Table 11.3, the corresponding dimensional wavelengths appear in Table 11.6 for two values of the baroclinic Rossby radius, λ . Although these wavelengths are seen to be quite long, they are not necessarily inconsistent with observed frontal meander patterns, which result from the superposition of a continuum of wavelengths ranging from short to very long.

Table 11.7 displays the characteristics of the fastest growing mode in Band 1 for $V_\infty = 0.6$ in order to examine the sensitivity to changes in V_∞ . Only those parameters that are dependent upon V_∞ are included in this table. While the data in Table 11.3 show that the real part of ω does not change substantially with increasing δ_0 for $V_\infty = 0.2$, the data in Table 11.7 reveal that $\text{Re}(\omega)$ is far more sensitive to changes in δ_0 for $V_\infty = 0.6$. As δ_0 changes by a factor of 5, from 0.1 to 0.5, $\text{Re}(\omega)$ decreases by a factor of 7, from 0.155 to 0.023. At $V_\infty = 0.2$, $\text{Re}(\omega)$ was monotonically decreasing only for increasing δ_0 greater than 0.2. For $V_\infty = 0.6$, however, $\text{Re}(\omega)$ decreases with increasing δ_0 between 0.1 and 0.5. As V_∞ increases from 0.2 to 0.6, the phase velocity at $\delta_0 = 0.1$ decreases only slightly, while at $\delta_0 = 0.5$ it decreases by nearly a factor of 5. As in Table 11.3, C_{ph} is monotonically decreasing with increasing δ_0 . For fixed δ_0 the change in group velocity as V_∞ increases from 0.2 to 0.6 is larger than the corresponding change in C_{ph} . C_{gr} is again monotonically decreasing with increasing δ_0 at $V_\infty = 0.6$. The period in days at latitudes of 20° , 30° , 40° and 50° corresponding to the tabulated values of $\text{Re}(\omega)$ constitute the last four columns in Table 11.7. Since $\text{Re}(\omega)$ is considerably more sensitive to variations in δ_0 at $V_\infty = 0.6$ than it is at $V_\infty = 0.2$, the periods in Table 11.7 exhibit far more variation with δ_0 at a given latitude than those in Table 11.5. The maximum period is 63.57 days at $\delta_0 = 0.5$ and 50° latitude. For intermediate values of δ_0 , where $\text{Re}(\omega)$ at $V_\infty = 0.6$ is not drastically

different from its corresponding value at $V_{\infty}=0.2$, the periods in Table 11.7 and 11.5 are not greatly different. Except at $\delta_0=0.4$ and $\delta_0=0.5$, even at $V_{\infty}=0.6$, the disturbance periods are thus reasonably consistent with the observational data of Maul, et al., (1978). As a general conclusion, with increasing V_{∞} , the disturbance period is progressively less sensitive to the change in V_{∞} as δ_0 decreases.

Using the same format as Table 11.7, data for V_{∞} between zero and 2.00 are summarized in Table 11.8.

TABLE 11.2

Maximum and Minimum Normalized

Wavenumber for Bands 1 and 2

$\frac{\delta_0}{\lambda}$	Band 1 $k\lambda_{\max}$	Band 2 $k\lambda_{\min}$
0.1	0.154	≈ 0.77
0.2	0.248	≈ 0.88
0.3	0.321	≈ 1.77
0.4	0.406	> 2.00
0.5	0.490	> 2.00

TABLE 11.3

Characteristics of the Fastest
Growing Mode, Band 1, $V_\infty = 0.2$

δ_o	$\kappa\lambda$	$\text{Re}(w)$	$\text{Im}(w)$	C_{ph}	C_{gr}	$F_b=0.05$	τ_d $F_b=0.20$
0.1	0.063	0.180	-0.263	2.85	1.17	14.03	8.76
0.2	0.111	0.182	-0.290	1.65	0.54	12.72	7.94
0.3	0.147	0.166	-0.297	1.13	0.26	12.42	7.75
0.4	0.189	0.145	-0.293	0.77	0.08	12.59	7.86
0.5	0.237	0.117	-0.281	0.49	-0.05	13.13	8.19

TABLE 11.4

Values of the Coriolis
Parameter as a Function of Latitude

<u>LAT (Deg)</u>	<u>f(Sec⁻¹)</u>
0	0
10	2.526×10^{-5}
20	4.974×10^{-5}
30	7.272×10^{-5}
40	9.349×10^{-5}
50	1.114×10^{-4}
60	1.260×10^{-4}
70	1.376×10^{-4}
80	1.432×10^{-4}
90	1.454×10^{-4}

TABLE 11.5

Period at Various Latitudes

Period in Days at Latitude in Degrees

<u>Re (w)</u>	<u>20°</u>	<u>30°</u>	<u>40°</u>	<u>50°</u>
0.180	8.12	5.56	4.32	3.63
0.182	8.03	5.49	4.27	3.59
0.166	8.81	6.02	4.69	3.93
0.145	10.08	6.90	5.36	4.50
0.117	12.50	8.55	6.65	5.58

TABLE 11.6
Wavelength for Various Values of $k\lambda$
and Rossby Radius

<u>$k\lambda$</u>	Wavelength (km)	
	<u>$\lambda = 50$ km</u>	<u>$\lambda = 100$ km</u>
0.063	4987	9973
0.111	2830	5661
0.147	2137	4274
0.189	1662	3324
0.237	1326	2651

TABLE 11.7

Characteristics of the Fastest Growing

Mode, Band 1, $V_{\infty} = 0.6$

δ_0	$Re(w)$	C_{ph}	C_{gr}	Period in Days at Latitude in Degrees			
				20°	30°	40°	50°
0.1	0.155	2.46	0.77	9.43	6.45	5.02	4.21
0.2	0.138	1.24	0.14	10.59	7.25	5.64	4.73
0.3	0.107	0.73	-0.14	13.66	9.35	7.27	6.10
0.4	0.069	0.37	-0.32	21.19	14.49	11.27	9.46
0.5	0.023	0.10	-0.45	63.57	43.48	33.82	28.38

TABLE 11.8

V_{∞}	δ_0	Re(w)	C_{ph}	C_{gr}	Period in Days at Latitude in Degrees			
					20°	30°	40°	50°
0.00	0.1	0.193	3.06	1.37	7.57	5.18	4.03	3.38
	0.2	0.204	1.84	0.74	7.17	4.90	3.81	3.20
	0.3	0.195	1.33	0.46	7.50	5.13	3.99	3.35
	0.4	0.170	0.90	0.28	8.60	5.88	4.58	3.84
	0.5	0.165	0.70	0.15	8.86	6.06	4.71	3.96
0.05	0.1	0.190	3.02	1.32	7.69	5.26	4.09	3.44
	0.2	0.199	1.79	0.69	7.35	5.03	3.91	3.28
	0.3	0.188	1.28	0.41	7.78	5.32	4.14	3.47
	0.4	0.173	0.92	0.23	8.45	5.78	4.50	3.77
	0.5	0.153	0.65	0.10	9.55	6.54	5.08	4.27
0.20	0.1	0.180	2.85	1.17	8.12	5.56	4.32	3.63
	0.2	0.182	1.65	0.54	8.03	5.49	4.27	3.59
	0.3	0.166	1.13	0.26	8.81	6.02	4.69	3.93
	0.4	0.145	0.77	0.08	10.08	6.90	5.36	4.50
	0.5	0.117	0.49	-0.05	12.50	8.55	6.65	5.58
0.40	0.1	0.168	2.67	0.97	8.70	5.95	4.63	3.89
	0.2	0.160	1.44	0.34	9.14	6.25	4.86	4.08
	0.3	0.136	0.93	0.06	10.75	7.35	5.72	4.80
	0.4	0.107	0.57	-0.12	13.66	9.35	7.27	6.10
	0.5	0.070	0.30	-0.25	20.88	14.29	11.11	9.32
0.60	0.1	0.155	2.46	0.77	9.43	6.45	5.02	4.21
	0.2	0.138	1.24	0.14	10.59	7.25	5.64	4.73
	0.3	0.107	0.73	-0.14	13.66	9.35	7.27	6.10
	0.4	0.069	0.37	-0.32	21.19	14.49	11.27	9.46
	0.5	0.023	0.10	-0.45	63.57	43.48	33.82	28.38

TABLE 11.8

V_{∞}	δ_0	Re(w)	C_{ph}	C_{gr}	Period in Days at Latitude in Degrees				
					20°	30°	40°	50°	
0.80	0.1	0.142	2.25	0.57	10.30	7.04	5.48	4.60	
	0.2	0.116	1.05	-0.06	12.60	8.62	6.71	5.63	
	0.3	0.077	0.52	-0.34	18.99	12.99	10.10	8.48	
	0.4	0.031	0.16	-0.52	47.16	32.26	25.09	21.05	
	0.5	-0.024	-0.10	-0.65	-60.71	-41.67	-32.41	-27.20	
1.00	0.1	0.130	2.06	0.37	11.25	7.69	5.98	5.02	
	0.2	0.093	0.84	-0.26	15.72	10.75	8.36	7.02	
	0.3	0.048	0.33	-0.54	30.46	20.83	16.21	13.60	
	0.4	-0.007	-0.04	-0.72	-208.84	-142.86	-111.12	-93.24	
	0.5	-0.067	-0.28	-0.85	-21.82	-14.93	-11.61	-9.74	
1.50	0.1	0.098	1.56	-0.13	14.92	10.20	7.94	6.66	
	0.2	0.038	0.34	-0.76	38.47	26.32	20.47	17.18	
	0.3	-0.026	-0.18	-1.04	-56.23	-38.46	-29.92	-25.10	
	0.4	-0.102	-0.54	-1.22	-14.33	-9.80	-7.63	-6.40	
	0.5	-0.190	-0.80	-1.35	-7.69	-5.26	-4.09	-3.44	
2.00	0.1	0.067	1.06	-0.63	21.82	14.93	11.61	9.74	
	0.2	-0.018	-0.16	-1.26	-81.22	-55.56	-43.21	-36.26	
	0.3	-0.108	-0.73	-1.54	-13.54	-9.26	-7.20	-6.04	
	0.4	-0.196	-1.04	-1.72	-7.46	-5.10	-3.97	-3.33	
	0.5	-0.309	-1.30	-1.85	-4.73	-3.24	-2.52	-2.11	

NOTE: Negative Disturbance Periods Reflect The Sign of Re(w)

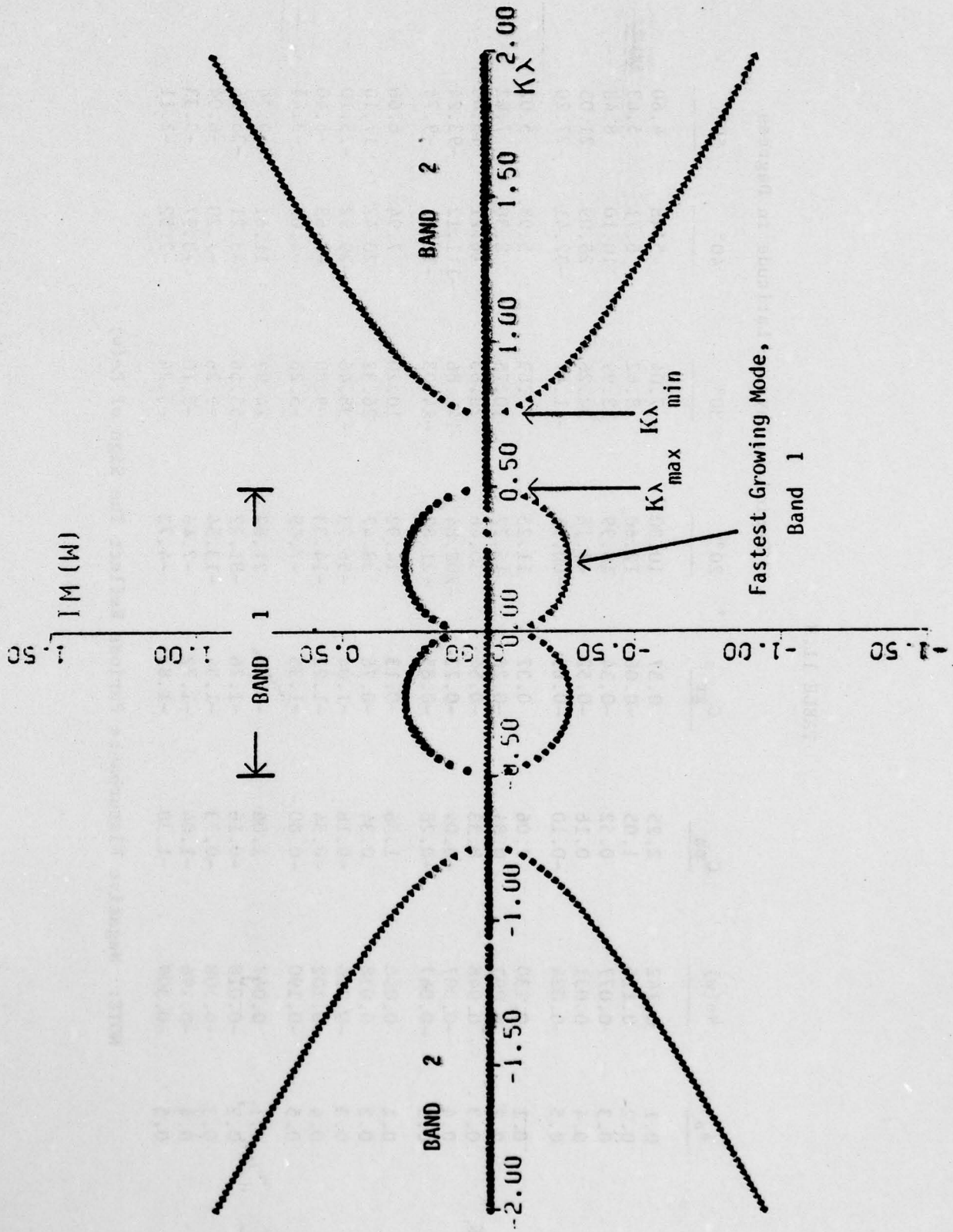


Figure 11.2(a): $s_0 = 0.500$

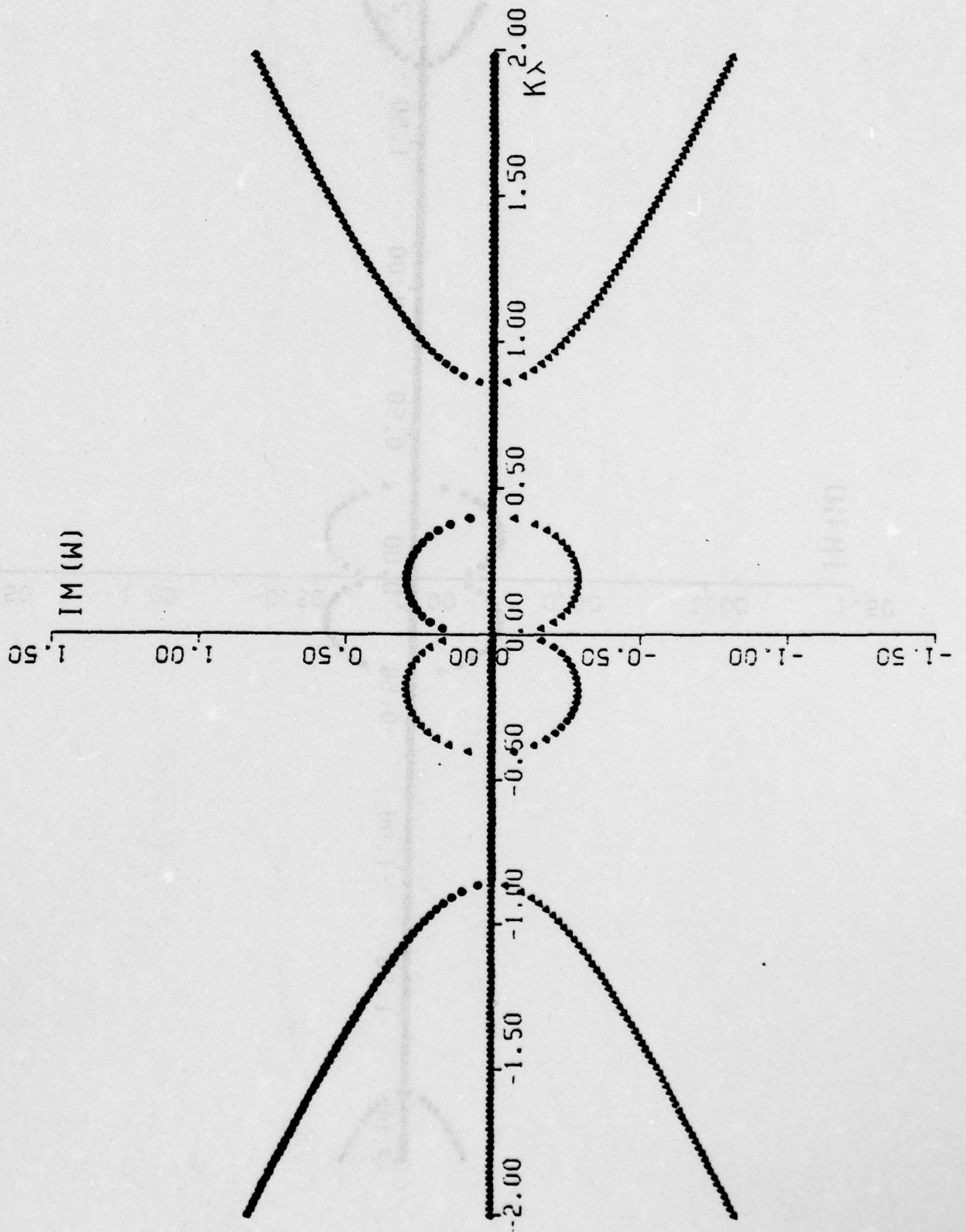


Figure 11.2(b): $\lambda = 0.400$

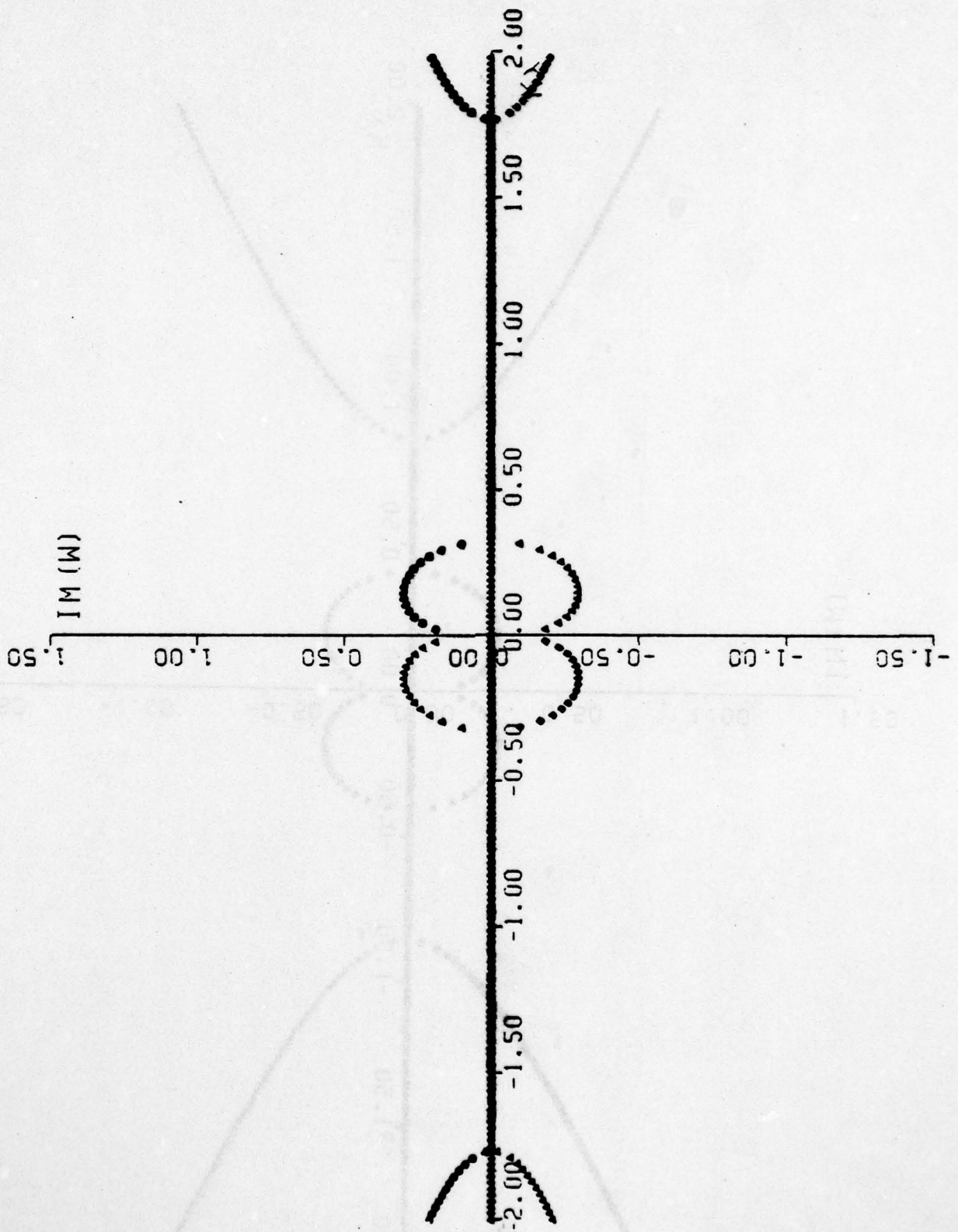
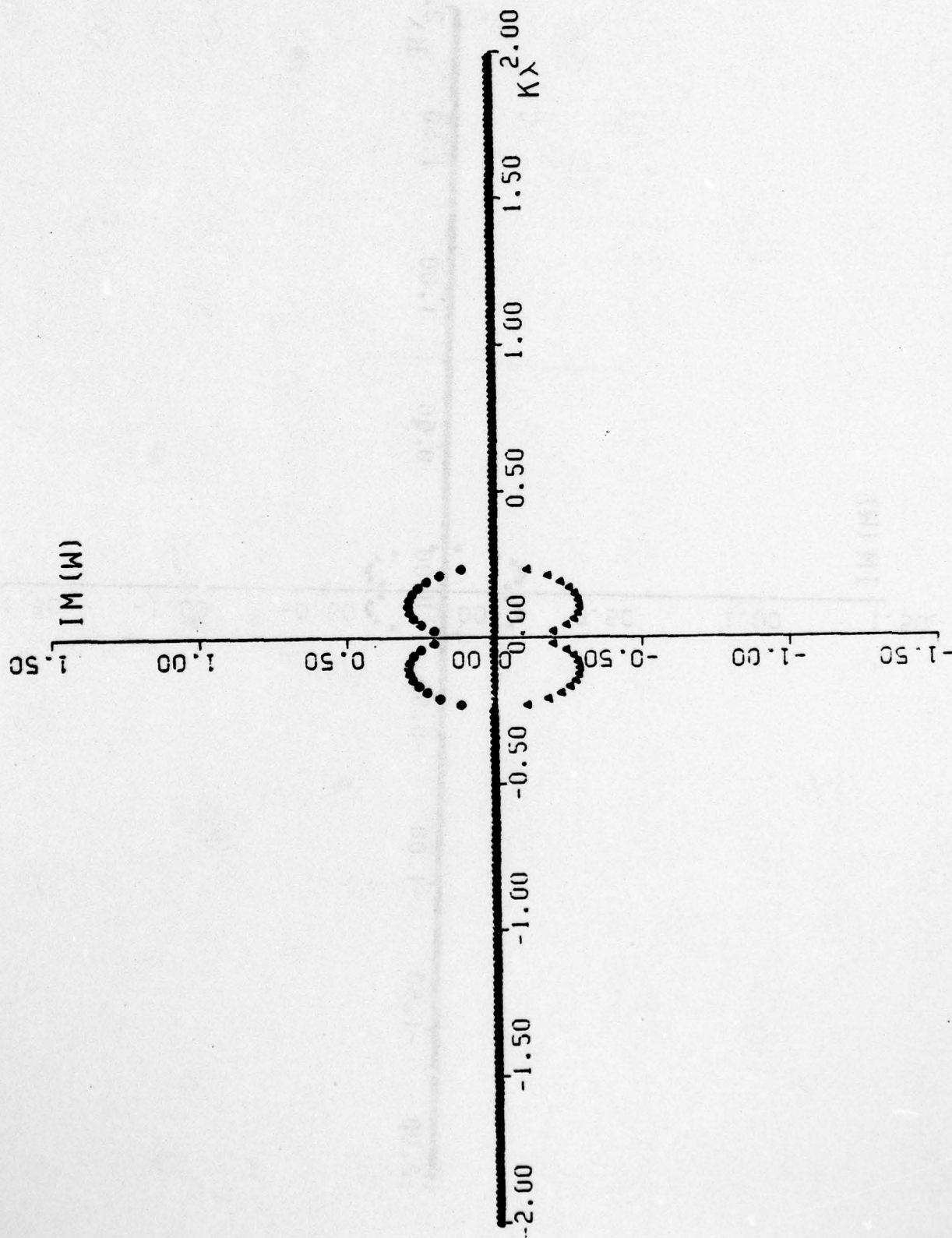


Figure 11.2(c): $\delta_0 = 0.300$



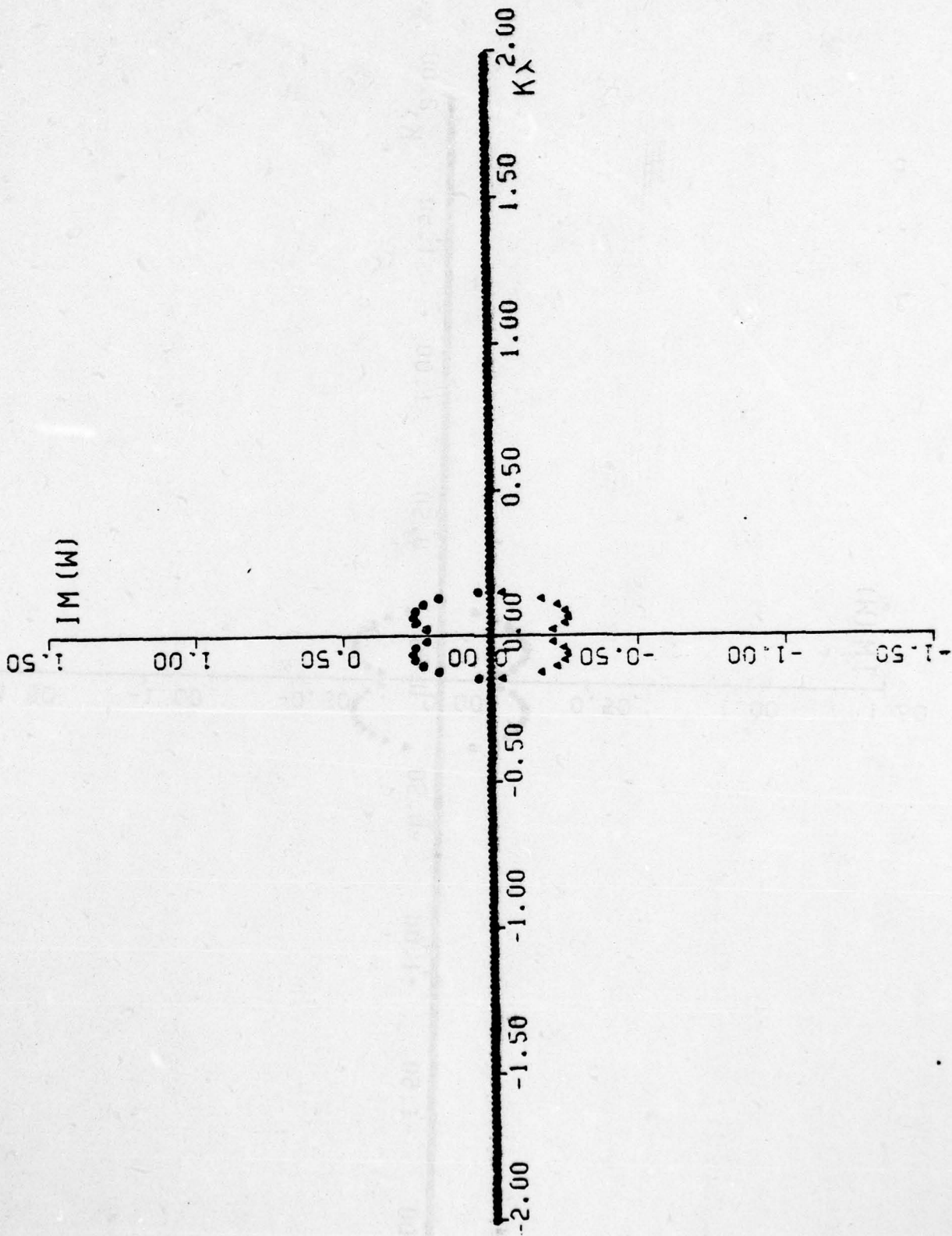


Figure 11.2(e): $\delta_0 = 0.100$

PARAMETER VALUES FOR FIGURES 11.3 THROUGH 11.6

<u>FIGURE</u>	<u>δ_0</u>	<u>V_∞</u>
11.3(a)	0.5	0.2
(b)	0.4	0.2
(c)	0.3	0.2
(d)	0.2	0.2
(e)	0.1	0.2
11.4(a)	0.4	0.5
(b)	0.4	0.4
(c)	0.4	0.3
(d)	0.4	0.2
(e)	0.4	0.1
11.5(a)	0.5	0.2
(b)	0.4	0.2
(c)	0.3	0.2
(d)	0.2	0.2
(e)	0.1	0.2
11.6(a)	0.4	0.5
(b)	0.4	0.4
(c)	0.4	0.3
(d)	0.4	0.2
(e)	0.4	0.1

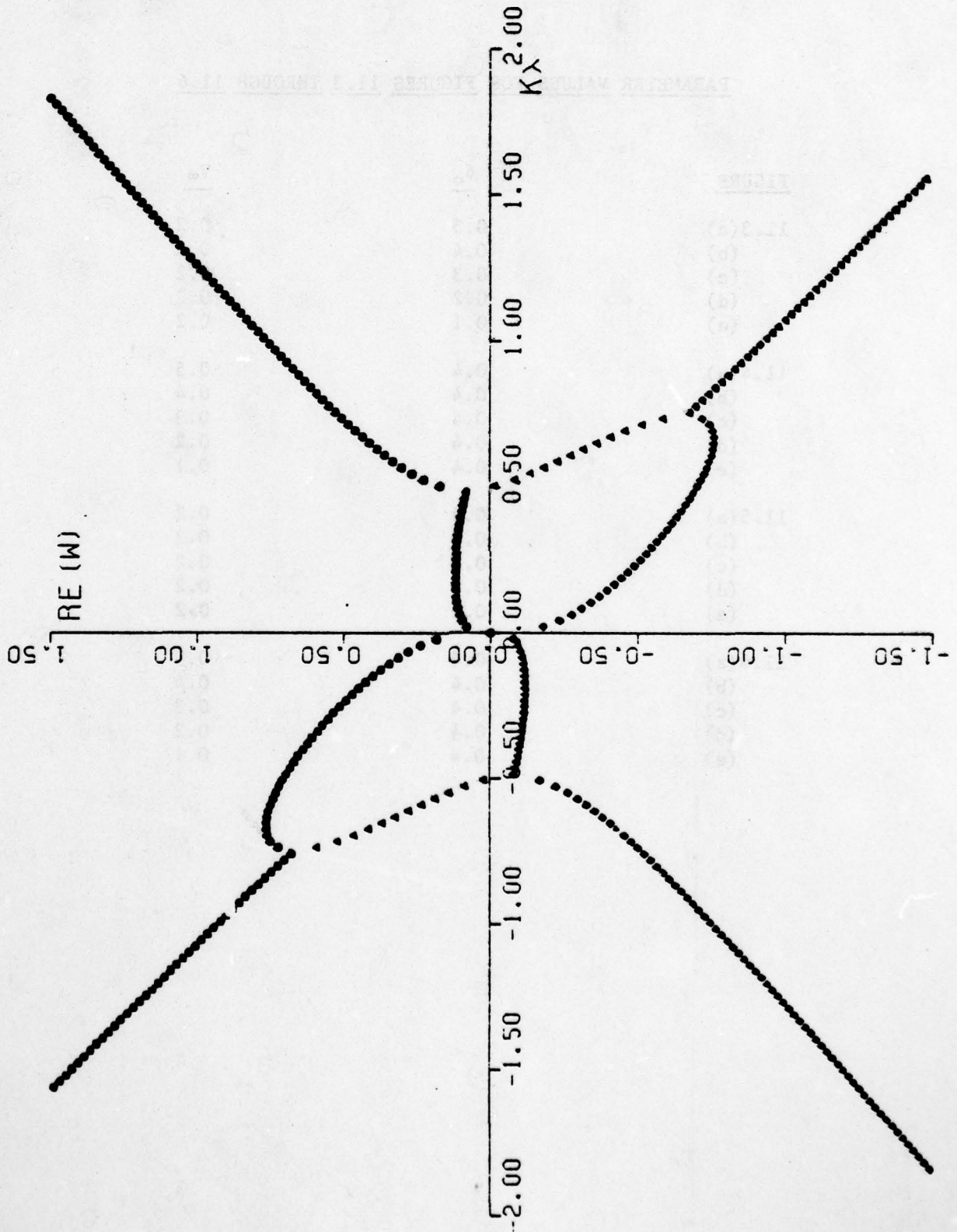


Figure 11.3(a)

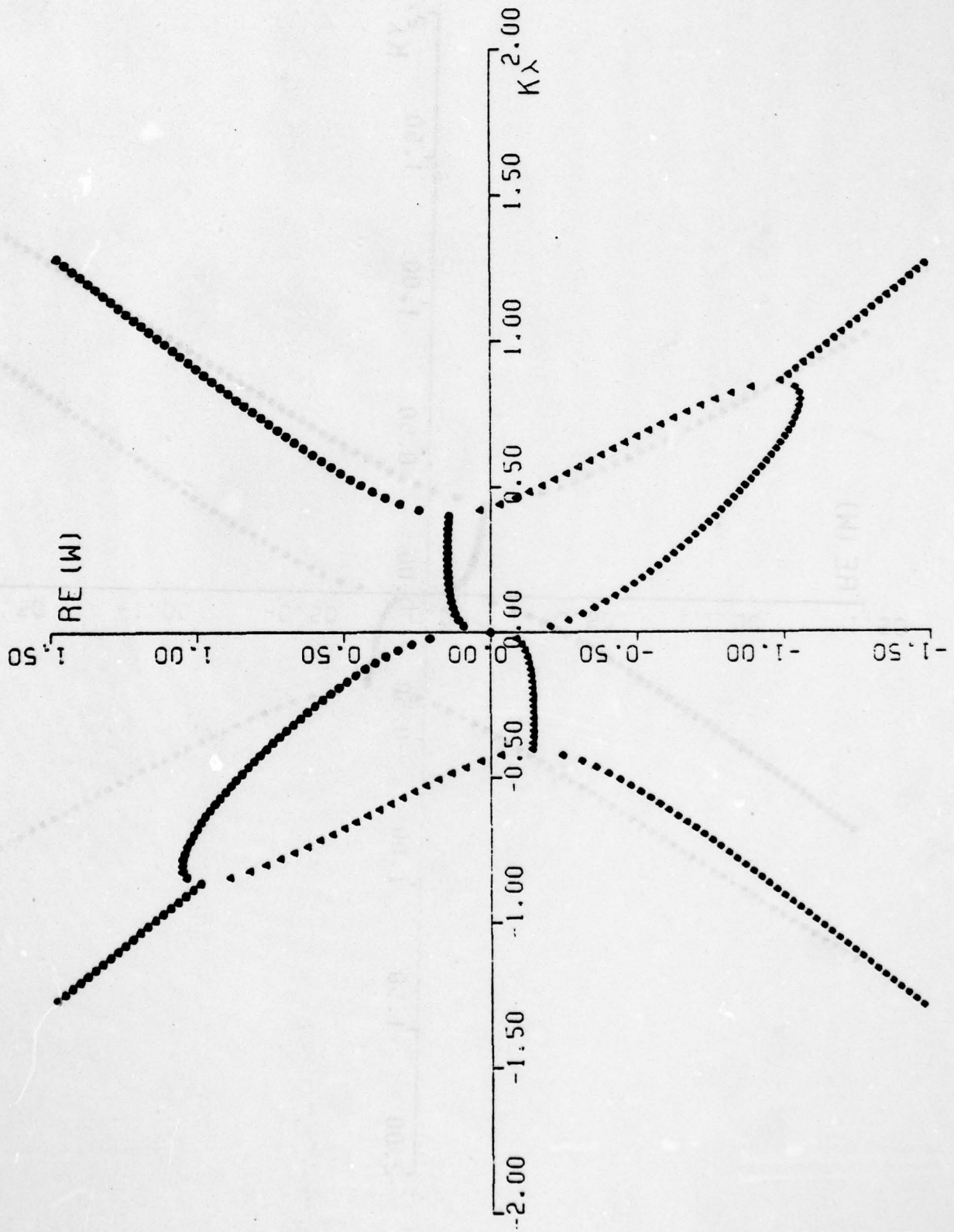


Figure 11.3(b)

AD-A076 248

DELAWARE UNIV NEWARK COLL OF MARINE STUDIES

F/6 8/10

WAVELIKE BAROCLINIC DISTURBANCES ON SHALLOW UPPER OCEAN DENSITY--ETC(U)

MAR 79 R A FORMATO

N00014-78-C-0071

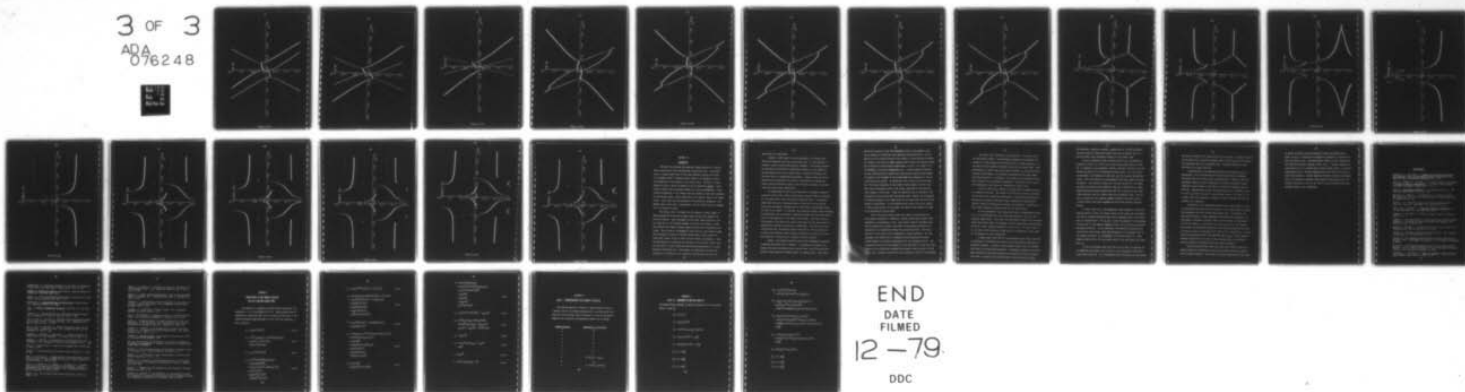
UNCLASSIFIED

CMS-C-1-79

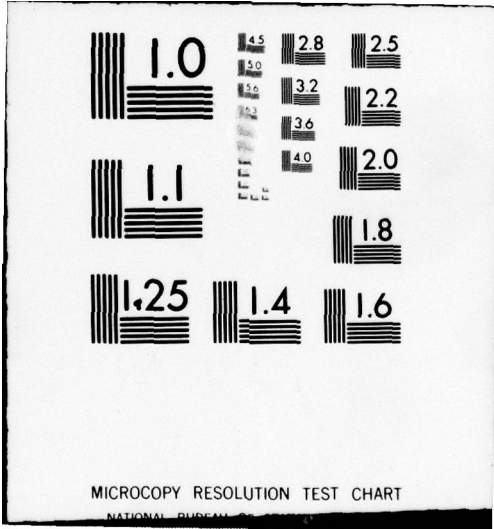
NL

3 OF 3

ADA
076248



END
DATE
FILMED
12-79
DDC



MICROCOPY RESOLUTION TEST CHART
NATIONAL BUREAU OF STANDARDS-1963-A

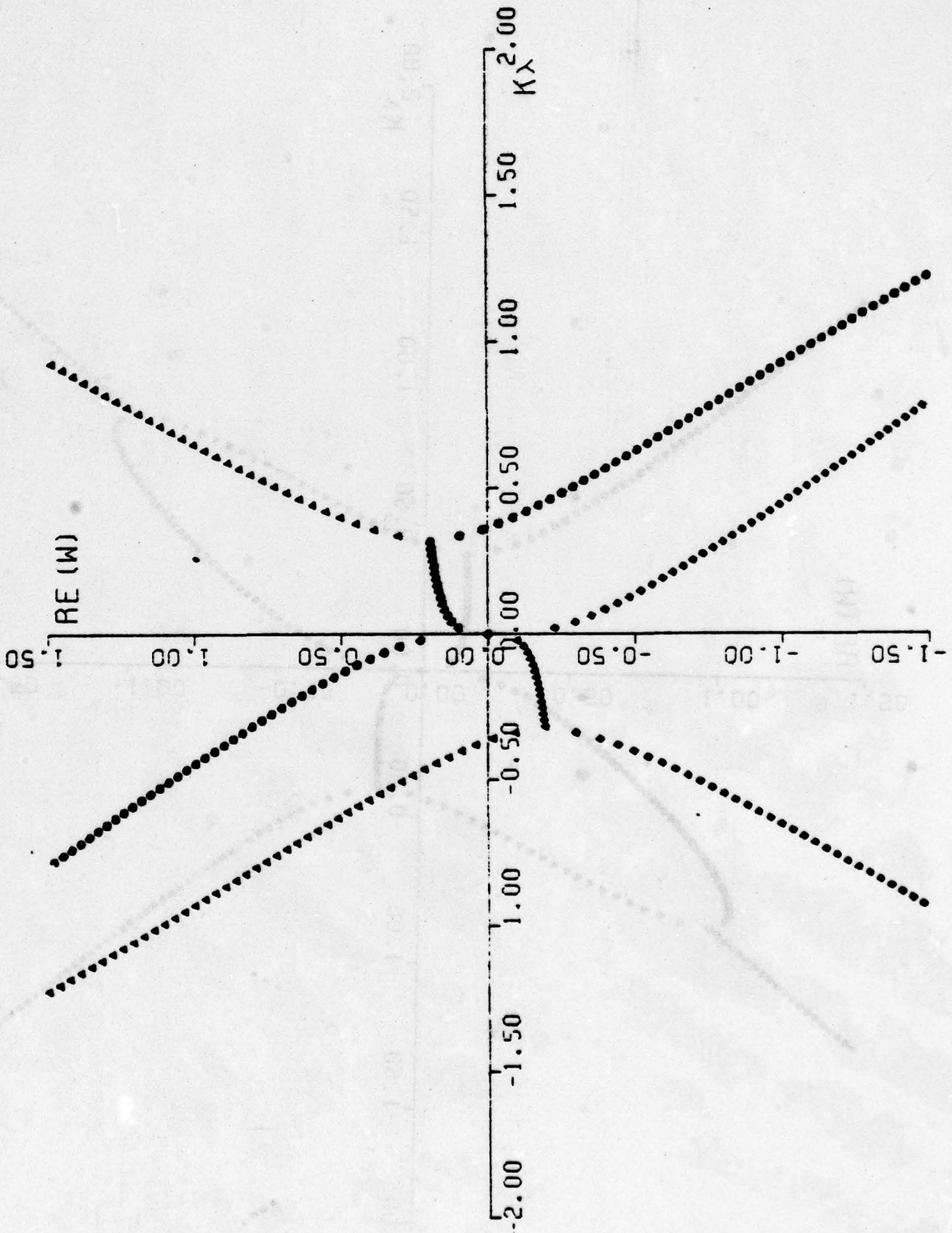
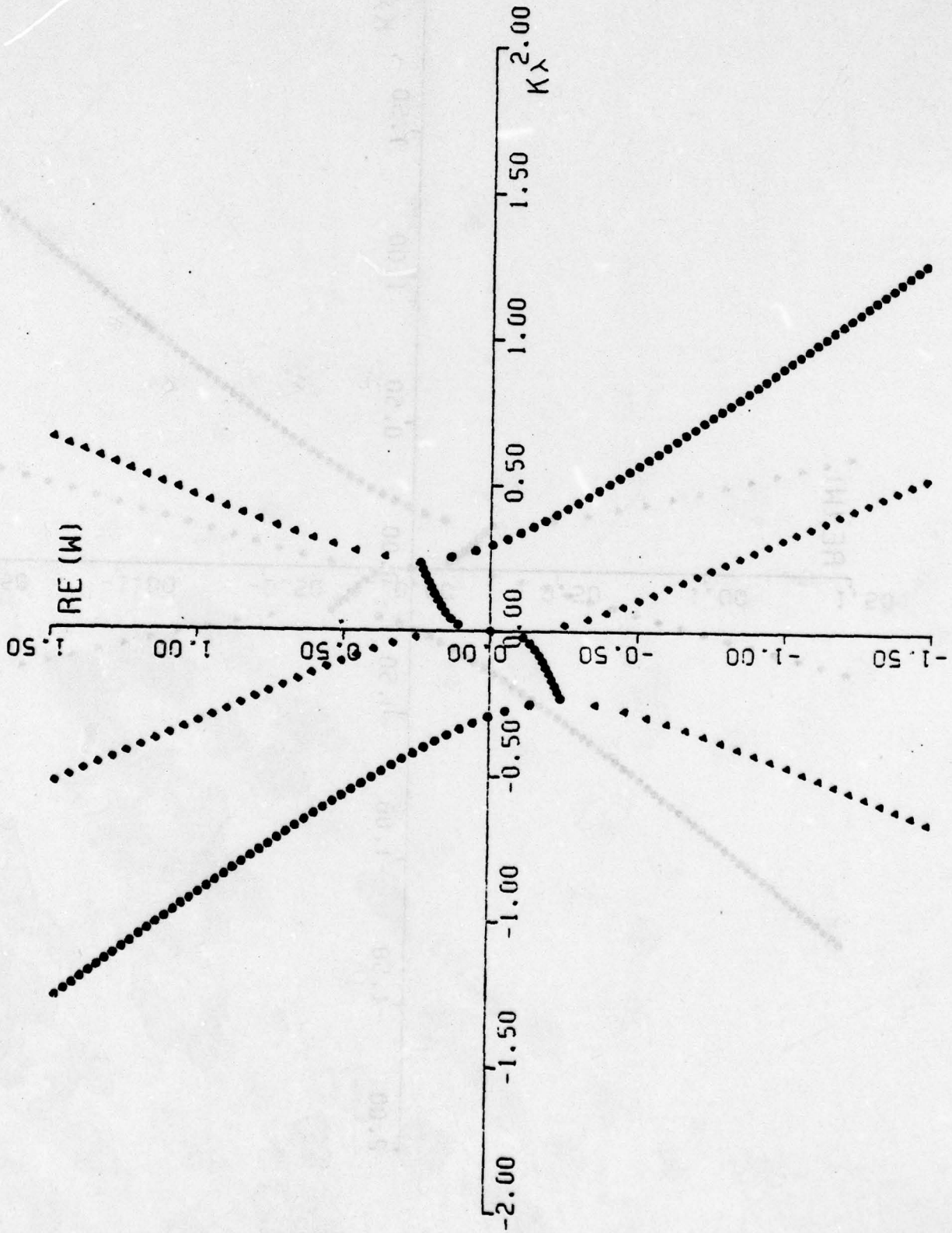


Figure 11.3(c)



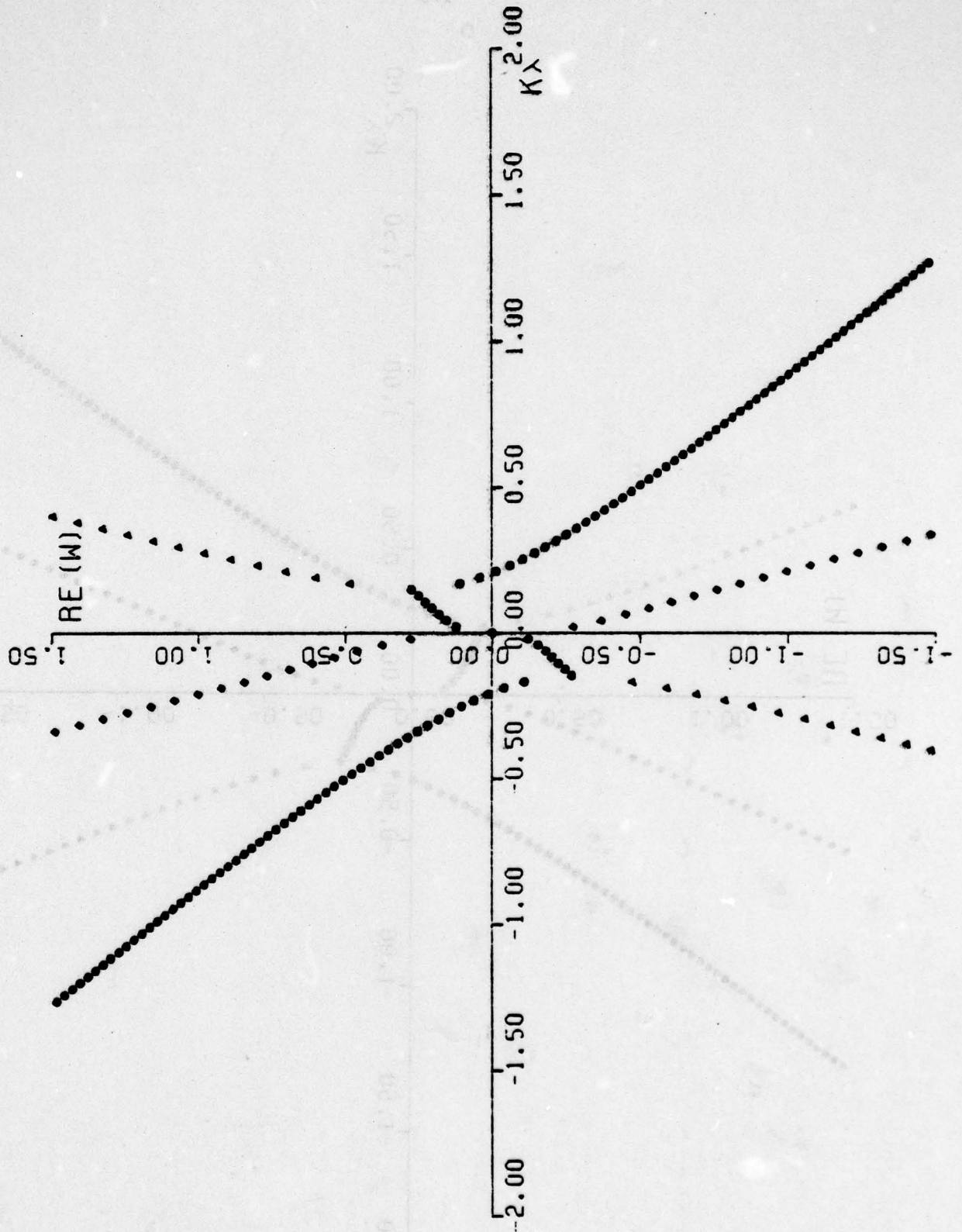


Figure 11.3(e)

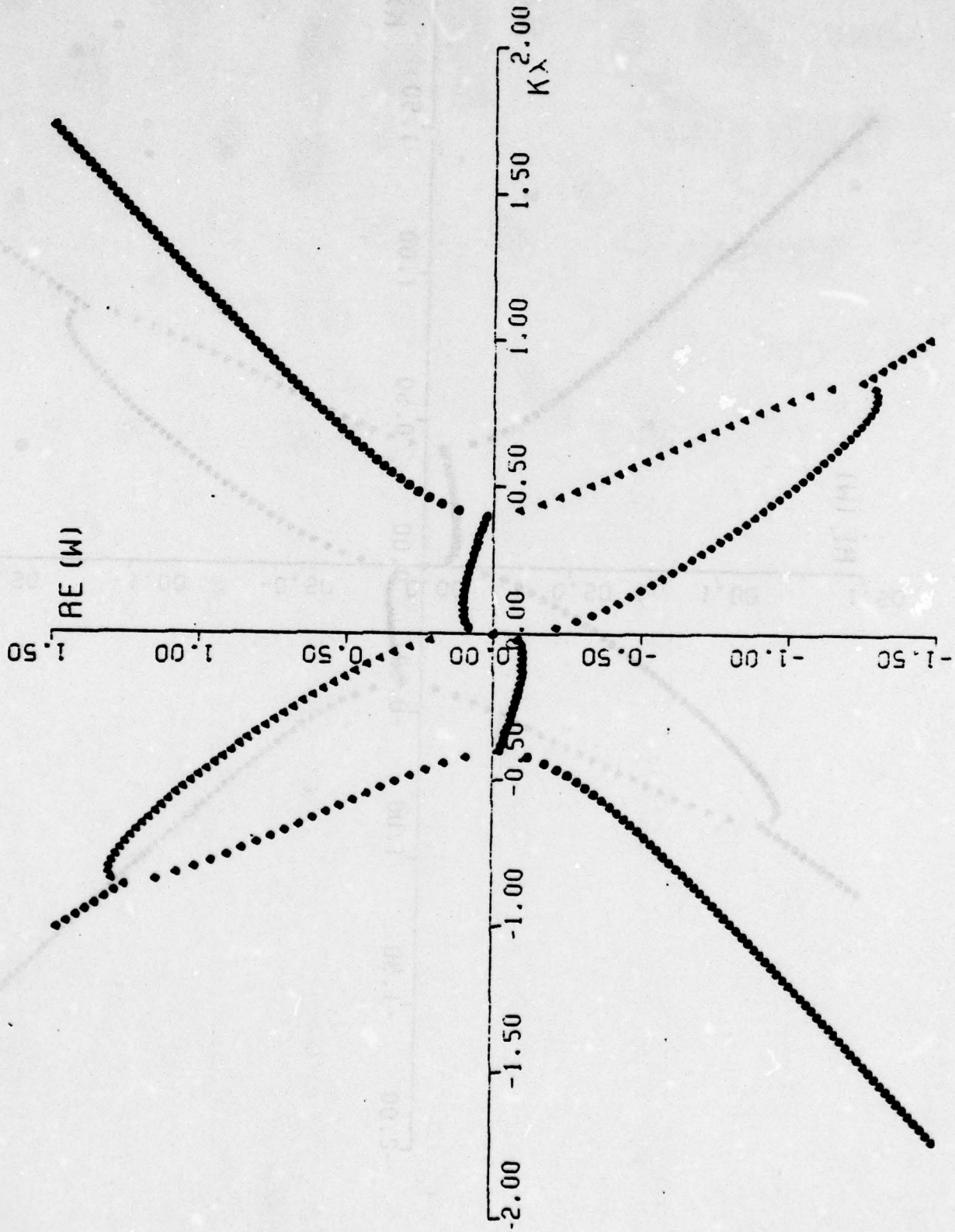


Figure 11.4(a)

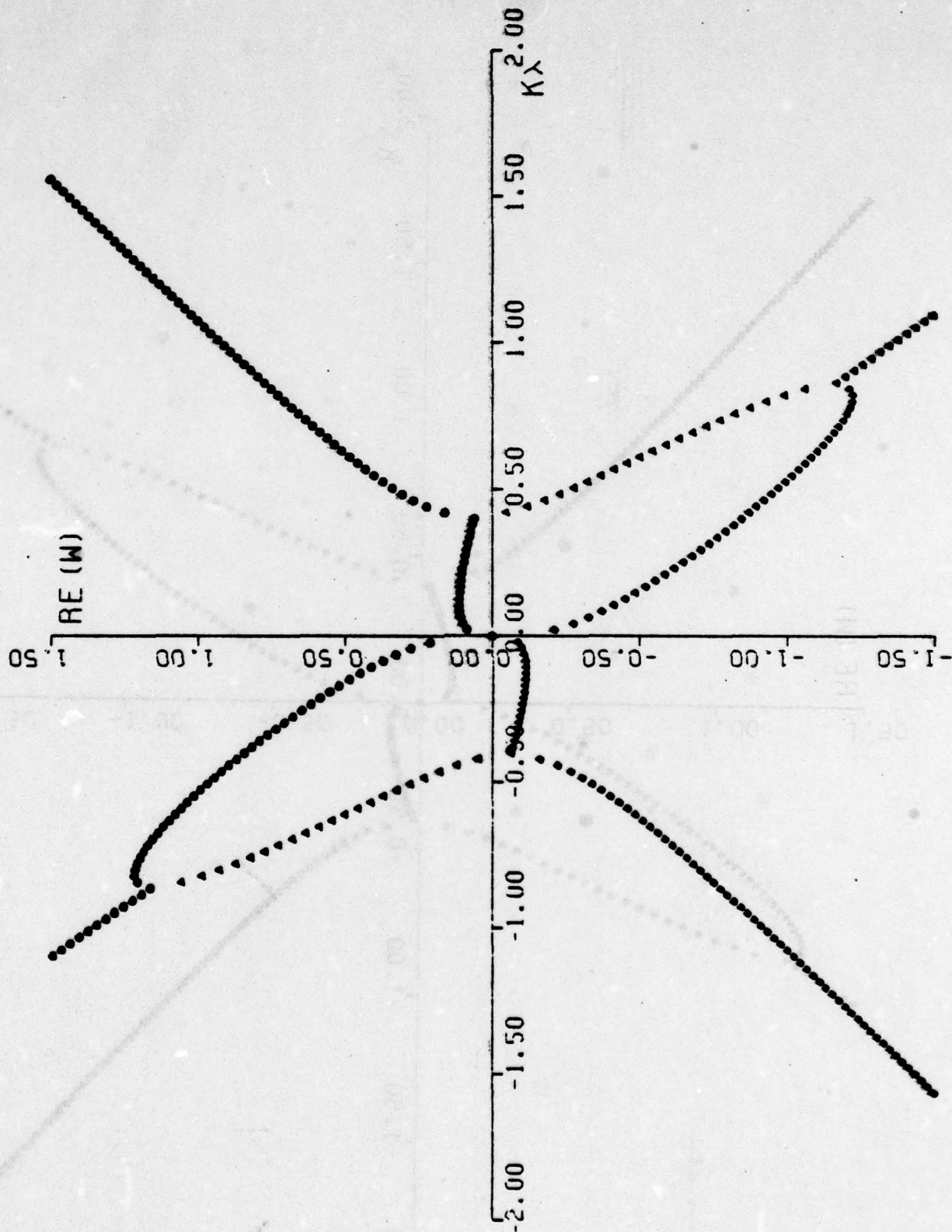


Figure 11.4(b)

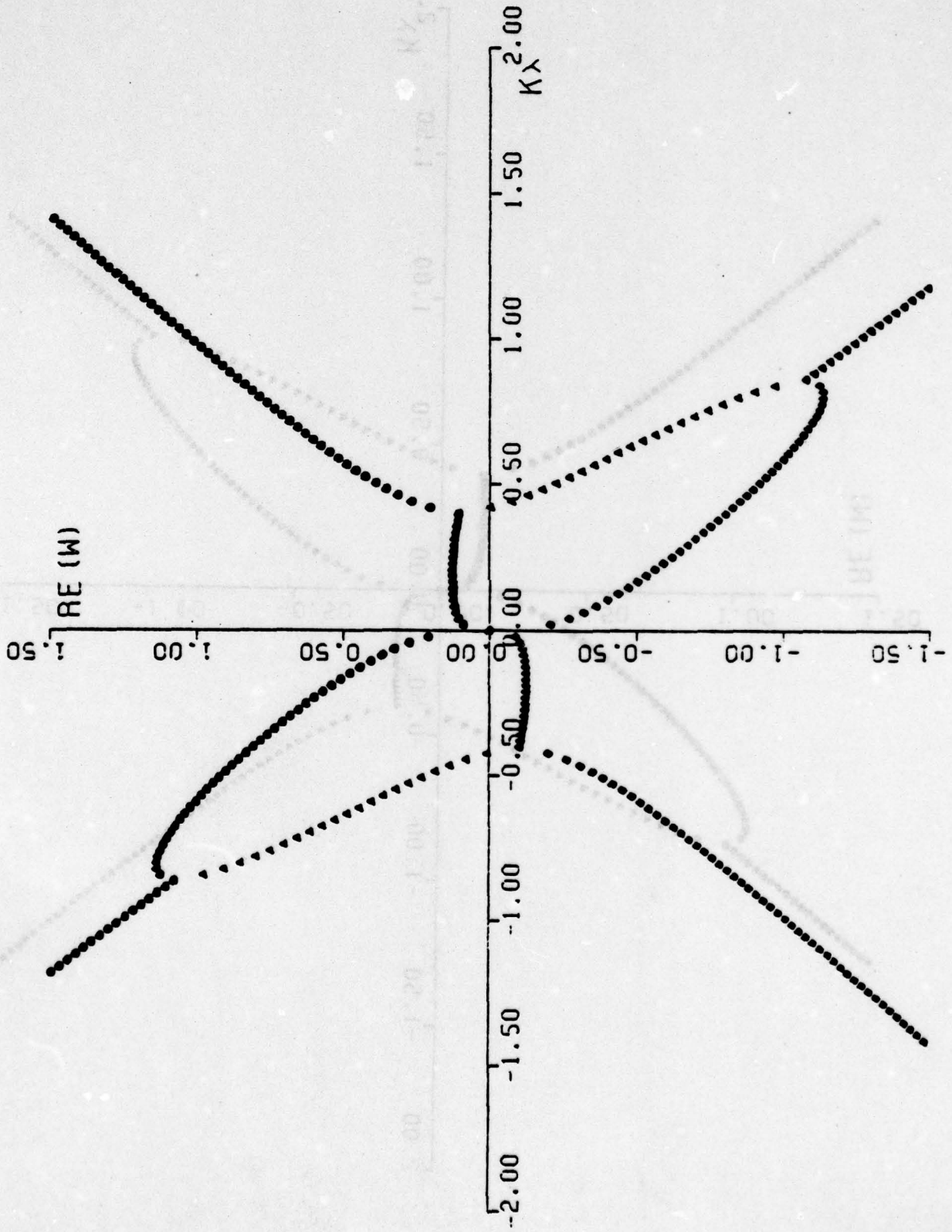


Figure 11.4(a)

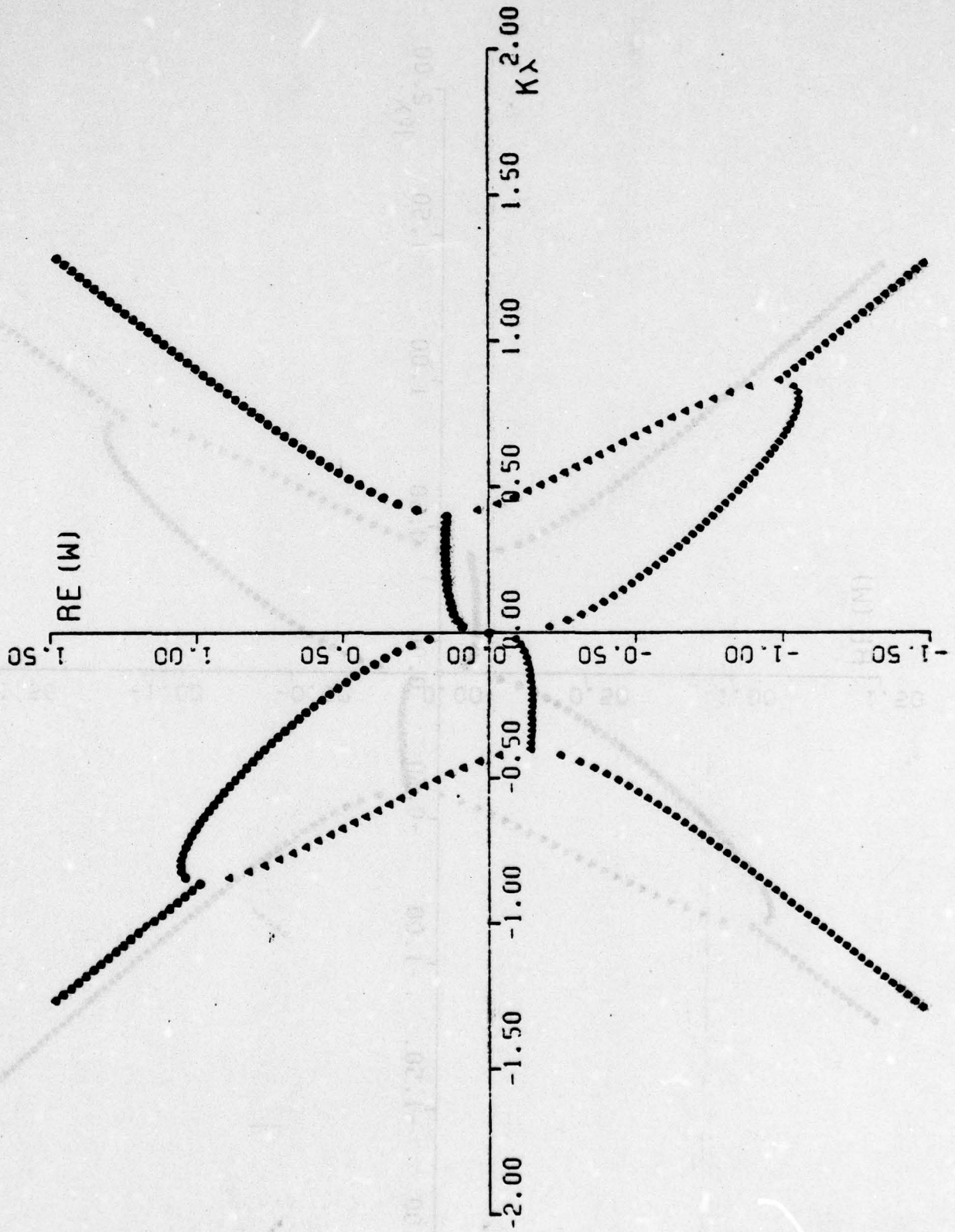


Figure 11.4(d)

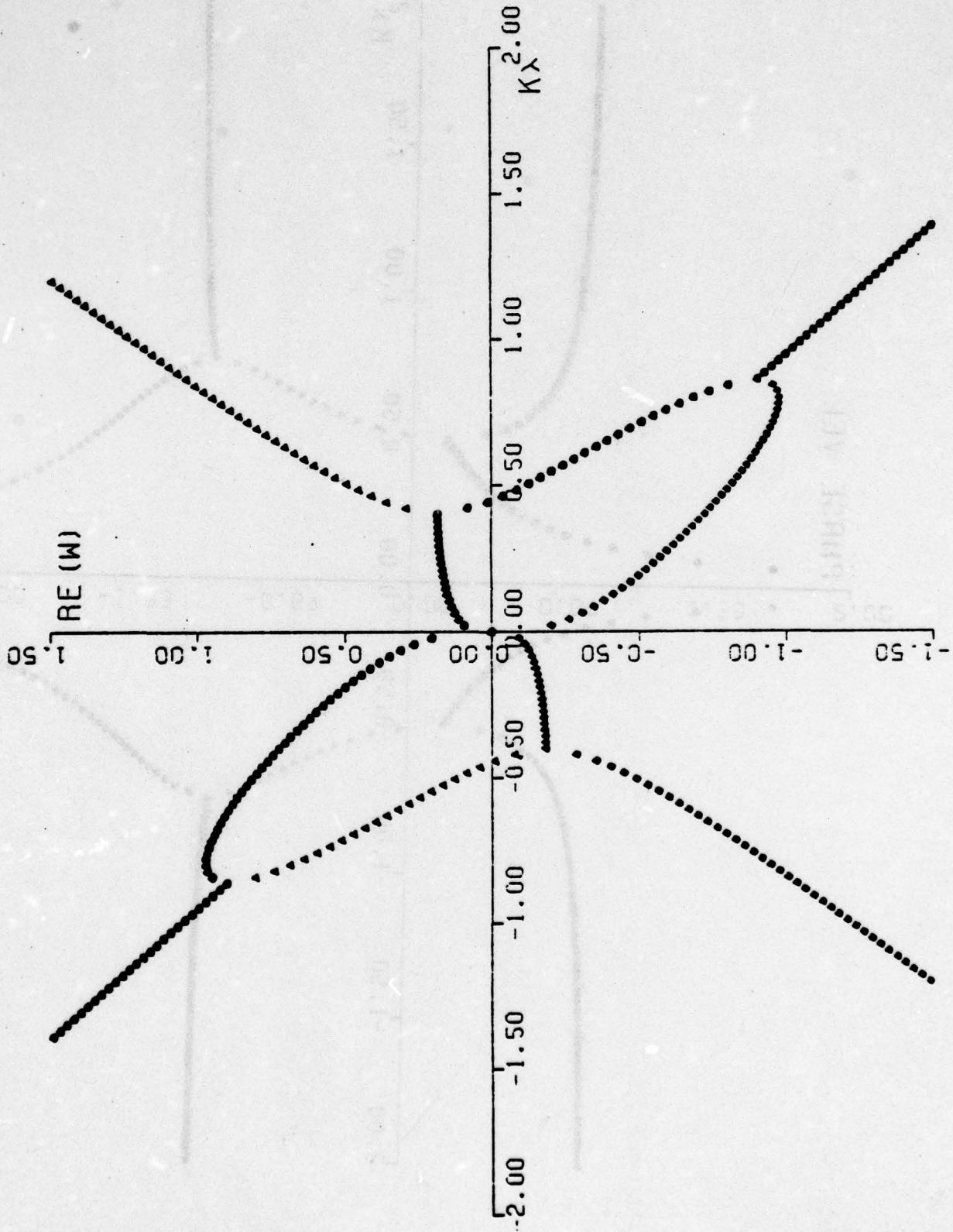


Figure 11.4(e)

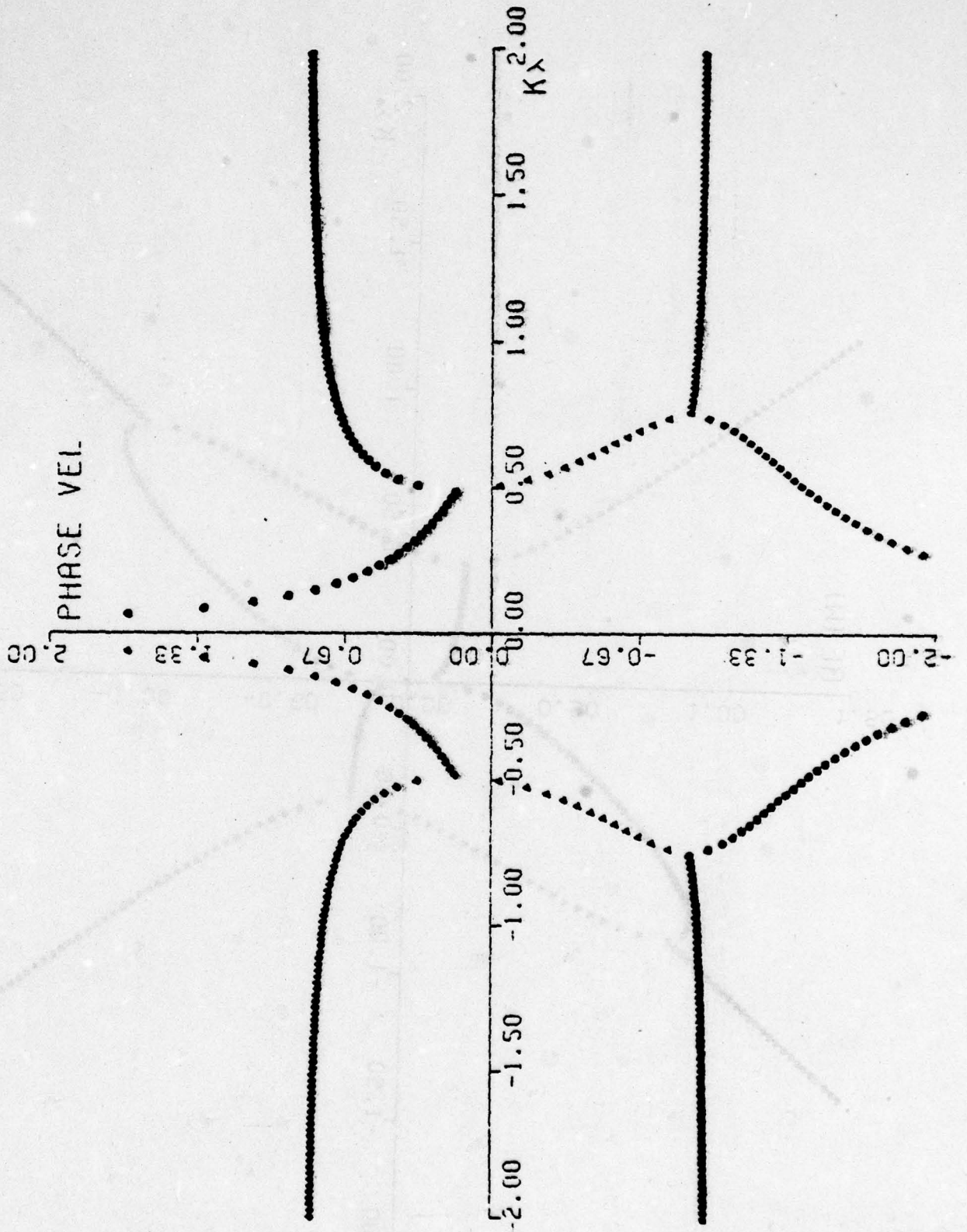


Figure 11.5(a)

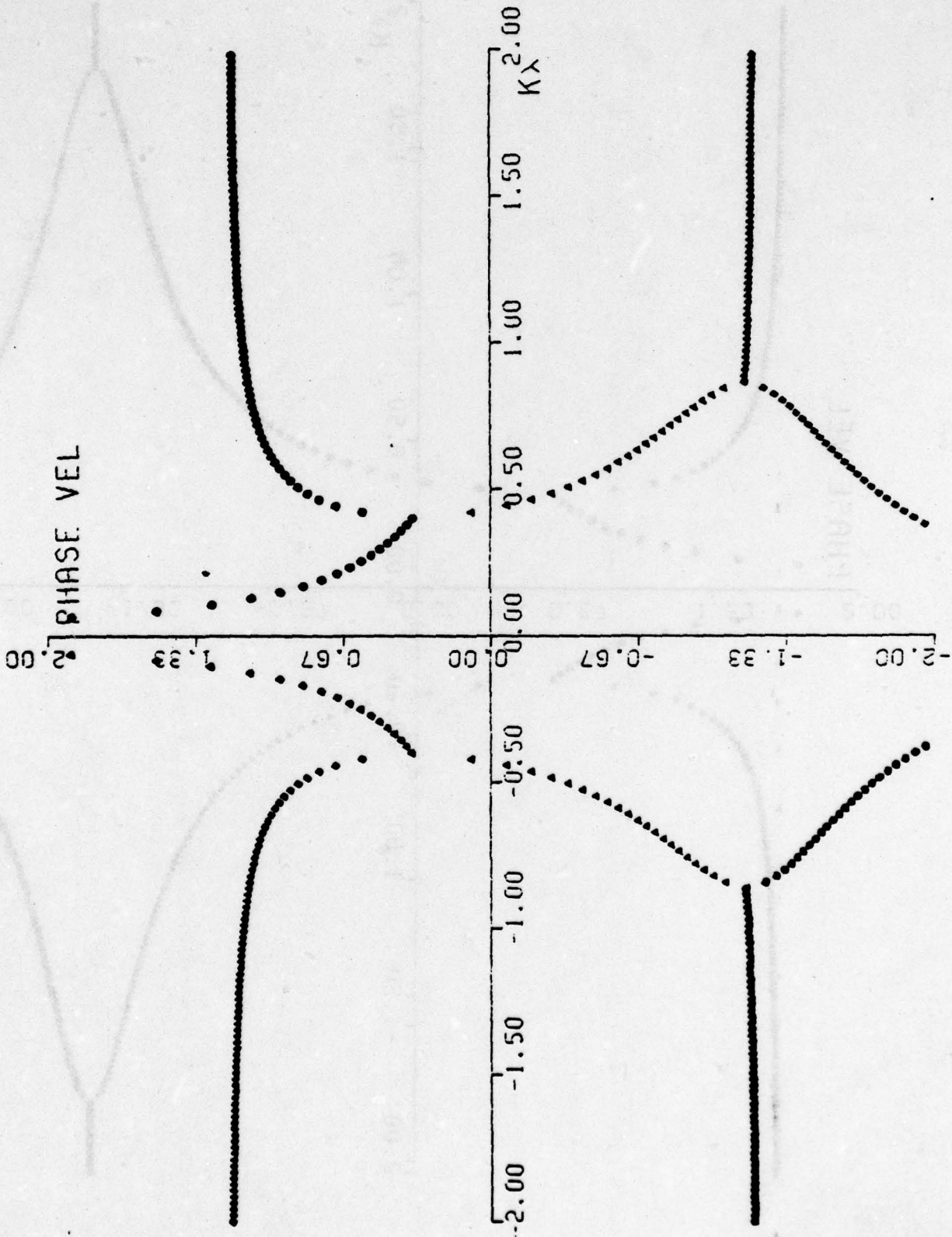


Figure 11.5(b)

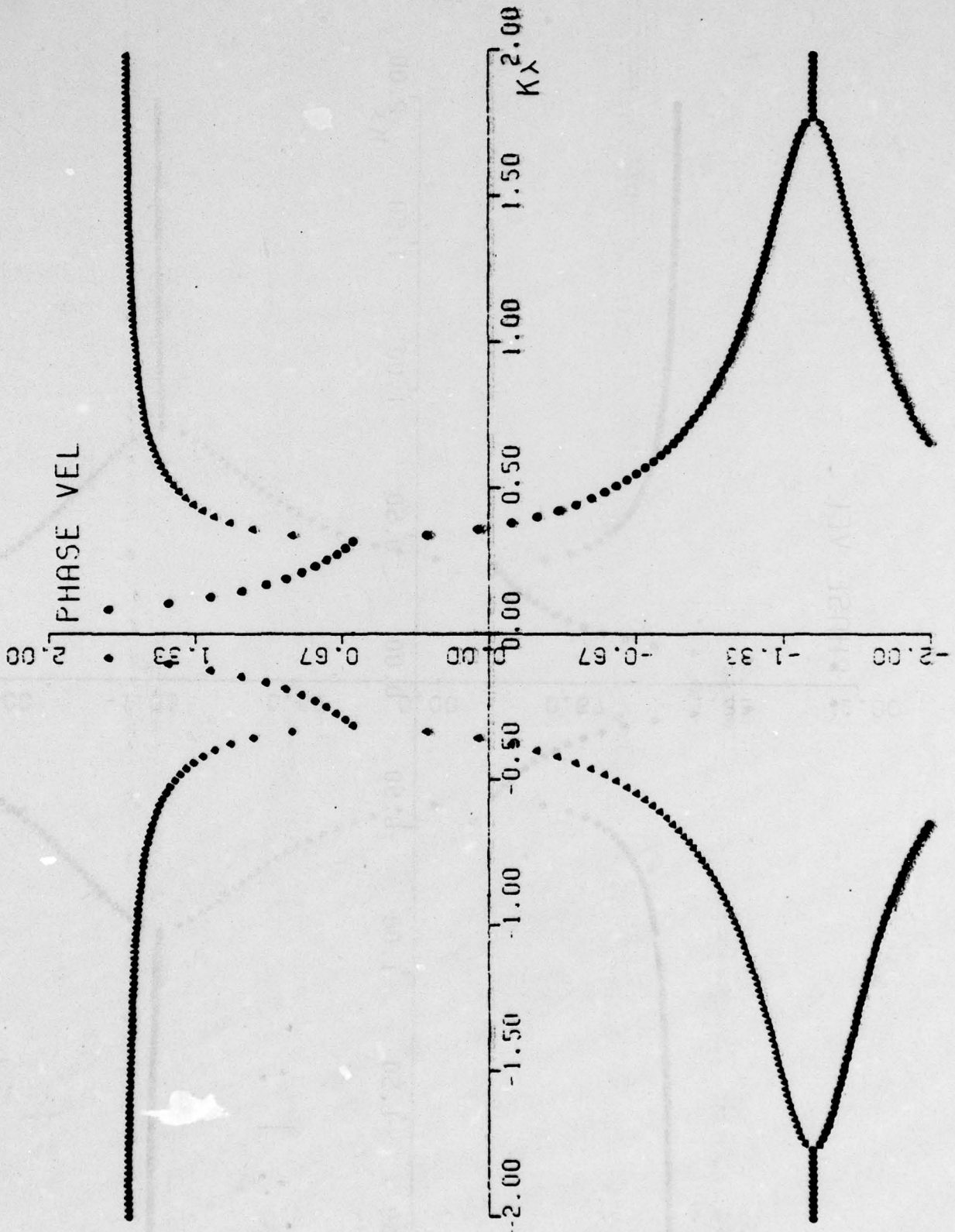


Figure 11.5(c)

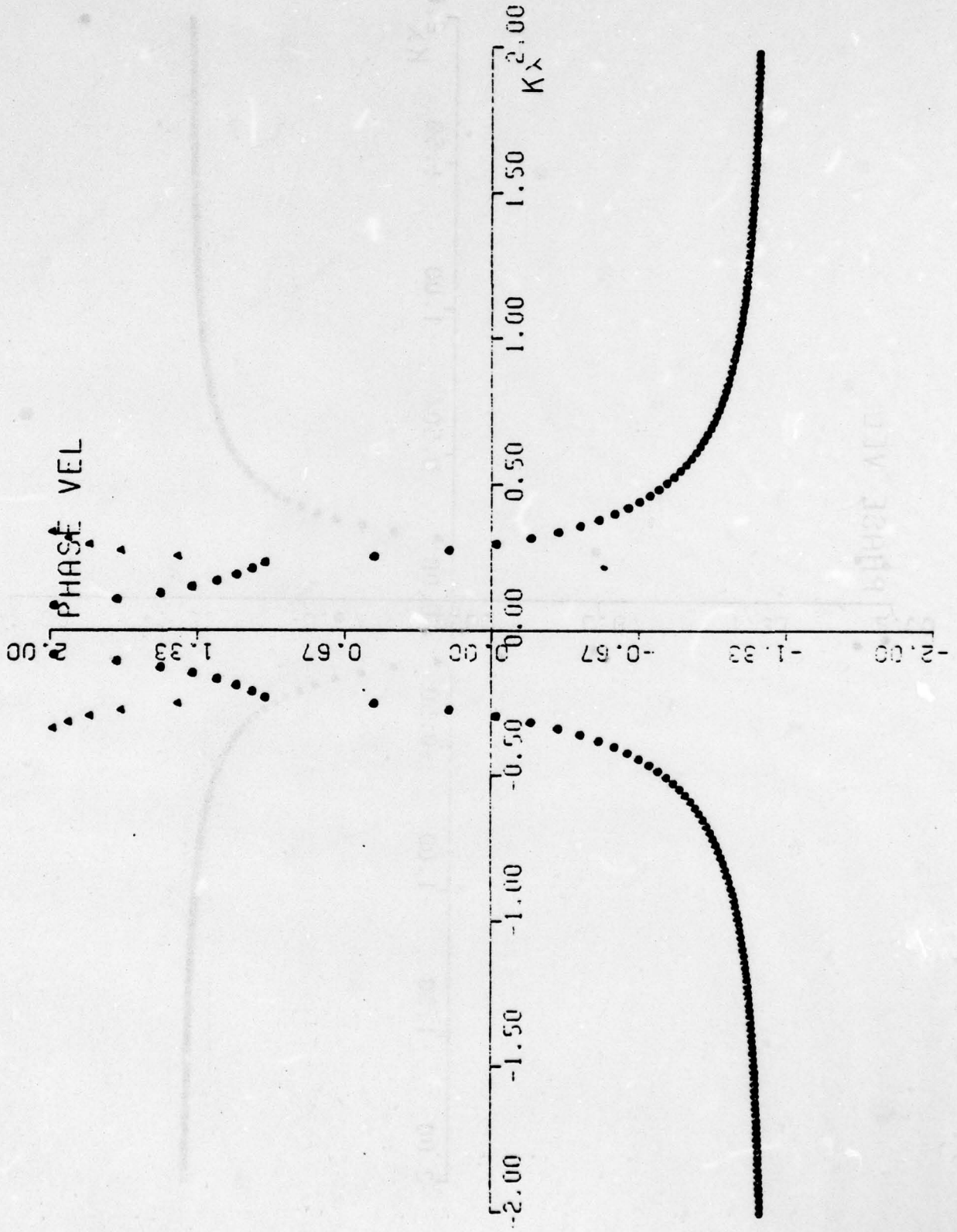


Figure 11.5(d)

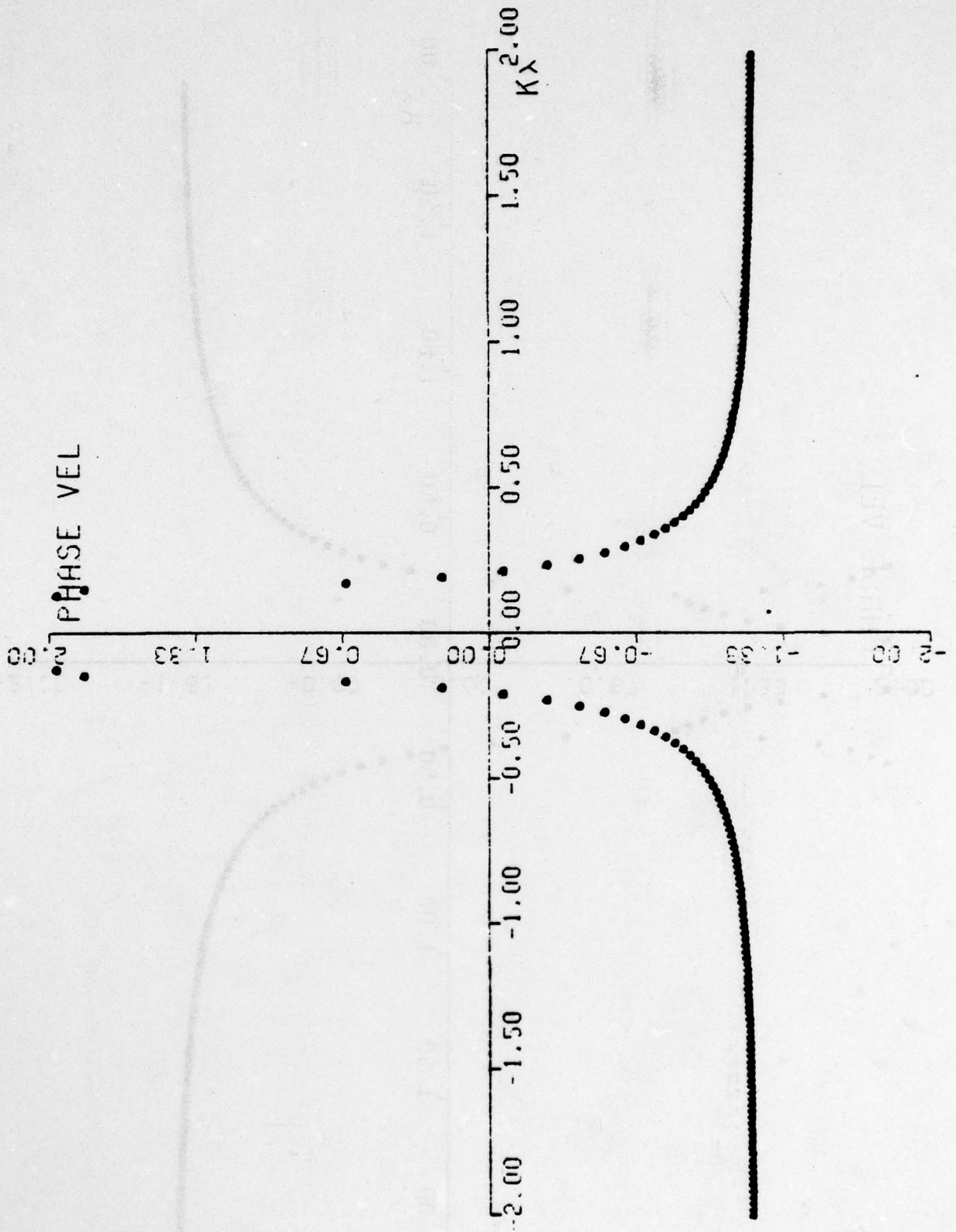


Figure 11.5(e)

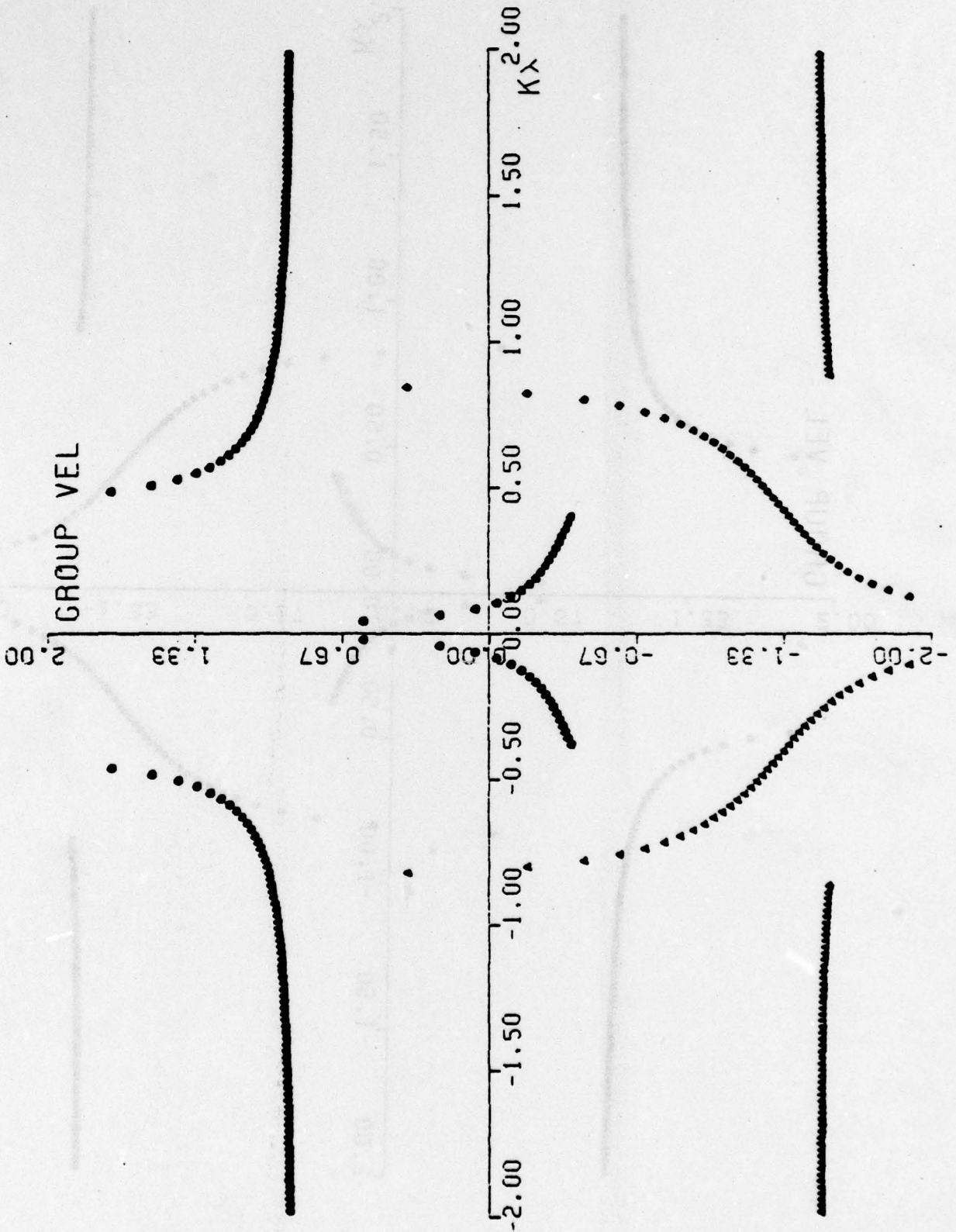


Figure 11.6(a)

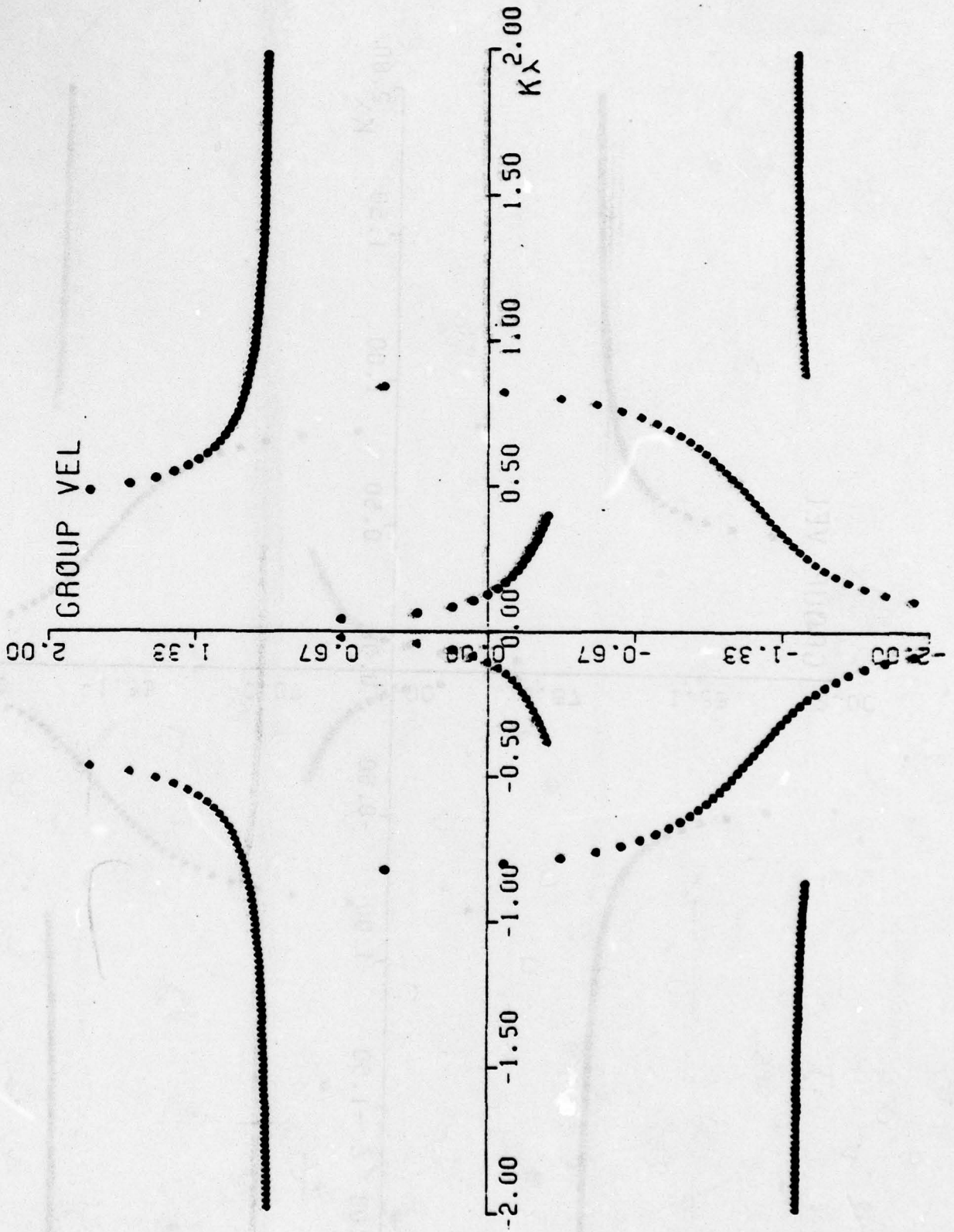


Figure 11.6(b)

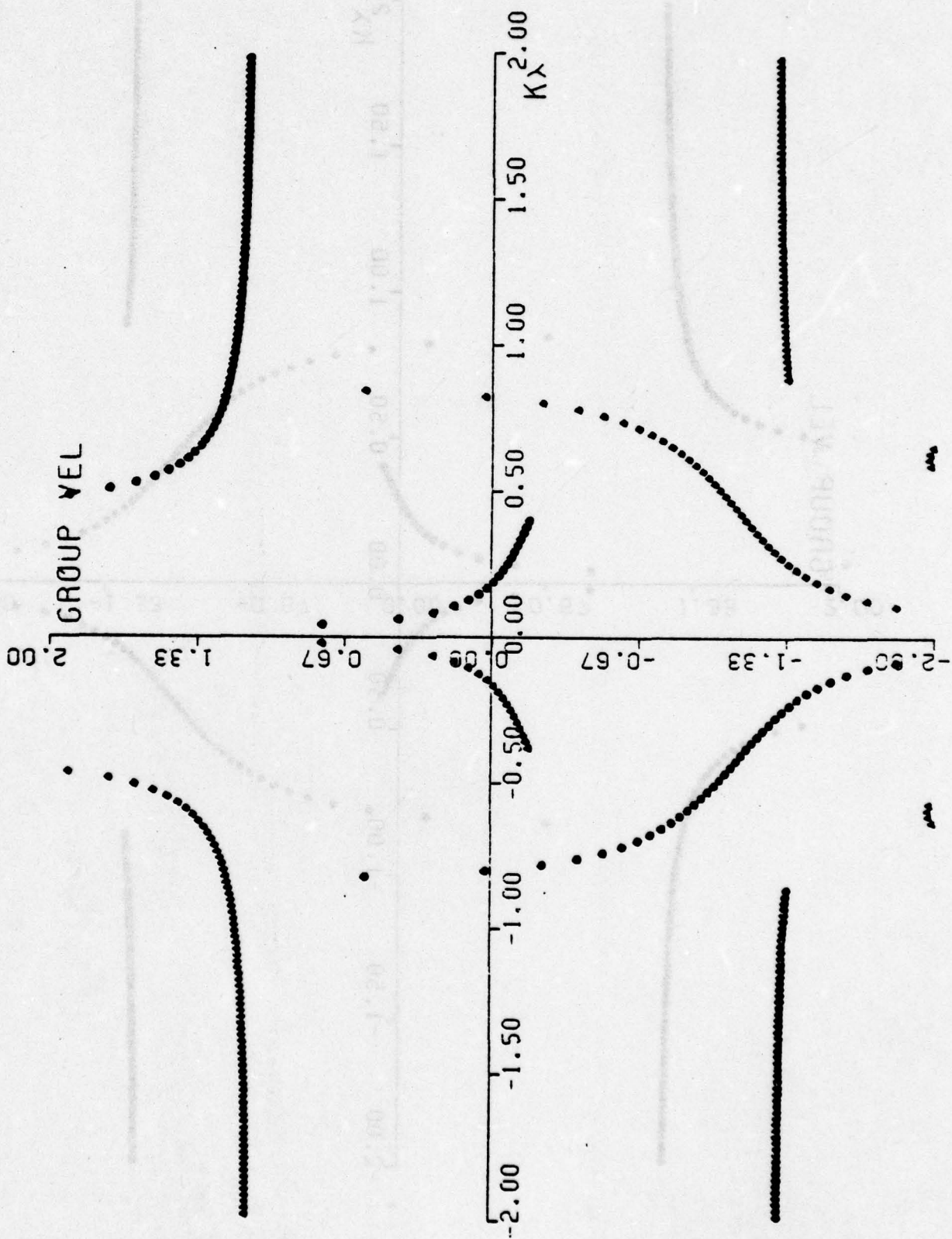


Figure 11.6(c)

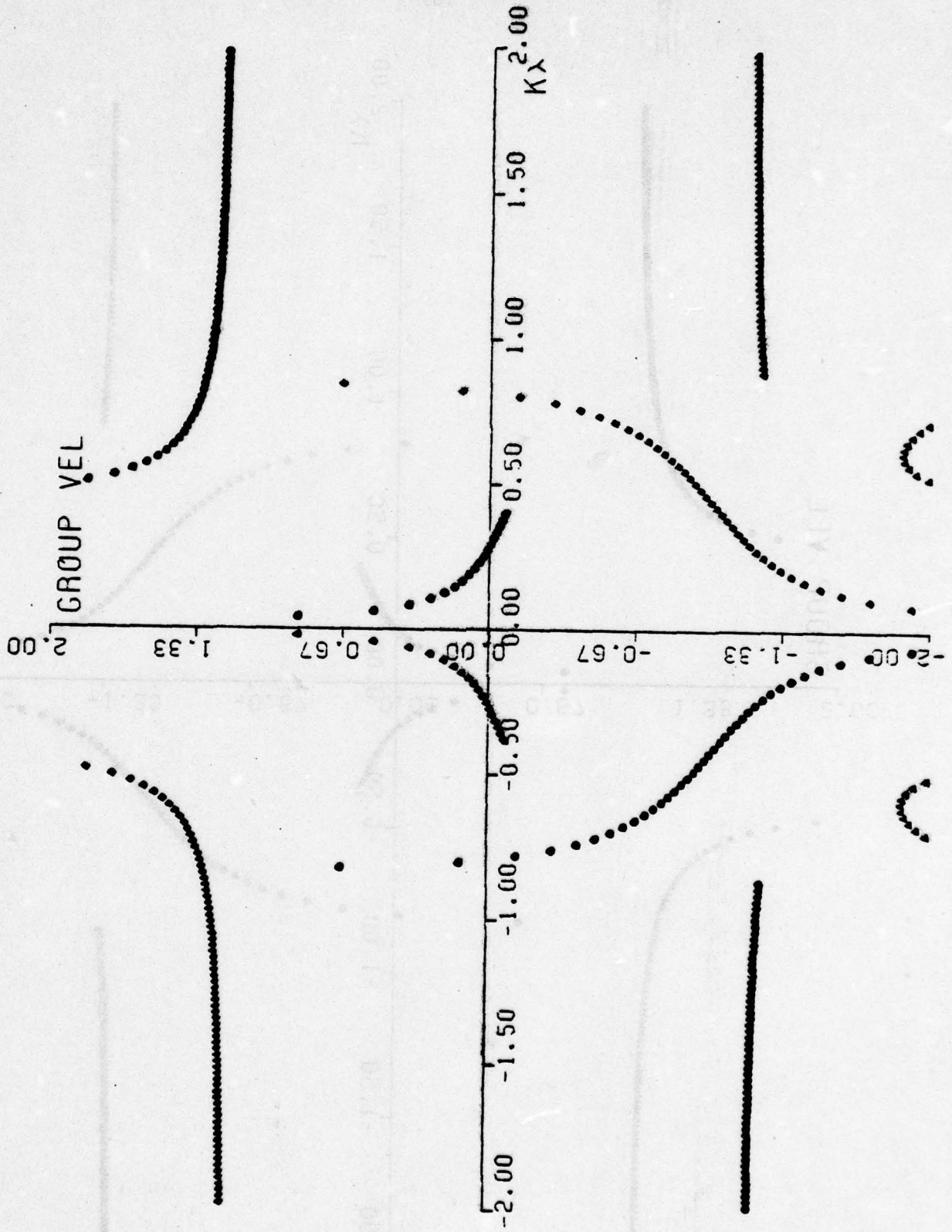


Figure 11.6(d)

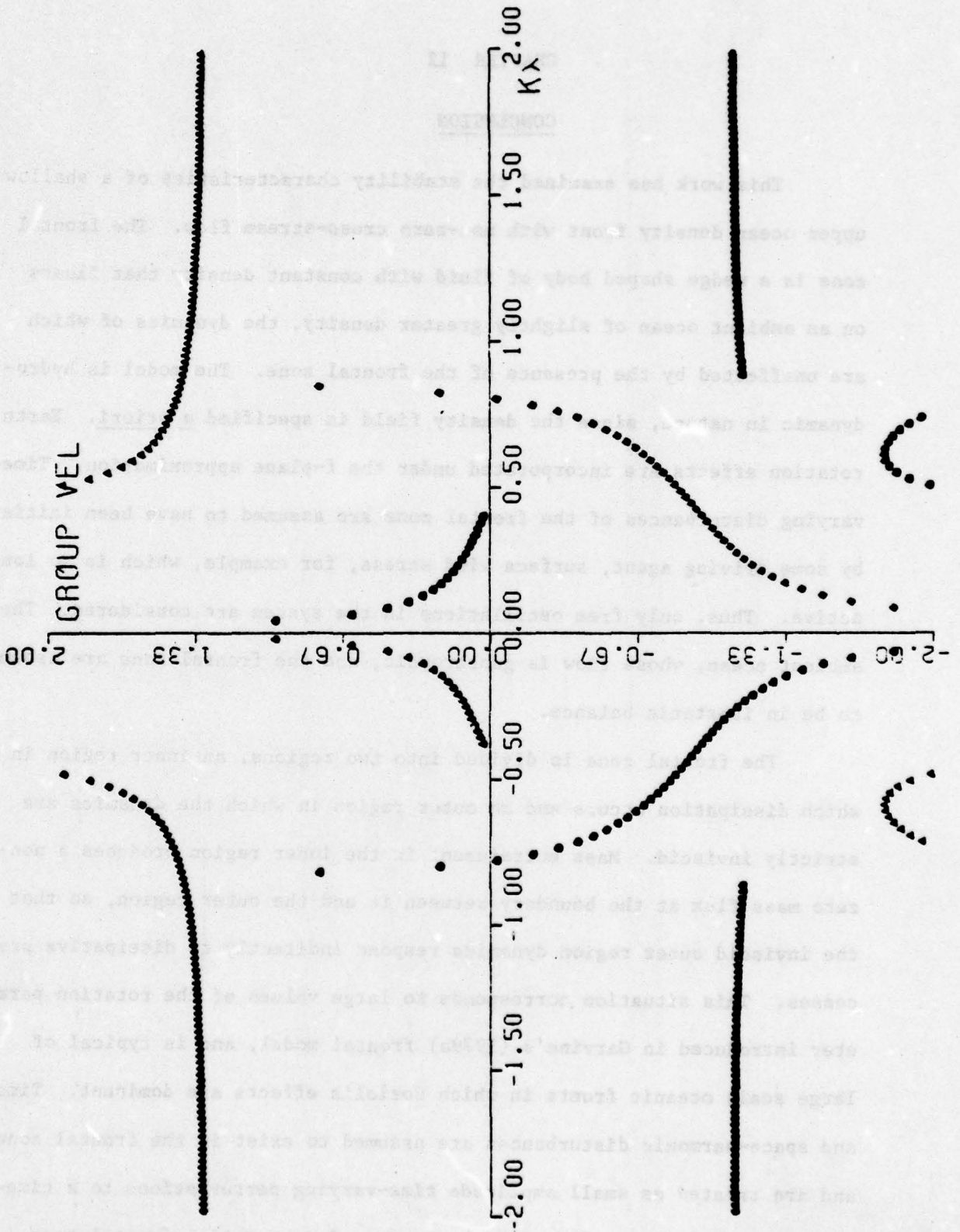


Figure 11.6(e)

CHAPTER 12

CONCLUSION

This work has examined the stability characteristics of a shallow upper ocean density front with non-zero cross-stream flow. The frontal zone is a wedge shaped body of fluid with constant density that floats on an ambient ocean of slightly greater density, the dynamics of which are unaffected by the presence of the frontal zone. The model is hydrodynamic in nature, since the density field is specified a priori. Earth rotation effects are incorporated under the f-plane approximation. Time-varying disturbances of the frontal zone are assumed to have been initiated by some driving agent, surface wind stress, for example, which is no longer active. Thus, only free oscillations in the system are considered. The ambient ocean, whose flow is geostrophic, and the frontal zone are assumed to be in isostatic balance.

The frontal zone is divided into two regions, an inner region in which dissipation occurs and an outer region in which the dynamics are strictly inviscid. Mass entrainment in the inner region produces a non-zero mass flux at the boundary between it and the outer region, so that the inviscid outer region dynamics respond indirectly to dissipative processes. This situation corresponds to large values of the rotation parameter introduced in Garvine's (1979a) frontal model, and is typical of large scale oceanic fronts in which Coriolis effects are dominant. Time- and space-harmonic disturbances are assumed to exist in the frontal zone, and are treated as small amplitude time-varying perturbations to a time-invariant equilibrium flow. Both planar and exponential frontal zone geometries are considered, with respective equilibrium flows that are

geostrophic and aeostrophic.

Duxbury's (1963) model of wave disturbances on a planar front, which was formulated with zero cross-stream flow, is first extended to include a nonzero cross-stream velocity component. The initial analysis in this paper is performed in dimensional variables, as was Duxbury's. The equilibrium flow for the planar front is spatially invariant, and the basic state is consequently geostrophic. Constant long- and cross-stream velocity components are driven by the sloping sea surface and frontal zone discontinuity surface, both of which are planes, which motivates the planar front nomenclature.

By eliminating the velocity perturbations as dependent variables, a general seventh order ordinary differential equation (ODE) is developed for the planar front depth perturbation amplitude (DPA). An asymptotic normal form solution is presented which is valid far from the surface front, and an integral representation of the solution is developed which is valid in any region. In addition, the connection between these solutions is established, and it provides an important insight into the proper decay scale for perturbations to the planar front system. With these results, the problem of the planar front with cross-stream flow has been solved in principle by reducing its solution to quadratures. For the case of zero cross-stream flow, the general seventh order ODE for the DPA reduces to a second order equation, whose integral representation solution is evaluated explicitly to recover all of Duxbury's earlier results.

However, the analysis described above raises fundamental questions concerning the planar front's dynamics. In dimensional variables, the system with zero cross-stream flow is second order, while the system with nonzero cross-stream flow, however small, is seventh order. This result

raises the question of what the fundamental order of the system is and why it changes so drastically with vanishing cross-stream flow. The answers lie in the proper scaling of the problem, in which spatial variables are scaled to the inviscid region characteristic length (the Rossby radius) and an advective characteristic length which, in fact, is so small as to be imbedded in the narrow dissipative zone. A small parameter expansion is then introduced which involves the cross-stream internal Froude number (a measure of the strength of the cross-stream flow normalized to the internal wave phase speed). At zeroth and first orders in the Froude number, the system normalized by the inviscid scale length is second order, while the corresponding zeroth order system normalized by the advective scale length is fifth order. Since the advective zone is imbedded in the dissipative region located near the surface front, however, the assumption of inviscid dynamics is no longer valid and the model with the fifth order system is inapplicable. On the inviscid scale, which is the only region of direct applicability of this model, the planar front dynamics are seen to be fundamentally second order.

The inviscid scale planar front with nonzero cross-stream flow thus reduces essentially to Duxbury's original second order system, which exhibited no instabilities at all. This result, which is available only with an appropriate scaling of the planar front problem, motivates consideration of the exponential front with cross-stream flow. The entire analysis in this latter case is performed in scaled variables. For completeness, the planar front is reexamined using essentially the same scaling scheme in a parallel development with the exponential front. The dispersion relation for each geometry is then developed at zeroth and first orders in the cross-stream internal Froude number, which is used to introduce a small parameter expansion for each dependent variable in the problem.

The lowest order dispersion characteristics of the planar front are particularly simple. The disturbance frequency and wavenumber are related by a linear equation which involves only a single parameter, V_∞ , the shear velocity between the ambient fluid and the frontal zone. Wave disturbances to lowest order in the small parameter F_b , the cross-stream internal Froude number, are therefore non-dispersive with equal phase and group velocities. In addition, real values of the wavenumber correspond to purely real disturbance frequencies. The planar front is therefore dynamically stable under all conditions at lowest order.

At first order in F_b , however, the planar front dispersion results are somewhat surprising. The system of differential equations satisfied by the first order perturbation amplitudes is internally self-consistent and meets the boundary conditions without imposing any characteristic relation between the disturbance frequency and wavenumber. Therefore, no first order dispersion relation exists for the planar front.

For the exponential front, whose basic state is formulated in Chapter 5, the equilibrium flow is not spatially invariant, and it is consequently ageostrophic. Both exact and approximate solutions for the equilibrium interfacial depth are developed, with the approximate solution again involving a small parameter expansion in terms of F_b . At lowest order in F_b , the basic state interfacial depth profile is exponential, which leads to the exponential front nomenclature.

A single second order ODE for the exponential front DPA at order F_b^0 is developed by eliminating the velocity field perturbation amplitudes as dependent variables. Analysis of this equation reveals that the exponential front is sub-inertially dominated. Disturbances leading to non-divergent solutions for the depth perturbation amplitude far from the surface front must, in general, have periods greater than the inertial period.

This existence condition, moreover, depends only on a single parameter, the shear velocity between the frontal zone and the ambient fluid, as did the lowest order dispersion relation for the planar front.

For the exponential front at zeroth order in F_b , the dispersion relation is linear in ω and $k\lambda$, as it was for the planar front at order F_b^0 . It depends on two parameters, however, the shear velocity V_∞ and the interfacial depth δ_0 at the coordinate system origin. For real values of wavenumber, the frequency is also real, and the system is dynamically stable. Wave disturbances are non-dispersive with equal phase and group velocities. With realistic values for the shear velocity V_∞ , the phase and group velocities will be positive along the $+y$ direction in a right-handed coordinate system oriented such that the $+x$ axis is in the cross-stream direction into the frontal zone from the ambient fluid. This result is consistent with observed meander patterns on the Gulf Stream, in which frontal zone waves propagate northward and eastward along the Stream.

At first order in F_b , the exponential front possesses a cubic dispersion relation, which, for certain values of the purely real wavenumber, can lead to complex frequencies with nonzero imaginary parts, and, therefore, to instabilities. Both V_∞ and δ_0 enter as parameters in determining the real part of the complex frequency, which, in turn, governs the phase and group velocities. On the other hand, the stability characteristics of the first order system, which are determined by the imaginary part of the complex frequency, are independent of the shear velocity V_∞ . They depend instead only on the interfacial depth at the inner/outer zone boundary, δ_0 .

In the low frequency limit as ω and $k\lambda$ go to zero, an unstable and an evanescent mode always exist as a pair on the exponential front with equal phase velocities. The corresponding group velocities are also equal,

and equal one-third of the phase velocity for each mode. The phase velocity of the stable wave in the low frequency limit is twice that of the unstable and evanescent waves and of opposite sign. Its group velocity is also one-third of its phase velocity.

Instabilities of the exponential frontal zone vanish as $F_b \rightarrow 0$, or, equivalently, as the equilibrium state cross-stream velocity vanishes. The growth time for unstable waves is proportional to $\ln(1/F_b)$, and thus approaches infinity as $F_b \rightarrow 0$, reflecting a continuous transition from an inherently stable system at order F_b^0 to a potentially unstable system at order F_b^1 . Computational results for typical values of δ_0 between 0.1 and 0.5 with F_b between 0.05 and 0.2 show doubling times on the order of 1 to 2 weeks, which seem reasonable, although no direct observational data are available for comparison.

Calculation of the disturbance periods over a wide range of δ_0 and V_∞ values shows that they are also typically 1 to 2 weeks, which is in general agreement with Gulf Stream observational data. In addition, the wave periods exhibit a strong dependence upon the Coriolis parameter, or, equivalently, geographic latitude, which is also evident in observations of the Gulf Stream. In particular, for $V_\infty=0.2$ and $\delta_0=0.3$, both reasonable values, the disturbance periods for the fastest growing mode are 8.81, 6.02 and 4.69 days at latitudes of 20° , 30° and 40° , respectively. At latitudes of approximately 27°N , 33°N and 38°N , Maul, *et al.*, (1978) observed dominant periods of 10, 5.8 and 4.8 days, respectively, by performing a spectral analysis of available satellite infra-red imagery.

The work presented here shows that upper ocean density fronts can exhibit baroclinic instabilities, while all previous theoretical efforts have concluded otherwise. The system's stability characteristics are seen

to depend critically upon the existence of some cross-stream flow, which, in turn, is supported by dissipative processes in a narrow zone near the surface front. The quasi-steady dynamics of this region have been modelled elsewhere (Garvine, 1979a, 1974). A natural extension of this work would be to consider earth rotation effects under a beta-plane approximation and to include coupling between the frontal zone and ambient ocean dynamics. Another important extension would be the development of an energetics analysis, which should provide insight into the physical processes at work in the frontal zone and perhaps display the physical origin of the instability.

BIBLIOGRAPHY

Abramowitz, M., and Stegun, I., Handbook of Mathematical Functions with Formulas, Graphs and Mathematical Tables, AMS Series 55, U.S. National Bureau of Standards, Washington, D.C., 1970

Amos, A., Langseth, M., and Markl, R., "Visible Oceanic Saline Fronts" in Studies in Physical Oceanography, A. L. Gordon, Editor, Gordon and Breach, Publishers, London, 1972, p. 49

Beebe, W., The Arcturus Adventure, G. P. Putnam and Sons, Inc., New York and London, 1926, Ch. III, pp. 41-70

Bernstein, R., Breaker, L., and Whritner, R., "California Current Eddy Formation: Ship, Air and Satellite Results", Science, 195, 4276, 28 January 1977, p. 353

Charney, J. G., "The Gulf Stream as an Inertial Boundary Layer", Proc. Nat. Acad. Sci., Washington, D.C., 41, 1955, p. 731

Conte, S. D., and deBoor, C., Elementary Numerical Techniques, 2nd. ed., McGraw-HillPub. Co., New York, 1972, Ch. 5

Cromwell, T., and Reid, J., "A Study of Oceanic Fronts", Tellus, 8, 1956, p. 94

Duxbury, A., "An Investigation of Stable Waves Along a Velocity Shear Boundary in a Two-Layer Sea With a Geostrophic Flow Regime", Jour. Marine Res., 21, 3, 1963, p. 246

Garvine, R., and Monk, J., "Frontal Structure of a River Plume", Jour. Geophysical Res., 79, 15, May 20, 1974, p. 2251

Garvine, R., "Dynamics of Small-Scale Oceanic Fronts", Jour. Physical Oceanography, 4, 4, October, 1974, p. 557

Garvine, R., "An Integral Hydrodynamic Model of Upper Ocean Frontal Dynamics: Part I, Development and Analysis", Jour. Physical Oceanography, 9, 1979a

Garvine, R., "An Integral Hydrodynamic Model of Upper Ocean Frontal Dynamics: Part II, Physical Characteristics and Comparison With Observations", Jour. Physical Oceanography, 9, 1979b

Gradshteyn, I., and Ryzhik, I., Tables of Integrals, Series and Products, Academic Press, New York, 1965, 4th ed.

Grammeltvedt, A., "Numerical Simulation of the Motion of Atmospheric Fronts Using a Two-Layer Model", *Tellus*, 22, 6, 1970, p. 625

Handbook of Mathematical Tables, First Edition, Chemical Rubber Publishing Co., Cleveland, Ohio, 1962

Hansen, D., "Gulf Stream Meanders Between Cape Hatteras and the Grand Banks", *Deep-Sea Research*, 17, 1970, p. 495

Hildebrand, F., Advanced Calculus for Applications, Prentice-Hall, Inc., Englewood Cliffs, N.J., 1962

Ince, E., Ordinary Differential Equations, Dover Pub. Co., New York, 1956

Ingram, R. G., "Characteristics of a Tide-Induced Estuarine Front", *Jour. Geophysical Res.*, 81, 12, April 20, 1976, p. 1951

Kao, T., Park, C., and Pao, H., "Buoyant Surface Discharge and Small-Scale Oceanic Fronts: A Numerical Study", *Jour. Geophysical Res.*, 82, 12, April 20, 1977, p. 1747

Kao, T., Pao, H., and Park, C., "Surface Intrusions, Fronts and Internal Waves: A Numerical Study", *Jour. Geophysical Res.*, 83, C9, September 20, 1978, p. 4641

Kasahara, A., Isaacson, E., and Stoker, J., "Numerical Studies of Frontal Motion in the Atmosphere - I", *Tellus*, 18, 3, 1965, p. 261

Kasahara, A., and Rao, D., "Instability of Frontal Motions in the Atmosphere", *Jour. Atmospheric Sciences*, 29, September, 1972, p. 1090

Katz, E., "Further Study of a Front in the Sargasso Sea", *Tellus*, 21, 2, 1969, p. 259

Knauss, J., "An Observation of an Oceanic Front", *Tellus*, 9, 2, 1957, p. 234

Maul, G., and Hansen, D., "An Observation of the Gulf Stream Surface Front Structure by Ship, Aircraft and Satellite", *Remote Sensing of the Environment*, 2, 1972, p. 109

Maul, G. A., deWitt, P. W., Yanaway, A., and Baig, S. R., "Geostationary Satellite Observations of Gulf Stream Meanders: Infrared Measurements and Time Series Analysis", *Jour. Geophysical Research*, 83, C12, December 20, 1978, p. 6123

Morgan, G. W., "On the Wind-Driven Ocean Circulation", *Tellus*, 8, 1956, p. 301

- Mysak, L., and Schott, F., "Evidence for Baroclinic Instability of the Norwegian Current", *Jour. Geophysical Research*, 82, 15 May 20, 1977, p. 2087
- Newton, C., "Fronts and Wave Disturbances in Gulf Stream and Atmospheric Jet Stream", *Jour. Geophysical Res.*, 83, C9, September 20, 1978, p. 4697
- Orlanski, I., "The Influence of Bottom Topography on the Stability of Jets in a Baroclinic Fluid", *Jour. Atmospheric Sciences*, 26, November, 1969, p. 1216
- Orlanski, I., "Instability of Frontal Waves", *Jour. Atmospheric Sciences*, 25, March, 1968, p. 178
- Pak, H., and Zaneveld, R., "Equatorial Front in the Eastern Pacific Ocean", *Jour. Physical Oceanography*, 4, October, 1974, p. 570
- Stoker, J., "Dynamical Theory for Treating the Motion of Cold and Warm Fronts in the Atmosphere", New York University Institute for Mathematics and Mechanics, Report No. IMM-NYU-195, June, 1953
- Stommel, H., "Examples of the Possible Role of Inertia and Stratification in the Dynamics of the Gulf Stream System", *Jour. Marine Research*, 12, 2, 1953, p. 184
- Stommel, H., The Gulf Stream, Library Reprint Series Edition, Univ. of California Press, Berkeley, 1976
- Uda, M., "On the Nature of the Kuroshio, Its Origin and Meanders", in Studies in Oceanography, K. Yoshida, Editor, Univ. of Tokyo Press, Tokyo, 1964, pp. 89-107
- Voorhis, A., "The Horizontal Extent and Persistence of Thermal Fronts in the Sargasso Sea", *Deep-Sea Research*, 16, 1969, p. 331
- Webster, F., "A Description of Gulf Stream Meanders Off Onslow Bay", *Deep-Sea Research*, 8, 1961, p. 130
- Whitham, G. B., "Dynamics of Meteorological Fronts", New York University Institute for Mathematics and Mechanics, Report No. IMM-NYU-195, June, 1953
- Wooster, W., "Equatorial Front Between Peru and Galapagos", *Deep-Sea Research*, 16, 1969, p. 407
- Zaneveld, R., Andrade, M., and Beardsley, G., "Measurements of Optical Properties at an Oceanic Front Observed Near the Galapagos Islands", *Jour. Geophysical Research*, 74, 23, October, 1969, p. 5540

APPENDIX 1

COEFFICIENTS OF THE GENERAL EQUATION

FOR $Z(x)$ FOR THE PLANAR FRONT

The operators L_1 through L_5 and the operator polynomial $\Delta(p)$ appearing in (3.11) are defined in (3.10). These operators may be expanded and substituted into (3.11) to yield the final form of the depth perturbation amplitude ODE in (3.13), with the constants v_n and γ_n given by:

$$v_0 = ia_1 g' k^2 \omega^3 (f^2 - \omega^2) \quad (\text{A.1a})$$

$$\begin{aligned} \gamma_0 = & (f^2 - \omega^2) \{ a_2 g' k \omega^3 + i \{ g' k^2 \omega^3 (D_f(0) + a_2 y) \\ & - a_1 g' k \omega^2 f + \omega^3 (f^2 - \omega^2) \} \} \\ & + 2a_1 g' k^2 \omega^2 \bar{u} (f^2 - 3\omega^2) \end{aligned} \quad (\text{A.1b})$$

$$v_1 = a_1 g' k^2 \omega^2 \bar{u} (3f^2 - 5\omega^2) \quad (\text{A.1c})$$

$$\begin{aligned} \gamma_1 = & g' k^2 \omega^2 \bar{u} (3f^2 - 5\omega^2) (D_f(0) + a_2 y) \\ & + 2a_1 g' k \omega \bar{u} f (2\omega^2 - f^2) \\ & + ia_1 g' \omega (\omega^2 (\omega^2 - f^2) + 4k^2 \bar{u}^2 (6\omega^2 - f^2)) \\ & + a_2 g' \omega^2 f (f^2 - \omega^2) \\ & + ia_2 g' k \omega^2 \bar{u} (5\omega^2 - 3f^2) \\ & - \omega^2 \bar{u} (10\omega^2 f^2 - 3f^4 - 7\omega^4) \end{aligned} \quad (\text{A.1d})$$

$$v_2 = ia_1g'w\{k^2u^{-2}(10w^2-3f^2) + w^2(w^2-f^2)\} \quad (\text{A.1e})$$

$$\begin{aligned} \gamma_2 &= ig'w(D_f(0)+a_2y)\{k^2u^{-2}(10w^2-3f^2) + w^2(w^2-f^2)\} \\ &+ a_1g'u\{2k^2u^{-2}(18w^2-f^2) + w^2(11w^2-5f^2)\} \\ &+ ia_1g'ku^{-2}f(f^2-6w^2) \\ &+ a_2g'ku^{-2}w(10w^2-3f^2) \\ &+ 2ia_2g'wuf(2w^2-f^2) \\ &- iwu^{-2}(21w^4-20w^2f^2+3f^4) \end{aligned} \quad (\text{A.1f})$$

$$\begin{aligned} v_3 &= a_1g'u\{f^2(f^2-4w^2) + 5w^4+k^2u^{-2}(10w^2-f^2)\} \\ &+ ia_1g'kf u^{-2}(w^2-f^2) \end{aligned} \quad (\text{A.1g})$$

$$\begin{aligned} \gamma_3 &= g'u(D_f(0)+a_2y)\{f^2(f^2-4w^2)+5w^4+k^2u^{-2}(10w^2-f^2)\} \\ &+ ig'kf u^{-2}(D_f(0)+a_2y)(w^2-f^2) \\ &- 2a_1g'kwu^{-3}f \\ &+ ia_1g'wu^{-2}(9f^2-24k^2u^{-2}-34w^2) \\ &+ a_2g'u^{-2}f(6w^2-f^2) \\ &+ ia_2g'ku^{-3}(f^2-10w^2) \\ &- u^{-3}(35w^4+f^4-20w^2f^2) \end{aligned} \quad (\text{A.1h})$$

$$\begin{aligned} v_4 &= 2a_1g'kfwu^{-3} \\ &+ 5ia_1g'wu^{-2}(f^2-2w^2-k^2u^{-2}) \end{aligned} \quad (\text{A.1i})$$

$$\begin{aligned}
\gamma_4 &= 2g'kfwu^{-3}(D_f(0)+a_2y) \\
&+ 5ig'\omega u^{-2}(f^2-2\omega^2-k^2u^{-2})(D_f(0)+a_2y) \\
&+ a_1g'u^{-3}(5f^2-46\omega^2-6k^2u^{-2}) \\
&- 1a_1g'kfu^{-4} \\
&- 5a_2g'kwu^{-4} \\
&- 41a_2g'\omega u^{-3}f \\
&+ 1\omega u^{-4}(35\omega^2-10f^2)
\end{aligned} \tag{A.1j}$$

$$v_5 = a_1g'u^{-3}(2f^2-10\omega^2-k^2u^{-2}) - 1a_1g'kfu^{-4} \tag{A.1k}$$

$$\begin{aligned}
\gamma_5 &= g'u^{-3}(D_f(0)+a_2y)(2f^2-10\omega^2-k^2u^{-2}) \\
&- 1g'kfu^{-4}(D_f(0)+a_2y) + 291a_1g'\omega u^{-4} \\
&- a_2g'fu^{-4} + 1a_2g'ku^{-5} - u^{-5}(2f^2-21\omega^2)
\end{aligned} \tag{A.1l}$$

$$v_6 = 51a_1g'\omega u^{-4} \tag{A.1m}$$

$$\begin{aligned}
\gamma_6 &= 5ig'\omega u^{-4}(D_f(0)+a_2y) + 7a_1g'u^{-5} \\
&- 71\omega u^{-6}
\end{aligned} \tag{A.1n}$$

$$v_7 = a_1g'u^{-5} \tag{A.1o}$$

$$\gamma_7 = u^{-5}\{g'(D_f(0)+a_2y) - u^{-2}\} \tag{A.1p}$$

APPENDIX 2

PART I - CORRESPONDENCE WITH DUXBURY'S NOTATION

The notation employed in Duxbury's (1963) analysis, which is a special case of the problem addressed here, is sufficiently different that the following table is included in order to conveniently summarize the notational correspondence between the two models.

<u>Duxbury Variable</u>	<u>Designation in This Model</u>
s	a_1
x	y
y	-x
U	\bar{v}
Z	Z
k	k
w	-w
σ	σ
κ	$(\omega^2 - f^2)/g' + fa_1k/\omega$
α	α_d
z	$z = (2k/a_1)(D_f(0) + a_1x)$

APPENDIX 2

PART II - CONSTANTS IN THE DPA EQUATION

The dimensionless constants \tilde{v}_n and $\tilde{\gamma}_n$ appearing in (4.2) are given below to order F_x^2 .

$$\tilde{v}_0 = 1\sigma^3(1-\sigma^2)$$

$$\tilde{v}_1 = k\lambda F_x \sigma^2(3-5\sigma^2)$$

$$\tilde{v}_2 = 1\sigma\{\sigma^2(\sigma^2-1) + (k\lambda F_x)^2(10\sigma^2-3)\}$$

$$\tilde{v}_3 = k\lambda F_x(1-4\sigma^2+5\sigma^4) + O(F_x^3)$$

$$\tilde{v}_4 = 51(k\lambda F_x)^2\sigma(1-2\sigma^2) + O(F_x^3)$$

$$\tilde{v}_5 = 0 + O(F_x^3)$$

$$\tilde{v}_6 = 0 + O(F_x^4)$$

$$\tilde{v}_7 = 0 + O(F_x^5)$$

$$\begin{aligned}\tilde{\gamma}_0 &= (1-\sigma^2)\{F_x \sigma^2 (2k\lambda - \sigma/F_y) \\ &+ (i\sigma^3/F_y)\{(\tau/k\lambda)(1-\sigma^2) - k\lambda\tau - F_x \tilde{\gamma} - F_y/\sigma\}\end{aligned}$$

$$\begin{aligned}\tilde{\gamma}_1 &= k\lambda F_x \sigma \{(\sigma/F_y)(5\sigma^2 - 3)(k\lambda\tau + F_x \tilde{\gamma}) + 2(2\sigma^2 - 1)\} \\ &+ (F_x \sigma^2/F_y)\{\sigma^2 - 1 + \tau(7\sigma^4 + 3 - 10\sigma^2)\} \\ &+ i\sigma\{\sigma^2(\sigma^2 - 1) + k\lambda F_x^2\{(\sigma^2/F_y)(3 - 5\sigma^2) + 4k\lambda(2\sigma^2 - 1)\}\end{aligned}$$

$$\begin{aligned}\tilde{\gamma}_2 &= k\lambda F_x \{\sigma^2(11\sigma^2 - 9) + (k\lambda F_x \sigma/F_y)(3 - 10\sigma^2)\} \\ &- (i\sigma/F_y)\{\sigma^2(k\lambda\tau + F_x \tilde{\gamma})(\sigma^2 - 1) + (k\lambda F_x)^2 \tau(10\sigma^2 - 1)\} \\ &+ ik\lambda F_x^2 \{k\lambda(1 - 6\sigma^2) + (\sigma/F_y)\{2(1 - 2\sigma^2) + \tau(20\sigma^2 - 21\sigma^4 - 3)\}\} \\ &+ o(F_x^3)\end{aligned}$$

$$\begin{aligned}\tilde{\gamma}_3 &= -(k\lambda F_x/F_y)(k\lambda\tau + F_x \tilde{\gamma})(1 - \sigma^2) \\ &+ i(k\lambda F_x)^2 \{((1 - \sigma^2)/F_y)(k\lambda\tau + F_x \tilde{\gamma}) + 17\sigma(1 - 2\sigma^2)\} \\ &+ o(F_x^3)\end{aligned}$$

$$\tilde{\gamma}_4 = 5i(k\lambda F_x)^2 (\sigma\tau/F_y)(2\sigma^2 - 1)$$

$$\tilde{\gamma}_5 = 0 + o(F_x^3)$$

$$\tilde{\gamma}_6 = 0 + o(F_x^4)$$

$$\tilde{\gamma}_7 = 0 + o(F_x^5)$$